

**MORPHOLOGICAL STUDIES ON *KLUYVEROMYCES MARXIANUS* VAR.
MARXIANUS NRRLY2415 IN SUSPENSION CULTURE: A STUDY
INCORPORATING COMPUTER AIDED IMAGE ANALYSIS**

A thesis presented for the
degree of Ph.D.

by

Daniel G. O'Shea BSc.


Under the supervision of
Dr. Padraig Walsh

School of Biological Sciences
Dublin City University

February 1998

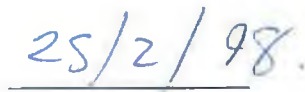
I hereby certify that this material, which I now submit for assessment on this programme of study leading to the award of Ph.D. is entirely my own work and has not been taken from the work of others save to the extent that such work has been cited and acknowledged within the text of my work.

Signed:

A handwritten signature in blue ink that reads "Daniel O'Shea". The signature is written in a cursive style and is positioned above a horizontal line.

Daniel G. O'Shea

Date:

A handwritten date in blue ink that reads "25/2/98". The date is written in a simple, clear style and is positioned above a horizontal line.

25th February 1998

To Sinead.....

ACKNOWLEDGEMENTS

I would like to sincerely thank my supervisor Dr. Pádraig Walsh for all his input. Thanks for having the faith in me to take me on, when I knocked on your door in '93. Special thanks for the extreme proofing and heated scientific debates at the end!

I would like to thank all staff members in the School of Biological Sciences for their friendship and assistance. I would like to particularly thank Dr. Patricia Kieran, Dr. Greg Foley, Ms. Angela O'Toole and Prof. Richard O'Kennedy for all their support. I would also like to thank all the technical staff I have had the pleasure of working with over the years, particularly Mr. Brian Corcoran and Mr. Ben Austen, without whose technical support I would have been lost.

I would like to thank the BERG crew, particularly Miriam O'Shea, Audrey McNulty, Tony McCarthy and Una Cusack. I would like to particularly thank my good friend Tony for all the invaluable brainstorming sessions (coffee breaks) throughout the years, without his help and brilliance I would not be here. To Miriam, my sister, flatmate and co-worker, thanks for putting up with me. I would also like to thank all members of the postgraduate fraternity, both past and present, for their friendship.

Thanks to all the fourth years whom I had the pleasure of working with over the years, many of whom worked on projects related to this work. I wish them all luck in the future. I would especially like to thank Mr. Dan Hourigan, Mr. Nigel Plant and Ms. Miriam Porter for their assistance.

To Dara and all in BRI, thanks for being so understanding when the pressure was on.

To my fellow travellers of eight years, Kevin Blackwell, Marianne O'Sullivan and Paula Meleady. Long may we remain good friends.

To Kev, Eddie, Andrew and Robbie who have remained my good friends throughout all my college days. I hope I'll have more time (and money) for poker now!

To Mom and Dad and Seamus, without whose understanding and support, none of this would ever have been possible. At last I'm leaving the nest!

To Sinead, thanks for being there and putting up with me when times were bad. Without you this thesis would not exist. This thesis is dedicated to you....

PUBLICATIONS ASSOCIATED WITH THIS WORK

O'Shea D.G. and Walsh, P.K. (1996) Morphological characterisation of the dimorphic yeast *Kluyveromyces marxianus* var. *marxianus* NRRLy2415 by semi-automated image analysis, *Biotechnol. Bioeng.*, **51**, 679-690.

McCarthy, A.A., O'Shea, D.G., Murray, N.T., Walsh, P.K. and Foley, G. (1998). Effect of cell morphology on dead-end filtration of the dimorphic yeast *Kluyveromyces marxianus* var *marxianus* NRRLy2415., *Biotechnol. Prog.*, **14**, 279-285.

TABLE OF CONTENTS

Abstract	i
Nomenclature	ii
List of Figures	vi
List of Tables	xv
Abbreviations	xvii
CHAPTER 1 – INTRODUCTION	1
CHAPTER 2 – FUNGAL MORPHOLOGY AND ENVIRONMENT	
2.1 INTRODUCTION	4
2.2 FUNGAL MORPHOLOGY IN SUSPENSION CULTURE	5
2.2.1 Unicellular Fungi (Yeast)	5
2.2.2 Filamentous Fungi	6
2.2.3 Pelleted Fungi	7
2.2.4 Dimorphic Fungi	8
2.3 EFFECT OF BIOREACTOR ENVIRONMENT ON MORPHOLOGY	8
2.3.1 Mechanical Shear	9
2.3.1.1 <i>Problems with experimental design</i>	10
2.3.1.2 <i>Breakage or acceleration of old age?</i>	11
2.3.1.3 <i>How does agitation damage fungal hyphae?</i>	11
2.3.1.4 <i>Fungal adaption to agitation.</i>	12
2.3.1.5 <i>Agitation and pelleted growth</i>	13
2.3.2 Other Environmental Effects	13
2.4 BROTH RHEOLOGY	15
2.4.1 Fluid Rheology	15
2.4.2 The Consequence of Cell Morphology on Broth Rheology	16
2.5 FUNGAL DIMORPHISM	19
2.5.1 Morphologies Exhibited by Dimorphic Organisms	19
2.5.2 Sub Classification of Dimorphic Organisms	20
2.5.3 Pathogenic Yeast-Like Fungi	21

2.5.4 Non-Pathogenic Yeast-Like Fungi	23
2.5.5 Dimorphic True Yeast	27
2.5.6 Dimorphic Imperfect Yeast	31
2.6 A MECHANISM FOR DIMORPHISM IN YEAST	31
2.6.1 Cell Wall Composition and Significance in Morphology	32
2.6.2 Cell Wall Development	32
2.6.3 Cell Division	35
2.7 SUMMARY	36
CHAPTER 3 – MATERIALS AND EXPERIMENTAL METHODS	
3.1 ORGANISM	38
3.2 AUTOCLAVING PROCEDURE	38
3.3 MEDIA PREPARATION	38
3.3.1 YEPD Medium	38
3.3.2 YEPD Medium (Solid)	38
3.3.3 YEPL Medium	38
3.3.4 Whey-Based Medium	39
3.4 CULTURING ON SOLID MEDIUM	39
3.5 SHAKE FLASK CULTURES	39
3.6 10L “MICOGEN” FERMENTER (BATCH CULTURE)	39
3.6.1 Fermenter Configuration	40
3.6.2 Fermenter Setup	40
3.6.3 Fermenter Operation	41
3.7 2L “LIFE SCIENCES” FERMENTER (CHEMOSTAT)	41
3.7.1 Fermenter Configuration	42
3.7.2 Fermenter Setup	43
3.7.3 Fermenter Operation	44
3.8 DETERMINATION OF FERMENTATION PARAMETERS	44
3.8.1 Sugar Concentration	44
3.8.2 Ethanol Concentration	45

3.8.3 Cell Enumeration	45
3.8.4 Cell Dry Weight	45
3.8.5 Viscosity of Cell Suspensions	46
3.8.6 pH	47
3.8.7 Cell Dry Matter per Unit Cell Volume (δ)	47
3.8.8 Fermenter k_La	48

CHAPTER 4 – INITIAL MORPHOLOGICAL OBSERVATIONS AND DEVELOPMENT OF A MORPHOLOGICAL CLASSIFICATION REGIME.

4.1 INTRODUCTION	50
4.2 MORPHOLOGICAL VARIATION IN <i>Kluyveromyces marxianus</i>	51
4.3 FURTHER CLASSIFICATION OF PSEUDOHYPHAE	58
4.4 CONCLUSIONS	58

CHAPTER 5 – IMAGE ANALYSIS METHODS

5.1 INTRODUCTION	60
5.2 APPROACHES TO INFORMATION EXTRACTION FROM IMAGES	60
5.2.1 Image Segmentation Based on Colour or Greyscale Thresholding	60
5.2.2 Edge-Based Segmentation	61
5.2.3 Pattern Recognition	61
5.2.4 Colour Indexing	62
5.3 IMAGE ANALYSIS HARDWARE	62
5.3.1 Image Generator	63
5.3.2 Framegrabber Board	63
5.3.3 Image Analysis Software	63
5.4 APPLICATIONS OF IMAGE ANALYSIS IN BIOLOGICAL SCIENCES	64
5.5 IMAGE ANALYSIS OF FUNGI IN SUSPENSION CULTURE	67
5.5.1 Yeast	67
5.5.2 Fungal Pellets	70
5.5.3 Filamentous Fungi	71

5.5.4 Dimorphic Organisms	75
5.6 IMAGE ANALYSIS HARDWARE	77
5.6.1 Computer Configuration	77
5.6.2 Camera	77
5.6.3 Microscope	77
5.7 IMAGE ANALYSIS SOFTWARE	77
5.7.1 Introduction	77
5.7.2 Grey Image Acquisition	78
5.7.3 Grey Image Processing	78
5.7.4 Image Segmentation (Feature Detection)	78
5.7.5 Binary Image Manipulation	79
5.7.6 Feature Measurement	79
5.7.7 Program Development Utility (QUIPS)	79
5.8 SLIDE PREPARATION FOR IMAGE ACQUISITION	80
5.9 OBJECTIVES FOR DEVELOPED ALGORITHMS	80
5.10 OVERVIEW OF PROGRAM “ACQUIRE”	81
5.11 OVERVIEW OF PROGRAM “MEASURE”	86
5.11.1 Preliminary Cell Classification	86
5.11.2 Primary Segmentation	87
5.11.3 Secondary Segmentation	88
5.11.3.1 Segment 2	88
5.11.3.2 Segment 3	88
5.11.3.3 Segment 4	89
5.11.4 Classification and Measurement of Single Cells	89
5.11.5 Skeletonization and Measurement of Pseudohyphal Cells	89
5.11.6 Sorting and Presentation of Data	92
5.12 VALIDATION OF PROGRAM “MEASURE”	92
5.12.1 Validation of Correct Geometric Shape	92
5.12.2 Test Fermentation Development	96
5.12.3 Classification Error Estimation	100
5.12.4 Establishment of Suitable Sample Size	100

5.12.5 Examination of Sample Processing Time	102
5.13 DISCUSSION	104
CHAPTER 6 – FERMENTATION KINETICS FOR BATCH AND CONTINUOUS CULTURES OF <i>Kluyveromyces marxianus</i>	
6.1 ETHANOL FORMATION IN YEAST FERMENTATIONS	106
6.2 MATHEMATICAL MODEL DESIGN	109
6.2.1 $Y_{x/s}$ aerobic	109
6.2.2 $Y_{p/s}$ theoretical	111
6.2.3. J_s critical	111
6.2.4 $Y_{p/s}$ anaerobic	112
6.2.5 $Y_{x/s}$ anaerobic	112
6.2.6 Substrate Uptake	114
6.2.7 Implementation of Model	116
6.2.8 Examination of model sensitivity	117
6.2.9 Adaption of Model to Batch Culture Growth	122
6.3 INTRODUCTION TO EXPERIMENTAL WORK	123
6.4 CHEMOSTAT CULTURE RESULTS	123
6.4.1 Overview of Kinetic Data	123
6.5 BATCH CULTURE RESULTS	128
6.5.1 Overview of Whey-Based Batch Culture Studies	128
6.5.2 Substrate Uptake Rates	131
6.5.3 The Effect of k_{La} on J_s critical	133
6.5.4 Overview of YEPD and YEPL Batch Fermentations	134
6.6 CONCLUSIONS	136
CHAPTER 7 - THE CONSEQUENCES OF GROWTH CONDITIONS ON THE MORPHOLOGY OF <i>Kluyveromyces marxianus</i>	
7.1 INTRODUCTION	139
7.2 EFFECT OF AGITATION ON MORPHOLOGY IN BATCH CULTURE (WHEY BASED MEDIUM)	140

7.3 EFFECT OF DIFFERENT MEDIA ON CELL MORPHOLOGY IN BATCH CULTURE	145
7.4 MORPHOLOGY IN CHEMOSTAT CULTURE	151
7.4.1 Introduction	151
7.4.2 Chemostat Morphological Classification Data.	151
7.4.3 Geometric Properties of Cells	160
7.4.4 Pseudohyphal Growth Unit	166
7.5 GEOMETRIC CONSIDERATIONS FOR MORPHOLOGICAL TRANSITIONS	167
7.6 CONCLUSIONS	171
CHAPTER 8 – POPULATION DISTRIBUTIONS OF VARIOUS MORPHOLOGIES OF <i>Kluyveromyces marxianus</i>	
8.1 INTRODUCTION	174
8.2 INITIAL INVESTIGATIONS	175
8.3 DISTRIBUTIVE CHARACTERISTICS OF CELL SUB-POPULATIONS	178
8.3.1 Single cells	179
8.3.2 Double cells	182
8.3.3 Pseudohyphae	185
8.4 GENERATION OF CUMULATED DISTRIBUTION FUNCTION	187
8.5 APPLICATION OF THE SUMMED DISTRIBUTION TO CELL LENGTH AND CELL WIDTH	189
8.6 APPLICATION OF DISTRIBUTION TO FERMENTATION DATA	192
8.7 CONCLUSIONS	196
CHAPTER 9 – THE STRUCTURAL DEVELOPMENT OF <i>K. marxianus</i> PSEUDOHYPHAE IN CONTINUOUS CULTURE	
9.1 INTRODUCTION	198
9.2 MANUAL IMAGING PROTOCOL	198

9.3 INITIAL OBSERVATIONS	200
9.4 PROPOSED MODEL FOR PSEUDOHYPHAL DEVELOPMENT	204
9.5 ANALYSIS OF SUBUNIT BEHAVIOUR	205
9.5.1 Introduction	205
9.5.2 Subunit Lengths Relative to Position in Pseudohyphae	205
9.6 ANALYSIS OF BRANCH DEVELOPMENT	210
9.6.1 Introduction	210
9.6.2 Branch Extension Rates	212
9.7 EFFECT OF ENVIRONMENT ON PSEUDOHYPHAL DEVELOPMENT	214
9.7.1 Effect of Operating Conditions on Branching Pattern	214
9.7.2 Effect of Growth Conditions on Pseudohyphal Subunit Length	218
9.8 NOTE ON THE CLASSICAL VALUE OF L_e	220
9.9 CONCLUSIONS	220
CHAPTER 10 - SUMMARY AND RECCOMENDATIONS FOR FURTHER WORK	
10.1 SUMMARY	224
10.2 OVERALL CONCLUSIONS	230
10.3 POSSIBLE AREAS OF FUTURE RESEARCH	232
10.3.1 Image Analysis	232
10.3.2 Kinetic Modelling	232
10.3.3 Morphology Studies	232
BIBLIOGRAPHY	234

ABSTRACT

MORPHOLOGICAL STUDIES ON *KLUYVEROMYCES MARXIANUS* VAR. *MARXIANUS* NRRLy2415 IN SUSPENSION CULTURE: A STUDY INCORPORATING COMPUTER AIDED IMAGE ANALYSIS

The morphology of the lactose fermenting organism, *Kluyveromyces marxianus* var. *marxianus* NRRLy2415 was studied in batch and continuous culture. The morphology of the organism was observed to vary significantly from a budding yeastlike form to a branched pseudohyphal form depending on the operating conditions. The following morphological classes were deemed important for the complete description of culture morphology: yeast, elongated yeast, filament, double yeast, double elongated yeast, double filament and pseudohyphae.

Image analysis was used to implement the classification system, due to its objectivity in measurement of visual phenomena. The protocol developed was also capable of measuring geometric properties of the cell population including volume, length and width for all cells and hyphal growth unit length for pseudohyphae.

The predominant morphology observed for the organism in fully aerobic batch culture was yeast-like. When the agitation rate was decreased, an increased heterogeneity in the morphology was observed, with the generation of more elongated yeast and filamentous forms. This was attributed to partial oxygen limitation in the fermentations.

In chemostat culture, the morphology observed was predominantly pseudohyphal. This morphological form was found to dominate over a large range of dilution rates ($0.1-0.45\text{h}^{-1}$) and substrate feed concentrations (5 to 20g/L lactose). At both extrema of dilution rates a reversion to a yeastlike morphology was observed. The mycelial morphology was attributed to substrate limitation and was demonstrated to be of ecological advantage under substrate limited conditions.

Kinetic modelling of substrate metabolism was undertaken for continuous and batch culture results. It was demonstrated that, the stoichiometry of the metabolic pathways studied was identical under all operating conditions. This is significant, as the morphology of the organism varies significantly from batch to continuous culture.

A population model was developed which was capable of describing the distributions of cell geometric parameters based on summed lognormal distributions of selected morphological classes.

The ultrastructure of pseudohyphae was examined. This study demonstrated significant differences in methods of formation between pseudohyphae and true hyphae and highlighted key issues that need to be addressed if successful modeling of such growth is to be undertaken.

NOMENCLATURE

Symbol	Definition	Units	Dimensions
A	Projected area of pellet	μm^2	L^2
A	Cross sectional area of cell	μm^2	L^2
$A_{\text{estimated}}$	Estimated cell cross sectional area	μm^2	L^2
A_{measured}	Observed cell cross sectional area	μm^2	L^2
C_L^*	Concentration of oxygen in liquid phase at 100% saturation	---	---
C_{L_0}	Oxygen concentration at time 0	---	---
C_{L_t}	Oxygen concentration at time t	---	---
C_L	Concentration of oxygen in liquid phase	---	---
C_m	Biomass concentration	gL^{-1}	ML^{-3}
D	Diameter of the daughter cell	μm	L
D	Distance in direction of examination	variable	L
D	Dilution rate	h^{-1}	T^{-1}
D_f	Double filaments		
D_I	Impeller diameter	mm	L
D_t	Tank diameter	mm	L
D_y	Double yeastlike cells		
F	Flowrate into bioreactor	Lh^{-1}	L^3T^{-1}
F	Filaments		
F_{ac}	Fraction of substrate used in ethanol production	---	---
H	Length of the daughter cell	μm	L
I	Intensity	---	---
J_s	Substrate flux	gh^{-1}	MT^{-1}
$J_{s \text{ critical}}$	Critical substrate flux at which ethanol production ensues	gh^{-1}	MT^{-1}

k	Power law constant	Pa	$\text{ML}^{-1}\text{T}^{-2}$
k_1	Initial substrate concentration dependence constant	gL^{-1}	ML^{-3}
k_c	Casson constant	$(\text{Pa s})^{0.5}$	$(\text{L}^{-1}\text{MT}^{-1})^{0.5}$
k_{LA}	Volumetric oxygen, gas-liquid mass transfer coefficient	s^{-1}	T^{-1}
k_s	Saturation constant in Monod eq.	gL^{-1}	ML^{-3}
L	Cell length	μm	L
L	Feret length of cell	μm	L
L_c	Effective hyphal length	μm	L
L_{hgu}	Hyphal growth unit length	μm	L
L_i	Length of segment i	μm	L
L_t	Total hyphal length	μm	L
M	Mycelium		
M_p	Mass of cell pellet	g	M
M_I	Morphology index	---	---
N	Consistency index	---	---
N	Cell number	L^{-1}	L^{-3}
N	Number of subdivisions	---	---
N	Number of tips per hyphae	---	---
N_{df}	Numerical fraction of double filaments	---	---
N_{dy}	Numerical fraction of yeastlike double cells	---	---
N_f	Numerical fraction of filaments	---	---
N_m	Numerical fraction of mycelium	---	---
N_t	Total population size	cells	---
N_v	Rate of Vesicle Supply	---	T^{-1}
N_y	Numerical fraction of yeastlike single cells	---	---
P	Power input	W	L^2MT^{-3}
P	Concentration of product	gL^{-1}	ML^{-3}
$p(x)$	Probability of x	---	---

R_s	Specific substrate uptake rate	g substrate /g cell / h	T^{-1}
R_{vsc}	Rate of VSC movement	---	LT^{-1}
S	Diameter of the mother bud interface	μm	L
S	Substrate concentration	gL^{-1}	ML^{-3}
S_0	Initial substrate concentration	gL^{-1}	ML^{-3}
S_{yeast}	Surface area of yeastlike cells	μm^2	L^2
$S_{f/m}$	Surface area of filamentous/mycelial cells	μm^2	L^2
S_v	Surface area to volume ratio	μm^{-1}	L^{-1}
S_L	Surface area to length ratio	μm	L
t	Time	s,h	T
t_c	Circulation time	s	T
V	Overall cell volume	μm^3	L^3
\bar{V}	Mean cell volume	μm^3	L^3
V	Bioreactor Volume	L	L^3
V_i	Volume of segment, i	μm^3	L^3
W	Cell width	μm	L
W	Feret width of cell	μm	L
w	Histogram bucket width	variable	variable
x	Distance in x direction	---	L
X	Cell dry mass concentration	gL^{-1}	ML^{-3}
X_0	Biomass concentration at time 0	gL^{-1}	ML^{-3}
$X_{aerobic}$	Aerobically produced biomass	gL^{-1}	ML^{-3}
$X_{anaerobic}$	Anaerobically produced biomass	gL^{-1}	ML^{-3}
X_{total}	Total biomass	gL^{-1}	ML^{-3}
y	Yeastlike cells (Yeast and elongated yeast)		
$Y_{p/s aerobic}$	Yield of ethanol per unit substrate metabolised anaerobically.	g ethanol/ g lactose	---
$Y_{p/s theoretical}$	Theoretical yield of ethanol per unit substrate	g ethanol/ g lactose	---

$Y_{x/s}$ aerobic	Aerobic yield of cells per unit substrate	g cell/ g lactose	---
$Y_{x/s}$ anaerobic	Anaerobic yield of cells per unit substrate	g cell/ g lactose	---
z	Length of major axis		
δ	Cell dry weight:wet weight ratio	---	---
ε	Pellet voidage	---	---
ε_A	Error function	---	---
ε_c	Energy dissipation/circulation function	$W m^{-3} s^{-1}$	$ML^{-4} T^{-3}$
γ	Shear rate	s^{-1}	T^{-1}
η	Viscosity	Pa s	$L^{-1}MT^{-1}$
μ_m	Maximum specific growth rate	h^{-1}	T^{-1}
σ	Population standard deviation	variable	variable
$\sigma_{\ln x}$	Standard deviation of natural log of population	Variable	Variable
τ	Shear stress	Pa	$ML^{-1}T^{-2}$
τ_0	Yield stress	Pa	$ML^{-1}T^{-2}$
τ_0	Casson yield stress	Pa	$ML^{-1}T^{-2}$

LIST OF FIGURES

- Figure 3.1** Fermenter configuration for chemostat operation
- Figure 4.1** Fermentation sample displaying predominantly yeast-like morphology. (a) Sample magnification at 200x, (b) Sample magnification at 400x. Bars = 20 μ m
- Figure 4.2** Example of pseudohyphal cells taken from chemostat culture. Sample magnification at 200x. Bar = 20 μ m
- Figure 4.3** Example of intermediate cells taken from batch culture. (a) Sample magnification at 200x. (b) Sample magnification at 400x. Bar = 20 μ m.
- Figure 4.4** Morphological forms displayed by *K. marxianus* NRRLy2415 (a) yeast (b) elongated yeast (c) double yeast (d) double elongated yeast (e) filament (f) double filament (g) mycelium. Bar = 10 μ m
- Figure 5.1** Application of contour rotation method (adapted from Huls *et al.* (1992))
- Figure 5.2** Overview of algorithms used in programs ACQUIRE and MEASURE
- Figure 5.3** Preliminary image processing state (a) Image A: (portion of) initial grey image; (b) Image B: unedited binary image; (c) Image C: edited binary image. For clarity, only a portion (approximately one third) of the full image frame is displayed.
- Figure 5.4** Morphological operations for secondary image processing: (a) Segment 2; (b) Segment 3; (c) Segment 4. Bar = 10 μ m.
- Figure 5.5** Skeletonisation and characterisation of mycelium; (a) original grey image, (b) binarised version of largest mycelium, (c) binary image after application of skeletonisation operator, (d) pruned to remove artefact branches, (e) number of tips.
- Figure 5.6** Error function (ϵ_A) for increasing measured cell cross-sectional area (a) 200x magnification, (b) 400x magnification.

- Figure 5.7** Comparison of distributions of cross-sectional area, length and width of a single cell population measured at 200× and 400× magnification
- Figure 5.8** Test fermentation growth profile for *K. marxianus*
- Figure 5.9** Distribution of cell morphologies during the test fermentation
- Figure 5.10** Frequency distribution of cell properties during fermentation run. (a) volume, (b) length
- Figure 6.1** $Y_{x/s}$ aerobic versus dilution rate for *K. marxianus* grown in lactose-limited chemostat (800 rpm, 1 vvm)
- Figure 6.2** Determination of critical substrate flux for *K. marxianus* grown in lactose-limited chemostat (whey medium, 800rpm, 1 vvm)
- Figure 6.3** Schematic of the proposed mechanism for substrate bypass of the reactor
- Figure 6.4** Sensitivity analysis on model parameter f , long dash ($f = 0.0$), solid line ($f = 0.03$), short dash ($f = 0.06$)
- Figure 6.5** Sensitivity analysis on model parameter k_s ; long dash ($k_s = 0.0036$), solid line ($k_s = 0.036$), short dash ($k_s = 0.36$).
- Figure 6.6** Sensitivity of model to variation in S_0 ; long dash ($S_0 = 15\text{g/L}$), solid line ($S_0 = 20\text{g/L}$), short dash ($S_0 = 25\text{g/L}$).
- Figure 6.7** Sensitivity analysis on model parameter J_s ; long dash ($J_s = 2.02\text{g/L/h}$), solid line ($J_s = 3.02\text{g/L/h}$), short dash ($J_s = 4.02\text{g/L/h}$).
- Figure 6.8** Chemostat fermentation 1-Kinetic overview of 20g/L run (a) biomass (b) ethanol (c) residual substrate and pH. Solid lines - model prediction of data ($S_0 = 19.5\text{ g/L}$)
- Figure 6.9** Chemostat Fermentation 2 - Kinetic overview of 15g/L run (a) biomass (b) ethanol (c) residual substrate and pH. Solid lines - model prediction of data. ($S_0 = 14.5\text{ g/L}$)
- Figure 6.10** Chemostat fermentation 3 - Kinetic overview of 10g/L run (a) biomass (b) ethanol (c) residual substrate and pH. Solid lines - model prediction of data ($S_0 = 10.0\text{ g/L}$)

- Figure 6.11** Chemostat Fermentation 4 - Kinetic overview of 5g/L run (a) biomass (b) ethanol (c) residual substrate and pH. Solid lines - model prediction of data ($S_0 = 5.2$ g/L)
- Figure 6.12** Batch Fermentation 1 – 800rpm, 1vvm whey medium. Broken Line – stoichiometric prediction for substrate concentration
- Figure 6.13** Batch Fermentation 2 – 400rpm, 1vvm whey medium. Broken Line – stoichiometric prediction for substrate concentration
- Figure 6.14** Batch Fermentation 3 – 300rpm, 1vvm whey medium. Broken Line – stoichiometric prediction for substrate concentration
- Figure 6.15** Batch Fermentation 4 – 200rpm, 1vvm whey medium. Broken Line – stoichiometric prediction for substrate concentration
- Figure 6.16** Estimated Specific Substrate uptake rates (R_s) versus time for whey fermentations
- Figure 6.17** The effect of k_La on $J_{s\text{ critical}}$ in whey media batch culture
- Figure 6.18** Batch Fermentation 5 – 800rpm, 1vvm YEPD medium. Broken Line – stoichiometric prediction for substrate concentration
- Figure 6.19** Batch Fermentation 6 – 200rpm, 1vvm YEPD medium. Broken Line – stoichiometric prediction for substrate concentration
- Figure 6.20** Batch Fermentation 7 – 800rpm, 1vvm YEPL medium. Broken Line – stoichiometric prediction for substrate concentration
- Figure 6.21** Batch Fermentation 8 – 200rpm, 1vvm YEPL medium. Broken Line – stoichiometric prediction for substrate concentration
- Figure 7.1** Morphology distribution versus time for whey batch culture grown at 800 rpm, 1vvm. Black – Yeast; Red – Double yeast; Green – Elongated yeast; Yellow - Double elongated yeast; Dark Blue – Filaments; Purple – Double filaments; Light Blue – Pseudohyphae
- Figure 7.2** Morphology distribution versus time for whey batch culture grown at 400 rpm, 1vvm (Legends Figure 7.1)
- Figure 7.3** Morphology distribution versus time for whey batch culture grown at 300 rpm, 1vvm (Legends Figure 7.1)

- Figure 7.4** Morphology distribution versus time for whey batch culture grown at 200 rpm, 1 vvm (Legends Figure 7.1)
- Figure 7.5** Morphology distribution versus time for YEPL batch culture grown at 800 rpm, 1 vvm (Legends Figure 7.1)
- Figure 7.6** Morphology distribution versus time for YEPD batch culture grown at 800 rpm, 1 vvm (Legends Figure 7.1)
- Figure 7.7** Mean geometric parameters of cells in batch cultures grown at 800 rpm, 1 vvm on various media. (a) mean cell volume, (b) mean cell length, (c) mean cell width. filled circles - YEPL, open circles - YEPD, open triangles - Whey. Data presented versus biomass concentration due to differences in inoculum size and initial substrate concentration
- Figure 7.8** Morphology distribution versus time for YEPL batch culture grown at 200 rpm, 1 vvm (Legends Figure 7.1)
- Figure 7.9** Morphology distribution versus time for YEPD batch culture grown at 200 rpm, 1 vvm (Legends Figure 7.1)
- Figure 7.10** Mean geometric parameters of cells in batch cultures grown at 200 rpm, 1 vvm on various media. (a) mean cell volume, (b) mean cell length, (c) mean cell width. filled circles - YEPL, open circles - YEPD, open triangles - Whey. Data presented versus biomass concentration due to differences in inoculum size and initial substrate concentration
- Figure 7.11** Classification data for 20g/L chemostat fermentation (based on cell volume fraction in each class)
- Figure 7.12** Classification data for 20g/L chemostat fermentation (based on cell numerical fraction in each class)
- Figure 7.13** Classification data for 15g/L chemostat fermentation (based on cell volume fraction in each class)
- Figure 7.14** Classification data for 15g/L chemostat fermentation (based on cell numerical fraction in each class)

- Figure 7.15** Classification data for 10g/L chemostat fermentation (based on cell volume fraction in each class)
- Figure 7.16** Classification data for 10g/L chemostat fermentation (based on cell numerical fraction in each class)
- Figure 7.17** Classification data for 5g/L chemostat fermentation (based on cell volume fraction in each class)
- Figure 7.18** Classification data for 5g/L chemostat fermentation (based on cell numerical fraction in each class)
- Figure 7.19** Plot of Power law constant (k) and Power law index (n) versus dilution rate for 20 g/L chemostat fermentaton
- Figure 7.20** Mean geometric parameters of cells for 20g/L chemostat fermentation; (a) cell volume, (b) cell length, (c) cell width
- Figure 7.21** Mean geometric parameters of cells for 15g/L chemostat fermentation; (a) cell volume, (b) cell length, (c) cell width
- Figure 7.22** Mean geometric parameters of cells for 10g/L chemostat fermentation; (a) cell volume, (b) cell length, (c) cell width
- Figure 7.23** Mean geometric parameters of cells for 5g/L chemostat fermentation; (a) cell volume, (b) cell length, (c) cell width
- Figure 7.24** Mean L_{hgu} versus dilution rate for four initial substrate concentrations
- Figure 7.25** Plots of S_V and S_L versus dilution rate for 10g/L chemostat fermentation (a) S_V (b) S_L
- Figure 7.26** Plots of S_V versus Biomass concentration for various batch culture fermentations. (a) 800rpm (b) 200rpm
- Figure 8.1** Lognormal and Gaussian volume distributions for Sample 1. Solid line – lognormal distribution, Dashed line – normal distribution (sample size=302)
- Figure 8.2** Lognormal and Gaussian volume distributions for Sample 2 Solid line – lognormal distribution, Dashed line – normal distribution (sample size = 297)

- Figure 8.3** Lognormal and Gaussian volume distributions for Sample 3 Solid line – lognormal distribution, Dashed line – normal distribution (sample size = 250)
- Figure 8.4** Volume distribution of single cells for Sample 1. Solid line – lognormal distribution, Dashed line – normal distribution (sample size = 95)
- Figure 8.5** Volume distribution of single cells for Sample 2. Solid line – lognormal distribution, Dashed line – normal distribution (Sample size = 101)
- Figure 8.6** Volume distribution for single filaments in Sample 2, solid line - lognormal distribution, dashed line – normal distribution (Sample size = 72)
- Figure 8.7** The use of the summed distribution of yeastlike cells and filaments to describe the overall volume distribution of single cells for sample 2. ($N_y = 0.29$, $N_f = 0.71$)
- Figure 8.8** Volume distribution of double cells for Sample 1, solid line – lognormal distribution, dashed line – normal distribution (sample size = 201)
- Figure 8.9** Volume distribution of double cells for Sample 2, solid line – lognormal distribution, dashed line – normal distribution (Sample size = 221)
- Figure 8.10** The use of the summed distribution of yeastlike cells and filaments to describe the overall distribution of double cells for sample 2. ($N_{dy} = 0.41$, $N_{df} = 0.59$)
- Figure 8.11** Distribution of pseudohyphae for Sample 2, solid line – lognormal distribution (sample size = 146)
- Figure 8.12** Distribution of pseudohyphae for Sample 3, solid Line – lognormal distribution. (Sample size = 164)
- Figure 8.13** Summed population distribution for sample 1, $N_y = 0.31$, $N_{dy} = 0.63$, $N_f = 0.02$, $N_{df} = 0.03$, $N_m = 0.00$ (sample size = 302)

- Figure 8.14** Summed volume distribution for sample 2, $N_y = 0.10$, $N_{dy} = 0.09$, $N_f = 0.25$, $N_{df} = 0.34$, $N_m = 0.23$ (sample size = 297)
- Figure 8.15** Summed volume distribution for sample 3, $N_y = 0.01$, $N_{dy} = 0.09$, $N_f = 0.02$, $N_{df} = 0.20$, $N_m = 0.68$ (sample size = 250)
- Figure 8.16** Summed length distribution for yeast-like Sample 1. $N_y = 0.31$, $N_{dy} = 0.63$, $N_f = 0.02$, $N_{df} = 0.03$, $N_m = 0.00$ (sample size = 302)
- Figure 8.17** Summed length distribution for intermediate Sample 2. $N_y = 0.10$, $N_{dy} = 0.09$, $N_f = 0.25$, $N_{df} = 0.34$, $N_m = 0.23$ (sample size = 297)
- Figure 8.18** Summed length distribution for pseudohyphal Sample 3. $N_y = 0.01$, $N_{dy} = 0.09$, $N_f = 0.02$, $N_{df} = 0.20$, $N_m = 0.68$ (sample size = 250)
- Figure 8.19** Summed width distribution for yeast-like Sample 1 $N_y = 0.31$, $N_{dy} = 0.63$, $N_f = 0.02$, $N_{df} = 0.03$, $N_m = 0.00$ (sample size = 302)
- Figure 8.20** Summed width distribution for yeast-like Sample 2. $N_y = 0.10$, $N_{dy} = 0.09$, $N_f = 0.25$, $N_{df} = 0.34$, $N_m = 0.23$ (sample size = 297)
- Figure 8.21** Summed width distribution for pseudohyphal Sample 3. $N_y = 0.01$, $N_{dy} = 0.09$, $N_f = 0.02$, $N_{df} = 0.20$, $N_m = 0.68$ (sample size = 250)
- Figure 8.22** Distribution of volume for selected dilution rates for chemostat with 20g/L feed substrate concentration: (a) 0.12 h^{-1} (b) 0.20 h^{-1} (c) 0.3 h^{-1} (d) 0.4 h^{-1} (e) 0.49 h^{-1}
- Figure 8.23** Distribution of volume for selected dilution rates for chemostat with 5g/L feed substrate concentration: (a) 0.10 h^{-1} (b) 0.20 h^{-1} (c) 0.3 h^{-1} (d) 0.4 h^{-1} (e) 0.47 h^{-1}
- Figure 8.24** Distribution of volume for selected time points for whey media batch culture fermentation at 800rpm 1vvm (a) 2.5 h (b) 4.5 h (c) 6.5 h (d) 8.5 h
- Figure 8.25** Distribution of volume for selected time points rates for YEPL media batch culture fermentation at 200rpm 1vvm (a) 2.5 h (b) 4.5 h (c) 6.5 h (d) 8.5 h
- Figure 9.1** Example of pseudohyphal coding system employed in the study of *K. marxianus* pseudohyphae.

- Figure 9.2** The initiation of pseudohyphal formation with the lead subunit budding a long thin subunit
- Figure 9.3** The development of the second bud from the lead subunit
- Figure 9.4** New bud formation at the tip of branch 1 and on subunit 2 in the main hypha
- Figure 9.5** Development of third bud from lead subunit
- Figure 9.6** Development of a second bud on the first branch concurrent with the development of a third bud on the second subunit on main hyphae
- Figure 9.7** Unusual morphological structure in “old” pseudohyphae
- Figure 9.8** Diagrammatic representation of pseudohyphal development for *K. marxianus*
- Figure 9.9** Lengths of subunits in main hyphae (5g/L feed, $D = 0.4\text{h}^{-1}$). Additional graph demonstrates the standard deviations on the values obtained for six subunits in the main hypha.
- Figure 9.10** Development of subunits in main hyphae with respect to main hyphal length development of subunit two, (b) development of subunit three. (20g/L, $D = 0.4\text{h}^{-1}$)
- Figure 9.11** Relationship between the length of mother and daughter subunits. Solid line – parity plot. Dashed Line - linear regression ($r^2 = 0.38$)
- Figure 9.12** The relationship between the fully grown length of the first and second progeny of a subunit. Solid Line –parity plot, dashed Line - linear regression ($r^2 = 0.46$)
- Figure 9.13** Extension of branches from lead subunit (1.0); Unfilled symbols, first branch; filled symbols second branch; dashed line - parity plot (20g/L $D = 0.4\text{h}^{-1}$)
- Figure 9.14** Extension rate differences between branches generated from first and second subunit on main hyphae. (20g/L $D = 0.2\text{h}^{-1}$)
- Figure 9.15** Effect of dilution rate and substrate feed concentration on the structure of pseudohyphae (a) 5g/L substrate feed concentration, (b)

10g/L substrate feed concentration, (c) 15 g/L substrate feed concentration, (d) 20 g/L feed concentration.

Figure 9.16 The effect of agitation on the structural characteristics of pseudohyphae ($D = 0.2 \text{ h}^{-1}$)

Figure 9.17 Branching pattern analysis for various subunits under different agitation conditions (a) pseudohyphae with three subunits in main hyphae, (b) pseudohyphae with four subunits in main hyphae (c) pseudohyphae with five subunits in main hyphae ($D = 0.2 \text{ h}^{-1}$)

Figure 9.18 The effect of agitation on the mean subunit lengths of subunits within pseudohyphae of various chain lengths.

Figure 9.19 The effect of dilution rate and substrate feed rate on the mean subunit length of subunits within pseudohyphae of various chain lengths (a) 5g/L substrate feed concentration, (b) 10g/L substrate feed concentration, (c) 15g/L substrate feed concentration, (d) 5g/L substrate feed concentration.

Figure 10.1 Overview of possible morphological pathways based on experimental observations

LIST OF TABLES

Table 3.1	YEPD medium formulation
Table 3.2	10L Micogen Fermenter Configuration
Table 3.3	2 L Life Sciences Fermenter Configuration
Table 4.1	Operating conditions used to obtain samples of varying morphology
Table 5.1	Morphologies displayed by <i>K. marxianus</i> var <i>marxianus</i> NRRLy2415. Classification and volume estimation
Table 5.2	Filters for preliminary cell classification
Table 5.3	Classification of single and double cells
Table 5.4	Classification of filaments/unbranched mycelia (in Image H)
Table 5.5	Comparison of mean width (μm) of 20 manually measured mycelia with the mean width of the same 20 mycelia measured by program MEASURE
Table 5.6	Classification of segmentation errors made by algorithm (t=12h)
Table 5.7	Effect of sample size on cell categorisation (based on cell numbers)
Table 5.8	Time taken to perform the individual stages of the image analysis algorithm (t=12h)
Table 6.1	Constants used in model
Table 6.2	Constants required to calculate the residual substrate curves
Table 6.3	The effect of agitation on $k_L a$ in 10L batch whey fermentations
Table 8.1	Origins of samples used for population model development
Table 8.2	Summary of classification breakdown for single cells for Samples 1 and 2
Table 8.3	Summary of classification breakdown for double cells for Samples 1 and 2
Table 9.1	Relative extension rates of subunits post budding (5g/L feed, $D = 0.4\text{h}^{-1}$)

Table 9.2 Classification (numerical fraction) data for samples used in Figure 9.16

ABBREVIATIONS

AMP	Adenosine monophosphate
ATP	Adenosine triphosphate
BOD	Biochemical oxygen demand
CSTR	Continuous stirred tank reactor
DEY	Double elongated yeast
DF	Double filament
DNS	3,5-dinitrosalicylic acid
DY	Double yeast
EDTA	Ethylenediamine tetraacetic acid
EY	Elongated yeast
F	Filament
GA	Gibberellic acid
GUI	Graphical user interface
Hgu	Hyphal growth unit
M	Mycelium
NCYC	National Collection of Yeast Cultures
NRRL	National Regional Research Laboratories
psi	Pounds per square inch
RNA	Ribonucleic acid
Rpm	Revolutions per minute
SEM	Scanning electron microscopy
STR	Stirred tank reactor
TCA	Tricarboxylic acid
UDP	Uridine di phosphate
UV	Ultra Violet
VSC	Vesicle supply centre
vvm	Volumes/volume/minute
Y	Yeast
YEPD	Yeast Extract, Peptone, Dextrose
YEPL	Yeast Extract, Peptone, Lactose

CHAPTER 1

INTRODUCTION

Fungal morphology is of great interest both from a biological and biochemical engineering viewpoint. Biologically, it can reflect an organism's adaptation to stress, its pathogenic potential and can also be used in its identification. Within the realm of biochemical engineering, fungal morphology can influence fermentation broth rheology, nutrient mass transfer, productivity and product recovery (Oolman and Liu, 1991). Within any environment, two morphologies exist for any organism, microscopic and macroscopic. Microscopic morphology refers to the shape and size of a single organism whereas macroscopic morphology refers to the structure formed by the interaction of several of the above. For example, the microscopic morphology of a yeast is generally ovoid and budding whereas its macroscopic morphology can be unicellular or flocculent in liquid culture or as a colony on an agar plate, whose texture, shape or size can be used in the yeast's identification. Macroscopic morphology can be either strongly dependent on, or completely independent of, the microscopic morphology.

In microbiology, few more unusual observations can exist than that of fungal dimorphism. This phenomenon is referred to as "the process by which the mycelial habit of growth, with cells in hyphal or filamentous form, is transformed by some change in cultural or environmental conditions, so that a yeast-like or unicellular morphology is adopted at the cellular level." (San-Blas and San-Blas, 1984). Many pathogenic and industrially important fungi are known to be dimorphic and are so, for reasons of ecological advantage. From an engineering perspective, the alteration of microbial morphology in fermentation can have several deleterious effects on process performance making the assessment of such dimorphic switches in fermentations essential.

Currently, there is a strong trend towards quantifying microbial morphology in suspension cultures using image analysis (Thomas and Paul, 1996). Image analysis allows the quantitative extraction of information from images. Image analysis

provides more detailed information about microbial morphology than previous methodologies such as “Coulter” counting and is much faster than methods involving digitising tablets and manual measurements from photomicrographs (Adams and Thomas, 1988). As computing power has increased over the years, so has the complexity of the algorithms used for the quantification of morphology. Currently, researchers are generating images directly from the bioreactor using laser technology to allow the quantification of yeast morphology *in situ* (Suhr *et al.*, 1995); are examining the use of image analysis to quantify intracellular enzymatic reactions *in situ* using fluorescent techniques (Thomas, personal communication); and are training neural networks to recognise different cell morphologies (Guterman and Shabtai, 1996).

Kluyveromyces marxianus is an organism of great industrial importance. It produces a myriad of enzymes such as lactase (β -galactosidase) (Ku and Hang, 1992), inulinase (2,1 β -D-fructan fructanhydrolase), used in the degradation of inulin, a polymer of approximately 35 fructose molecules with a glucose molecule at the end, to a value added fructose syrup and invertase (Rouwenhorst *et al.*, 1990), and polygalacturonase (pectinases) (Schwan and Rose, 1994). The pectinases are a group of enzymes that degrade pectin-containing substances and are widely used in the food industry to improve the cloud stability of fruit and vegetable nectars (Harsa *et al.*, 1993). It also produces some primary metabolites, namely ethanol and glycerol, from a variety of industrial substrates, including cheese whey permeate and Jerusalem artichoke. Cheese whey contains lactose, a disaccharide of the reducing sugars, glucose and galactose. Whey is the primary by-product of the cheese-making industry, representing 80-90% of the volume of milk transformed and is composed primarily of water (94%), lactose (5%), proteins and salts. The high Biochemical Oxygen Demand (BOD) of whey (50g/L) makes it difficult to dispose of and it is generally used as a low-grade animal feed. The proteins are recovered using ultrafiltration but the resultant permeate still has a high BOD. Yeast fermentations can reduce the BOD of this permeate while simultaneously converting lactose to ethanol or glycerol. The fact that *Saccharomyces cerevisiae* does not possess the necessary enzymes for this fermentation makes *K. marxianus*

the obvious choice. In Ireland, a commercial process is in operation, which ferments cheese whey permeate to ethanol. The resultant alcohol is used in the liqueur industry.

K. marxianus has been reported as being dimorphic in suspension culture. Walker and O'Neill (1990) quantified the morphology of the organism in two forms, yeast-like and filamentous. They observed that the organism developed in filamentous form when grown under aerobic conditions and in yeast-like form when grown in anaerobic conditions. This was compared to the dimorphic fungus, *Mucor rouxii*, where the primary cause of morphological alteration is attributed to environmental change. Currently, some researchers are asserting that the term dimorphism is inadequate and that the terms polymorphism or pleomorphism are more suitable (Kerridge, 1993). Other workers are trying to improve the quantification of dimorphic suspension cultures (Bartnicki-Garcia and Gierz, 1993; Odds, 1993). The above suggests the inadequacy of a two class system in describing the morphology of such organisms.

The aim of the present work is to;

- 1) develop an hypothesis regarding yeast – mycelium dimorphism in fungi,
- 2) improve the classification system currently used for *K. marxianus*,
- 3) develop a fully automated image analysis algorithm to quantify the morphology of *K. marxianus*,
- 4) verify the findings of Walker and O'Neill (1990), that the presence or absence of oxygen is critical for the morphological transition of the organism,
- 5) assess the effect of changing morphology on the performance of the organism, grown on cheese whey permeate in both batch and continuous culture,
- 6) explain the development of the hyphal structure based on mathematical analysis.

CHAPTER 2

FUNGAL MORPHOLOGY AND ENVIRONMENT

2.1 INTRODUCTION

Several diverse microorganisms are classified within the broad group of protists called the fungi. However, they do share some typical features that distinguish them as fungi, from other microbes. These distinguishing features are based on the physiology and morphology of cells. The fungal cell is distinguished from the bacterial cell by its size (generally greater than 1-2 μm in diameter) and its eucaryotic structure is similar to that of plant and animal cells (having distinct membrane-bound organelles such as nuclei, mitochondria). Bacterial cells, which lack these organelles, are termed procaryotic. Fungal cells divide by mitosis (asexual reproduction) and by meiosis (sexual reproduction); bacterial cells divide by binary fission.

Like animals, the fungi are heterotrophic organisms that cannot manufacture their own food by photosynthesis, as plants and algae can. They require oxygen for growth (aerobic) and generally prefer an acidic environment (below pH 7) unlike the bacteria which are anaerobic and aerobic and generally grow in basic environments (at or above pH 7). Fungi utilise preformed organic material from other organisms as sources of energy and building blocks for their cellular synthesis. Soluble nutrients are absorbed from the growth substrate following the breakdown of complex polymers by extracellular enzymes (proteinases, cellulases, pectinases etc.) secreted by fungal cells.

The fungi have diverse morphologies especially in spore production, which is the basis for identification. But, they are commonly recognised as yeasts (single-celled thallus), moulds (filamentous thallus called a mycelium consisting of tubular cells in long, branched, thread-like structures called hyphae) and mushrooms (macroscopic fungi with considerable differentiation of tissues and hyphae in the mushroom, the sporulating portion of the thallus, which is fed by a massive underground mycelium). Fungi, like bacteria, are very susceptible to drying and,

are therefore generally found in very moist, if not aquatic habitats. They can resist desiccation by producing thick, melanised walls which are often seen in aerial spores, in hyphal strands, and in sclerotia that enable the fungus to survive sub-optimal growing conditions in the soil for several years. The fungal wall usually consists of layers of chitin, a linear polysaccharide polymer of N-acetylglucosamine, embedded in and often covered by glucans, branched polymers of glucose and other sugars. Some species of fungi in the Class Oomycetes such as *Phytophthora* and *Pythium* have walls predominantly of cellulose rather than chitin. The melanin components consist of branched polymers of phenolic material similar to the lignins of plant cell walls (Smith, 1975).

2.2 FUNGAL MORPHOLOGY IN SUSPENSION CULTURE

Suspension culture is not a natural environment for fungi, whose primary role is the surface colonisation and degradation of their preferred substrate. Certain fungi have high aerobic requirements but are also highly sensitive to shear. Supplying enough oxygen to a suspension culture typically requires vigorous mixing, thus generating a high shear environment. Certain morphological phenotypes are artefacts of their artificial environment and would never appear in such morphologies in their natural environment. This is particularly true of fungal pellets. Four morphological groupings can be identified within the fungal kingdom grown in submerged culture; free filamentous fungi, pelleted fungi, yeast and dimorphic fungi.

2.2.1 Unicellular Fungi (Yeast)

Yeast are defined as unicellular fungi that reproduce by budding and fission (Flegel, 1977). This is regarded, by Kreger-van Rij (1984), as the most precise definition currently available. Within yeast, three families are evident; the ascosporogeneous yeast, the basidosporogeneous yeast and the imperfect yeast. The imperfect yeast is a grouping for imperfect forms of ascosporogeneous and basidosporogeneous species.

Within yeast, morphology is one of the primary tools for species classification (Kreger-van Rij, 1984). Generally, yeast are regarded as ovoid and budding yet

often this is not the case. Many yeast morphologies are evident. The primary example of a morphological difference in yeast is dictated by their ability to reproduce. The processes of budding, and fission result in dramatically different morphologies for double cells. *S. cerevisiae* and *Schizosaccharomyces pombe* are examples of budding and fission yeast respectively. Other differences exist between strains and species but such differences generally involve changes in aspect ratio or volume. Little work has been done on the development of image analysis routines as a cost-effective method of inter-species differentiation.

There has been much interest in the relationship between morphological observations in yeast and physiological criteria such as growth rate and vitality of the cells present. Examples include the correlation of yeast cell growth rate with cell volume, a technique using a Coulter counter, validated using information taken from photomicrographs (Tyson *et al.*, 1979) and the examination of vacuolation in yeast populations as an indicator of vitality (Ohsumi *et al.*, 1993).

2.2.2 Filamentous Fungi

Filamentous fungi are of considerable importance in biotechnology, producing a diversity of hydrolytic enzymes, secondary metabolites and consumable biomass. They are cultivated extensively in bioreactors. The morphology displayed by filamentous fungi significantly alters bioreactor performance. This is due to rheological problems caused by high concentrations of fungal biomass in suspension culture. Fungal fermentation broths are generally power law in nature, displaying consistency indices as low as $n = 0.2$. Values in this range result in extremely heterogeneous mixing patterns, often resulting in stagnant regions close to the reactor wall (Olsvik and Kristiansen, 1994).

The terminology used to describe the development of fungal cells is as follows. Each individual fungal structure is termed a *hypha*. A culture of disperse hypha is termed a *mycelium*. A hypha can present itself as either *true hypha* or *pseudohypha*. True hyphae are made up of continuous cylinders segmented internally by *septa* whereas pseudohyphae are segmented by constrictions at

interfaces. True hyphae predominate among fungi which permanently remain in a filamentous form. Pseudohyphae are characteristic of dimorphic fungi. The total length of the hypha is described as the *total hyphal length* (L_t). Hyphae generally grow in an exponential manner by forming branches at almost regular intervals along the mycelium. Each actively growing end of the hypha extends at an almost linear rate and is known as a *tip*. Each hypha has a longest hyphal element known as the *effective hyphal length* (L_e). This particular length is important in quantifying the amount of time that the hypha has been in existence. The hypha develops exponentially, whereas the effective hyphal length develops linearly with respect to time, making it a more useful indicator of cell age. The hypha can be divided down into *hyphal growth units* (L_{hgu}), which defines the average length along mycelium between branches. This length proves quite consistent and is useful in evaluating the foraging power of a hyphal element. For example a low L_{hgu} suggests a dense tightly packed mycelium whereas a high L_{hgu} suggests a much looser structure with greater foraging power (Trinci, 1974).

2.2.3 Pelleted Fungi

Pellets are the macroscopic result of adverse environmental conditions on filamentous fungi. Many industrially important fungi are known to form pellets under specific environmental conditions. Examples of fungi that are capable of forming pellets in suspension culture include *Rhizopus oryzae* and *Penicillium chrysogenum*. Pellets are formed when the spores of certain fungi agglomerate with each other resulting in the formation of a complex matrix of mycelium which generate into a spherical object which can assume sizes on a scale of centimetres. As pellets are generally spherical, morphological alterations are generally related to diameter changes or to the texture of the pellet surface. Pellets are referred to as *hairy* or *smooth* depending on the amount of free mycelial growth protruding from the surface of what is known as the *core*, the dense region in the interior of the pellet. The growth of filamentous fungi in the form of pellets reduces or negates rheological problems but leads to other problems such as substrate limitation in the interior of larger pellets. This can result in the development of hollow regions,

caused by cell autolysis, in the interior of pellets resulting in a drop in volumetric productivity (Metz and Kossen, 1977).

2.2.4 Dimorphic Fungi

Dimorphic fungi are unusual in their ability to alter their morphology in response to changing environmental conditions. The morphological transitions exhibited generally involve the transformation of a typically filamentous organism to a yeast-like morphology or vice versa. The transition of yeast-like cells to a triangular morphology has also been reported (Sentheshanmuganathan and Nickerson, 1962^{a,b}). The morphology of dimorphic organisms is generally described using a combination of terms derived from yeast and filamentous fungal morphology. The only requirement for terminology specific to dimorphic fungi is when a hybrid morphology exists. A hypha growing directly from a yeast cell is called a *germ tube*. Dimorphic fungi will be discussed in greater detail in Section 2.6.

2.3 EFFECT OF BIOREACTOR ENVIRONMENT ON MORPHOLOGY

The environment within a bioreactor is composed of several elements. The system usually has three phases; solid (organism, insoluble substrate), liquid (medium) and gas (aeration). The interaction of all three phases and resultant mass transfer between each element can result in a myriad of complex environmental conditions. Mechanical shear and medium composition are crucial factors in the determination of the growth environment.

Cell morphology within the bioreactor can be altered by two methods:

- 1) the application of sufficient mechanical shear to the culture can result in physical damage to the cell structure resulting in a change in morphology,
- 2) changing environmental conditions can result in a change in cell physiology which subsequently leads to a change in morphology.

Often it is difficult to establish which of the above is occurring when the level of agitation is the variable.

2.3.1 Mechanical Shear

Typically, fungi are cultured in stirred tank reactors (STR) which are traditionally agitated by a set of Rushton turbines, named in recognition of J.H. Rushton and co-workers who carried out extensive research on mixing and agitators in the 1950s (Nienow, 1990). Agitation is supplied to suspension cultures to ensure good mass transfer and to prevent nutrient limitation. Agitation is also essential in the dispersion of gasses (predominantly oxygen). Reduction of bubble size dramatically increases the surface area for gas-liquid mass transfer. Due to the viscous nature and/or high oxygen consumption rate of many fungal fermentations, vigorous agitation has to be supplied and this can have deleterious effects on fungal morphology.

There are three regimes under which agitation can influence morphology:

- Agitation is poor enough to initiate mass transfer limitations in the environs of cells
- Agitation is adequate in providing good mass transfer to the cells in the broth
- Excessive agitation is mechanically damaging the cell/pellet causing cell rupture and the release of intracellular components.

Unfortunately, the three regimes are usually not mutually exclusive. Within a fungal fermentation containing large concentrations of biomass, usually two of the above regimes will exist. If agitation is too low, vital parameters such as heat, mass and oxygen transfer coefficients, will be insufficient in regions of low shear (near reactor walls) while being adequate in regions closer to the impeller, thus reducing productivity. Yet if the agitation is increased sufficiently to provide good mixing in the entirety of the bioreactor, the consequences may be mechanical damage to cells in regions of high shear, again reducing productivity. The process designer is left with a choice between partial oxygen limitation and high shear breakage, generally selecting whichever yields greater productivity.

2.3.1.1 Problems with experimental design

Much experimentation has been performed on the consequences of high agitation on morphology but often the experimental design has been poor. This is because of several reasons.

- The experimental methodology often involves culturing the cells at a specific impeller tip speed in chemostat culture, at a fixed dilution rate and assessing steady state morphology using computer-aided image analysis. While this may seem like the most ideal method of studying growth and morphology simultaneously, the underlying problem usually is whether the high concentration of biomass in the reactor is causing a rheological effect, nullifying any attempt to quantify observed phenomenon using conventional recirculation theory.
- Unsteady state methods of broth extraction from a bioreactor at steady state and its subsequent agitation in a separate vessel for short periods does not take account of the effect of starvation on cell morphology, although most of such experiments are of short duration.
- The effective hyphal length assessed by most researchers can often be a misleading parameter (fully explained in Section 9.8) and does not usually represent the true physiological length (to be defined later in Section 9.8) of the cell.

The ideal approach to assess the effect of agitation on morphology is to culture cells in suspensions containing excess dissolved oxygen and nutrients, avoiding the problem of poor mass transfer which, itself, can have deleterious effects on morphology. It is possible to culture cells in very low substrate concentrations, generating broths with low biomass and low (even Newtonian) apparent viscosity. In these cultures, where conventional mixing theory applies, the effect of agitation on cell morphology can be assessed without the need for cell starvation.

2.3.1.2 Breakage or acceleration of old age?

Consider a chemostat culture at steady state, containing a fixed number of hyphal elements. As feed is added, effluent is removed containing the same concentration of hyphal elements. As the culture is in steady state the rate of hyphal element removal has to be equal to the rate of hyphal breakage. With filamentous fungi, there is a natural progression from actively growing mycelial tips to vacuolated regions to dead regions (Paul *et al.*, 1994a). When experiencing sufficient mechanical shear, breakage will occur in dead regions in preference to younger regions, due to a greater degree of structural weakness. Paul *et al.* (1994b) suggested a similar hypothesis stating that mycelial breakage was both due to applied shear and microbial physiology. When excessive mechanical shear is applied, breakage will occur in actively growing regions. Evidence has shown an increasing presence of intracellular metabolites with increasing agitation (Reuss, 1988). Such metabolites should not be present in aging and dead regions of the hyphae, suggesting that a reduction of hyphal length in such cases is due to simple breakage.

2.3.1.3 How does agitation damage fungal hyphae?

The effect of agitation on particulate damage has been assessed in many biological and non-biological applications. Historically, it was thought that the size of a particle in a reactor was related to the power input per unit volume. However, van Suijdam and Metz (1981) suggested that this was untrue. By looking at complex phenomena such as the size and energy of turbulent eddies and energy dissipation rates, they identified key issues concerning the breakage of hyphae in stirred tank reactors. Hyphae can only break when local turbulent eddies are in the same scale as the dimensions of the organism. This typically only occurs in a region surrounding the impeller. As energy dissipates with respect to distance from the impeller, eddies get progressively larger and the scale is no longer correct for breakage. Therefore there exists a “breakage zone” surrounding each impeller and the probability of a cell breaking is proportional to the number of times the cell enters the zone. Breakage is related to parameters describing circulation time rather than those relating to power input. This finding has been validated by Smith *et al.*

(1990) who observed radically different morphologies in different size stirred tanks with the same power inputs per unit volume. This group adapted the work of van Suijdam and Metz (1981) and developed the following useful parameter, ε_c , for the correlation of *P. chrysogenum* hyphal fragment size with agitation intensity,

$$\varepsilon_c = \frac{P}{D_i^3} \frac{1}{t_c} \quad (2.1)$$

where P is the power input, D_i is impeller diameter and t_c is the circulation time. The energy dispersion zone is simulated using the P and D terms, while how often a cell enters the dispersion zone is related to the t_c term. Jüsten *et al.* (1996) demonstrated the usefulness of such an approach, by correlating mean total hyphal length and mean projected area (a measure of clumping) with an energy dissipation/circulation function, for a number of impeller geometries. Attempts were made to generate correlations based on power input, which proved unsuccessful.

2.3.1.4 Fungal adaption to agitation

Agitation in fermenters containing filamentous cells has been observed to significantly decrease hyphal lengths and alter productivity. Makagiansar *et al.* (1993) observed a decrease in mean effective hyphal length and in hyphal growth unit with increasing agitation speed for *P. chrysogenum*. The former reduction can be explained in terms of mechanical breakage whereas the latter can only be explained in terms of fungal adaption to environmental stress. It is possible that a denser branching pattern may protect the organism from the higher agitation environment. Other workers have observed this phenomena of a change from long sparsely branched hyphae to short, strongly branched hyphae upon increase of agitation intensity (Dion *et al.*, 1954; van Suijdam and Metz, 1981; Smith *et al.*, 1990).

2.3.1.5 Agitation and pelleted growth

Certain organisms will grow in pellet form if a low shear rate environment is provided. *Aspergillus niger*, a typically pelleted fungus, can be cultured in free filamentous form if sufficient agitation is supplied (Mitard and Riba, 1988). This applies for several other species that adopt pelleted growth in suspension culture. Other phenomena that occur under vigorous agitation include, the formation of “sclerotic pellets”, which are hollow with a toughened exterior, and the disintegration of existing pellets (Metz and Kossen, 1977). It can generally be stated that, as agitation intensity increases, the diameter of pellets will decrease (Nielsen *et al.*, 1995).

2.3.2 Other Environmental Effects

Environmental changes that do not involve the application of mechanical shear can only influence the morphology of the organism indirectly by changing the cell physiology. There are significantly fewer studies on morphology changes related to cell physiology than mechanical shear (Paul *et al.*, 1994^a). There are four factors that can influence the cell's morphology as a consequence of altering cell physiology; medium composition, dissolved oxygen tension, growth rate and growth in substrate limited chemostat.

Fungi, particularly filamentous fungi, can be very heterogeneous in nature, with different regions of the mycelium existing in different physiological states, ranging from new biomass to aged material. Autolysis of older cells can be a factor in the breakage of hyphae causing a general shortening of mean hyphal length. Righelato *et al.* (1968) studied the morphology of *P. chrysogenum* grown in continuous culture and observed considerable hyphal breakage when nutrients were supplied at the maintenance rate. This was related to an increase in hyphal vacuolation and degeneration. Paul *et al.* (1994^b) utilised image analysis to quantify the degree of vacuolation and observed a significant drop in hyphal length when hyphae were heavily vacuolated (at low growth rates).

When microorganisms are grown in a chemostat they evolve and become better adapted to the environment (Novick and Szilard, 1950). In chemostat cultures, neutral mutants (that neither have a selective advantage nor disadvantage when grown in competition with the parental strain) accumulate in the population at linear rates. Certain mutants develop that have a selective advantage over the parental strain, generally related to having a higher maximum specific growth rate (μ_m) or a lower k_s term (allowing the uptake of lower trace concentrations of substrate). Morphological mutants have been isolated from continuous cultures that have been highly branched compared to the parental strain (Trinci *et al.*, 1990). Withers *et al.* (1994) claim to be the first to have isolated a morphological mutant with a lower branching intensity than the parental strain of *Aspergillus oryzae*.

Changing gaseous environments in filamentous fermentations have resulted in some unusual morphological changes. *Aspergillus nidulans* was observed to alter morphologically when experiencing low dissolved oxygen concentrations. McIntyre and McNeil (1997) observed an increase in the effective hyphal length, mean branch length and mean hyphal growth unit length with increasing CO₂ concentration. This was accompanied by a decrease in citrate production. Large isodiametric cells were observed and the formation of free conidia occurred (Carter and Bull, 1971). Smith and Ho (1985) observed the formation of spherical or yeast-like cells when *P. chrysogenum* was cultured in high CO₂ partial pressures.

Other effects observed in fungal fermentations include the control of pelleted versus free filamentous growth in *P. chrysogenum* by the alteration of culture pH (Pirt and Callow, 1959). Furthermore, the length of hyphae varied considerably with pH. Joung and Blaskovitz (1985) observed that by altering the concentration of ammonium nitrate in their medium, three distinct morphologies could be achieved; a) vegetative hyphae, b) morphology comprising of fruiting bodies and hyphae and c) short, branched and bent hyphae with bulbous and horny masses. The second and third morphologies were found to overproduce citrate. Papagianni *et al.* (1994) also observed high levels of citric acid production in conjunction with shorter hyphae for the same organism.

2.4 BROTH RHEOLOGY

Rheological effects in reactor broths can be detrimental to bioreactor performance. The rheological characteristics of a fermentation fluid can directly affect the mixing behaviour, mass transfer and heat transfer, and can therefore have a profound influence not only on the course and outcome of a fermentation but also on the response of sensors used to monitor fermentation parameters on line. Such changes in broth rheology are generally attributed to morphological observations, yet significantly, no strong (universal for all organisms) correlations have been devised between any morphological parameter currently measured and rheological parameters. The following section describes the assessment of the rheology of fungal fermentation broths and the attempts to correlate morphological parameters with broth rheology.

2.4.1 Fluid Rheology

The Newtonian rheological model (2.2) describes a linear response of the shear rate (movement of the fluid) with respect to an applied shear stress.

$$\tau = \eta\dot{\gamma} \quad (2.2)$$

where τ represents the shear stress in the fluid, $\dot{\gamma}$ represents the resultant shear rate and η is the viscosity of the fluid. In many cases the above relationship does not hold. Fluids whose viscosities can not be described by the above relationship are known as non-Newtonian fluids. Most filamentous fungal broths display non-Newtonian characteristics. While many models exist to describe the rheological characteristics of non-Newtonian fluids most can be summarised by the following general relationship.

$$\tau = \tau_0 + k\dot{\gamma}^n \quad (2.3)$$

where n represents the power law index, τ_0 represents a yield stress (where an initial shear stress is required to result in fluid movement) and k is a constant. If $\tau_0 = 0$ then the model is power law where $n < 1$ represents pseudoplastic or shear thinning fluids, $n > 1$ represents dilatant or shear thickening fluids. The constant k under

such circumstances is known as the consistency index. If $\tau_0 > 0$ and $n=1$ then the equation is referred to as the Bingham model. The Bingham model suggests the presence of a yield stress, a finite shear stress required to induce fluid flow. The Casson equation is another example of a rheological model with a yield stress component. ($\tau^{0.5} = \tau_0^{0.5} + k_c \gamma^{0.5}$).

Herschel Bulkley ($\tau = \tau_0 + k\gamma^n$), imply that the solution of cells and culture broth does not behave like an ideal fluid. Any fluid that requires a finite stress to generate flow is not strictly a liquid. Many parties have debated the presence or absence of a yield stress in such fermentation broths. Allen and Robinson (1990) have suggested utilising physical methods to determine yield stress, such as those outlined by De Kee *et al.* (1980) and to compare the experimental values calculated for yield stress, to those extrapolated from rheograms.

2.4.2 The Consequence of Cell Morphology on Broth Rheology

The morphology of an organism is the description of the external form and structure of an organism. Equal volume fractions of yeast and fungal mycelial biomass can have clearly different rheological characteristics, yeast-like cell suspensions being Newtonian in nature up to 85% yeast volume fraction whereas mycelial fermentation broths can develop Non-Newtonian characteristics at less than 5% volume fraction (Reuss *et al.*, 1982). The fact that most cell free fermentation broths (bar those of cells secreting exopolysaccharides) have a Newtonian viscosity very close to that of water (1.0 mPa.s) suggests a strong role for cell morphology in broth rheology. The long, cylindrical and branched nature of the hyphal structure allows the interaction of such particles with each other hence aiding in the restriction of fluid flow, leading to stagnant fluid in regions of low shear. In regions of high shear, such interactions are easily dispersed, leading to well-mixed regions close to the impeller.

Many groups have investigated the effects of fungal morphology, primarily using image analysis methods. Attempts have been made to correlate the biomass concentration present with rheological parameters, but with the variety of

rheological parameters and morphological measurements used, it is difficult to make comparisons. The development of a unified approach to research and data analysis must occur before any progress can be made in achieving such correlations. Reuss *et al.* (1982) demonstrated the ability of all models discussed previously (Power law, Casson and Herschel-Bulkley) to describe *P. chrysogenum* fermentation broth data assessed using a turbine viscometer over a decade of shear rate ranges. However, the extrapolated curves on either side of the measured data deviate significantly from each other. It was also suggested that the inconsistency of much published experimental data lies within the measurement approach, placing particular blame on the use of standard rotational viscometers. This finding is in disagreement with Charles (1978) who indicated that the viscosities measured remained within 5% of the original viscosity for over two minutes of continuous monitoring for a 10g/L *A. niger* culture broth. The problem possibly lies in the inconsistency of organism and strain used for experimentation rather than the apparatus. Secondly, a standardisation of the rheological model used to fit the experimental data is necessary. The use of the Herschel-Bulkley equation seems most appropriate as it contains both variable yield stress and power law index terms, thereby allowing the rheological description of all fluid types. The problem with such an approach is the quality and quantity (both in terms of data point density and range of experimental shear rate, typically three orders of magnitude are required) of data required to solve for the many constants in the equation. If all data was treated in this manner, then comparative analysis may become a possibility.

It is however, still possible to draw important conclusions from research completed in this area. Firstly, for dispersed filamentous cultures the rheology of the suspension is dependent on individual hyphal characteristics, as suggested by Roels *et al.* (1974). In fact, Metz *et al.* (1979) suggested the following relationship to correlate gross morphological data with broth rheology.

$$\tau_0 = 1.67 \times 10^{-4} C_m^{2.5} L_e^{0.8} \quad (2.4)$$

$$K_c = 5.454 \times C_m^{1.0} L_{\text{hgu}}^{0.6} \quad (2.5)$$

τ_0 is the Casson yield stress, K_c the Casson constant and C_m the biomass concentration.

The use of L_e and L_{hgu} suggests a role for both overall length and branching intensity in rheological response.

Other groups believe that the characteristics of the individual hyphae are irrelevant and more detailed attention should be paid to aggregate characteristics. Fatile (1985) was the first to attempt to correlate measured aggregate characteristics with respect to the Power law parameters. His correlations relied on both biomass concentration and the equivalent circular diameter of the aggregates. This work was followed by a more detailed study by Tucker and Thomas (1993) who used the aggregate parameters, “fullness” and “roughness”, along with biomass to correlate morphology with rheological parameters.

In conclusion, if the study of the rheology of filamentous fermentations is to develop, certain key issues need to be addressed. A set of consistent protocols need to be established for researchers, incorporating viscometers of choice, range of measurements and rheological model to be used. There is a lack of standardisation in the above parameters. Furthermore, there has to be a realisation that the material being examined is biological and that cell-cell interactions are generally surface based. While the morphology of the organism is important in the interaction of surfaces, the overall “stickyness” is controlled by cell wall biochemistry.

2.5 FUNGAL DIMORPHISM

Dimorphism in micro-organisms is a well documented phenomenon with many occurrences to be found in both the fungal and bacterial kingdoms. It is defined as

"The process by which the mycelial habit of growth, with cells in hyphal or filamentous form, is transformed by some change in cultural or environmental conditions, so that a yeast-like or unicellular morphology is adopted at the cellular level." (San-Blas and San-Blas, 1984).

The term "dimorphic" is defined as "existing or occurring in two distinct forms" (Oxford English Dictionary, 3rd edition). In microbial dimorphism however, many intermediate forms are usually present. Currently, authors are stating that the term dimorphism is inadequate and that polymorphism or pleomorphism are more suitable (Kerridge, 1993). Following the discovery of dimorphism in the yeast-like fungus *Mucor* by Berkeley in 1838 and Bail in 1857 much curiosity was aroused in researchers. Earlier work was directed along two paths, firstly, the possible use of fungal dimorphism as a model for eucaryotic cell differentiation and secondly, establishing the reason for the high occurrence of this phenomenon in clinically important fungi. The latter has dominated dimorphism research since the above discovery. Recently, emphasis has been placed on possible optimisation of economically important fermentations based on the organism's morphological characteristics (Hill and Robinson, 1988; Walker and O'Neill, 1990).

2.5.1 Morphologies Exhibited by Dimorphic Organisms

If a yeast reproduces exclusively by budding the mature bud may either detach itself immediately or remain attached to the mother cell and eventually give rise to either clusters or chains of cells, resulting in the formation of *pseudohyphae*. Evans and Richardson (1989) defined pseudohyphae as "fragile chains of cells (usually yeast, which have arisen by budding and have elongated without detaching from adjacent cells), with morphological characteristics intermediate between a chain of

yeast cells and a hypha". Five different pseudomycelium structures have been observed and illustrated by Langerton and Talice (1932).

Although yeast do not reproduce by the exclusive formation of hyphae, numerous taxa will form true septate branching hyphae under suitable conditions. True hyphae proliferate by continuous growth of the hyphal tip followed by the formation of septa. Three distinct phases of yeast morphology have been described above. These phases, however, can be accompanied by intermediate morphologies. Wickerham (1951) applied three criteria to differentiate between pseudohyphae and true hyphae, basing observations on the terminal cells of the hyphae. Primarily, true hyphae have refractive, straight septa whereas pseudohyphae have not. Pseudohyphal forms show only a small percentage of cells separated by septa. Secondly, the terminal cell of true hyphae is usually considerably longer than its predecessor whereas in pseudohyphae the terminal cell is shorter. Pseudohyphae terminal cells are rarely longer than the adjacent cell. Thirdly, true hyphae show little or no constriction at the septa or where the septum will be formed whereas in pseudomycelium constriction is evident.

The term filament is used to describe an abnormally long cell and generally a pseudohypha is composed of a chain of filaments (the term filament is usually used in the description of bacteria). Any terms specific to a flora of microbes not covered in the above review will be explained as required. A more detailed review of the topic is given by Kreger-van Rij (1984).

2.5.2 Sub Classification of Dimorphic Organisms

Many different causes for dimorphism are presented in the literature and there appears to be much confusion over the unifying cause of the phenomenon. This confusion can be related to the broad range of species that are dimorphic. If dimorphic organisms are sub-classified into suitable groupings then more common trends can be identified. Two main groupings can be immediately seen, (1) the yeast-like fungi and (2) yeast. The yeast-like fungi are classified as fungi whose primary morphological form is filamentous (Scherr and Weaver, 1953). Such

organisms typically revert to yeast-like morphology when certain environmental stresses are applied. With yeast, the converse applies, as yeast are defined as unicellular fungi that reproduce by budding or fission (Flegel, 1977). This breakdown is therefore based on the dominant morphology of the organism in question.

Yeast-like fungi can be sub-classified into pathogenic and non-pathogenic. Pathogenic yeast-like fungi that display dimorphism (*Blastomyces dermatitidis*, *B. brasiliensis*, *Histoplasma capsulatum*, *Sporotrichum schenckii*, *Coccidioides immitis*) typically all change from the mycelial or saprophytic form to the yeast-like or parasitic form by elevation of incubation temperature from 30°C to 37°C (Deacon, 1984). This is known as thermal dimorphism and is believed to be of ecological advantage to the organisms in question. Dimorphic, yeast-like, parasitic fungi are known as the only fungi that cause deep-seated mycoses in both humans and animals. It is thought that a transition from a mycelial to a yeast-like morphology allows the organism motility within the blood stream and therefore allows it to establish colonies within the body. Parasitic fungi that do not possess the ability to make this transition are restricted to surface infections. Another factor that helps this transition is a higher pCO₂ (not in all cases). The 37°C and higher pCO₂ both indicate conditions present in humans and animals.

2.5.3 Pathogenic Yeast-Like Fungi

Blastomyces dermatitidis is the agent of North American blastomycoses (Gilchrist's disease) and *B. brasiliensis* is the agent of South American blastomycoses (Lutz's disease). Both organisms have a similar mycelial morphology but differ slightly in their parasitic morphology. At room temperature they exhibit a regular septate mycelium; *in vivo* they appear as spherical yeast bounded by a thick-walled membrane (Mariat, 1969). It was demonstrated by Hamburger (1907) that the growth temperature of *B. dermatitidis* had a major influence on its morphology. It was later established by Levine and Ordal (1946), that no matter what the medium composition was, temperature was the sole factor dictating transitions in morphology for the organism. The optimum temperatures for the growth of the

mycelial and yeast phases were 33°C and 37°C respectively. The phrase "thermal dimorphism" was coined to describe this reversible phenomenon (Nickerson and Edwards, 1949). They also showed that the oxygen consumption of the yeast phase was five to six times that of the mycelial phase.

H. capsulatum is present in soil and causes histoplasmosis or Darling's disease, a systemic mycosis characterised by the presence of small yeast in the cells of the reticulo-endothelial system. As with *B. dermatitidis*, its mycelial phase occurs at room temperature with the yeast-like phase occurring *in vivo* at 37°C. A temperature of 37°C is generally required for a mycelium to yeast conversion although with medium containing certain compounds, lower temperatures are equally effective. The compounds found favourable for the growth of the yeast phase include, Zn^{2+} , Mg^{2+} , glucose, citric and α -keto glucaric acids, cystine, cysteine and methionine; and a mixture of glutamic acid, aspartic acid and cysteine. As is the case of some of the previous examples, the effects of CO_2 , sulphhydryl groups and chelating agents all positively affect the mycelium to yeast conversion. (Mariat, 1969; Gupta and Howard, 1971).

As with the two previous yeast-like parasitic fungi, the *Sporotrichum schenckii* yeast-like phase occurs *in vivo*, is parasitic and requires a temperature of 37°C for a mycelium to yeast-like conversion. With this organism, a higher pCO_2 appears to promote the conversion from mycelium to yeast-like at the above temperature. Physiological studies have suggested that both the nucleic acid composition and respiratory metabolism of both phases differ to a large extent (Mariat, 1969).

Coccidioides immitis is the agent of an important mycosis limited to certain geographical regions. *In vitro* this organism has branched septate filaments, whereas *in vivo*, the fungus has a round structure bounded by a thick wall. This spherule contains developing round endospores, which when developed, are released by a rupture of the membrane. Temperature seems to be a determining factor in the development of the spherule, 34-35°C appears to be optimum, but with

low inocula, the presence of 10% pCO₂ appears to prevent mycelium formation. (Lones and Peacock, 1960; Brooks and Northey, 1963; Mariat, 1969).

2.5.4. Non-Pathogenic Yeast-Like Fungi

There are a small number of non-pathogenic, dimorphic, yeast-like fungi described in the literature, *Mucor* sp. and *Aureobasidium pullulans*, which are well documented for their dimorphic behaviour. Both present unusual and unrelated reasons for their dimorphic behaviour. Several *Mucor* species are characterised by their dimorphism. On a historical note, *Mucor* sp. was the first organism observed to exhibit mould-yeast dimorphism; Bail (1857) concluded that the yeast-like form of *Mucor Rouxii* was *Hormiscium cerevisiae* (a former name for *S. cerevisiae*) and that this organism and *Mucor* were developmental stages of the same fungus. Pasteur later rejected this concept of species transmutation and later demonstrated the importance of oxygen in the control of mould-yeast dimorphism in *Mucor* (Pasteur, 1876). *Mucor* presents a myriad of causes for its dimorphism including atmospheric alterations, hexose source and concentration, presence of chelating agents (EDTA) and concentration cyclic AMP.

Several conflicting reports have been published on the environmental conditions governing the dimorphism phenomenon, all relating to the atmospheric environment in which the cells were grown. The three basic parameters, relating dimorphism to environment, were anaerobiosis, CO₂, and the acidity caused by high pCO₂. Bartnicki-Garcia and Nickerson (1962a) established that both carbon dioxide and oxygen controlled dimorphism. Carbon dioxide was found to induce yeast-like growth, oxygen was found to have the converse effect. Under an inert atmosphere (nitrogen) the organism grew in filamentous form. By increasing the pCO₂ of this environment a gradual shift to yeast-like morphology occurred. The introduction of air even at low pO₂ levels nullified this effect. The effect of CO₂ was due to dissolved CO₂ and not to HCO₃⁻ (Bartnicki-Garcia and Nickerson, 1962b). Haidle and Stork (1966) verified the above conclusions using cytochrome oxidase analysis techniques. It was found that by exposing cells to air, the morphology of the organism changed to filamentous and the rate of cytochrome

oxidase synthesis increased simultaneously. Cytochrome oxidase synthesis is a strong indicator of a switch from oxido-reductive to oxidative metabolism. Using mitochondrial inhibitors, they interrupted the production of cytochrome oxidase and found a concomitant reversion to yeast-like morphology. They also found that another compound that caused morphological reversion (phenethyl alcohol) had no effect on cytochrome oxidase levels, demonstrating that the absence of cytochrome oxidase was not required for yeast-like growth. Furthermore they showed that under pure N₂ conditions (i.e. without any traces of O₂) the yeast-like form prevailed. This answered the last question regarding dimorphism in *Mucor*. It showed that under completely O₂ deprived conditions, the yeast-like form will dominate and that the dimorphism phenomenon in *Mucor* is respiratory based.

Bartnicki-Garcia (1968) also disclosed that under anaerobic conditions, the hexose source and concentration had a considerable effect on the morphology of *Mucor rouxii*. Glucose was the most effective hexose for eliciting yeast-like growth, followed in order by fructose, mannose and galactose. At 100% pCO₂, the effects were dramatic, with pure yeast-like or mycelial cultures developing, according to the glucose concentration present. At 30% pCO₂, the effect was less dramatic with high glucose concentrations only causing mixtures of mycelium and yeast. Inderlied and Sypherd (1978) also examined this hexose phenomenon and reasoned that the need for CO₂ and hexose in the maintenance of the yeast-like form of *Mucor racemosus* was related to the high flux of carbon through the glycolytic and pentose phosphate pathways of the organism while in yeast-like form. This observation was not noted for the mycelial form.

The effects of certain chemicals on the morphology of *Mucor* have also been observed. At concentrations increasingly inhibitory to growth, chelating agents of the N-acetic acid type, such as EDTA, progressively nullified the morphogenetic effect of CO₂, and cultures reverted to the filamentous form of development. Both the inhibition of growth and the morphogenetic effects were impeded by adding transition-group metal ions. This indicates that the effect of these compounds was

due to metal chelation and it was thought that in particular, zinc was the cause of the inhibition (Bartnicki-Garcia and Nickerson, 1962b).

A. pullulans is a non pathogenic yeast-like fungus which synthesises the α -glucan, pullulan. The organism has a complex life cycle exhibiting a variety of forms ranging from yeast-like cells through multicellular filaments to chlamydo spores. Interest in the morphology of this organism developed when it became clear that synthesis of the polysaccharide pullulan was affected by the amounts of either morphology present (Catley, 1980). It was also noticed that the generation of the polysaccharide was at an optimum concurrent with the formation of blastospores and that the nitrogen source present influenced this phenomenon. It was noted by Ono *et al.* (1977) that changing initial pH altered the production of pullulan. When the pH was lowered from 6.0 to 2.5, production of the polysaccharide fell dramatically. It was then noted that the morphology of both cultures was different, the pH 6.0 culture contained a far greater level of yeast cells than the pH 2.5 culture. They stated that morphological appearance indicates the ability to produce pullulan. This result was also observed by Heald and Kristiansen (1985) who concluded that it was possible that the yeast-like form of the organism was the primary producer of the polysaccharide. In the first Continuous Stirred Tank Reactor (CSTR) studies, McNeil *et al.* (1989) demonstrated that the specific productivity of the yeast-like phase drops sharply with increasing pH and that the optimum rate of pullulan production is found in cultures containing 50% yeast. This work replaced the concept of a producing and non-producing morphology and suggested a relationship between morphology and productivity. Many studies have linked nutritional limitations with morphology changes in the organism. Cooper and Gadd (1984) showed that the use of yeast extract induced yeast to mycelium transitions, the same effect being achieved by the addition of adenosine (Cooper *et al.*, 1985). In fact, Reeslev *et al.* (1991) who studied the effect of pH and yeast extract on the morphology of the organism, concluded that variations in both pH and yeast extract levels on the morphology of the organism were significant. They demonstrated that significant differences existed in the morphology of the organism grown at different pH values (3.5 and 6.5) when yeast extract was absent from the

medium. They found a greater percentage of yeast-like biomass at the higher pH. This difference was not observed when the concentration of yeast extract was increased to 4g/L. They concluded that limitation of a component in yeast extract was responsible for the morphological transition, however, the magnitude of the morphological transition was dependent on the pH of the culture. Reeslev and Jensen (1995) demonstrated that this mycelium to yeast transition was due to Zn^{2+} and Fe^{3+} limitation. They observed that the concentration of yeast extract (0.4 g/L) utilised in previous studies caused limitation of the above metals and suggested the utilisation of a higher concentration of yeast extract (4g/L) for improved growth and biomass production. For the production of pullulan, limitation of Zn^{2+} was found to be superior to limitation of Fe^{3+} . Limitation of Zn^{2+} also resulted in a greater quantity of yeast biomass.

From a biochemical engineering perspective, the changing morphology of *A. pullulans* has been seen to affect both reactor performance and downstream processing. Due to the production of a viscous polysaccharide and a changing morphology, *A. pullulans* fermentations present a complex rheological problem (McNeill and Harvey, 1993). It has been observed that fermentation broths with the highest concentrations of pullulan often have the lowest apparent viscosity (McNeil and Kristiansen, 1987). This result is due to the “pullulan producing” form of the organism being predominantly yeast-like, thus contributing little to the overall viscosity of the broth, whereas non-producing fermentations are predominantly filamentous and consequently pseudoplastic. The morphology distribution of the cells in the broth was seen to affect the performance of cross-flow membrane filtration systems (Yamasaki *et al.*, 1993a, 1993b). The specific resistance of the microbial cake was lowered dramatically when the yeast-like population was predominant. *A. pullulans* was also the centre of an interesting study on the use of neural network classification of cell morphology (Guterman and Shabtai, 1996).

2.5.5. Dimorphic True Yeast

The dimorphic, true yeast include *S. cerevisiae*, *Hansenula anomola*, *Saccharomycopsis fibulgera* and the organism used in the present work, *K. marxianus*. Imperfect, dimorphic yeast include *Candida albicans* and *T. varibilis*.

A number of common trends are evident. Firstly, dimorphism in *S. cerevisiae* seems to be caused by substrate limitation in continuous culture (Kuriyama and Slaughter, 1995). It was found that cells elongated considerably and exhibited filamentous and pseudomycelial morphology at intermediate dilution rates where glucose concentration was believed to be at its lowest (Hill and Robinson, 1988). Limitation of both glucose and nitrogen have been related to this change. Morphological alterations due to nitrogen have been explained by Brown and Hough (1965). Under nitrogen limiting conditions, elongated cells predominated and a decrease in the amount of sulphhydryl groupings in the sulphhydryl-disulphide balance occurs which consequently affects morphology (Nickerson and Falcone, 1956).

Yanagishima (1963) found that a cytoplasmic mutant strain of *S. cerevisiae*, deficient in aerobic respiration and under the influence of 10-20 mg/mL, indwell-3-acetic acid and α -naphthaleneacetic acid, exhibited cell elongation, while acetic acid had no such effect. An antiauxin, 2, 4, 6-trichlorophenoxyacetic acid, completely reversed the affect of the auxin. This effect was observed before any significant cell multiplication occurred. A similarity to the effects noted with the shoots of higher plants was observed. Cell length increased while cell width remained unchanged and the effect was antagonised by the addition of an antiauxin. In a later paper (Yanagishima, 1964), it was demonstrated that even with respiration sufficient cells, under ordinary cultural conditions, the cell elongation effect of auxin can be shown if the auxin is accompanied by gibberellic acid (GA). Since GA seems to make cells susceptible to the auxin action, it was assumed that some cellular substance responsible for the auxin action is produced by the effect of GA. After treating extracts from the GA treated cells with RNase, removing the RNase and reapplying the extracts to cells treated with auxin no elongation was noted, whereas

the extracts not treated with RNase showed considerable elongation. It was then suggested that the active substance produced by GA was in fact RNA. It is also possible that the substance was a protein coded for by the RNA in question and promoted by GA.

Gimeno *et al.* (1993) studied pseudohyphal growth of *S. cerevisiae* on solid medium and suggested that pseudohyphae may be vectors to deliver assimilative yeast cells to regions with plentiful nutrients, suggesting that pseudohyphae behave as foraging cells in times of environmental stress:

They identified the following key requirements for pseudohyphal growth.

- 1) Cell shape changes – cells could not change from one morphological form to another, but rather generated progeny whose morphology was different from the parent cell, suggesting that a cell has to be manufactured in a particular morphology and cannot change, once formed, from one morphology to another. This is similar to both the germ-tube formation (Odds, 1988) and clear opaque transitions (Bergen *et al.*, 1988) in *C. albicans*.
- 2) Nitrogen starvation or growth on a poorly assimilated form of nitrogen for example proline - this observation was made after cells grown on solid medium containing low amounts of ammonium sulphate or proline as the nitrogen source, initiated pseudohyphal growth. This also agrees with the work of Brown and Hough (1965) and Hill and Robinson (1988)
- 3) Unipolar cell division – to develop true pseudohyphae, unipolar growth is essential, in order to ensure that the cell develops away from substrate limited regions. This is genetically controlled in *S. cerevisiae*. The mating type locus programmes cell type specific budding patterns probably by regulating budding pattern genes and consequently controlling pseudohyphal growth as this requires the diploid budding pattern.

4) Invasiveness – pseudohyphae penetrated the surrounding agar. This was attributed to two possible factors, the pressure exerted by the tip of a pseudohypha is greater than that exerted by budding yeast thus initiating penetration, or the secretion of hydrolytic enzymes may assist in the penetration of the agar.

Lipke *et al.* (1976) found that by exposing the yeast to a sex pheromone produced by mating-type α cells, considerable elongation and enlargement of cells occurred. It was also shown that the cells in question contained more glucan and less mannan in their walls than the control cells.

Sundhagul and Hendrick (1966) demonstrated that by growing *Hansenula schneegii*, correctly known as *Hansenula anomala* var. *schneegii*, (Kreger-van Rij, 1984) in tryptophan-glucose medium, considerable elongation and pseudomycelium formation occurred. Tryptophan was the only amino acid to cause this elongation. When the cells were grown in the above medium along with the addition of other amino acids yeast-like growth predominated. It was found that there was 2.5 times as much mannan in the elongated cell walls than in the yeast cell walls. This transition was reversed when proline was added to the culture medium. On examination of the biomass curves for this experiment, it can be seen that tryptophan is a vastly inferior nitrogen source than ammonium sulphate. It can be hypothesised, in this case, that nitrogen is limiting, causing the observed elongation. *Saccharomyces fibulgera* has been reported as being dimorphic and again the nitrogen source is of great importance. Experimental results also point towards the above conclusion. Complex medium yielded 6.48 g/L biomass (yeast-like). All other nitrogen sources (except methionine) yielded approximately 1 g/L biomass, which was again yeast-like. Methionine on the other hand yielded an intermediate amount of biomass (3.46 g/L) plus extensive pseudo-hyphal growth. This result displays the effect of nitrogen on morphology and has strong implications for this work as well.

S. fibulgera, an organism used extensively for the production of biomass from starchy wastes and for amylase production, has been shown to be dimorphic by Nécas and Svoboda (1981). During growth on complex medium, mycelial biomass and yeast-like blastospores can be produced. Upon the introduction of defined medium it was found that methionine was required for vigorous growth and pseudomycelium production. As sulphur is implicated in the control of dimorphism in *C. albicans*, it was thought that cysteine would also affect the morphology of the organism in a manner similar to methionine. This proved not to be the case and hence it was assumed that methionine was essential for transmethylation reactions such as in the methylation of homocysteine, nucleic acids, steroids and phospholipids.

K. marxianus has been studied in the past also (Walker and O'Neill, 1990). The results indicated that oxygen had a major contribution in the morphological alterations of the organism. The present work will reveal that the above finding was erroneous and demonstrates an example of the dangers of comparing completely dissimilar organisms (*i.e. Mucor*) for dimorphic criteria. This will be discussed in some detail in Chapter 7.

Moser and Kung (1986) demonstrated the potential of exploiting a dimorphic organism as a biological test system to assess bioreactor performance. They utilised the dimorphic, strictly aerobic (*sic*) yeast, *Trichosporon cutaneum* in their fermentation studies and observed that by changing the orientation of the fermenter from vertical to horizontal, completely different end point morphologies were observed.

2.5.6. Dimorphic Imperfect Yeast

Imperfect yeast, *Candida albicans* and *Trigonopsis varibilis* are the only reported dimorphic organisms in their class. In fact it has been stated that

“Few fields of biological science based on so simple an observation, can have generated such a confused and contradictory literature as that of dimorphism in *Candida albicans*” (Odds, 1988).

Candida is a pathogen, but unlike all other dimorphic pathogens, its morphological transition is not exclusively regulated by temperature. In fact, *Candida* occurs as both yeast and mycelia in both the saprobic and pathogenic states. As with the previous organisms discussed, the ability of *Candida* to form hyphae is thought to be an important virulence factor (Soll, 1991) but evidence is not conclusive for this organism. The molecular basis for the switch is not understood. Factors affecting the transition in morphology include pH, temperature, and the presence of amino acids and carbohydrates.

Trigonopsis varibilis does not follow the traditional yeast-like mycelium transition but instead has an ellipsoidal-triangular transition. Again, Methionine is related to the transition (Sentheshanmuganathan and Nickerson, 1962^b). The transition is also initiated using a combination of choline and inositol in the presence of ammonium sulphate. This indicates a strong link between phospholipid synthesis and dimorphism in this organism.

2.6 A MECHANISM FOR DIMORPHISM IN YEAST

A hypothesis for the dimorphic growth of many organisms is presented below. This is strongly based on the review of San-Blas and San-Blas (1984), the work of Shepherd and Gopal (1993) who deal with the nature and growth of cell wall biosynthesis, Bartnicki-Garcia and Gierz (1993) who discuss modelling of the development of cell shape and the studies of Nécas and Svoboda (1981) on protoplast regeneration in the well-studied *S. cerevisiae*.

2.6.1 Cell Wall Composition and Significance in Morphology

The cell wall is the primary determinant of cell shape (Sentandreu *et al.*, 1993). When protoplasts (wall free cells) were formed with yeast and mycelial forms of dimorphic organisms, all protoplasts were spherical and cells remained spherical as new wall developed (Svoboda and Nécas, 1974). Therefore, a change in either cell wall composition or structure is necessary for a change in morphology and it is also apparent that the environment in which the wall develops is critical for cell morphology. The cell wall of *C. albicans* (typical for other fungal cells) makes up about 30% of the total weight of the cell and a number of studies have shown that it is composed of glucans (60-80%), mannoproteins (20-30%), chitin (0.6-2.7%), protein (5-15%) and lipid (2-5%) (Chattaway *et al.*, 1968). Glucans can be further broken down into β -1,3 (25-35%) and β -1,6 (35-45%) linked glucans. Two lines of evidence indicate that the β -glucans impart the structural strength. Firstly, osmotically sensitive cells are generated after degradation of whole yeast cells with a purified β -1,3-glucanase (Gopal *et al.*, 1984^a) and secondly, it has been shown that with *C. albicans*, protoplasts regenerated in a simple medium give osmotically-resistant cells that have not incorporated mannoprotein in the wall (Gopal *et al.*, 1984^b). If cell morphology is to be altered, therefore, the structural component (*i.e.* glucans) has to be changed either in structure or method of deposition.

Mannoproteins are composed of both a carbohydrate and a protein portion. The major portion is an α -1,6 linked polymannose (mannose - a hexose closely related to glucose). This is joined to a protein via a chitobiose bridge and asparagine. Mannoproteins have been linked to virulence in *C. albicans*.

It is known that the cell wall also contains a number of enzymes including N-acetyl glucosaminidase, acid phosphatase, proteinase, glucanase and chitinase.

2.6.2 Cell Wall Development

The importance of the cell wall in dictating the morphology of the fungal cell has been stressed to date. The concept of altered methods of wall formation leading to

differing end morphologies will now be addressed. Cell wall formation can be divided into two stages, primary and secondary wall development.

In primary wall development, cell wall precursors are assembled in the endoplasmic reticulum and are dispensed to the cell wall in vesicles (Moor, 1967). These vesicles contain new material for the plasma membrane as well as membrane bound enzymes, soluble enzymes, highly-processed mannoproteins and perhaps a number of cell wall polymer primers. These vesicles are guided to the point of growth along actin fibrils and at the plasma membrane there is an accumulation of this new wall material from the vesicle into the plasma membrane. After fusion of the vesicles with the plasma membrane, the mannoproteins are released into the cell wall. Chitin and glucan are synthesised by transmembrane enzymes catalysing the vectorial synthesis of these polymers with the precursors UDP N-acetylglucosamine and UDP (uridine di phosphate) - glucose inside the cell and the products are extruded through into the wall. The insertion of materials into the existing wall is facilitated by localised glucanases that allow clipping and insertion of new material into glucan strands. The operation and control of these enzymes is not well understood.

A secondary phase of wall development is also known to exist - particularly in the subapical regions of the developing hyphae. This involves a cross-linking of the polysaccharides already present in the cell wall. This is thought to be mediated by localised glucanases that clip the glucan molecules and allow new polymer to be inserted and also a branching enzyme located in the cell wall. The rate of growth and the final morphology are clearly regulated by both temporal and spatial control of enzymes and involve the delivery of appropriate polymers to the relevant position in the wall. Nombela *et al.* (1992) hypothesised that the regulation of these glucanases point towards a role in cellular morphogenesis. Staebell and Soll (1985) demonstrated for *C. albicans* that the resultant shape of the cell was completely controlled by the ratio of apical to secondary growth. They observed that 70% of the budding cell's expansion was achieved by apical growth and the remaining 30% was achieved by general expansion after apical growth had ceased at approximately

two thirds of the cell's final volume. For germ-tubes, less than 10% of cell growth was attributed to general surface expansion with the remainder coming from continuous apical expansion. This whole process of cell wall development and morphogenesis has been simulated using a mathematical equation known as the hyphoid equation (Bartnicki-Garcia and Gierz, 1991).

$$y = x \cot \left(\frac{xR_{\text{vsc}}}{N_v} \right) \quad (2.6)$$

The hyphoid equation provides a mathematical foundation for the cellular basis for dimorphism. Its parameters, N_v and R_{vsc} , define two morphogenetically important parameters: the amount of wall building vesicles produced per unit time and the rate of advance of a theoretical entity the Vesicle Supply Centre (VSC) (x and y are geometric coordinates) (Girbardt, 1957). The VSC has been observed in higher fungi as an organelle known as the Spitzenkörper found in the growing tips of hyphae and, in lower order fungi, accumulations of vesicles have been found using electron microscopy near where the theoretical VSC would lie for both yeast (Moor, 1967) and filamentous fungi (Grove and Bracker, 1978). High values of this $R_{\text{vsc}} : N_v$ ratio led to the development of hyphae; low values led to a yeast-like morphology. The assumptions of the model are as follows. All vesicles originate from a point source known as the VSC, and vesicles can travel in any direction in the cell. The movement of the VSC was found to control morphology completely. If the VSC is held stationary while vesicles are released, then a spherical cell is produced; if the VSC is advanced continuously, then a hyphal tube is produced. It was found that, by pulsing the advance of the VSC, budding yeast cells could be simulated. By lengthening the pulse, pseudohyphae could be created. The ability of this simple model to predict the varied morphologies exhibited by dimorphic fungi suggests a simple mechanism behind dimorphism, which lies inherently in the formation of wall structure.

If secondary wall formation follows closely behind the cell's apex, then this will restrict the lateral extension of the cell wall in regions close to the apex, forcing the

cell to project outwards in a cylindrical fashion. If secondary wall formation is slow, this will allow the insertion of cell wall components more evenly over the entire cell surface, leading to the formation of more ovoid cells.

2.6.3 Cell Division

The hypotheses by which cell elongation can occur have been outlined, but such hypotheses do not take into account the lack of cell division that often occurs concurrently with cell elongation. The life cycle of the haploid phase of *S. cerevisiae* has been well studied and an overview of this life cycle, with particular emphasis on cell division will be presented here.

The initial stages of bud formation involve a weakening of the cell wall caused by the action of lytic enzymes that attack polysaccharides in the cell wall. The bud is formed when new cell wall material is laid down at the site of bud initiation. As the bud becomes larger, the deposition of new material becomes localised in the tip of the bud. When the bud becomes full sized then a complex septum is laid down in the neck of the bud which contains chitin as well as glucan and mannan. The biosynthesis of chitin, which is found in the bud scar and represents one of the layers of the dividing wall formed during bud formation, has been studied. The enzyme responsible for chitin synthesis has been found to be present in the plasmalemma as a zymogen, an inactive form of the enzyme. The formation of active chitin synthase is achieved by the action of an activation protein. This occurs by proteolytic cleavage of the zymogen. The activation protein is restricted to the neck of the bud, preventing widespread chitin synthesis. An inhibitor of the activator protein ensures this (Berry, 1982). Chitin seems to have a consequential effect on cell morphology in *C. albicans* as higher concentrations of chitin have been found in mycelial forms of the cell along with higher concentrations of chitin synthase. This may be explained by differences in cycle times of chitin synthesis in conjunction with differences in inhibitor activity. This may allow a more uniform degree of chitin synthesis throughout the cell rather than at the mother-bud junction, causing a failure of cells to separate. This also concurs with the suggestion that dimorphism is not caused by quantitative changes in the synthesis of any cell

division cycle component but rather by an alteration in the timing of cell division events. It has been shown for *C. albicans*, that no difference between protein synthesis in yeast-like and mycelial forms of the organism was observed, and that the filament ring found at the mother bud junction in budded forms appears 30 minutes later and 2 μ m further down the evaginated tube in mycelial forms.

2.7 SUMMARY

For monomorphic organisms, the primary controller of morphology is agitation or mechanical shear. Mechanical damage can result in hyphal fragmentation and pellet disintegration. Adaptions to agitation include the intensifying of the branching process in free filaments and sclerotic pellet formation. Mechanical shear has been correlated to hyphal or pellet disruption in terms of an energy dissipation/circulation function.

The consequences of other environmental parameters on morphology are either poorly investigated or are categorised as dimorphism. The effect of medium composition on morphology has been poorly investigated and could result in beneficial morphological effects such as the reduction of viscosity.

The major deleterious consequence of filamentous fungal morphology is that of increased broth viscosity. The rheological properties of filamentous fermentation broths are non-Newtonian, typically being described by the power law rheological model. At sufficiently high biomass concentrations, a yield stress has been observed by certain authors. This means that the fluid requires the application of a finite shear stress before fluid motion will occur. This fluid property results in unmixed regions in the bioreactor. The morphology of fungi has been related to the rheological characteristics of the fermentation with little success. This is probably due to the use of different rheological models and viscometers.

Both the cause and mechanism of dimorphism in fungi are complex phenomena. Dimorphism primarily appears to be caused by changes in the growth environment of the organisms in question and, in many cases, such morphological transitions in

response to environmental changes have been shown to be advantageous to the organism. For example, the mycelial - yeast transition in pathogenic yeast-like fungi allows greater motility and penetration into the host. Several experiments examining the effect of single medium components on morphology often do not address the effect of changing concentrations on physiology.

The cell cycle of yeast cells is a complex series of biochemical events, each contributing to the final morphology of the cell. The process can be described in two stages, cell enlargement and cell separation. Cell enlargement can be divided into two processes, the primary enlargement that predominantly occurs in the apical region of the bud and secondary enlargement which occurs over the entire surface of the bud and is mediated by glucanases that clip the existing polymer and allows new polymer to be inserted. The process of cell enlargement has been modelled using the hyphoid equation. The two primary parameters in this equation are (1) the movement of a theoretical entity, known as the vesicle supply centre (VSC), represented in higher fungi as an object known as the Sptizenkörper, and possibly representing the endoplasmic reticulum in yeast, and (2) the rate of supply of vesicles (packages of wall building materials) from the VSC. It was found that by controlling the rate of movement of the vesicle supply centre, the morphology of the organism could be altered to any morphological form observed.

Cell division is also impaired by yeast - mycelial transitions. The cell division mechanism in yeast is based on the establishment of a chitin septum between the mother and daughter cell. This septum is established using a complex series of enzymatic steps. A higher concentration of chitin in mycelial cells of *C. albicans* has been observed, along with a higher concentration of chitin synthase suggesting a defective septum establishment pathway.

Current theories on dimorphism suggest that transitions in morphology are not caused by quantitative changes in the production of cell division cycle proteins but is rather a change in the timing of different cellular events that control cell division. The timing of such events are thus altered by external environmental changes.

CHAPTER 3

MATERIALS AND EXPERIMENTAL METHODS

3.1 ORGANISM

The organism used for all studies was *Kluyvromyces marxianus* var. *marxianus* (formerly *fragilis*) NRRLy2415 (Northern Regional Research Laboratories, Peoria, IL). This organism is also recognised as NCYC1425 (National Collection of Yeast Cultures, England).

3.2 AUTOCLAVING PROCEDURE

All media, both solid and liquid, were sterilised by autoclaving at 121°C (15 psig) for 15 minutes in a Tomy SS-325 autoclave (Tomy Seiko Co., Ltd., Japan).

3.3 MEDIA PREPARATION

3.3.1 YEPD Medium

YEPD medium contained the components listed in Table 3.1, resuspended in deionised water.

Table 3.1. YEPD medium formulation

Constituent	Manufacturer	Concentration (g/L)
Yeast extract	Oxoid	10
Bacteriological peptone	Oxoid	20
glucose monohydrate	BDH	20

3.3.2 YEPD Medium (Solid)

As in Table 3.1, along with the addition of 30g/L Oxoid (Basingstoke, England) Technical Agar No. 3.

3.3.3 YEPL Medium

As in Table 3.1 but with the replacement of glucose monohydrate by 20g/L of lactose monohydrate (BDH, Poole, England).

3.3.4 Whey-Based Medium

Whey based medium was prepared by ultrafiltering 1kg whey powder (Avonmore plc, Kilkenny, Ireland) in 35L deionised water in a Romicon PM40 hollow fibre ultrafiltration unit (Romicon Inc. Woburn, MA). This yielded a permeate with a lactose concentration of approximately 20g/L. The permeate was subsequently supplemented with 10g/L yeast extract and 5g/L ammonium sulphate (BDH) to ensure adequate supplies of inorganic nitrogen and trace elements. The resultant medium was diluted accordingly to generate media of various lactose concentrations and the pH was adjusted to 4.5 using concentrated HCl (BDH).

3.4 CULTURING ON SOLID MEDIUM

The organism was maintained on solid YEPD agar plates. Subculturing was done on a monthly basis to ensure viable cultures. A loopful of cells from a single colony was taken from a stock plate and streaked on a fresh YEPD plate. Plates were incubated at 30°C for 24 hours and thereafter stored at 4°C.

3.5 SHAKE FLASK CULTURES

All starter cultures for both batch and continuous fermentations were grown in 1L Erlenmeyer flasks containing 400mL YEPL medium. A loopful of cells from a single colony was transferred to the flask and the flask was incubated at 30°C on an orbital shaker (200 rpm) for 24 hours.

3.6 10L “MICOGEN” FERMENTER (BATCH CULTURE)

The Micogen fermenter (New Brunswick Scientific, USA) had two primary advantages over other culturing systems available. Firstly, the fermenter was autoclavable *in situ* and secondly, due to the large culture volume, repetitive samples could be taken without significantly reducing the culture volume. A dissolved oxygen probe (Mettler Toledo, Switzerland) was also available for this fermenter.

3.6.1 Fermenter Configuration

The fermenter used was a 16L stainless steel vessel (10L working capacity) with numerous access ports at different levels in the fermenter. It contained a self-sterilising sampling port at the base of the fermenter. Agitation was supplied from a belt driven stainless steel shaft on which three Rushton turbine impellers were mounted. Aeration was supplied using a nozzle sparger on the base of the fermenter. For a detailed description of the fermenter configuration see Table 3.2.

Table 3.2 10L Micogen Fermenter Configuration

Measurement	Quantity
Tank diameter (D_T)	220 mm
Tank depth	500 mm
Impeller diameter (D_i)	70mm
Number of impellers	3
Blades per impeller	6
Dimensions of blade	20mm x 20mm
Interimpeller distance	100 mm
Sparger to 1 st impeller	70 mm

3.6.2 Fermenter Setup

The fermenter was initially cleaned thoroughly and rinsed with deionised water. The pre-prepared medium was then added through one of the ports on top of the fermenter. The dissolved oxygen probe was inserted into another of the top ports. The vessel was sealed by uniform tightening of the bolts on the head plate. Agitation was set at 400rpm to improve heat transfer. The vessel was autoclaved *in situ* by passing steam at 20psi through the baffles in the tank. Once the vessel temperature was greater than 105°C, steam was injected into the media, as no steam condensation occurred in the vessel under pressure. Once the vessel reached 121°C, it was held at this temperature for 25 minutes due to the large volume of the media it contained. Once the cycle was complete, the steam supply was terminated and the vessel was cooled by passing water through the fermenter baffles. As the

vessel temperature decreased towards 100°C the pressure in the vessel had to be prevented from falling below atmospheric pressure. This was achieved by sparging with air. A working pressure of 5psig was maintained in the bioreactor from this point onwards.

3.6.3 Fermenter Operation

Once the vessel had been stabilised at the cultivation temperature, the vessel pressure was dropped momentarily to allow removal of one of the top ports for inoculation. Inoculation was completed aseptically using a blowtorch to sterilise the area around the port and the neck of the Erlenmeyer flask. The contents of the flask were poured rapidly into the fermenter and the vessel was quickly resealed and a working pressure of 5psig re-established.

Agitation was controlled using a potentiometer, which regulated motor speed between 0 and 1200 rpm. Vessel temperature was controlled using a heating element which heated, when necessary, water passing through the baffles. All fermentations were maintained at 30°C. Aeration was provided from a central compressor via a regulator at 20 psi. The supply to the vessel was regulated by a rotameter mounted on the front of the fermenter control panel. Air sterilisation was achieved by a 0.22µm Dominick Hunter (Durham, UK) air filter. The filter was steam sterilised *in situ*. Aeration was supplied at 10L/min (1VVM) for all batch fermentations.

Sampling was achieved via a port at the base of the vessel that allowed for inter-sample sterilisation. Samples were forced out of the vessel due to the positive pressure within.

3.7 2L “LIFE SCIENCES” FERMENTER (CHEMOSTAT)

Due to the large working volume (V) in the Micogen fermenter it would have been impractical to operate this fermenter in chemostat mode due to the substantial quantity of feed substrate (F) required daily. Thus a smaller vessel had to be used for this purpose.

$$D = \frac{F}{V} \quad (3.1)$$

where D is dilution rate (h^{-1})

3.7.1 Fermenter Configuration

The bioreactor (Life Sciences Laboratories, Luton, U.K.) was fabricated in borosilicate glass mounted in a stainless steel collar supported on a three membered frame and base ring. The vessel had a hemispherical base and was surrounded by an external jacket to allow for heat transfer. The vessel had eleven ports on the head plate. During continuous culturing, ports were used for the following; feed addition, effluent removal, air addition, off gas outlet with condenser, antifoam addition and inoculum addition. The vessel was agitated using a top driven stainless steel shaft mounted with two Rushton turbine impellers. During trials, the fermenter was aerated with a nozzle sparger but this was found to be ineffective after operating periods of approximately one week due to blockage by biomass. The nozzle was removed and the fermenter was subsequently aerated by open pipe aeration. For a schematic of the fermenter see Figure 3.1. For measured parameters see Table 3.3.

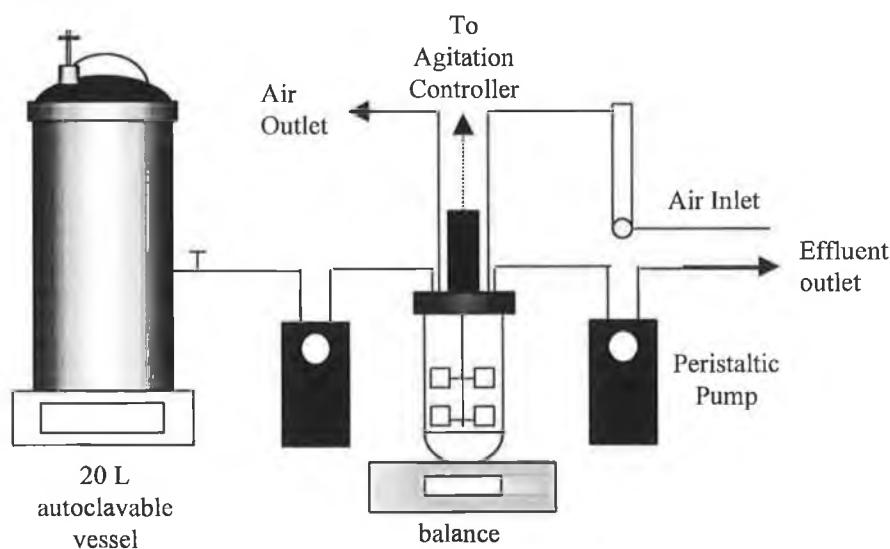


Figure 3.1 Fermenter configuration for chemostat operation

Table 3.3 2 L Life Sciences Fermenter Configuration

Measurement	Quantity
Tank diameter (D_T)	110 mm
Tank depth	230 mm
Impeller diameter (D_i)	55mm
Number of impellers	2
Blades per impeller	6
Dimensions of blade	10mm x 10mm
Interimpeller distance	70 mm
Sparger to 1 st impeller	20 mm

3.7.2 Fermenter Setup

As the fermenter was being operated in chemostat mode, certain additional requirements were necessary for fermenter set-up. Firstly, the bioreactor required a means of maintaining constant volume. The effluent was removed using a weir system, set at a height that allowed the working volume of the bioreactor to remain at 1L. The volume in the fermenter was monitored by a balance placed underneath the bioreactor. Secondly, the aseptic addition of sterile feed media was required. In trial runs, two 5L interchangeable vessels were used with a working volume of 4L. The small operational time per vessel and frequent contamination of the fermenter forced a change to a larger container. The container used was a modified autoclave (Dixons Surgical Instruments Ltd, Sheffield, England) which had a maximum autoclavable volume of approximately 20L. A feed line ran from a port in the side of the autoclave to the fermenter, which was closed during autoclaving. A sterile air filter (Millipore Millex 0.22 μ m) was placed on a port on top of the autoclave to allow the vessel compensate for the loss of media volume during feeding. Pumping of both feed medium and effluent was achieved using Watson Marlow peristaltic pumps (Cornwall, England) through silicone tubing. The inlet pump was calibrated prior to use, using similar grade silicon tubing (5mm internal diameter). A pump setting was chosen, the pump primed and the output volume was collected for a fixed time interval. Thus pump setting was related to feed rate.

The outlet pump setting was set to ensure the required steady state volume in the bioreactor.

3.7.3 Fermenter Operation

Agitation in the fermenter was set using a potentiometer on the front of the fermenter controller. Agitation was maintained at 800RPM for all chemostat culturing. Temperature was regulated at 30°C by circulating water through the jacket from a heating-cooling water bath (B. Braun, Buckinghamshire, U.K.). Aeration was supplied from a fish pump regulated by a rotameter (Platon) (2 L/min maximum air throughput). Air sterilisation was achieved using in line autoclavable Millipore Millex (Molsheim, France) 0.22µm air filters. Aeration was maintained at 1L/min (1VVM) for all chemostat culturing. Organic antifoam (Sigma, St. Louis, Missouri) was added manually through a septum port on top of the vessel using a sterile syringe and needle.

The primary problem with chemostat culturing was the identification of steady state in the bioreactor. Steady state was defined as the point when both morphology and kinetic parameters cease to change with respect to time. It was apparent from trials that the organism morphology was the parameter that took longest to reach steady state. It was found that the simplest assessment of morphological steady state was achieved using viscosity measurements. Once the viscosity of the exit stream was observed to reach a constant value, the culture was deemed to be in morphological steady state. This technique was verified using image analysis data. The fermenter typically reached steady state after a throughput of 3-4 L of medium.

3.8 DETERMINATION OF FERMENTATION PARAMETERS

3.8.1 Sugar Concentration

All reducing sugar concentrations were determined using a minor modification of the dinitrosalicylic acid method of Miller (1959). A 0.5 mL quantity of suitably diluted sample was added to 1.5 mL of DNS Reagent. The solution was boiled for 10 minutes and rapidly cooled by the addition of 5mL deionised water. The optical

density of the resultant solution was read at 540nm on a uv/vis spectrometer (Pye Unicam) and values were read off a standard curve. DNS Reagent was composed of 1.0g 3,5-dinitrosalicylic acid (Aldrich Chemical Co.) and 1.6g NaOH (BDH) dissolved in 100mL of deionised water. The assay was found to be linear from 0.0-1.5g/L glucose and galactose and from 0.0-3.0 g/L lactose. This method was validated using kit assays (Boheringer Mannheim GmbH, Mannheim, Germany) for glucose, lactose and galactose. The ability of the assay to quantify equimolar solutions of glucose, lactose and galactose was established allowing the preparation of a single standard (i.e. glucose) for all reducing sugars to be quantified.

3.8.2 Ethanol Concentration

Ethanol concentration was determined using a Carla Erba HRGC S300 Mega Series gas chromatograph (Carla Erba Strumentazione, Milan, Italy) with flame ionisation detection. The column was packed with 5% carbowax 20M on chromosorb WAW 80/100 mesh. Injector and detector temperatures were set at 170°C with a column temperature of 120°C. Carrier gas flowrate through the column was approximately 15 mL/min. A 1µL quantity of cell free sample was applied to the top of the column using an Exmire 10µL microsyringe (Ito Corporation, Fuji, Japan). Ethanol concentration was determined from peak heights obtained on a Linseis L6512 chart recorder.

3.8.3 Cell Enumeration

Cell enumeration was performed using a Improved Neubauer bright-line haemocytometer (Brand GmbH, Hamburg, Germany). Samples were suitably diluted in deionised water in order to perform counts. Cells were counted as single units irregardless of subunit number or size. This allowed the counts to be used in conjunction with image analysis data.

3.8.4 Cell Dry Weight

Cell dry weight was determined using the following protocol. Whatman (Kent, U.K.) No. 1 filter papers (70mm diameter) were predried overnight at 105°C. These were quickly removed from the oven and weighed on an analytical balance

when required. A predetermined quantity of culture fluid was passed through the filter in a Buchner funnel apparatus. The resultant supernatant was refiltered through the filter paper to ensure the removal of all cells. The filter cake was then washed with 100mL of deionised water to remove any soluble media components, which would add to the cake mass. The paper was then returned to the oven and dried overnight. The difference in filter weight was converted to cell dry weight in grams per litre.

3.8.5 Viscosity of Cell Suspensions

Viscosity of cell suspensions were used as a measure of steady state in the chemostat bioreactor. Viscosities were determined on two Brookfield digital viscometers, a cone and plate viscometer (model DV-1+), and a bob and cup viscometer (model DV-2+), (Brookfield Engineering Laboratories, MA, USA). The cone and plate viscometer had a shear rate range of 0-750 s⁻¹, the bob and cup viscometer had a shear rate range of 0-122.4 s⁻¹. Due to the pseudoplastic nature of some of the broths, viscosities were measured at many shear rates on both machines for a variety of samples. On analysis of the results it was found that the problems exhibited by such viscometers for other fungi such as entrapment of the fungi in the small interstitial space between the cone and plate thus causing higher viscosity readings or the settling of fungi due to the laminar flow regime of the bob and cup viscometer did not occur with this organism. The data generated from both viscometers overlapped well and no time dependent effect was found for either viscometer. All samples viscosities were read at 25°C. The cone and plate had an operational volume of 0.5mL. The bob and cup viscometer had an operational volume of 16mL. The constants of the power law model were determined from the following equation

$$\tau = k\gamma^n \quad (3.2)$$

Where τ is the shear stress and γ is the shear rate. By taking the log of both sides

$$\ln \tau = n \ln \gamma + \ln k \quad (3.3)$$

By plotting the $\ln \tau$ versus $\ln \gamma$ the slope is equal to the power law index, n , the intercept equals k , the power law constant.

3.8.6 pH

Sample pH was determined using a WTW (Weilheim, Germany) Microprocessor Precision-pH/mV-Meter meter. Supernatant generated from the dry weight procedure was used in preference to cell containing samples.

3.8.7 Cell Dry Matter per Unit Cell Volume (δ)

Two methods were employed for the assessment of this parameter. The first was based on data generated from image analysis where

$$\delta = \frac{X}{n\bar{V}} \quad (3.4)$$

X Cell dry mass concentration (g/L)

n Cell count (cells/L)

\bar{V} Mean cell volume determined using image analysis (cm^3)

The second method used to determine the volume fraction of cells in the culture was based on a method used to calculate the interstitial water in a cell pellet as suggested by Ju and Ho (1988). A fixed volume of culture was centrifuged in a Heraeus Labofuge 400 centrifuge at 3500 rpm (2383 g) for 10 minutes. The supernatant was discarded and the pellet washed by resuspending with deionised water. This was recentrifuged and the wash was discarded. The resultant pellet was weighed and the volume of the pellet was determined using the hypothesis that the pellet density is close to water thus the volume of the pellet is equal to the mass. The pellet was resuspended in 2mL of filtered 10% w/v dextran and the solution was recentrifuged. The dextran is diluted by the interstitial water in the pellet but does not interact with the cells due to its high molecular weight. The

volume of water in the pellet is thus calculated by measuring the difference in concentration between the solution added before and the solution obtained post centrifugation.

$$\delta = \frac{X}{M_p(1-\varepsilon)} \quad (3.5)$$

M_p Mass of cell pellet

ε Pellet voidage

3.8.8 Fermenter $k_L a$

The rate of change of oxygen concentration in a sterile fermentation broth with respect to time can be determined using the following equation.

$$\frac{dC_L}{dt} = k_L a (C_L^* - C_L) \quad (3.6)$$

Where C_L is the concentration of oxygen in the liquid phase, C_L^* is the concentration of oxygen in the liquid phase at 100% saturation and $k_L a$ is the volumetric oxygen mass transfer coefficient.

On rearrangement of the above,

$$\int_{C_{L_0}}^{C_{L_t}} \frac{dC_L}{C_L^* - C_L} = \int_0^t k_L a dt \quad (3.7)$$

Where C_{L_0} is the oxygen concentration at time 0 and C_{L_t} is the oxygen concentration at time t.

Integration yields,

$$\ln \frac{C_L^* - C_{L,n}}{C_L^* - C_{L,i}} = k_L a t \quad (3.8)$$

By plotting the left hand side of the equation versus time (s), the slope of the line equals the $k_L a$ (s^{-1}).

Experiments were performed on autoclaved whey medium. The medium was degassed by sparging with oxygen free nitrogen (Air Products) until an oxygen saturation close to zero was obtained. The nitrogen flow was stopped and the air supply initiated at 1vvm. The change in saturation was recorded at 5-second intervals until the medium was close to saturation. The results obtained were processed on Sigmaplot™ graphing and data processing package (Jandel Scientific, Erkrath, Germany) and the above plots were generated (Doran, 1995).

CHAPTER 4

INITIAL MORPHOLOGICAL OBSERVATIONS AND DEVELOPMENT OF A MORPHOLOGICAL CLASSIFICATION SYSTEM

4.1 INTRODUCTION

It is currently accepted that the term dimorphism is inadequate to morphologically describe organisms that fit within this frame of examination (Kerridge, 1993). It is suggested that terms such as “polymorphism” or “plaeomorphism” should replace the term dimorphism. Both of these terms suggest the presence of more than two classifications (i.e. yeast and filamentous) within organisms displaying dimorphism. Walker and O’Neill (1990) examined the morphology of *Kluyveromyces marxianus* var. *marxianus* NRRLy2415 under various environmental conditions, and while a diversity of morphologies were observed, the authors retained the traditional two class approach. This often resulted in plots showing a constant 100% yeast like or 100% filamentous cells over the timecourse of the fermentations. A larger number of classes imparts a greater amount of information to the observer. It may be argued that classification systems are redundant while the organism predominantly occupies only one morphological form. One consequence of increasing the number of classifications is the introduction of a greater degree of subjectivity in the classification system. Whatever classification system is used has to be one of sufficient flexibility as to allow adequate description of the morphology, yet be easy to implement and unaffected by operator variation.

The aim of this initial investigation is to uncover the diversity of morphology displayed by *Kluyveromyces marxianus* var. *marxianus* NRRLy2415. This is to be achieved by varying the environmental conditions experienced by the organism. Once the range of morphological variation has been established, a classification system can be designed that truly describes the morphology of the organism. This system will allow the development of an image analysis protocol that will assist in the classification of the organism.

4.2 MORPHOLOGICAL VARIATION IN *Kluyveromyces marxianus*

As stated in section 4.1 the following examples of morphology have been achieved by varying environmental parameters such as agitation rate in batch culture and substrate feed concentration and dilution rate in continuous cultures. Many different culturing conditions were examined, many of which will be discussed subsequently in the following sections, but for the purpose of brevity only those examples that demonstrate significant changes in morphology will be exhibited. All examples are of *K. marxianus* cultured in suspension. Table 4.1 lists the environmental conditions experienced by the examples shown.

Figure 4.1 shows, what could only be described as, a population of budding yeast. By simple observation it is apparent that the population can be broken into single and double cells. Hence the first two observed classes, namely "Yeast" and "Double Yeast".

Table 4.1 Operating conditions used to obtain samples of varying morphology

Figure Number	Fermenter	Medium	Operation Mode	Volume	Agitation	Aeration
Figure 4.1	10 L Micogen	2% Whey Medium	Batch	10 L	800 RPM	1 vvm
Figure 4.2	1 L Life Sciences	2% Whey Medium	Continuous	1 L	800 RPM	1vvm
Figure 4.3	10 L Micogen	2% YEPL Medium	Batch	10 L	300 RPM	1 vvm



(a)



(b)

Figure 4.1 Fermentation sample displaying predominantly yeast-like morphology. (a) Sample magnification at 200x, (b) Sample magnification at 400x, bars = 20 μ m.

Figure 4.2 presents an example of the hyphal form of the organism. This population is composed of long, thin, branched pseudohyphae, which in themselves are composed of filamentous-like cells. Cells of this nature will be termed “pseudohyphae” and make up the third class to be observed.



Figure 4.2 Example of pseudohyphal cells taken from chemostat culture. sample magnification at 200x, bar = 20 μ m.

The classes, yeast and pseudohyphae, represent the extremes of dimorphism. However, many intermediate forms were observed between the two described morphologies. Figure 4.3 shows such an example. As can be seen certain yeast-like cells have become more elongated in appearance and certain other cells are more filamentous in nature. Hence the choice of four new classes. The class “elongated yeast” describe cells that, in appearance, are yeastlike, but have elongated considerably in the major axis. Often this appears to be accompanied by a decrease in the yeast cell width. The cells are still ellipsoid in appearance. As these cells are present as both single and double forms the classifications are extended to include “Double elongated yeast”.



(a)



(b)

Figure 4.3 Example of intermediate cells taken from batch culture. (a) sample magnification at 200x (b) sample magnification at 400x, bars = 20 μ m.

Also present in the culture (Figure 4.3) are cells of a distinctly different phenotype. The cells appear cigar shaped (cylindrical with hemispherical ends) and are present either singly or in doubles. This generated the further classifications of “filaments” and “double filaments”. It is thought, on initial observation, that the filamentous forms are the precursors to pseudohyphae. Figure 4.4 shows good examples of different classes identified in culturing in suspension culture. It is apparent from the examination of many other cultures, grown under a diversity of environmental conditions that the morphology of each of the cultures was described adequately by the seven classes illustrated in Figure 4.4.

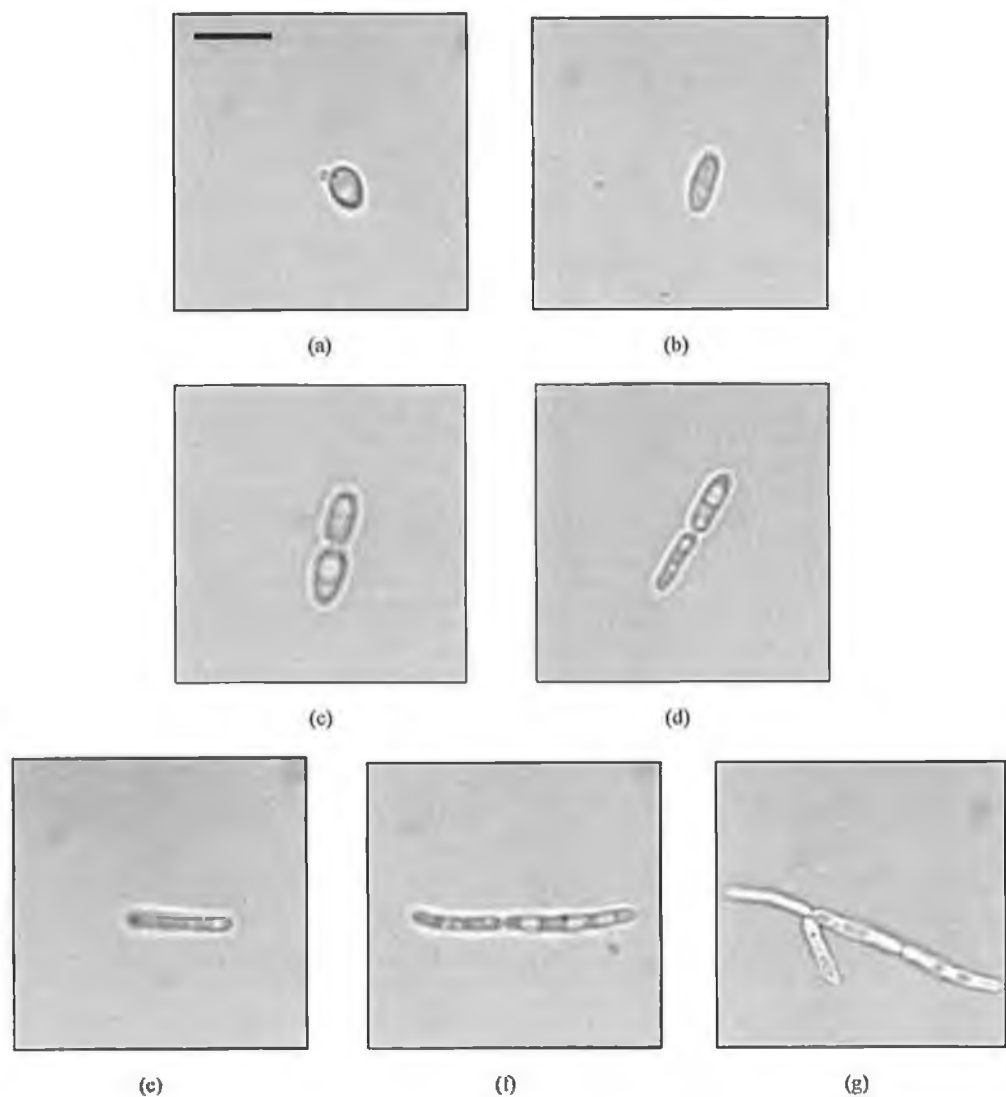


Figure 4.4 Morphological forms displayed by *K. marxianus* NRRLy2415 (a) yeast (b) elongated yeast (c) double yeast (d) double elongated yeast (e) filament (f) double filament (g) pseudohyphae, bar = 10 μ m.

4.3 FURTHER CLASSIFICATION OF PSEUDOHYPHAE

All the classes described, excluding pseudohyphae, have finite limits in size and shape, whereas pseudohyphae can range from the unbranched type, containing just three subunits (filaments) to branched pseudohyphae containing 20 subunits or more. Thus the pseudohyphae class cannot adequately describe the morphology of a culture containing predominantly pseudohyphae. Additional descriptors may be added to the classification in order to completely describe the culture's morphology. Examples of such descriptors include the mean length of a pseudohypha in terms of subunits and the mean number of branches per pseudohypha.

4.4 CONCLUSIONS

A classification system has been designed that allows the complete description of the morphology displayed by *Kluyveromyces marxianus* var. *marxianus* NRRLy2415, under all culture conditions utilised in this study. This does not definitively suggest that this is the extent of morphologies displayed by the organism, however, it does claim to represent the range of morphologies expected under normal bioreactor operating conditions, in typical media known to sustain yeast growth. Problems experienced with manual implementation of the classification system were significant, due to the large degree of inter-operator variation in the generated data and the problems experienced with the complete description of the morphology of pseudohyphae. It is apparent at this stage, that if the organism is to be classified correctly and the morphology of pseudohyphae be described correctly that a tool less subjective than the human eye be used for the purpose.

Image analysis has gained much attention recently due to its utility in physically quantifying biological phenomena (Thomas and Paul, 1996). Its potential to implement the extensive classification system, both non-subjectively and routinely, is appealing. Image analysis will also provide a measure of the geometric properties of cells. It was hoped, to develop an automatic protocol that would provide both classification and measurement of cell geometry, routinely for fermentation samples. This will be addressed in Chapter 5.

In terms of experimental work, it was hoped to re-examine the causes of dimorphism established by Walker and O’Niell (1990) for *K. marxianus*, as they do not fit the typical criteria responsible for dimorphism in similar yeast (Hill and Robinson, 1988). It is also hoped to apply a mathematical analysis to kinetic data, as the misinterpretation of data is widespread in this area of research. Many examples exist in the literature of attributing the presence or absence of a nutrient to a dimorphic transition in an organism, whereas it is apparent that the presence or absence of the nutrient affects the physiology, which in turn affects the morphology. For examples of the above see Section 2.8.5.

It was also hoped to assess the influence of morphology on the metabolism of the organism. *K. marxianus* is a known ethanol producer when growing on whey permeate and its kinetics have been modelled for chemostat culture growth on lactose (Castrillo and Ugalde, 1992). It was hoped to assess, based on kinetic modelling, how the performance of the organism varies between one morphological form and another. The above matters will be addressed in Chapters 6 and 7.

K. marxianus mycelium morphology, as can be seen in Figure 4.4 (g), is pseudohyphal. Pseudohyphal growth is defined in Section 2.8.1. Little work has been presented on the mechanism of pseudohyphal growth. In order to successfully model the growth and development of such morphologies, a means of describing such growth is necessary. It is hoped to address this matter in Chapters 8 and 9.

CHAPTER 5

IMAGE ANALYSIS METHODS

5.1 INTRODUCTION

Image analysis is the use of computer technology to extract quantitative information from a visual scene. The basic principle used in image analysis, is the simplification of the information content of an image, by converting the image into a matrix of image components known as pixels, each pixel containing a specific shade of grey, in the case of black and white images, or a series of numbers representing the colour and intensity of a pixel in the case of colour images (Jain, 1989).

5.2 APPROACHES TO INFORMATION EXTRACTION FROM IMAGES

5.2.1 Image Segmentation based on Colour or Greyscale Thresholding

The information content of an image can be overwhelming. It can be reduced significantly by binarisation of the matrix of image components. Giving pixels a value of 1 or 0, depending on their significance or insignificance to the observer, achieves this. This is known as segmentation, where pixels, within regions of interest or objects of interest, within the image are turned on (set to 1) and background pixels are turned off (set to 0).

Thresholding, either by colour or greyscale, is the most widely used and simplest process to extract an object from a background. If any scene is observed, any visible object in that scene has a property that makes it visible to the eye such as a distinct colour, intensity or texture. Thresholding is based on setting ranges of acceptable pixel colours or grey levels for segmentation based on the observation of a colour or grey-scale histogram. The histogram indicates the frequency of any colour or grey-scale in the image.

Following segmentation, the computer is able to distinguish the foreground from the background and can also determine the number of objects present in the image, based on simple binary connectivity. If a pixel, of value 1, is in contact with another pixel, of value 1, then they are both part of the same object. If a pixel, of value 1, is in contact with a pixel, of value 0, then the pixel of value 1 is a pixel on the edge of an object. By breaking the pixels of value 1 into sets of interconnecting pixels, then the number of sets is representative of the number of objects in the scene. This approach is not applicable to non-segmented images.

A disadvantage of this approach is that a lot of the textural information is discarded. This is an unfortunate, but necessary, consequence of segmentation. However, if an image is of good definition and contrast, simple grey-scale or colour thresholding is an adequate means of segmentation.

5.2.2 Edge-Based Segmentation

Edge-based segmentation utilise the sharp localised differences in intensity that occur as a transition is made from one edge to another. In essence, edge based detection examines changes in intensity with respect to distance in a single direction which is represented by dI/dD where I is the intensity and D is distance in the direction of examination. Edge-based segmentation can be useful in images where horizontal or vertical edges predominate, *i.e.* buildings, biological gel images *etc.* For circular objects, multiple directions of approach have to be used to fully describe the outline.

5.2.3 Pattern Recognition

Pattern recognition is based on novel neural network technology, which allows computers to learn an object's discriminate characteristics from a set of positive and negative instances. Positive instances would represent good examples of a pattern whereas negative instances are counter examples of a pattern. This technology is becoming a more popular method of industrial inspection, as a classifier can be trained to recognise flawed components simply by changes in pattern. This provides a high-speed alternative to the traditional approach of object-

based segmentation and measurement. Object orientation or scale does not limit such pattern recognition approaches.

Uses of pattern recognition include reading scanned document images (typed numeric and alphabetic characters have very well defined patterns), high speed flaw inspection and electronic circuitry inspection. Pattern recognition has difficulties when a large degree of variance exists between positive examples.

5.2.4 Colour Indexing

Colour indexing is a new approach to image segmentation developed by Swain and Ballard (1991). It works on the principle of dividing RGB space into equally spaced “colour cubes”. For example, each cube in a 16 x 16 x 16 matrix describing a 24 bit RGB image (8 bit x 3 colours) represents 4096 different colours out of a total of 16,777,216. Test images are assessed for their colour content and if any colour in a colour cube is present in the image, the colour cube is given the value 1. If all colours in a colour cube are unrepresented in the image, the colour cube is given the value of 0. The result of this training yields a three dimensional binary matrix with the colour information content of the test image. The data set is trained by exposing the colour cube to multiple test images in order to expose the data set to as much variability as possible. Once the data set has been fully trained it can be used to identify colour changes in test images from the normal range of colours experienced in the training images. This technique is very useful in the development of high-speed industrial inspection protocols, for example the screening for burn markings on filter casings (Duffy and Lacey, 1997). It is also a useful technique for image retrieval from a database.

5.3 IMAGE ANALYSIS HARDWARE

Image analysis hardware usually consists of three primary components.

1. Image generator
2. FrameGrabber Board
3. High Speed Computer

5.3.1 Image Generator

The image generator in visual image analysis usually consists of a CCD camera. The CCD or charged couple device was developed by AT&T Bell Labs in the early 1970's. The basic principle behind its operation is as follows. The crystal silicon is an array of atoms whose bonds can be broken by absorbing light at different wavelengths. In absorbing light, thus breaking bonds, electrons are released but, importantly maintained in that region (well) of the CCD chip. The potential well represents a pixel. The number of electrons released is proportional to the amount of light that hits the silicon crystal in that region. The term pixel is an acronym of sorts for the term "picture element" (Jain, 1989). A CCD camera is usually attached to a lens system to extract information from a scene, such as a microscope or photo-lens.

5.3.2 Framegrabber Board

The framegrabber board provides the interface between the hardware or image generator and the software. It has several functions, including the interpretation, if necessary, of the analogue signal arising from the camera and the generation of fixed images from the continuous stream of data arising from the camera. Framegrabbers may also include frame stores for the capture and manipulation of multiple images.

5.3.3 Image Analysis Software

Image analysis software allows the user to interface with the information stored on the framegrabber board or stored images. The software generally provides the following key services:

- 1) a graphical user interface (GUI) between the user and the framegrabber or image file, that allows the user to observe the image or any manipulations made to the image;
- 2) significant simplification of the process of image segmentation and processing, by the use of simple commands that complete complex mathematical transformations on the image;
- 3) the inclusion of an inbuilt “macro recording” facility that allows the user to record complex series of image processing events and to subsequently run them automatically on an image.

The third service can be overlooked if the developed software is not a multipurpose research tool, but rather, is a dedicated inspection system, designed for one task only. If the end user has sufficient programming skills, the development of an in-house image analysis software platform to interact with the framegrabber may be beneficial, as this allows manipulations of images often not supplied or possible using pre-designed software.

5.4 APPLICATIONS OF IMAGE ANALYSIS IN BIOLOGICAL SCIENCES

The general complexities of biological images create a certain degree of difficulty for image analysis. Medical applications include interpretation of data from various scanners such as MRI (Magnetic Resonance Imaging), ultrasound and X-ray and the subsequent three-dimensional representation of internal structures based on the above scans. The use of image analysis as an automated diagnostic aid has also come to the forefront with investigations into automated early melanoma recognition in ambiguous cases (LeBoit and Van Fletcher, 1987) and automated cancer diagnosis in histopathology sections based on nuclear grade and density (Melamed, 1996).

In agriculture, image analysis can also be used to sort agricultural produce (Marchant, 1990) and to identify strains of potato tubers and grain crops, for example, wheat and barley.

Within the realm of biotechnology, image analysis has proven essential in the quantification of information from gel images. Image analysis techniques were developed almost simultaneously with gel techniques, with the first programs written for supercomputers (Häder, 1992). Modern gel analysis systems can operate on standard computers and can correct for local distortions and “smiling” in gels.

Within plant biotechnology, image analysis has been used to quantify chlorophyll content in leaves, leaf morphology and the quantification of individual plant cell morphology in suspension culture (Kieran, 1993). Chi *et al.* (1996) used a neural network classification system, in association with Fourier transformations, to monitor changing morphology of somatic embryos. This technique related changes in the surface contour, using Fourier transformations to the correct classification of carrot somatic embryo. In the field of animal cell culture, image analysis has been demonstrated as an efficient means of quantification of hybridoma cell lines (Tucker *et al.*, 1994), being more consistent and less labour intensive than manual methods. It also proved more consistent when quantifying stained cells and provided information about cell shape. Maruhashi *et al.* (1994) demonstrated an image analysis system suitable for on-line monitoring of animal cell suspension culture. The system was also capable of monitoring cell viability using the assumption that viable cells are larger than dead cells. The resultant data correlated well with trypan blue staining as a method of viability testing. There is still much room for development within the animal cell culture field, particularly within the study of toxicology, where parameters such as changes in cell motility and cellular shape are indicators of drug toxicity. Image analysis is currently being investigated as a tool to assess the localised cellular toxicity of surgical implant materials (Remes Biomedical, Personal communication). The study examines the radial density of nuclei surrounding the implant, thus assessing cellular density with respect to distance from the implant-tissue interface.

Within microbiology, image analysis has been used extensively to study the growth and morphology of microbial colonies grown on solid substrates.

Wimpenny *et al.* (1995) suggested that the automated diagnosis of species, even strains, using image analysis, is a possibility. Due to the small size of bacterium, it is difficult to apply image analysis to monitoring the characteristics of individual cells. However, Tsuchido *et al.* (1994), utilised image analysis to evaluate bacterial injury by determination of bacterial motion. They identified intermediates between healthy cells and dead cells that developed upon moderate heating, thus suggesting bacterial injury rather than death. To monitor the morphology of individual bacteria, the use of advanced microscopy techniques such as Scanning Electron Microscopy (SEM), would be required. This would make the use of image analysis impractical as a bacterial fermentation monitor. Image analysis has been used to assess bacterial colony development in varied environments. Wirtanen *et al.* (1995) utilised image analysis to evaluate cleaning procedures in the elimination of biofilm from stainless steel surfaces in open process equipment. Prosser *et al.* (1994) utilised image processing to identify luminescence marked bacterial cells from among a mixed flora of microorganisms, by utilising staining (crystal violet and acridine orange).

Image analysis has been used to quantify various facets of surface and immobilised fungal growth. Walsh *et al.* (1996) quantified growth patterns of the yeast *S. cerevisiae* microcolonies in carrageenan and alginate gel particles and demonstrated a relationship between local alginate concentrations in the alginate bead and microcolony morphology. Surface growth of fungi on agar plates has also been monitored using image analysis (Larralde-Corona *et al.*, 1994). In an important study, image analysis has been applied to the quantification of the extension rate of fungal tips, leading to the discovery of pulsed growth in hyphal tips (López-Franco *et al.*, 1994). Prior to this study, fungal hyphae were assumed to extend in a uniform, linear fashion. While pulse frequency and amplitude varied for the different fungi examined, it was apparent that all fungi examined, possessed a pulse. Olsson (1995) was able to observe nutrient relocation by higher fungi (Basidiomycetes) across a nutrient gradient, utilising image analysis to quantify both biomass concentrations on either side of the gradient, by correlating pixel grey levels with biomass concentrations, and nutrient diffusion in conjunction with

a chemical assay for glucose. This work proved that certain higher fungi could relocate nutrients from regions of sufficient nutrition to regions of insufficient nutrition, often promoting greater growth in the latter regions.

In mathematics, a geometric shape that is complex and detailed in structure at any level of magnification is known as a *fractal*. Often fractals are *self-similar*—that is, they have the property that each small portion of the fractal can be viewed as a reduced-scale replica of the whole. Diverse phenomena in biological sciences display interesting scaling in the time and space domain, many of which have been described using a fractal power law model. Pons *et al.* (1995) used fractal-based descriptors of texture to try and differentiate between colonies of various organisms cultured on agar plates. While the study proved unsuccessful, it is one of the first to use grey level deviation as a measured parameter. One method of characterisation of the spatial distribution of hyphae within a mycelium is in terms of fractal dimension. Donnelly *et al.* (1995) demonstrated a rapid box counting algorithm for determining border fractal and mass fractal dimensions and indicates that the previously qualitative descriptors of fungal feeding versus foraging can now be described using fractal dimensions. Hitchcock *et al.* (1996), using complex analysis of skeletonised mycelial networks (see Section 5.5.3. for description of skeletonisation), estimated fractal dimensions for different mycelial networks and verifies the above conclusion. Such work has significance in quality control of mushroom inoculum production.

5.5 IMAGE ANALYSIS OF FUNGI IN SUSPENSION CULTURE

5.5.1 Yeast

Yeast, geometrically speaking, are regarded as prolate ellipsoids, with mother and daughter having the same geometric properties as each other. In a two-dimensional projection they project as slightly intersecting ellipses and this is how the imaging system perceives them. To infer a volume for each component of the cell can be a difficult process. The first attempt at generating volumes from observations was done by Wheals (1982), who manually measured the major and minor axes of each component of the yeast using a digitising tablet. The first application of image

analysis to the area was by Huls *et al.* (1992) who used a contour rotation method to assess the volume of cells present (Figure 5.1).



Figure 5.1 Application of contour rotation method (adapted from Huls *et al.* (1992))

The major axis (of length L) of the cell in figure 5.1(a) is subdivided into n_s equal divisions. A rectangle of width L/n_s with a length defined by the intersection of a line running perpendicular to the major axis intersecting the mid point of the major axis section with the edge of the two-dimensional projection of the cell is generated. The volume of each segment, i , of the cell is then calculated by

$$V(i) = \frac{\pi}{4} L_i^2 \left(\frac{L}{n_s} \right) \quad (5.1)$$

The overall volume of the cell was estimated from

$$V = \sum_{i=1}^{n_s} V(i) \quad (5.2)$$

If n_s is large, then the representation given by such a method is good but the technique is cumbersome in terms of processing time. Secondly, the two cell subunits have to be on the same major axis, which is often not the case. Pons *et al.* (1993) first exploited the approximate geometric properties of the yeast, namely its ellipsoidal nature, by estimating the major and minor axes of the subunits and estimating volume using the following calculation.

$$V = \frac{\pi}{6} (L_a W_a^2 + L_b W_b^2) \quad (5.3)$$

where a and b represent the subunits of the cell.

The major and minor axes were estimated by using the intersection of the “geodesic diameter”, the longest Feret diameter in the cell representing the major axis of the structure, with the “regional maxima” determined by a process of repeated erosion to a single point (removal of pixels in an ordered fashion from the surface of the cell until only one pixel remains in the centre of the cell(s)). Again, the drawback of this approach is the necessity of both cells being on the same major axis.

Two of the most significant pieces of work done to date on the quantification of yeast using image analysis are as follows. Zalewski *et al.* (1994) correlated the relative frequency of four cell aggregates or tetrads with specific growth rate of the culture. This was a significant advance as it demonstrated the use of image analysis as a monitor of fermentation performance. Suhr *et al.* (1994) demonstrated the use of an *in situ* microscopy system to quantify both cell growth and cell size. Both image generation (laser-based) and image processing are complex, yet they illustrate the use of image analysis on the same basis as any fermentation probe, providing real time data regarding the physiological state of the fermentation. This work also illustrated the use of image analysis as a non-invasive technology, capable of making measurements from the exterior of a reactor on its contents.

In a later paper, Zalewski and Bucholz (1996) demonstrated a fully automatic sampling and analysis method that was capable of dealing with yeast aggregates in the viewing chamber and was also capable of enumerating cells and counting vacuoles within cells.

Vincente *et al.* (1996) quantified yeast flocs by image analysis using an automated threshold. Automated thresholding, which is based on mathematical properties of the grey level histogram, leads to less user intervention and less variation on what is deemed to be the “correct” threshold. This group also made use of a statistical

analysis based on cumulative Gaussian distributions, each distribution describing single, double or other higher order flocs. This yielded a strong mathematical description of the data presented. A similar approach to data analysis was developed simultaneously in the present work to describe batch and continuous culture population distributions.

5.5.2 Fungal Pellets

The pellet is the macroscopic morphology of many filamentous organisms. Due to their nature, pellets contain within them an extremely heterogeneous environment. Pellets are formed by a process of agglomeration, whereby different hyphal elements or spores aggregate together or with solid particles in the media. Certain pellets have been reported to form from the germination of a single spore (Takahashi and Yamada, 1959). The morphology of fungal pellets is generally dictated by their growth environment, and several environmental parameters such as medium composition and agitation rate have been associated with alterations in pellet morphology. The typical classification system used to describe pellets is as follows.

- 1) Fluffy loose pellets – such pellets have a compact core with a much looser outer zone.
- 2) Compact smooth pellets – the whole pellet is compact and the exterior is smooth.
- 3) Hollow smooth pellets – the interior of the pellet is hollow due to autolysis and the exterior is smooth.

Quantification of pellet morphology can provide a significant amount of information about culture physiology. Prior to the introduction of image analysis to the field quantification of pellet morphology was based on qualitative descriptions of pellet morphology (Metz and Kossen, 1977) and time-consuming sieve analysis to determine pellet volume fraction distributions (Vecht-Lifchitz *et al.*, 1990). Reichl *et al.* (1992) and Cox and Thomas (1992) simultaneously demonstrated the use of image analysis as a quantifier of pellet morphology. Both groups capitalised

on two factors that make pellets suitable for image analysis, (a) the spherical nature of pellets and (b) the large difference in grey levels between the foreground, or pellet and the background. Using image analysis, the overall volume of a pellet is represented by

$$V = \frac{\pi}{6} \left(\sqrt{\frac{4A}{\pi}} \right)^3 \quad (5.4)$$

where A is the projected area of the pellet, a measurement easily determined using image analysis. Where pellets are “hairy” or fluffy, this approach can be inaccurate due to the often large volume occupied by voidage on the exterior of the pellet. The estimated volume of the pellet will be smaller than in reality. In such cases, the approach of researchers has been to calculate the volume the core or solid region and to provide what is typically referred to as the “pellet hairy length”.

5.5.3 Filamentous Fungi

The quantification of the morphology of filamentous fungi in suspension culture has always been of great interest to biochemical engineers as such quantification should (at least in theory) lead to a greater understanding of the behaviour of the fermentation broth and its constituent biocatalyst (the organism).

Filamentous fungi are generally regarded as being cylindrical in nature with hemispherical ends at hyphal tips. Most fungi grow in a branched structure, the development of which varies significantly with organism, strain and growth conditions. Plomley (1959) was the first to suggest that filamentous fungi have a growth unit that is duplicated at a constant rate during hyphal growth. This conclusion follows inevitably from the early observations that an individual hyphal strand extends at a linear rate whereby the whole hypha extends at an approximately exponential rate (Trinci, 1969). Trinci (1974) defined the Hyphal Growth Unit (HGU) as the total hyphal length divided by the number of hyphal tips. Using this definition, he further demonstrated its constant nature in relation to hyphal development for three organisms grown on agar covered in cellophane,

using time-lapse photomicroscopy. This approach was followed up with a study examining mitosis, branching and septation in *Aspergillus nidulans* on coverslip cultures (Fiddy and Trinci, 1976). This study involved the examination of the synchrony of division of nuclei within hyphae and found that synchronous nuclear division occurred until the hyphae contained 8 or 16 nuclei and subsequently became asynchronous. This study also demonstrated an increase in the hyphal extension rate with increasing hyphal length. The study was accompanied by a similar examination on *Geotrichum candidum* (Fiddy and Trinci, 1976) where exponential growth of the hyphal element was observed with respect to time and a general increase in extension rate of the primary branch and of the apical compartment (the compartment between the tip and the adjacent septa).

While such studies revealed much about the mechanisms of growth and differentiation of fungi, they did not involve the examination of fungi in suspension cultures. Metz *et al.* (1981) measured many of the morphological criteria used today on suspension cultures. The following are a list of measured parameters.

- L_t Total hyphal length = length of main hypha + branches
- L_e Effective hyphal length = length of main hypha
- n number of tips per hypha
- L_{hgu} Hyphal Growth Unit length

Metz *et al.* (1981) used a digitising tablet to measure the above parameters from photomicrographs, essentially a laborious and time consuming process if statistically significant numbers of hyphae are to be measured. This group continued this work with an important attempt to correlate engineering variables with morphology of *P. chrysogenum*, see Chapter 2 (van-Suidjam and Metz, 1981). Adams and Thomas (1988) introduced the first digital image analysis protocol for the quantification of filamentous fungi. They identified the usefulness of a morphological operator known as “skeletonisation”, a process by which pixels are sequentially removed from the surface of an object until a line one-pixel thick

remains. This operator has become the basis of most algorithms developed for filamentous fungi. The protocol, subsequent to object skeletonisation, made use of a light pen to identify branch points and the main hypha. It eliminated the need for photomicrographs and allowed the user to work in "real time". This protocol, while a significant improvement on previous approaches, still had a considerable amount of operator involvement. The development of an automatic image analysis protocol was the concern of Packer and Thomas (1990). They identified some other key features of a single pixel line such as the ability to remove pixels from the ends of such lines, a process known as *pruning*. This led them to be able to remove short artefact branches generated in the skeletonisation process and also to identify hyphal growth in clumped form based on closed loops, an artefact not present in freely dispersed hyphae. The use of logical operators also became apparent in this study. The main hypha was based on the longest interconnected distance in the skeletonised hypha. This skeletonised hypha was subsequently removed from the image and the remaining unattached branches were then measured. This work also introduced the concept of measuring clumped biomass, a term that will be used a great deal in following studies. In fact, it was found that in this study over 90% of the biomass (*P. chrysogenum*) remained in indispersable clumps for most of the fermentation. Tucker *et al.* (1992) developed the automated measurement of clumped biomass with the definition of morphological characteristics of clumped biomass such as projected area, perimeter, compactness and roughness. The geometry of a line is much simpler than that of a two-dimensional object and allows the calculation of hyphal length based on values such as half the line perimeter or the sum of all inter pixel distances. The use of such measurements have been used to quantify fungal morphology for the purposes of relating morphology to parameters such as broth rheology and to quantify the effect of agitation on the structure of hyphae.

The next phase in the study of hyphal structure came with the development of algorithms to study hyphal ultrastructure, particularly hyphae of *P. chrysogenum*. This information is essential for the development of structured mathematical models for growth and antibiotic production. The whole concept behind the work

is that biomass is not homogenous but, in fact, is composed of regions of varying degrees of vitality. The use of image analysis to non-invasively identify such zones is of obvious use. The first progress in this area came with the development of an algorithm by Packer *et al.* (1992) whereby the amount of vital *P. chrysogenum* was estimated using image analysis measurements. This group divided biomass into two discrete types, actively growing biomass and inactive biomass. They found that the inactive regions of the biomass contributed about 40% of the mass per unit volume of actively growing biomass. Paul *et al.* (1992) quantified the vacuolation of *P. chrysogenum* hyphae. The organism possesses clearly visible vacuoles and is thus an ideal candidate for such studies. It was discovered that vacuolation increased as the distance from the actively growing tips increased. The possibility of modelling the hyphal development of the organism using the results from such analysis was discussed and subsequently demonstrated by Paul *et al.* (1994c). This work also included an extension of the previous protocol to quantify the actively growing fungal tips based on their grey density (the tips appeared darker than other cell material). The first venture into colour-based image analysis of fungal cells was made by a collaborative effort between the Thomas and Pons groups, (Vanhoutte *et al.*, 1994). This work, based on hyphal staining and multiple stain recognition, demonstrated the presence of six metabolically distinct zones within the organism being cultured. It was regarded, at the time, as being too intensive from a processing perspective. However, the advent of more powerful computers has opened opportunities in the area of colour image analysis.

Quantification of the morphology of aggregated biomass generally requires classification of the organism into discrete morphological groupings. Generally, morphological alterations are continuous, but to aid the user, a discrete quantification system is often useful to help visualise the current morphological state of a culture. Many examples of such classification approaches exist. In yeast fermentations, the culture is often classified into groups of similar cells such as single cells, double cells, triple cells etc., where each cell grouping is normally distributed on a volumetric basis (Vincente *et al.*, 1996). This is an ideal system with very discrete visual groupings, yet the volumetric data often overlaps between

groupings. This is a typical example of the additional information that such classification systems can add to the morphological description of a culture. With filamentous biomass, classifications are made based on the degree of aggregation of the free filaments. Thomas's group demonstrated the presence of clumps of biomass that remained stable even after significant agitation. Tucker *et al.* (1992) developed the following classification system to describe the broad range of morphologies exhibited in filamentous fungal fermentations.

Free filaments \longrightarrow Clumps of free filaments \longrightarrow Pellets

While this classification system may encompass the entirety of displayed morphologies, it is often redundant due to the culture growing completely in one form of the three. This classification system has distinct difficulties in implementation, as there is a difficulty in perception between the groupings outlined and considerable inter-group variation. It is apparent from the general failure to relate the above morphological criteria to rheology (Olsvik and Kristiansen, 1994), that further study of the classification of such complex systems is necessary.

5.5.4 Dimorphic Organisms

With regard to dimorphic fungal growth, there have been few attempts to mathematically quantify the dimorphic transition exhibited by such organisms. Odds (1993) suggested a method for assessing the morphological transition in *C. albicans* based on three pertinent measurements.

- 1) the diameter of the mother bud interface (s)
- 2) the diameter of the daughter cell (d)
- 3) the length of the daughter cell (h)

These values were combined to generate the following equation.

$$M_1 = 2 + 1.78 \log_{10} \left(\frac{hs}{d^2} \right) \quad (5.5)$$

where M_1 is a morphology index related to the morphology of a subunit of a hypha or a budding yeast cell. This author feels the term, s , is often redundant due to the similarity between yeast and hyphal cell interfaces. Thus, in equation (5.5), the statement is simply a comparison between the length and width of the generated cell. While measurements of this nature may be easy to assess manually, they are difficult to automatically evaluate using computer aided image analysis.

In a much more interesting development, the use of neural network technology has been demonstrated in the classification of yeast-like and pseudohyphal forms of the dimorphic organism, *Aureobasidium pullulans* (Guterman and Shabtai, 1996). This procedure was termed a “self-tuning vision system” and was based on the training of a neural network with positive and negative examples of a given morphology. The ease of training led the authors to believe that the system could rapidly be adapted to different mixed morphology systems. While this method classifies the organism into visual groupings, it yields no information on the physical size of the organisms.

It is hoped that the present work can address the above problems by providing physical measurements along with the standard classification system. The organism chosen for this work displays several morphologies (Chapter 4) and even within the pseudohyphal class, is seen to vary greatly from linear chains of three cells to the large branched cells with up to 20 subunits.

5.6 IMAGE ANALYSIS HARDWARE

The hardware consisted of three main components, a personal computer, a TV camera (CCD type) and a microscope. Each component will be described in detail.

5.6.1 Computer Configuration

The computer supporting the image processing and analysis software contained a 66MHz Intel 486 DX2 processor. For input of live and frozen video-based images, the system contained an ELViS (Vision Dynamics) framegrabber board. The Monitor used was an AcerView 46L Low radiation 14'' colour monitor (Acer Peripherals Inc., Taiwan).

5.6.2 Camera

The camera used was a Sony XC-74CE monochrome video camera (Sony Corporation, Japan). This was attached to the microscope via a C-mount adapter.

5.6.3 Microscope

The microscope used for all studies was an Olympus BX40 brightfield microscope (Olympus Optical Company, Japan). The magnifications used for this work were 200× and 400×, yielding on screen magnifications of $0.414\mu\text{m}^2$ and $0.206\mu\text{m}^2$ per pixel respectively. Both lighting and condenser settings were maintained at constant levels to ensure as uniform an image as possible.

5.7 IMAGE ANALYSIS SOFTWARE

5.7.1 Introduction

The software used was a Windows based package (QWIN, Leica, Cambridge, England) which had the ability to:

- acquire and display a grey image on screen
- modify and enhance the acquired image to appropriate levels
- segment regions of interest from the grey image resulting in binary images
- subsequently modify the binary image both manually and automatically
- measure selected features contained in the binary image

- output the measured data in useable form
- program routines to automatically complete complex sequences of the above events

5.7.2 Grey Image Acquisition

Each image acquired and displayed on the screen is composed of 720×512 pixels, each pixel with a grey level ranging from 0 (representing black) to 255 (representing white), this is known as an 8 bit image due to division of grey into 2^8 discrete values. The 8 bit grey image is an industry standard. Initially, a live image is displayed in the image window and when an image of sufficient quality is viewed the image is frozen. This image is now available for subsequent processing. The package allowed the short-term storage of seven grey images in regions known as planes. The image planes were not only useful for storing multiple images but also allowed for the processing of images without overwriting the original.

5.7.3 Grey Image Processing

Acquired images often do not possess the required quality for image analysis. Problems commonly experienced are noise, unexplained variations in pixel grey values, and lighting aberrations. Grey image processing is necessary to correct such problems. Grey image processing is fundamentally the ability to alter a pixel's grey level based on the pixel's own or surrounding pixels' grey values. Such operators include edge enhancers and detectors, image smoothing and sharpening and image inversion. Such operators are used only if the acquired image is not of suitable quality to allow segmentation of the regions of interest.

5.7.4 Image Segmentation (Feature Detection)

Image segmentation is a necessary feature of all image analysis software packages. It is defined as the ability to isolate regions of interest in the image using some quality unique to the regions of interest. Many documented approaches to image segmentation are available such as edge- and region- based segmentation (Jain, 1989) but the QWIN software package simply uses detectable differences in grey levels between the regions of interest and the background. This approach is often

referred to as “thresholding”. Pixels with grey levels in the range of interest are subsequently defined in the matrix of pixels as “1” and background pixels are defined as “0”. This resultant matrix is defined as a binary image and is displayed on the screen with regions of interest coloured and background black. Image segmentation should not be confused with binary segmentation (an in-built binary morphological operator) to be described later.

5.7.5 Binary Image Manipulation

Once an image has been segmented the resultant binary image is easily manipulated due to its mathematical simplicity. Often segmented images lack the required quality to perform correct measurements on features and require enhancement. Such images require the use of the suite of in-built binary operators for improvement. Binary operators are also useful in the modification of a binary image, *i.e.* the separation of touching features, and, as will be discussed later, can be used in combination to provide some powerful morphological modifications to an image. Six binary image planes were provided to allow for multiple operations to be performed.

5.7.6 Feature Measurement

The software package allows the measurement of multiple parameters on any given feature in a binary image such as feature area, dimensions such as length and width, and other useful parameters including convex area (the area of a polygon circumscribing the object) and object orientation. Measurements can be used to add or eliminate features from binary images and are useful in categorising objects into groups.

5.7.7 Program Development Utility (QUIPS)

The software package also contained a utility to develop routines that will complete a complex sequence of events without the need for manual intervention. The facility provided programming operations such as the ability to input and output data from routines and conditionally execute certain events. QUIPS proved

to be an extremely flexible and user friendly method of creating image analysis routines.

5.8 SLIDE PREPARATION FOR IMAGE ACQUISITION

Many different slide preparations were attempted in order to find the most suitable for image analysis. The most effective method is outlined below. A 35 μ l aliquot of suitably diluted sample was applied to a 1.2mm thick Blue Star glass slide (Chance Propper Ltd., Warley, England). This was covered with a 22x22mm No. 1½ Glass cover slip (Chance Propper). This resulted in an image that was essentially monoplanar. Pseudohyphal samples were suitably diluted and vortexed for 10 minutes prior to slide preparation to break up any temporary aggregates that may have been present.

5.9 OBJECTIVES FOR DEVELOPED ALGORITHMS

Algorithms were developed to perform the following functions on a cell population:

- separation of the cells into the seven classes described in Chapter 4.
- estimation of the volume of individual cells and double cells (Table 5.1).
- measurement of the morphological properties of pseudohyphal cells, such as total length, mean width, volume (Table 5.1), and the extent of branching.

Two programs were developed to perform the above functions. This was necessary due to the slow speed of the processor in this system. The first program, ACQUIRE, was responsible for grey image acquisition, feature detection and binary image enhancement. The enhanced binary images were then stored. It was possible to acquire and store multiple samples each with multiple images. The second program, MEASURE, was responsible for the measurement and classification of cells in the binary images. This program was run overnight so as not to interfere with other researchers in the laboratory. The program was capable of outputting the data for several different samples separately. A more detailed

description of the operation of each program will now be given. For an overview of the algorithms used in each program see Figure 5.2.

5.10 OVERVIEW OF PROGRAM “ACQUIRE”

Program ACQUIRE consists of five distinct sections:

1. program setup and control of image logging
2. image acquisition
3. image segmentation (detection)
4. automatic image enhancement
5. manual image enhancement

Program setup and image management involve the initialisation of variables in the program and the logging of information about the image including:

1. sample name
2. user number
3. number of images to be logged

Table 5.1 Morphologies displayed by *K. marxianus* var. *marxianus* NRRLy2415. Classification and volume estimation.

Class	Description	Volume
Yeast	Spherical or ellipsoidal single cells	$LW^2\pi/6$
Elongated yeast	Elongated ellipsoidal single cells	$LW^2\pi/6$
Filament	Rod-like cell with no visible curvature except at the tips	$LW^2\pi/4^a$
Double yeast	Budding yeast containing a visible constriction at the mother-bud junction	$(L_1W_1^2 + L_2W_2^2)\pi/6$
Double elongated yeast	Budding elongated yeast containing a visible constriction at the mother-bud junction	$(L_1W_1^2 + L_2W_2^2)\pi/6$
Double filament	Joined filaments formed either by cell growth or pseudohyphal fragmentation	$(L_1W_1^2 + L_2W_2^2)\pi/4^b$ $LW^2\pi/4^c$
Pseudohyphae	Three or more cells joined together (usually composed of filaments) may be branched or unbranched	$LW^2\pi/4^d$

L and W are the feret length and width of a cell respectively. The subscripts refer to the first and second subunits of a double cell.

- ^a The length L of a filament is the feret length when it has been measured from Image G (Figure 5.2) and is the skeletonised length (where the cell has been reduced to a single pixel width and the length is measured as perimeter/ 2) when it has been measured from Image H (Figure 5.2).
- ^b Volume of double filament which has been successfully segmented in Image F (Figure 5.2).
- ^c Volume of double filament which could not be segmented in Image F (Figure 5.2).
- ^d L is the skeletonised length of a pseudohypha. W is the mean width of the cell and is equal to area/length.

This information is logged in data files along with the information from previous samples logged. The program now has the information required to log the images within the image database. The image logging database was developed primarily for this program but was found useful for other programs being developed in the laboratory.

The image acquisition stage required the operator to move the microscope stage to a region of interest (a live image was present on the screen at this stage). The image was frozen and stored in the image database (Image A, Figure 5.3). This process was repeated until the desired number of images was logged.

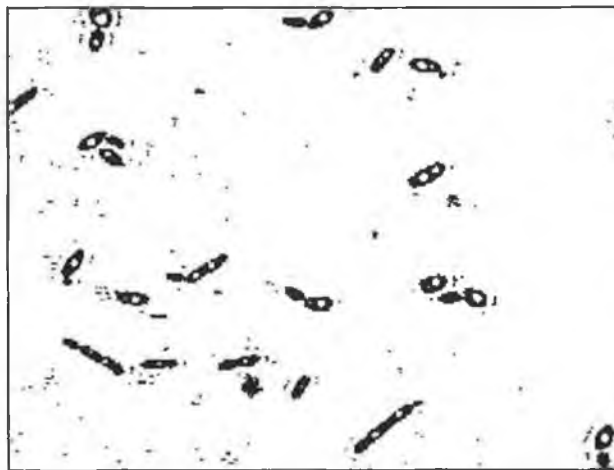
Image segmentation was performed using two different approaches. Cells in most images possessed white halos (Figure 5.3(a)) (an artefact of lighting) that were easily detectable. These halos were generally not present on debris and served as a useful method of isolating cells from background debris and lighting inconsistencies. Dark pixels within the white borders were deemed to be part of cells. Figure 5.3 outlines the approach to cell detection.

Pseudohyphae may possess inconsistent halos due to non-planarity and complexity of structure. A simpler approach to detection had to be implemented involving solely the detection of darker regions in cells. These regions were reconstructed to the whole cell using closure cycles and hole filling routines. The image resulting from this approach was often of poorer quality due to the presence of a greater quantity of debris being present. This debris had to be removed using size filters and in some cases manual intervention.

Once detection thresholds have been manually set for the first of a series of images, the remaining images are segmented and processed automatically, based on the assumption that the background grey levels in all images are similar. This was generally the case for all images taken off the same microscope slide. This greatly reduced operator intervention.



(a)



(b)



(c)

Figure 5.3. Preliminary image processing stage (a) Image A: (portion of) initial grey image. (b) Image B: unedited binary image. (c) Image C: edited binary image. For clarity, only a portion (approximately one third) of the full image frame is displayed.

The enhanced binary images were then presented to the operator for manual intervention if necessary. Problems that involved manual intervention included the elimination of debris not removed using size filters, the separation of touching cells and the repair of pseudohyphae exhibiting non planarity. Manual intervention was minimal for most images. Once images were deemed to be of sufficient quality they were stored for processing by the MEASURE program.

5.11 OVERVIEW OF PROGRAM “MEASURE”

Program MEASURE is responsible for the measurement, classification and output of data for cells in images recorded using program ACQUIRE. A graphical overview of program MEASURE is presented in Figure 5.2.

5.11.1 Preliminary Cell Classification

Single cells and pseudohyphae were separately identified on Image C and placed in separate binary image stores. Initially, a primary classification of single cells is performed on Image C, using two size/shape filters (Filters 1 and 2, as detailed in Table 5.2), giving rise to a preliminary “single cells” image (Image D, Figure 5.2). Pseudohyphal cells are then removed from Image C using a size and shape filter (Filter 3 in Table 5.2), resulting in a preliminary pseudohyphae image (Image E, Figure 5.2). Once the single cells and pseudohyphal cells have been removed from Image C the remaining cells are termed “possible double cells” (Image F, Figure 5.2).

Table 5.2. Filters for preliminary cell classification

Class	Filter number	Filter parameters
Single Cell	1	$8 < \text{area} < 14\mu\text{m}^2$
Double Cell	2	$14 \leq \text{area} < 24\mu\text{m}^2$ and $\text{perimeter}/\text{convex perimeter} < 1.12$
Pseudohyphae	3	$\text{Area} > 60 \mu\text{m}^2$

5.11.2 Primary Segmentation

Image F contains what are termed “possible” double cells, because, in addition to “true” double cells (both double yeast and double filaments), this image may also contain cells that are, in fact, either single cells or pseudohyphae, but that are not captured by the software filters described in Table 5.2. To classify these cells correctly, it was necessary to perform segmentation on each cell in Image F. The segment function is a system-inbuilt binary morphological operator that is used to separate automatically touching features by reconstruction from ultimate erosion markers. Primary segmentation proceeds by systematically (and automatically) removing the largest object in Image F and placing it in a separate image plane. If two cells of the same size are present in an image, a backup filter based on cell roundness is used to separate them. Cells have to be isolated before segmentation, because, sub-units generated from a cell during the segmentation process become independent of each other. Thus if more than one cell segments in the same image the sub-units generated cannot be reassociated with each other after measurement.

Once a cell has been isolated, a binary segmentation is then performed on this object and the number of entities in the frame is counted (this primary segmentation is hereafter termed Segment 1). If the cell separates into two subunits, the geometric properties of the subunits are measured and the cell is classified as a double yeast, a double elongated yeast or a double filament according to the criteria of Table 5.3. The cell is then removed from Image F and the cycle repeated until all cells are removed from Image F.

Table 5.3 Classification of single and double cells

Cell type	Classification
Yeast	$1 < L/W < 2.5$
Elongated Yeast	$2.5 \leq L/W < 4$
Filament	$L/W \geq 5$
Double Yeast	L_1/W_1 and $L_2/W_2 < 2.5$
Double Elongated Yeast	L_1/W_1 and $L_2/W_2 < 4 : L_1/W_1$ or $L_2/W_2 \geq 2.5$
Double filament	L_1/W_1 or $L_2/W_2 \geq 4$

5.11.3 Secondary Segmentation

There are a number of cell geometries in Image F, for which the application of the binary segment function either fails to separate double cells, or more than two subunits arise. Extended image processing must be performed on these cells if they are to be classified correctly and automatically. The use of a system-inbuilt binary “outline” morphological operator proved extremely useful in correctly classifying (and separating, if necessary) the aforementioned cells. Any cell in Image F which failed to segment into exactly two subunits after the application of Segment 1, was subjected to a series of operations (hereafter termed Segments 2, 3 and 4), which were applied in sequence and which are described in Figure 5.4.

5.11.3.1 Segment 2

This operation proved useful for separating double cells that segmented into more than two subunits when primary segmentation (Segment 1) was performed. The binary outline operator is applied to the cell. In Figure 5.4a, this results in the outline continuing through the cell-cell interface. Using logical arithmetic, the cell is seen to separate into two subunits. Using a number of logical and rebuild functions, it is possible to recreate the original cell image, whereby the cells are separated at the interface, as depicted in Figure 5.4a. The geometric parameters of the subunits are measured and their volume calculated as an ellipsoid or cylinder as required. The cell is then removed from Image F.

5.11.3.2 Segment 3

Some double cells do not possess the necessary degree of concavity at the cell-cell junction to separate into two subunits by primary segmentation (Segment 1) and also fail to separate when the series of outlining and logical operations in Segment 2 is applied (as depicted in Figure 5.4b). If, however, the segment operator is applied to the cell structure in place after outline removal as in Segment 2, and this successfully separates the cell into two subunits, the subunits may be rebuilt, measured and removed from Image F. This step is termed Segment 3. If following the application of the segment operator, three or more subunits are present, then the

cell is defined as a pseudohypha and is copied to Image H (the final pseudohyphal image) and simultaneously removed from Image F.

5.11.3.3 Segment 4

If, following the application of Segments 1, 2, and 3, the cell fails to separate (see Figure 4.4c) but where there is a significant difference (greater than three pixels) between the measured areas of the original cell and the image remaining after the applications of Segments 1,2 and 3, then the cell can be rebuilt, measured, and removed from Image F. (this sequence of operations is termed Segment 4). However, if the difference in area between the original cell and the segmented cell is three pixels or less, the cell is deemed to be a single cell. It is then removed from Image F and added to the final single cell image (Image H, Figure 5.2).

After these steps have been completed, all true double cells in the original “possible” double cells (Image F) have been classified (and their geometric properties have also been measured). If, after applying Segments 1, 2, 3 and 4, the original cell is still intact it is added to the original single cells image resulting in a final single cells image (Image G, Figure 5.2). If, after applying Segments 1, 2 and 3, the number of subunits is greater than two the cell is added to the original pseudohyphal cell image, resulting in a final pseudohyphal cells image (Image H, Figure 5.2)

5.11.4 Classification and Measurement of Single Cells

The individual cells in Image G are further classified as yeast, elongated yeast or filaments according to the criteria listed in Table 5.3. As the cells in this image are single cells and, hence, are discrete objects, measurement of geometric parameters can be performed on the entire image in a single pass.

5.11.5 Skeletonisation and Measurement of Pseudohyphal Cells

The algorithm for skeletonising a hypha and pruning the branches was developed in a manner similar to that described by Tucker *et al.* (1992). The binary skeletonisation function is a morphological transformation producing the medial

axis of an object in a binary image. A skeleton is produced by successive thinning from the edges inwards until single pixel centre lines are identified. This operator is very useful in the analysis of pseudohyphae due to their long thin morphology. On application of the skeletonisation operator to the pseudohyphae image, a single pixel line is generated representing the mid-line of the pseudohyphae. The fact that the line is one pixel thick has a number of advantages. Firstly, by determining the perimeter of the line, the length of the pseudohypha can be estimated from $L \cong \text{Perimeter}/2$.

Secondly, by using a pruning operator, which sequentially removes pixels from the end of single pixel lines, in conjunction with the skeletonisation operator, information about the branching pattern of the pseudohyphae can be extracted.

The largest cell in Image H is removed to a separate binary image plane (Figure 5.5(b)). The skeletonisation operator is then applied to the cell and this results in a single pixel line representative of the mid line of the pseudohypha (Figure 5.5(c)). Artifact branches are removed using the pruning operator (Figure 5.5(d)). This operator removes pixels from the ends of single pixel lines. Once artifact branches have been removed the operator is applied once more. Using a series of logical operations the end point pixels can be isolated and counted thus yielding the number of tips on the pseudohypha (Figure 5.5(e)). If the number of tips equals two then the pseudohypha is unbranched and can be measured and removed from Image H. The calculation of tip number was also necessary for correct length estimation. The total length of the pseudohypha (L_t) was estimated using the assumption that half the perimeter of the single pixel line yielded the length of the pseudohypha. The pruning operator removed pixels from each tip in its attempt to rid pseudohyphae of artefact branches thus the length of pixels removed from all the tips has to be added back to the measured area. After pseudohyphal length is determined, the skeleton is

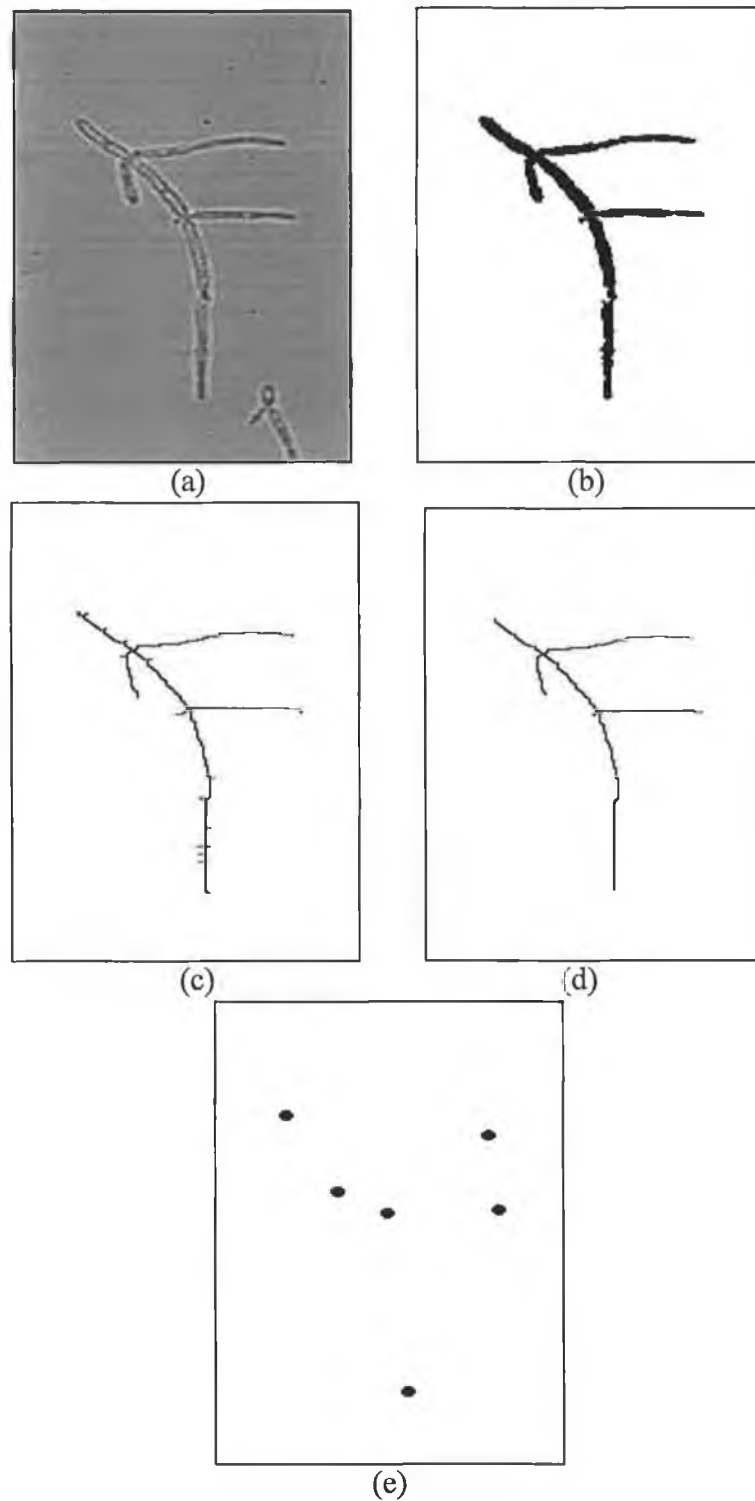


Figure 5.5 Skeletonisation and characterisation of pseudohyphae; (a) original grey image, (b) binarised version of largest pseudohypha, (c) binary image after application of skeletonisation operator, (d) pruned to remove artifact branches, (e) number of tips.

systematically pruned and branches are removed and measured yielding the effective hyphal length (L_e) and mean branch length.

Image H also contains some single filaments (which were not removed by the Table 5.2 filters) and double filaments, which segmented into more than two subunits even after applying the primary and secondary segmentation operations (Segments 1, 2, 3 and 4). Such cells were classified using the criteria in Table 5.4. The individual sizes of two subunits of the double filaments cannot be measured, but the volume of the entire unit is calculated as described in Table 4.1 and the unit is categorised using the criteria of Table 4.4.

Table 5.4 Classification of filaments/unbranched pseudohyphae (in Image H)

Class	Filter
Filament	$L \leq 18\mu\text{m}$
Double Filament	$18 < L \leq 36\mu\text{m}$
Unbranched pseudohyphae	$L > 36\mu\text{m}$

5.11.6 Sorting and Presentation of Data

The measured and calculated morphological data from single cells, double cells and pseudohyphae were sorted into the desired order and the results graphed with Sigmaplot™.

5.12 VALIDATION OF PROGRAM “MEASURE”

Three important validation steps had to be carried out before the program could be used for sample analysis.

5.12.1 Validation of Correct Geometric Shape

The assumed geometric shape of cells (i.e. prolate ellipsoids for yeast and elongated yeast and cylinders for filaments and pseudohyphae) have to be validated. The ellipsoidal nature of yeast and elongated yeast was validated by measuring the projected area of yeast and elongated yeast and then estimating the projected area using length and width measurements where.

Projected area for single yeast and elongated yeast was calculated as

$$A = \frac{\pi}{4} LW \quad (5.6)$$

Projected area for double yeast and elongated yeast was calculated as

$$A = \frac{\pi}{4}(L_1W_1 + L_2W_2) \quad (5.7)$$

An error estimate (ϵ_A) was based on the difference between observed ($A_{measured}$) and estimated cross sectional areas ($A_{estimated}$) where:

$$\epsilon_A = \frac{A_{measured} - A_{estimated}}{A_{measured}} \times 100 \quad (5.8)$$

Figure 5.6(a) shows ϵ_A plotted against measured cell projected area for single and double cells. The plot is scattered but little bias is evident in the data. The mean absolute error in estimation was found to be 6.34%. It was decided to examine the effect of magnification on ϵ_A . Cells were measured at 400× magnification and the results are shown in Figure 5.6(b). Again, little bias was evident but the mean absolute error was reduced to 3.62%. The effect of magnification on the measurement of projected area, length and width was then assessed by measuring the same population of cells at 200× and 400×. Figure 5.7 demonstrates clearly, that little difference exists between the measured lengths, widths and projected area at the two different magnifications.

Pseudohyphal cells possess a different geometric shape and the estimated parameter for pseudohyphal cells is width and not area as is the case for yeast cells. The error on estimated cell width was assessed by manually measuring the mean width of a pseudohyphal population and comparing the mean and standard deviation to that of the estimated values. As can be seen from Table 5.5 the mean

values and standard deviations for both measured and estimated values are within 5% error

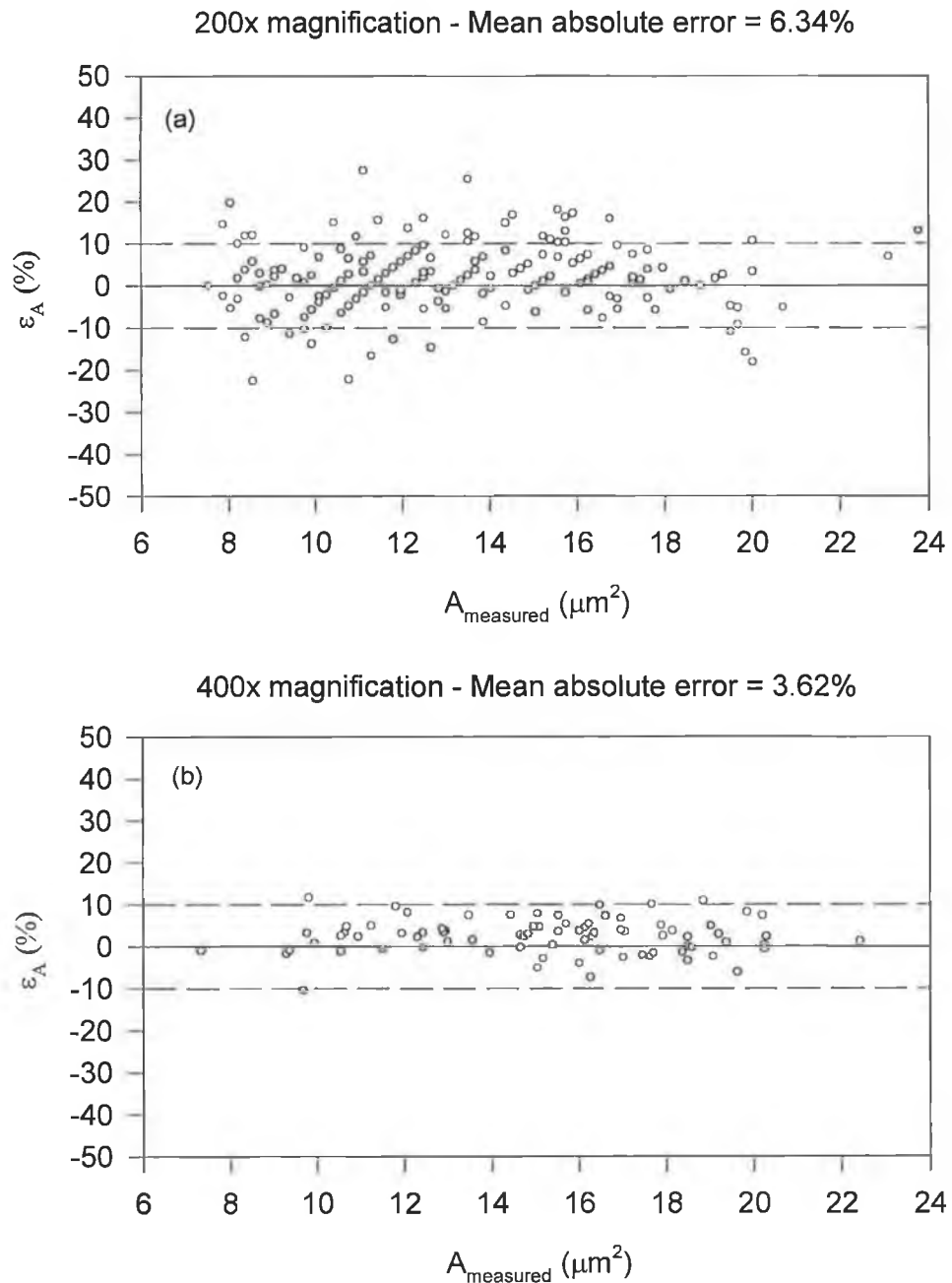


Figure 5.6 Error function (ϵ_A) for increasing measured cell cross-sectional area (a) 200 \times magnification, (b) 400 \times magnification. Dashed lines indicate $\pm 10\%$ on the expected value of ϵ_A

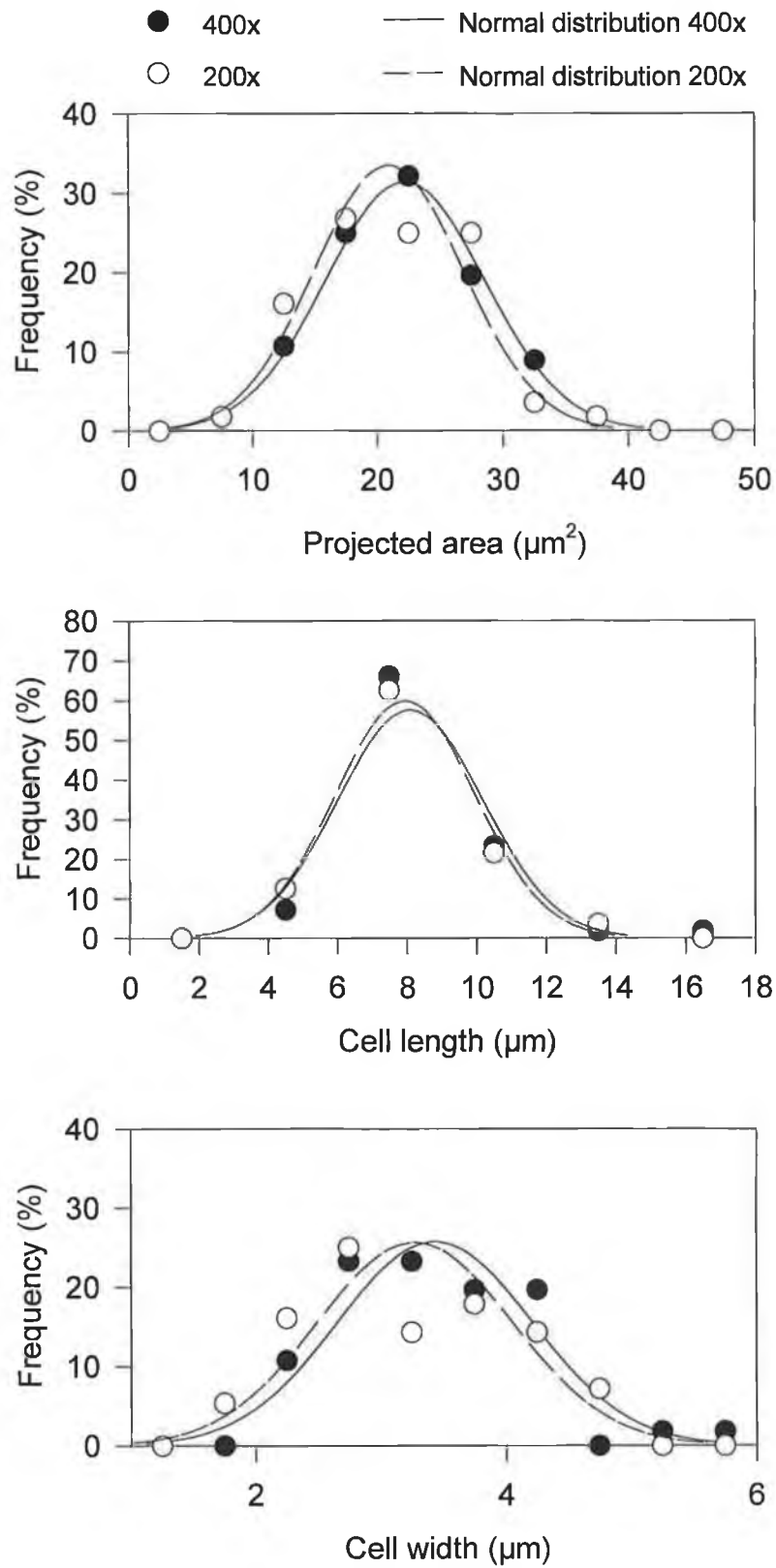


Figure 5.7 Comparison of distributions of cross sectional area, length and width of a single cell population measured at 200x and 400x magnification.

Table 5.5 Comparison of mean width (μm) of 20 manually measured pseudohyphae with the mean width of the same 20 pseudohyphae measured by program MEASURE

Sample number	Manual	Automatic	% error
1	2.10	2.21	+5.24
2	2.30	2.35	+2.17
3	1.75	1.65	-6.06
Mean % error			4.49

5.12.2 Test Fermentation Development

In order to fully test the protocol, a test fermentation was completed at 30°C at 133rpm in foil covered 250mL Erlenmeyer flasks containing 100mL of whey medium. The operating conditions described above were chosen because such conditions generate a diverse range of morphologies over the timecourse of the fermentation. The fermentation was sampled at three hourly intervals over a 24 hour period. Biomass, ethanol and residual substrate concentrations for the fermentation are presented in Figure 5.8. The fermentative nature of the run is evidenced by the preferential conversion of lactose into ethanol rather than cell mass.

The classification of cells at three-hourly intervals over the course of the fermentation is displayed in Figure 5.9. From 0 to 6 hours the percentage of single cells decreases initially and the number of double yeast increases, indicating biomass growth. In the period from 6 to 9 hours the percentage of double filaments increases dramatically. The development of many of these cells into pseudohyphae is seen to occur between 9 and 12 hours. As the medium is exhausted towards the latter stages of the fermentation, an increase in the percentage of single cells is noted at the expense of other forms. As the inoculum was taken from an overnight culture, the expected similarity in the distribution of cells at the beginning and towards the end of the fermentation can also be seen.

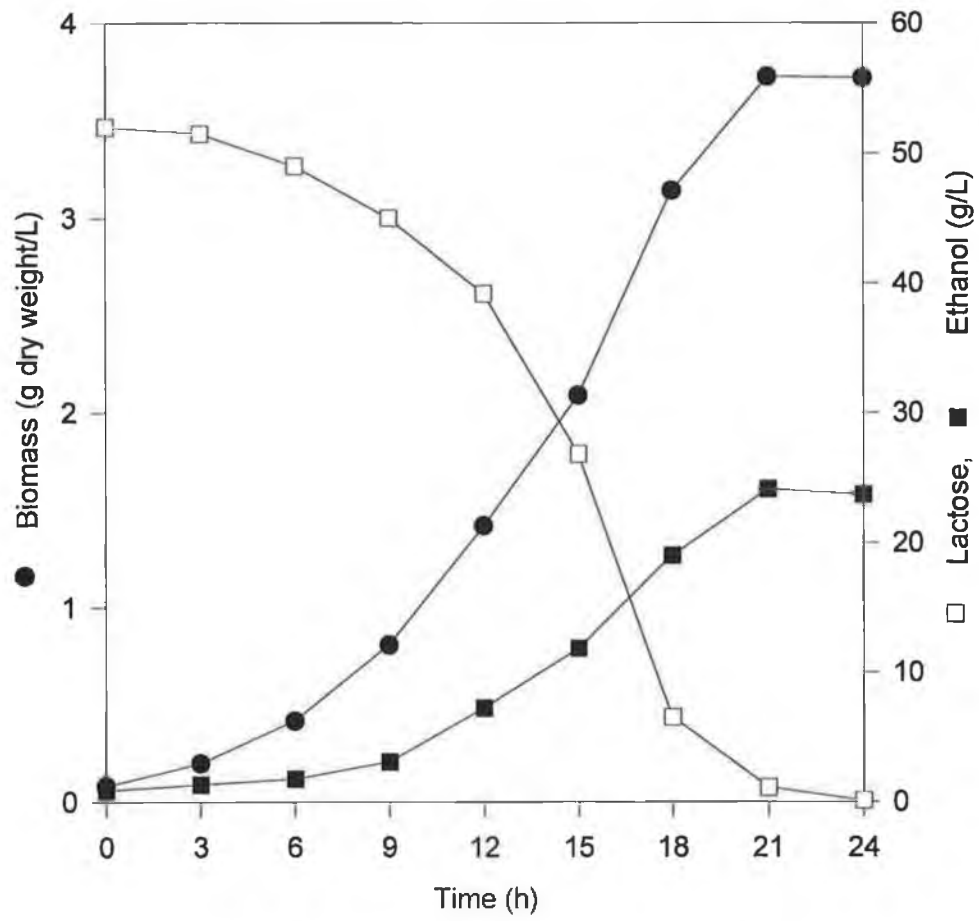


Figure 5.8 Test fermentation growth profile for *K. marxianus*

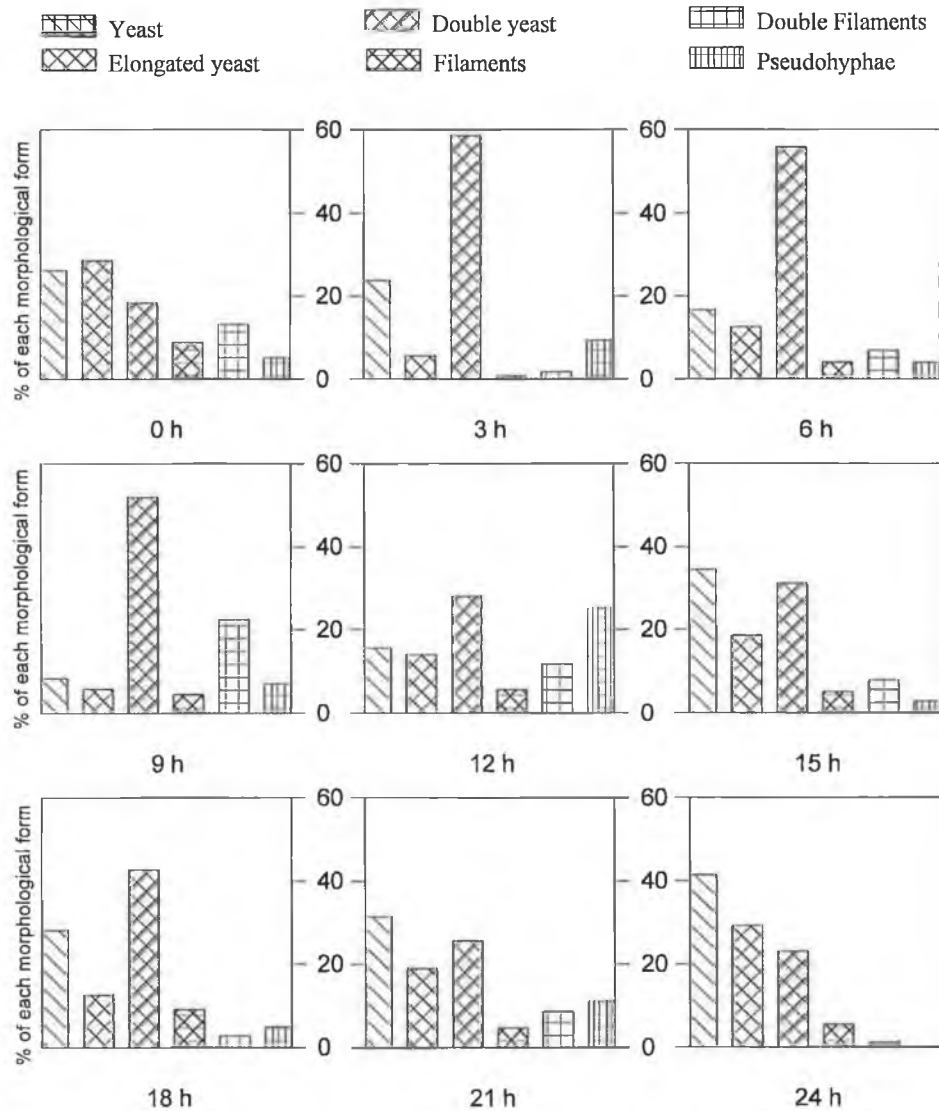


Figure 5.9 Distribution of cell morphologies during the test fermentation. Class percentages based on estimated volume fraction of each class.

The time course of the distribution of the volumes and lengths of cells is depicted in Figure 5.10. It can be seen that there is both a significant broadening of, and a modal increase in, the distribution of cell volumes in the first three hours, followed by a narrowing of, and a modal decrease in, the distribution over the remainder of the fermentation run. The pseudohyphae measured in the 12 hour sample of Figure 5.9 is seen to correspond in Figure 5.10(a) to a large number of cells whose volumes range from 100 to 250 μm^3 .

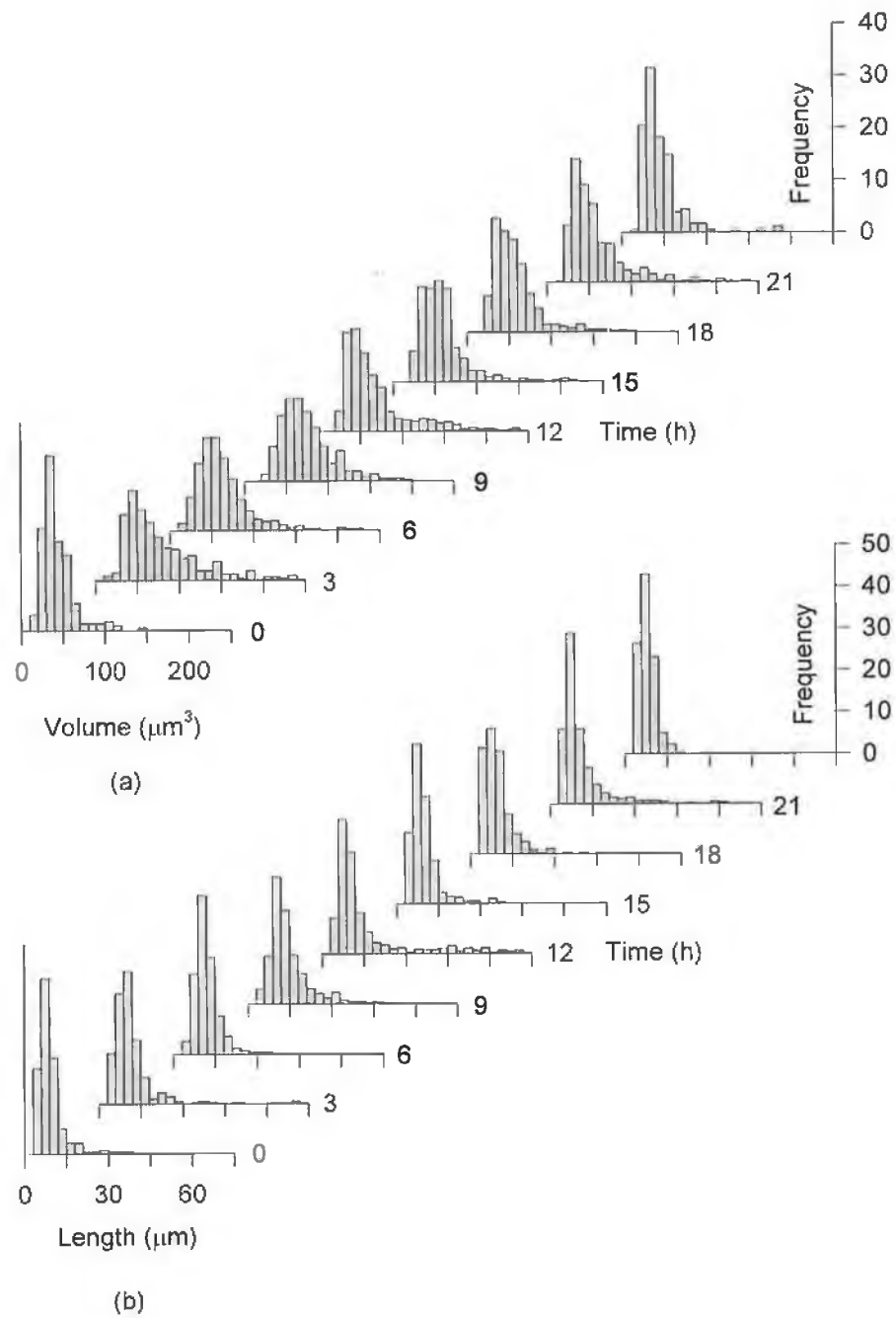


Figure 5.10 Frequency distribution of cell properties during fermentation run. (a) volume, (b) length

In Figure 5.10(b), the distribution of cell length is seen to broaden significantly during the growth phase, reflecting large numbers of pseudohyphae present at this stage. The length distribution is seen to narrow towards the latter stages of the fermentation run, with the distribution of the 24-hour sample closely resembling that of the original sample.

5.12.3 Classification Error Estimation

To check the accuracy of the automatic image analysis routine, the cells were also processed through the algorithm in such a manner that the operator was able to intervene manually and inspect the correctness of the cell classification technique. For the 12 hour sample of the test fermentation a total of 17 of the 302 cells (4.6%) were incorrectly classified due to errors in blob segmentation. The nature of these errors are detailed in Table 4.6. It can be seen, however, that two of the mistakes occurred where double cells segmented at the wrong location but where no error in categorisation took place and, in addition, a number of the other errors are self cancelling. In fact, in classification terms, there are only 8 differences between the automatic and manual categories (<3%).

5.12.4 Establishment of Suitable Sample Size

The number of cells that must be analysed is a compromise between the accuracy desired, the total time taken to analyse the sample and the amount of storage available for the images. The effect of sample size on the measured percentage of cells in each morphological category is presented in Table 5.7 for the test sample. To avoid any bias, the data for the sample was randomised each time before the first 100, 200, etc. cells were categorised. A sample size of 300 cells was determined to be sufficient in obtaining an accurate classification, at a significance level of 5%.

Table 5.6 Classification of segmentation errors made by algorithm (t = 12h)

Cell determined manually as	Cell classified by algorithm as	Count	Nature of error
Yeast	Double yeast	2	Single cell segments into two cells
Elongated yeast	Double yeast	2	"
Filament	Double yeast	2	"
Double yeast	Yeast	1	Double cell fails to segment
Double yeast	Elongated yeast	1	"
Double filament	Filament	4	Double cell segments in the wrong location
Double filament	Filament	2	"
Double yeast	Double filament	1	"
Double filament	Double yeast	2	"

Table 5.7 Effect of sample size on cell categorisation (based on cell number)

Class	Number of cells taken at random from a sample of 420 cells			
	100	200	300	400
Yeast	26%	24%	22%	21%
Elongated yeast	18%	23%	23%	23%
Double yeast	22%	22%	24%	26%
Filament	8%	9%	9%	9%
Double filament	8%	9%	8%	9%
Pseudohypha	16%	12%	14%	12%

5.12.5 Examination of Sample Processing Time

Due to the structure of the algorithm, some cells are categorised and measured quickly and others are subjected to a large number of processing operations. The effectiveness and limitations of the various components of the automatic image analysis routine can best be understood by observing the processing of a specific cell sample through the algorithm. This is demonstrated for the 12-hour sample in Table 5.8. This sample was chosen as the proportion (by cell number) of cells in any category is no less than 7% and no greater than 26%. Table 5.8 also illustrates the time taken to complete each section of the algorithm. A comparison of the relative time taken to perform an operation is probably more useful than the absolute time, as this is system dependent, and would be considerably quicker on a more powerful image analysis system.

Table 5.8 Time taken to perform the individual stages of the image analysis algorithm (t = 12 h)

Stage	Images	Unit Time	No. of cells	No. of fields	Total Time
Filter 1 (Table 5.2)	C→D	5 s/field	(45)*	6	30 s
Filter 2 (Table 5.2)	C→D	5 s/field	(96)	6	30 s
Filter 3 (Table 5.2)	C→E	5 s/field	(28)	6	30 s
Primary segmentation (<i>Segment 1</i>)	F	14 s/cell	58	----	812 s
Secondary segmentation (<i>Segment 2</i>)	F	37 s/cell	18	----	666 s
Cells sent to pseudohyphae image	F→H	37 s/cell	(27)	----	999 s
Secondary segmentation (<i>Segment 3</i>)	F	49 s/cell	1	----	49 s
Secondary segmentation (<i>Segment 4</i>)	F	49 s/cell	13	----	637 s
Cells sent to single cells image	F→G	45 s/cell	(16)	----	720 s
Single cell measurement	G	5 s/field	157	6	30 s
Branched pseudohyphae	H	41 s/cell	10	----	410 s
Unbranched pseudohyphae (Table 5.4)	H	20 s/cell	22	----	440 s
Filaments in pseudohyphae image (Table 5.4)	H	20 s/cell	11	----	220 s
Double filaments in pseudohyphae image (Table 5.4)	H	20 s/cell	12	----	240 s
Total			302		89 minutes

5.13 DISCUSSION

The bounds of filters in Table 5.2 and Table 5.3 were necessarily determined by trial and error. The primary function of these filters is to remove as many of the single cells and pseudohypha from the original image (Image C, Figure 5.7) at the earliest possible stage of the algorithm. The significance of this filtration process is evident from Table 5.8, which demonstrates that the application of the segmentation operations amounts to a large percentage of the total time. However, the upper bound of the single cell area and the lower bound of the pseudohyphal area must be chosen to minimise the number of double cells that would be incorrectly classified. The use of a perimeter/convex perimeter filter (Filter 2 of Table 5.2) was found to be very useful in avoiding the erroneous placement of double cells in the single cell image. The effectiveness of Filters 1 and 2 is demonstrated by the fact that 84% of single cells in the 12-hour sample are isolated in this manner. In addition, for the same sample, 68% of the cells in Image F ("possible" double cells) are finally classified as true double cells.

The greatest difficulties in the development of an automatic classification algorithm for the strain studied were encountered with filaments and double filaments. The lack of distinct concavity in these cells frequently resulted in their segmentation into three or more subunits at points of slight concavity. A second difficulty with the classification of filaments and double filaments was in distinguishing such cells from similar cells, typically double yeast and double elongated yeast, when relying solely on gross measures such as Feret length and Feret width. Slight curvature of filaments means that Feret width is an inappropriate measure of the mean cell width and, in the case of double filaments with an L-shaped morphology, Feret length and Feret width are both inappropriate parameters with which to estimate the true cell geometry. In addition, cells possessing such geometry tended to oversegment. The most suitable way to measure the necessary geometric parameters proved to be the skeletonisation of the cells in a manner similar to pseudohyphae. The inability to segment such filamentous forms properly necessitated an alternative means of classification, and the parameters chosen in Table 4.4 to distinguish between

filaments, double filaments and unbranched pseudohyphae were determined from measurements of a large number of cells.

The development of an automatic image analysis method to characterise a cell population containing such a wide variety of cell morphologies must involve an element of compromise. The classification system developed had to be truly automatic so that the routine could be run overnight on a range of samples from a fermentation. Some reduction in accuracy results from the use of the 200x magnification. In addition subtle differences in the boundaries of small cells are lost at the lower magnification, rendering segmentation more difficult. This is offset, however, by the increase in speed arising from the reduced number of original grey images required to perform a statistically meaningful analysis.

There is an obvious element of overlap in the categories chosen to describe the cell population. There is no sharp cut-off point between a long elongated yeast and a short filament, for instance. However, it is felt that the separation of the cells studied into seven distinct categories facilitates a good insight into the nature of the dynamic growth of a population of dimorphic cells. The image analysis method described above certainly provides a much more comprehensive picture of a fermentation than the simple reporting of populations in terms of the percentage yeast and filamentous cells (Reeslev and Jensen, 1995; Walker and O'Neill, 1990). Although the algorithm has only been tested on the strain described, it should be capable of categorising (with minimal tuning of parameters) any dimorphic strain that displays the same range of morphologies as *K. marxianus*.

Note

After a more comprehensive examination of culturing conditions it was decided to add the class double elongated yeast to the algorithm. This involved no significant changes in the above description of or testing of the algorithm, as double elongated yeast are a sub-class of the double yeast class referred to in this chapter.

CHAPTER 6

FERMENTATION KINETICS FOR BATCH AND CONTINUOUS CULTURES of *Kluyveromyces marxianus*

6.1 ETHANOL FORMATION IN YEAST FERMENTATIONS

Yeast fermentations are generally involved in the production of either biomass or ethanol from fermentable sugars such as glucose, fructose, or galactose. In a brewing process, the aim is to achieve the maximum concentration of ethanol possible while keeping biomass growth to a minimum. Whether yeast predominantly produce ethanol or biomass, is controlled by the capacities of various metabolic pathways within the cell. As sugar is taken up by the cell it enters either the glycolytic pathway or is used for raw materials in cell construction. Substrate (glucose) that enters the glycolytic pathway is converted into two pyruvate molecules. This form of metabolism results in the direct formation of two high energy ATP molecules from metabolism and the indirect formation under aerobic conditions of 4 moles of ATP from FADH_2 .

Once the glucose has been metabolised to pyruvate, the pyruvate can enter one of two kinetic pathways. The first is a short pathway whereby the pyruvate is converted to ethanol using two enzymes, namely pyruvate decarboxylase and alcohol dehydrogenase. This pathway provides no energy input to the cell and can be seen as an energy storage mechanism, as the two afore-mentioned enzymatic steps are reversible. The other option is to pass the pyruvate through a complex enzymatic pathway known as the TCA (tricarboxylic acid) pathway. This pathway requires the presence of oxygen and results in the metabolism of the pyruvate to CO_2 and H_2O with the net generation of 15 moles of ATP per mole of pyruvate. This pathway is the preferential method of metabolism of all pyruvate that passes through the cell. It requires 3 moles of O_2 per mole of pyruvate metabolised along the TCA cycle. Intermediates from both the glycolytic and TCA pathways are used in the biosynthesis of new cell materials.

A number of situations arise which result in the metabolism of pyruvate down the ethanol production pathway rather than the optimal TCA metabolic pathway. The first of these occurs when there is an insufficient supply of oxygen, preventing the

electron transport chain in the mitochondrial membrane from functioning properly. This results in a build-up of NADH in the mitochondrion and a deficit of NAD^+ . This in turn causes the TCA cycle to stop, which in turn causes a build-up of pyruvate in the cytoplasm. This build-up of pyruvate triggers the production of ethanol.

The second situation is where the ability of the yeast cell to fully metabolise the glucose to CO_2 and H_2O is compromised by a rate limiting step in the TCA cycle or in the transport of pyruvate across the mitochondrial membrane. This will result in the production of ethanol in the presence of excess carbohydrate substrate whether excess O_2 is present or not, hence the term *limited respiratory capacity* commonly used to describe this phenomenon. Limited respiratory capacity is common among yeast and it may result in the production of large quantities of ethanol in aerobic yeast culture. The location of the rate-limiting step has been debated by several authors. While Sonnleitner and Käppelli (1986) suggest that the bottleneck in metabolism lies at the start of the TCA cycle, Van Urk *et al.* (1988) propose that it is caused by the depletion of TCA cycle intermediates for amino acid synthesis and have observed the secretion of certain TCA cycle intermediates, on addition of a pulse of glucose to a glucose limited chemostat. While this finding may move the position of the bottleneck, the model of Sonnleitner and Käppelli (1986) is still the most widely accepted for the prediction of metabolism in *S. cerevisiae* (Nielsen and Villadsen, 1994).

The Sonnleitner and Käppelli model uses a simple approach which separates the metabolism of the organism into two distinct metabolic pathways; an aerobic pathway, resulting in the complete metabolism of substrate to CO_2 and H_2O , and an anaerobic pathway resulting in the metabolism of the substrate to ethanol and CO_2 . The biomass produced as a result of metabolism is calculated by associating a yield coefficient with each metabolic pathway. The flux of substrate through each metabolic pathway is controlled by a critical specific substrate uptake rate. If the substrate uptake rate for the cell is lower than the critical uptake rate then all sugars will be metabolised via the aerobic pathway whereas if the specific substrate uptake rate is higher than the critical value, then the difference between

the total uptake rate and the critical uptake rate will be metabolised via the anaerobic pathway.

Some studies have examined the metabolism of the *Kluyveromyces* species. Gonzalez Siso *et al.* (1996) observed that, irrespective of oxygen concentration, ethanol production was observed in both batch and continuous culture for the organism *Kluyveromyces lactis*. The production of ethanol in continuous culture started at a very low dilution rate of 0.1 h^{-1} . The work of Castrillo and Ugalde (1993, 1994) demonstrated that *Kluyveromyces marxianus* NCYC1424 could grow fully aerobically, if adequate supplies of oxygen are supplied. They proposed a model to predict the observed metabolic results simply based on the difference of substrate flux through the different metabolic pathways as outlined by Sonnleitner and Käppelli (1986). No morphological variation was described for this strain of *K. marxianus*.

A variation of the Castrillo and Ugalde model will be used in this work to interpret the results found for experimental fermentations. It is hoped to use this model to assess whether the organism's morphology is affected by its kinetic state or vice versa. It encompasses the following major differences from the model of Sonnleitner and Käppelli (1986).

- The organism does not suffer from a respiratory bottleneck, i.e. ethanol is not formed in oxygen saturated culture.
- Sonnleitner and Käppelli describe a specific substrate flux through the cell which dictates whether the organism develops a respiratory bottleneck or not. The flux referred to in this present work is a global substrate flux through the reactor with respect to the global utilisation of oxygen in the fermenter, as the cells' metabolism is completely controlled by the global availability of oxygen to metabolise the substrate.

6.2 MATHEMATICAL MODEL DESIGN

Chemostat fermentations operate at a steady state. This means that parameters, such as cell, substrate and product concentrations, are unchanging with respect to time.

A description of the model is as follows

- 1) Sugar is taken up by the cell
- 2) If enough oxygen is present to metabolise the sugar, then it is metabolised aerobically
- 3) If not enough oxygen is present to allow the complete aerobic metabolism of the sugar, then the excess is metabolised by anaerobic pathways
- 4) Cell yield per gram of lactose is different for aerobic and anaerobic pathways
- 5) The rate of oxygen supply to the bioreactor is constant irrespective of dilution rate
- 6) None of the ethanol produced is metabolised

The following parameters needed to be assessed to evaluate the model:

$Y_{x/s \text{ aerobic}}$ - The yield of cells per unit substrate metabolised aerobically (g cell/ g lactose)

$Y_{x/s \text{ anaerobic}}$ - The yield of cells per unit substrate metabolised anaerobically (g cell/ g lactose)

$Y_{p/s \text{ theoretical}}$ - theoretical yield of ethanol per unit substrate (g ethanol/ g lactose)

$Y_{p/s \text{ anaerobic}}$ - yield of ethanol per unit substrate metabolised anaerobically. (g ethanol/ g lactose)

$J_{s \text{ critical}}$ - The critical substrate flux at which ethanol production occurs (g lactose/h)

6.2.1 $Y_{x/s \text{ aerobic}}$

$Y_{x/s \text{ aerobic}}$ is determined by examining the non-ethanol producing regions of the dilution rate curves for all the substrate concentrations. The substrate feed concentration of 5 g/L is ideal for this purpose, as no ethanol is produced at this feed concentration over the range of dilution rates used. Figure 6.1 shows the $Y_{x/s \text{ aerobic}}$ for all 5 g/L data plus all other non-ethanol producing data points from other

runs. As can be seen a little deviation from the mean is found as dilution rate decreases below 0.2h^{-1} . This can be explained in terms of a maintenance coefficient, where the operations of the cell take precedent over cellular reproduction due to the slow growth rate and cause a decrease in the yield of cells. The regions affected by maintenance will not be addressed in this model for two reasons. The number of data points obtained in this region is small and as the model is predominantly based on actual cell metabolic pathways, maintenance is not fully understood in this context.

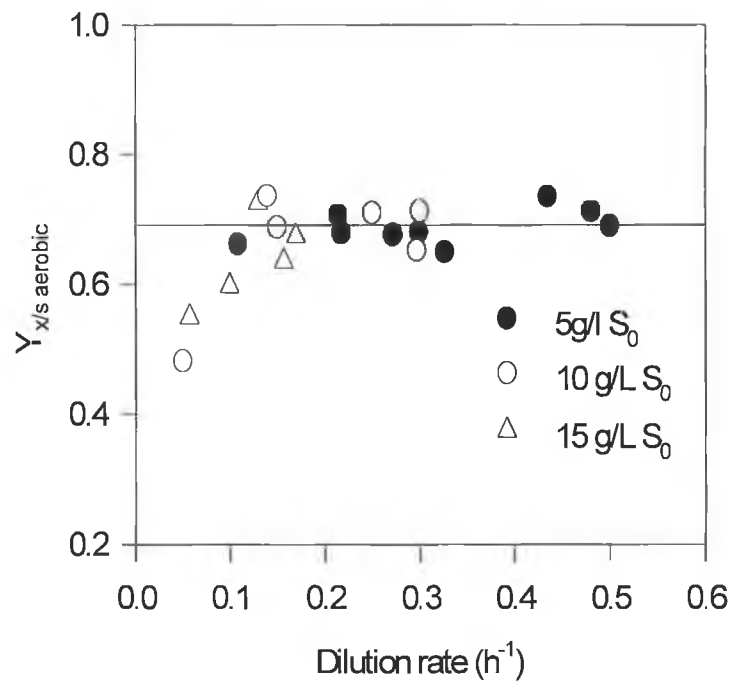


Figure 6.1 $Y_{x/s \text{ aerobic}}$ versus dilution rate for *K. marxianus* grown in lactose limited chemostat (800 rpm, 1 vvm)

The mean value of $Y_{x/s \text{ aerobic}}$ obtained for all points not affected by maintenance was $0.69 \text{ g cells/g lactose}$. This value is quite high compared to literature values. Castrillo and Ugalde (1993) determined the value at 0.54 g g^{-1} . The complex nature of the medium used in the present work compared to the above, minimises the synthesis of amino acids and other building blocks, allowing a greater fraction of the substrate to be used for energy production, resulting in a higher cell yield.

6.2.2 $Y_{p/s}$ theoretical

$Y_{p/s}$ theoretical was determined stoichiometrically from the following reaction



4 moles of ethanol are produced per mole of lactose entering metabolism. The water molecule is necessary in the equation as the lactose molecule has to be hydrolysed to glucose and galactose before it can be subsequently metabolised. On a mass basis the $Y_{p/s}$ theoretical is 0.54 g ethanol/ g lactose.

6.2.3 J_s critical

Substrate flux (J_s) refers to the quantity of substrate being utilised by the cell population per hour (g substrate/L/ h)

$$J_s = (S_0 - S) D \quad (6.2)$$

All fermentations were aerated at a rate of 1vvm. The rate of aerobic substrate metabolism should increase with increasing J_s and then remain constant when oxygen becomes limiting, the excess substrate being metabolised to ethanol. Figure 6.2 shows the effect of increasing substrate flux on ethanol production. Substrate metabolism is aerobic until substrate flux reaches a critical point ($J_{s \text{ critical}}$) where ethanol production begins. Beyond this point, the rate of ethanol production increases linearly with increasing substrate flux. The value obtained for $J_{s \text{ critical}}$ was 3.02 g lactose/L/h. It is assumed that any substrate supplied beyond this value is metabolised anaerobically.

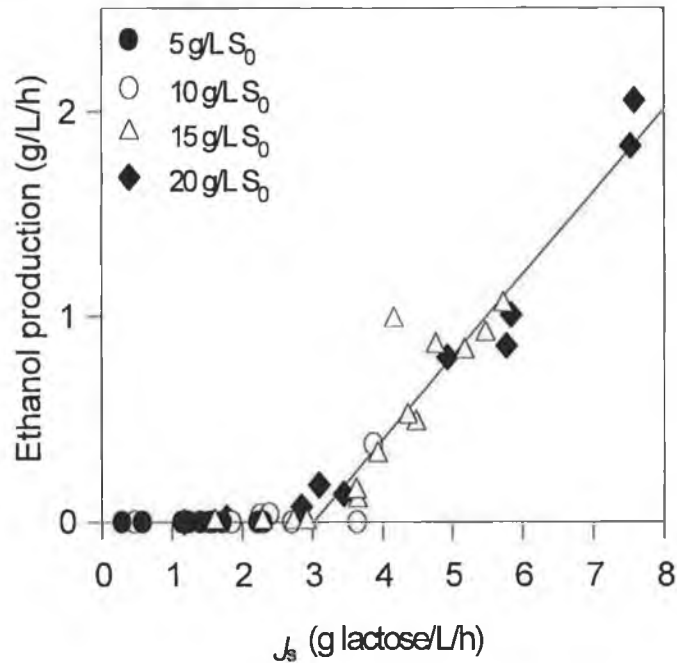


Figure 6.2 Determination of critical substrate flux for *K. marxianus* grown in lactose-limited chemostat (whey medium, 800rpm, 1vvm)

6.2.4 $Y_{p/s}$ anaerobic

When further analysis is carried out on Figure 6.2, it is possible to calculate the fraction of anaerobically metabolised lactose that is directly converted to ethanol ($Y_{p/s}$ anaerobic). The yield of ethanol per gramme of anaerobically metabolised lactose is 0.403g ethanol/g lactose. The theoretical yield is 0.54 g ethanol/ g lactose. Thus the organism is converting 74% of anaerobically metabolised sugars to ethanol. The fraction of anaerobically metabolised substrate used for energy production will be represented by F_{ae} (=0.74). This value of F_{ae} is similar to the value calculated from the data of Castrillo and Ugalde (0.7). The rest of the sugar is used as raw material to construct biomass.

6.2.5 $Y_{x/s}$ anaerobic

$Y_{x/s}$ anaerobic was calculated by determining the amount of aerobically produced biomass ($X_{aerobic}$) using the following equation.

$$DX_{aerobic} = \text{Min}(J_s Y_{x/s_{aerobic}}, J_{s_{critical}} Y_{x/s_{aerobic}}) \quad (6.3)$$

By subtracting X_{aerobic} from X_{total} , the amount of anaerobically generated biomass ($X_{\text{anaerobic}}$) was determined.

$$X_{\text{anaerobic}} = X_{\text{total}} - X_{\text{aerobic}} \quad (6.4)$$

$Y_{\text{x/s anaerobic}}$ was determined by dividing $X_{\text{anaerobic}}$ by the quantity of sugar going through anaerobic metabolism.

$$J_{\text{s anaerobic}} = \text{Max}(0, J_{\text{s}} - J_{\text{s critical}}) \quad (6.5)$$

$$Y_{\text{x/s anaerobic}} = \frac{DX_{\text{anaerobic}}}{J_{\text{s anaerobic}}} \quad (6.6)$$

Considerable scatter was found using this determination due to the small value for this constant compared to the error in the determination of ethanol, lactose and biomass. $Y_{\text{x/s anaerobic}}$ was estimated to be approximately 0.1 g cells/ g lactose. Sonnleitner and Käppeli (1985) showed that this value was in the range of 0.05-0.1 g cells/ g glucose for *S. cerevisiae*. It is also possible to compare this value to the value of g biomass/ mol ATP value of Barford (1990a,b). Theoretically, the metabolism of 1 mole of lactose for the formation of ethanol will result in the formation of 4 moles of ATP. Thus, at a $Y_{\text{x/s anaerobic}}$ of 0.1g/g and assuming 74% is metabolised yielding 4 moles of ATP per mole lactose, a value of 11.4 g biomass/ mol ATP is found. This compares to Barford's value of 10.5 g biomass/ mol ATP for the majority of yeast strains examined in that work.

Table 6.1. Constants used in model

Constant	Value
$Y_{\text{x/s aerobic}}$	0.69 g cell/ g substrate
$Y_{\text{x/s anaerobic}}$	0.10 g cell/ g substrate
$Y_{\text{p/s anaerobic}}$	0.403 g ethanol/ g substrate
$Y_{\text{p/s theoretical}}$	0.54 g ethanol/ g substrate
$J_{\text{s critical}}$	3.02 g substrate/L/hour

6.2.6 Substrate Uptake

It was assumed that substrate uptake into the cell could be described using the simple Monod model, however, when the data for residual substrate was examined there was an increase in S at any dilution rate, with increasing S_0 . As described in Chapter 3 the chemostat employed was based on a weir system, where feed is added to the surface of the liquid and overflow is also removed from the surface of the liquid. Due to previously undescribed variability in k_s with increasing S_0 , the potential of a mixing problem being present in the reactor was investigated.

If a mixing problem exists in the reactor the system can be treated as a reaction vessel with a bypass line. The bypass line feeds into the output from the reactor as described in Figure 6.3.

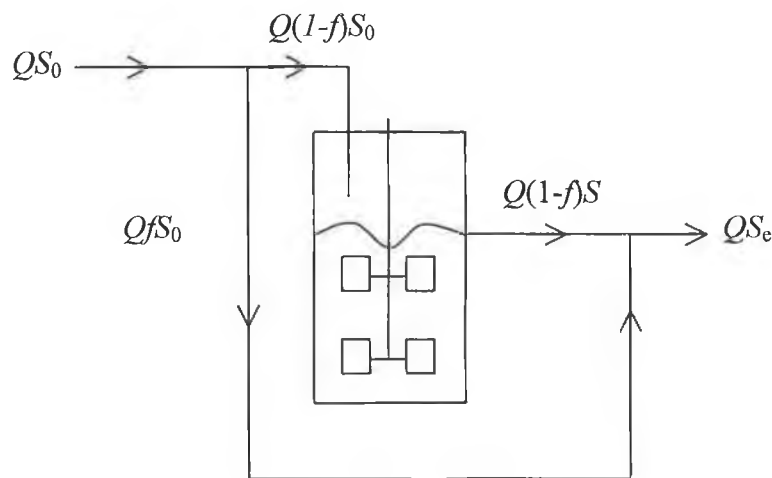


Figure 6.3 Schematic of the proposed mechanism for substrate bypass of the reactor

A mass fraction (f) of the overall feed flow Q is observed to bypass the reactor with the remaining fraction $(1-f)$ entering the reactor. The exit substrate concentration S_e is generated by combining the bypass stream and the exit stream with substrate concentrations of S_0 and S respectively. A mass balance on the above system yields the following equation

$$QfS_0 + Q(1-f)S = QS_e \quad (6.7)$$

rearrangement of Equation 6.7 yields

$$S = \frac{S_e - fS_0}{1-f} \quad (6.8)$$

Assuming Monod kinetics for substrate uptake within the reactor

$$\mu = \frac{\mu_m S}{k_s + S} \quad (6.9)$$

Substituting equation 6.8 into 6.9 yields

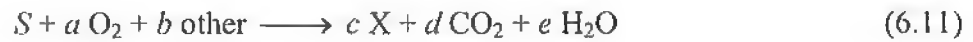
$$\mu = \frac{\mu_m (S_e - fS_0)}{(1-f)k_s + S_e - fS_0} \quad (6.10)$$

Observation of the data suggests that μ_m is approximately 0.5h^{-1} . The above equation thus contains two unknowns, f and k_s . The unknowns were estimated by curve-fitting the experimental data using the least squares method on Sigmaplot (Jandel Scientific, USA). The values for the constants used are presented in Table 6.2.

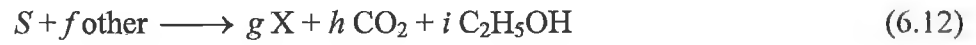
Table 6.2. Constants required to calculate the residual substrate curves

Constant	Value
μ_m	0.5 h^{-1}
k_s	0.036 g/L
F	0.034

Once the sugar enters the cell then it is either used to generate biomass by oxidative pathways or by oxido-reductive pathways. Aerobic metabolism can be summarised by the following equation



If a moles of oxygen are not provided, per mole of sugar, to the cell, the remainder will be metabolised anaerobically by the following pathway.



Therefore to predict the quantity of biomass the following equations are required,

$$D X_{\text{aerobic}} = \text{Min}(J_s, J_{s \text{ critical}}) Y_{x/s \text{ aerobic}} \quad (6.13)$$

$$D X_{\text{anaerobic}} = \text{Max}(0, J_s - J_{s \text{ critical}}) Y_{x/s \text{ anaerobic}} \quad (6.14)$$

$$X_{\text{total}} = X_{\text{aerobic}} + X_{\text{anaerobic}} \quad (6.15)$$

The amount of ethanol present is estimated by Equation 6.16.

$$D P_{(\text{ethanol})} = \text{Max}(0, J_s - J_{s \text{ critical}}) \cdot Y_{p/s \text{ anaerobic}} \quad (6.16)$$

6.2.7 Implementation of Model

The model was implemented using the following series of steps. The model was calculated using a Sigmaplot™ transform.

- 1) Select S_0
- 2) Calculate residual substrate concentrations for fermentation using Equation 6.10 and the model constants from Table 6.2.
- 3) Calculate J_s curve for data at 0.01 intervals using Equation 6.2.
- 4) Calculate biomass and ethanol traces using Equations 6.13-6.16.

6.2.8 Examination of model sensitivity

Figures 6.4 to 6.7 illustrate model sensitivity to different values of model parameters. When the parameters are not being varied, their values are as in Table 6.2 and S_0 is set at 20g/L. Variation in each model parameter by less than or equal to an order of magnitude causes large changes in at least one of the predicted parameters. While variation in the f constant does not significantly affect the resultant biomass and ethanol predictions, it is necessary to describe the residual substrate traces experienced in Figures 6.8 to 6.11.

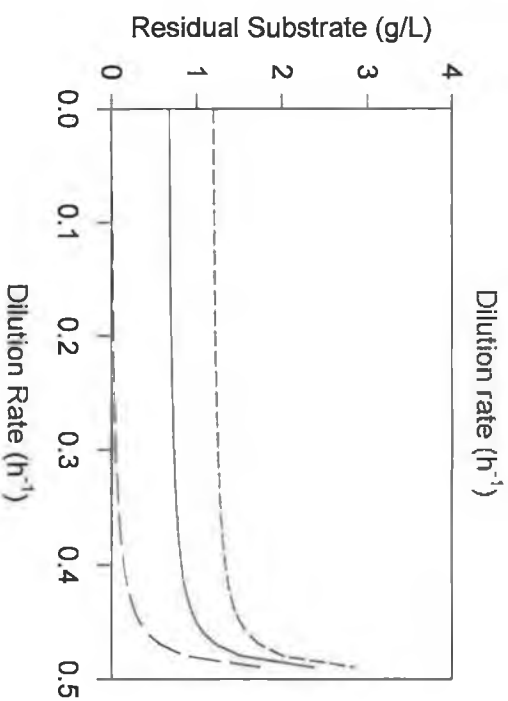
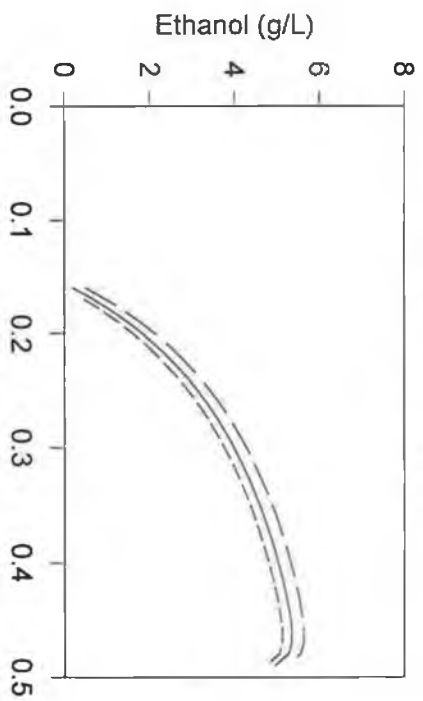
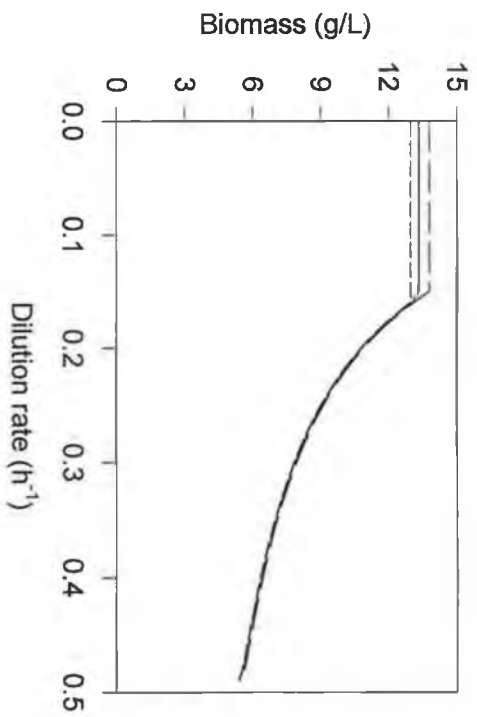


Figure 6.4 Sensitivity analysis on model parameter f ; long dash ($f=0.0$), solid line ($f=0.034$), short dash ($f=0.06$).



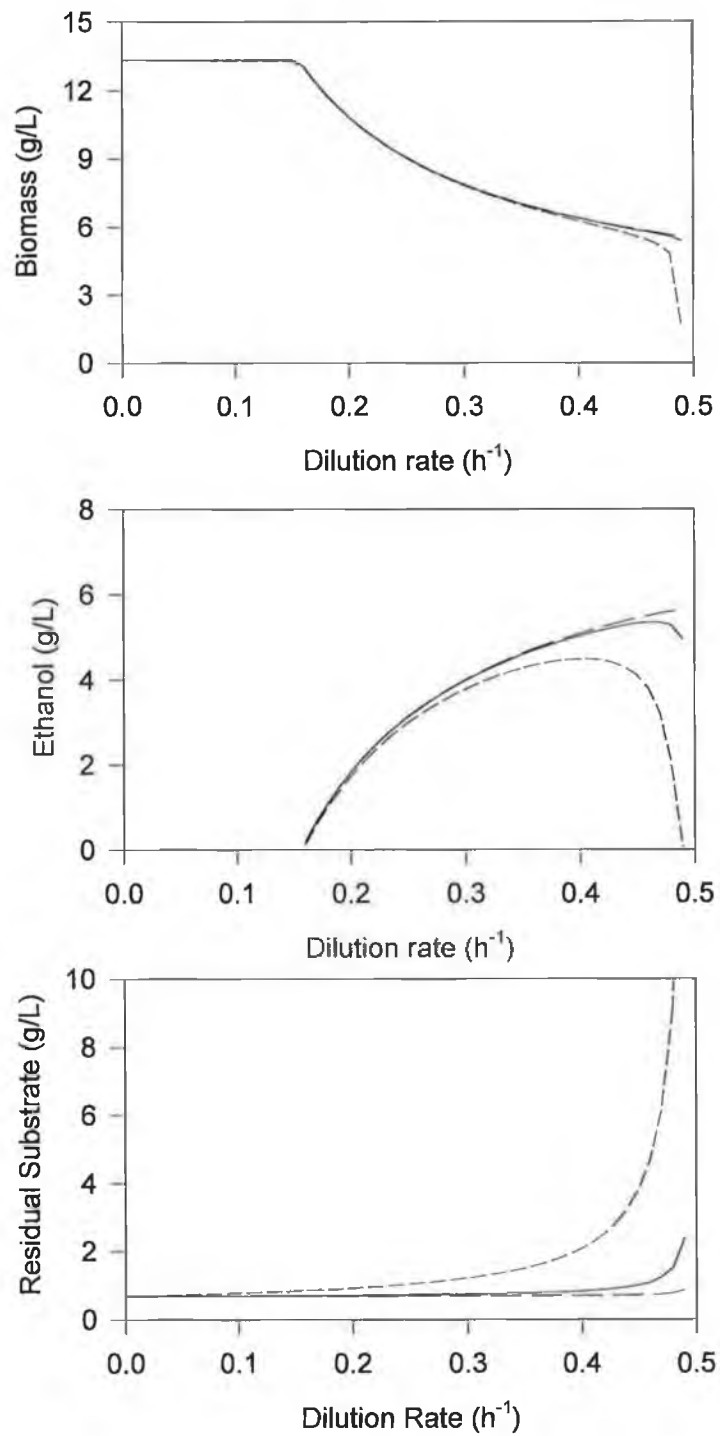


Figure 6.5 Sensitivity analysis on model parameter k_s ; long dash ($k_s = 0.0036$), solid line ($k_s = 0.036$), short dash ($k_s = 0.36$).

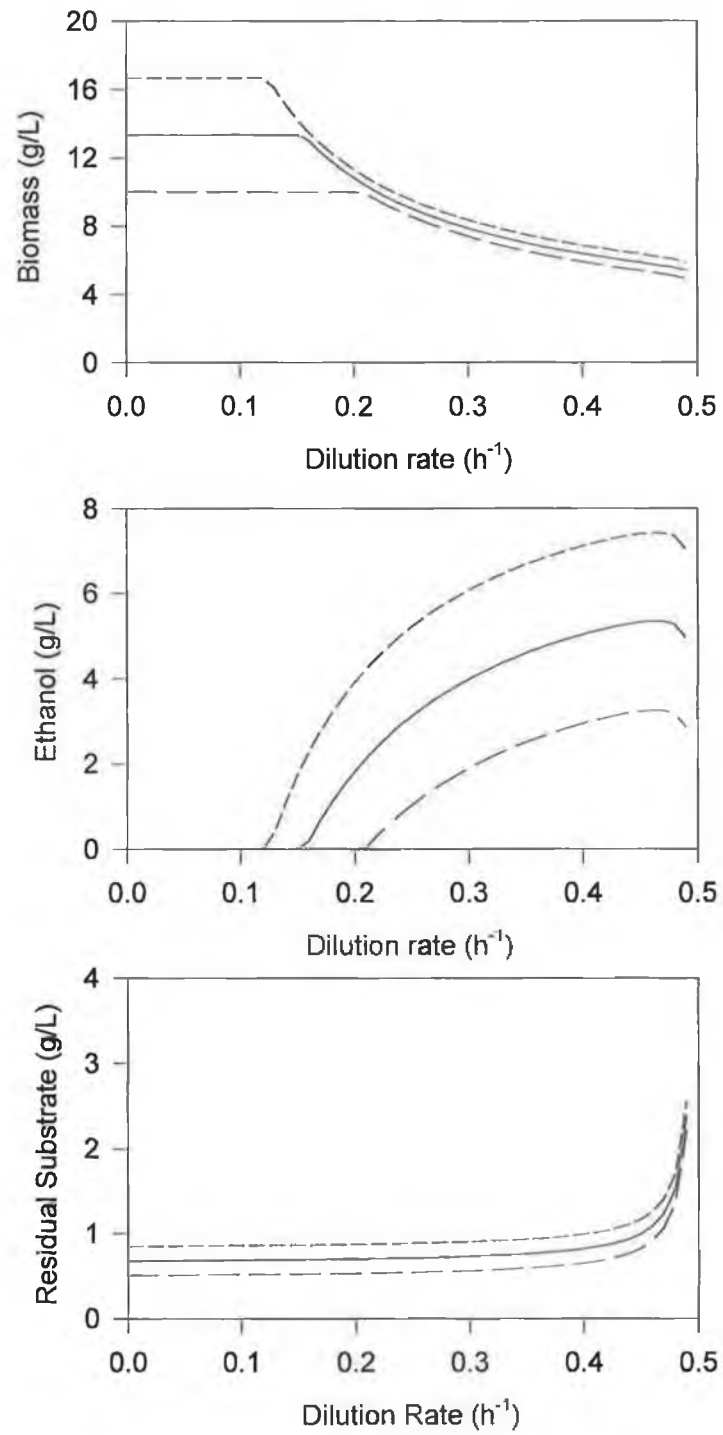


Figure 6.6 Sensitivity of model to variation in S_0 ; long dash ($S_0 = 15g/L$), solid line ($S_0 = 20g/L$), short dash ($S_0 = 25g/L$).

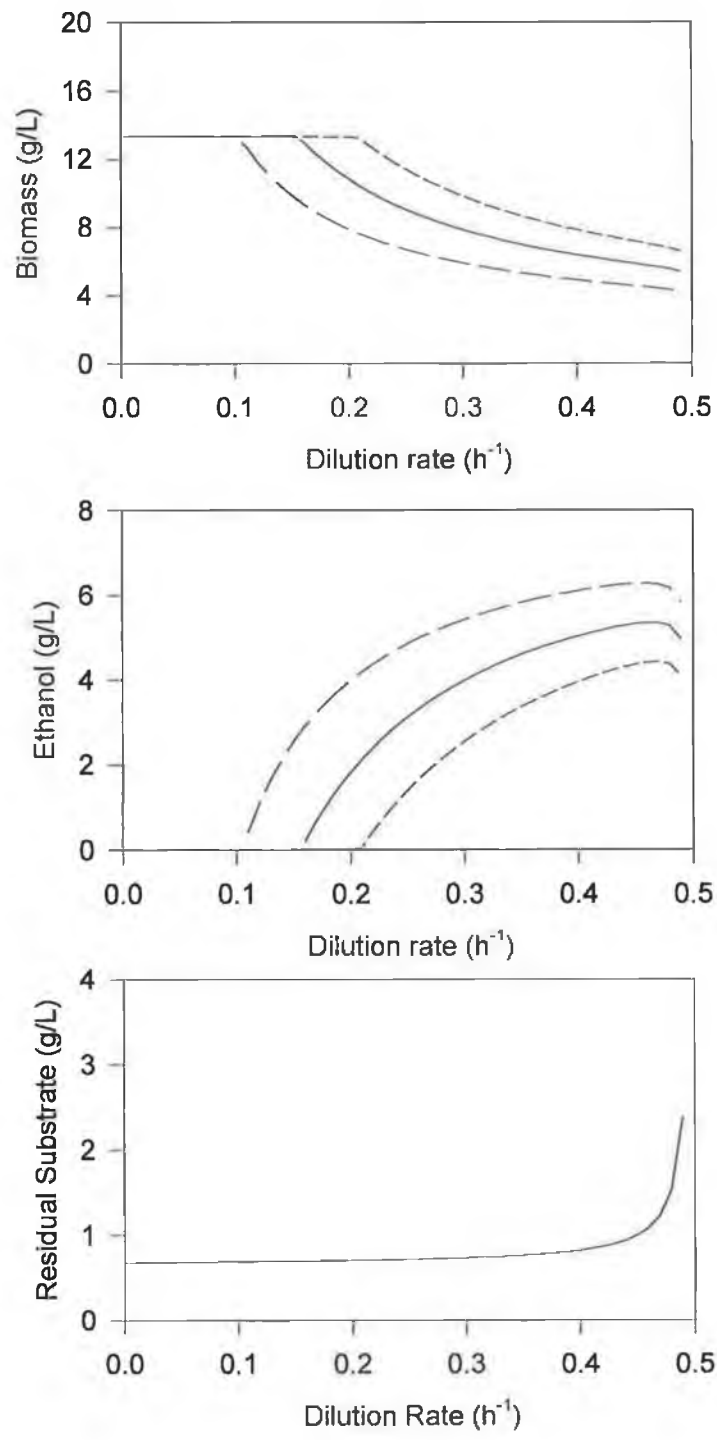


Figure 6.7 Sensitivity analysis on model parameter J_s ; long dash ($J_s = 2.02\text{g/L/h}$), solid line ($J_s = 3.02\text{g/L/h}$), short dash ($J_s = 4.02\text{g/L/h}$).

6.2.9 Adaptation of Model to Batch Culture Growth

Batch culture by its nature is dynamic, thus requiring a series of differential equations based on the above steady state model. The following additional steps are necessary in a batch culture.

- 1) The specific rate of substrate uptake is uncontrolled in batch culture. In chemostat this step can be ignored as substrate is consumed as quickly as it enters the fermenter.
- 2) The rate of oxygen supply is varying to the fermenter. To successfully model this process a relationship between a parameter such as $k_L a$ and metabolism will need to be established

It was decided to examine whether significant differences exist in the stoichiometry of cell populations grown in batch and continuous culture. It is possible to estimate the substrate trace for each fermentation, using the model constants determined from chemostat studies. The following procedure was adapted.

The amount of biomass generated as a direct result of ethanol formation was estimated using the following relationship

$$X(t)_{\text{anaerobic}} = \frac{P(t)}{Y_{p/s \text{ anaerobic}}} Y_{x/s \text{ anaerobic}} \quad (6.17)$$

Once this has been calculated, $X(t)_{\text{anaerobic}}$ is subtracted from the total measured biomass (along with X_0). The remainder is the amount of biomass formed as a result of aerobic fermentation $X(t)_{\text{aerobic}}$. The total sugar remaining in the fermentation at the time of examination is.

$$S(t) = S_0 - \left(\frac{X(t)_{\text{aerobic}}}{Y_{x/s \text{ aerobic}}} + \frac{X(t)_{\text{anaerobic}}}{Y_{x/s \text{ anaerobic}}} \right) \quad (6.18)$$

Figures 6.12 to 6.15 and Figures 6.18 to 6.21 illustrate the relationship between $S_{\text{predicted}}$ and $S_{\text{experimental}}$ determined using the DNS assay for both whey

fermentations and YEPD and YEPL fermentations. A good relationship between the measured and the experimental data is observed in all cases.

6.3 INTRODUCTION TO EXPERIMENTAL WORK

The importance of microbial physiology in determining the morphology of organisms was illustrated in Chapter 2. Varying fermentation parameters such as agitation and aeration considerably alters yeast physiology. To relate morphology to fermenter parameters requires the completion of well-characterised fermentations. Parameters required to be measured in typical yeast fermentations include, biomass concentration, residual substrate concentration, ethanol concentration, dissolved oxygen concentration, pH and off gas analysis of CO₂ and O₂.

The following series of continuous and batch fermentations are presented to allow greater insight into the physiology responsible for the morphology reported in Chapter 7. The model presented in Section 6.2 also allows the reader an insight into the kinetic workings of the organism and highlights some interesting phenomena which have not been previously described for this strain of yeast, growing on whey based media.

6.4 CHEMOSTAT CULTURE RESULTS

6.4.1 Overview of Kinetic Data

As can be seen from Figures 6.8 – 6.11, changing substrate feed concentration greatly affects the metabolism of the organism. At low dilution rates significant differences in biomass concentration for different feed concentrations are observed. Ethanol production ensues at different dilution rates for each substrate concentrations. For the 5g/L feed (Figure 6.11) concentration there is no ethanol production at any dilution rate. These experimental results suggest that the organisms' metabolism lacks a limited respiratory capacity. It is apparent that biomass concentration is reduced as the dilution rate passes the point at which ethanol production begins. Very little substrate remains in the effluent

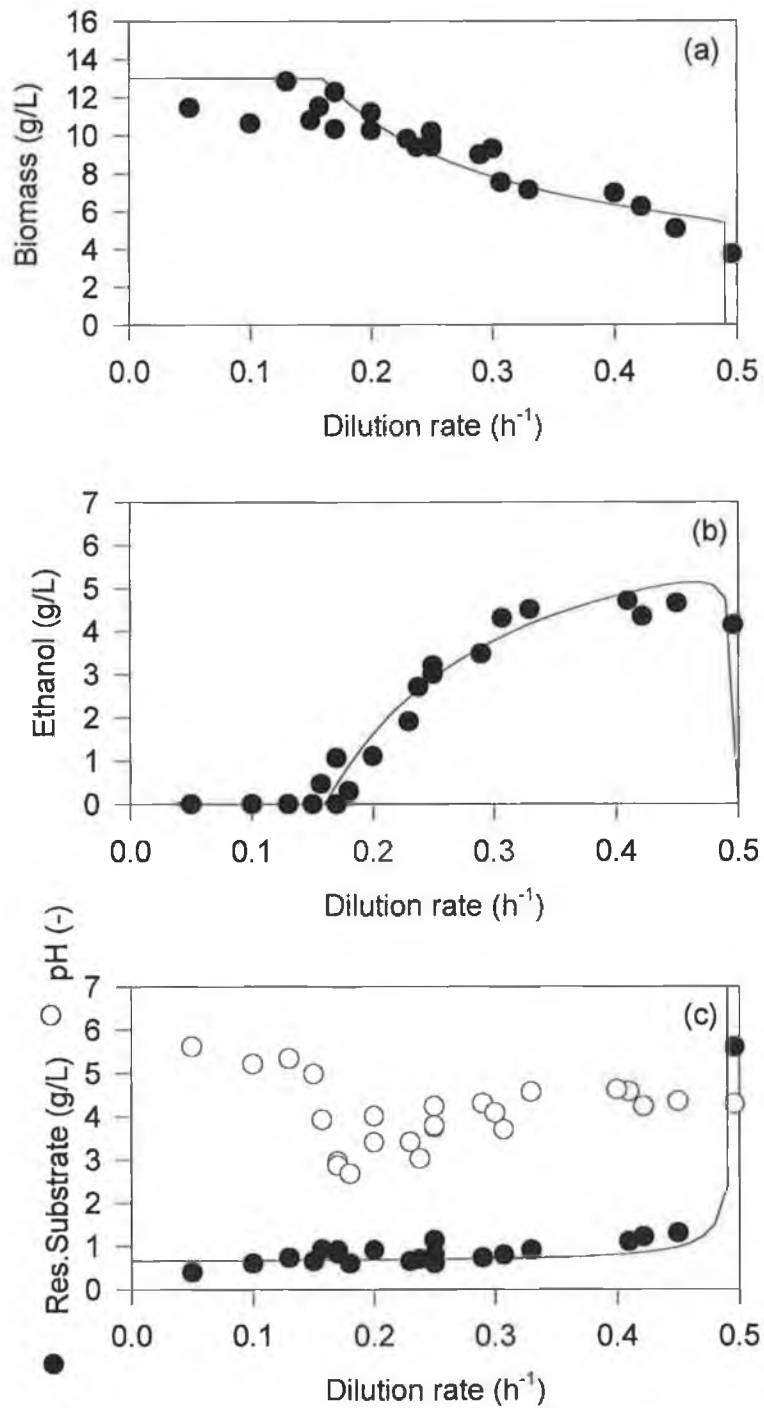


Figure 6.8. Chemostat fermentation 1-Kinetic overview of 20g/L run (a) biomass (b) ethanol (c) residual substrate and pH. Solid lines - model prediction of data ($S_0 = 19.5$ g/L).

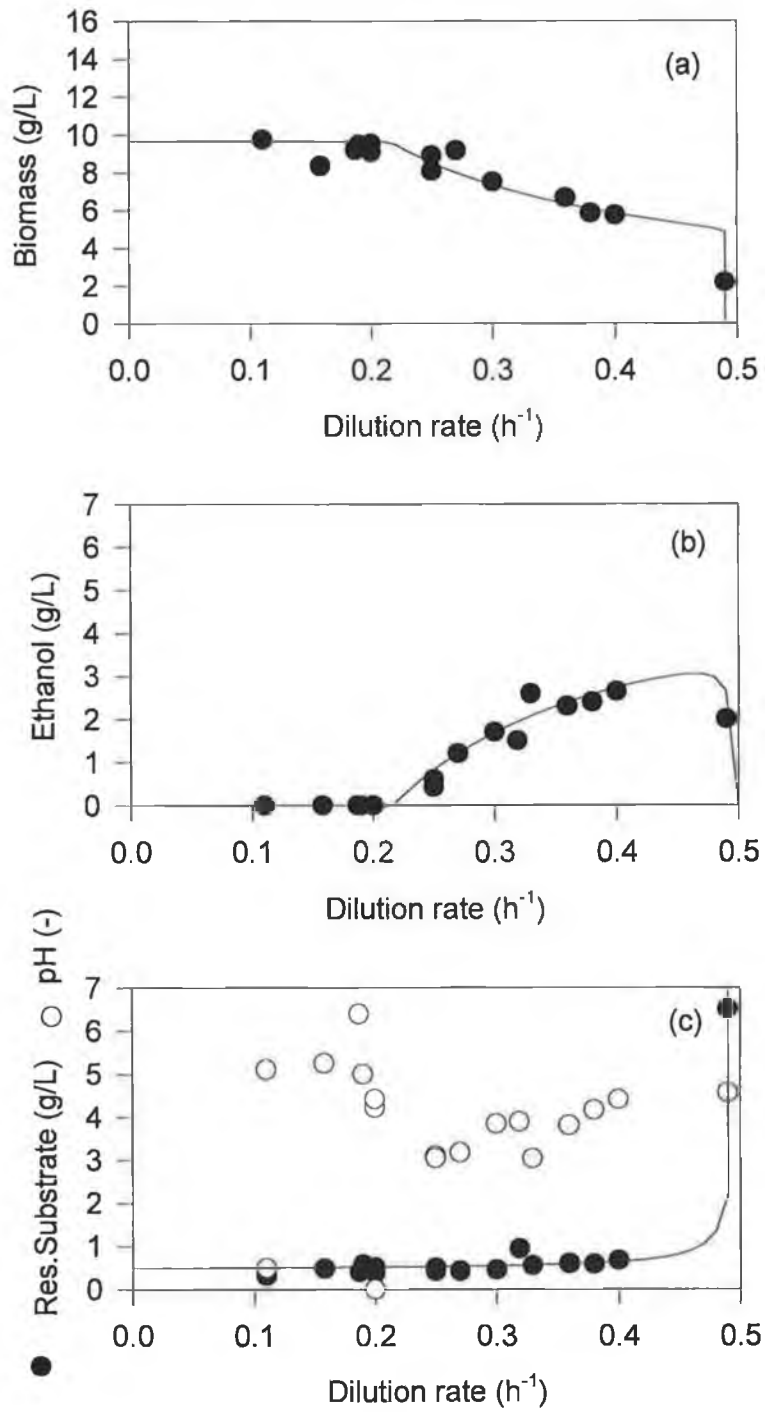


Figure 6.9. Chemostat Fermentation 2 - Kinetic overview of 15g/L run (a) biomass (b) ethanol (c) residual substrate and pH Solid lines - model prediction of data ($S_0 = 14.5$ g/L)

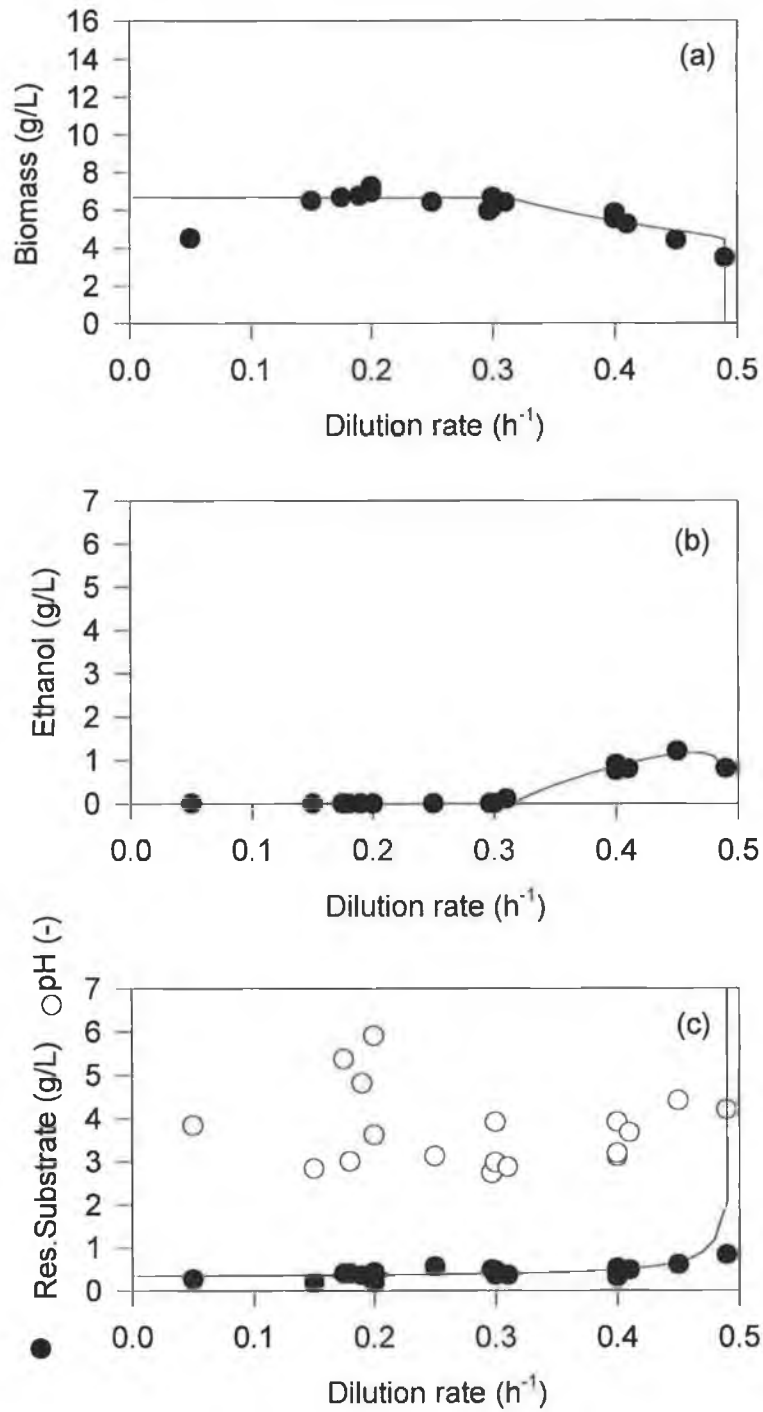


Figure 6.10. Chemostat fermentation 3 - Kinetic overview of 10g/L run (a) biomass (b) ethanol (c) residual substrate and pH. Solid lines - model prediction of data ($S_0 = 10.0$ g/L)

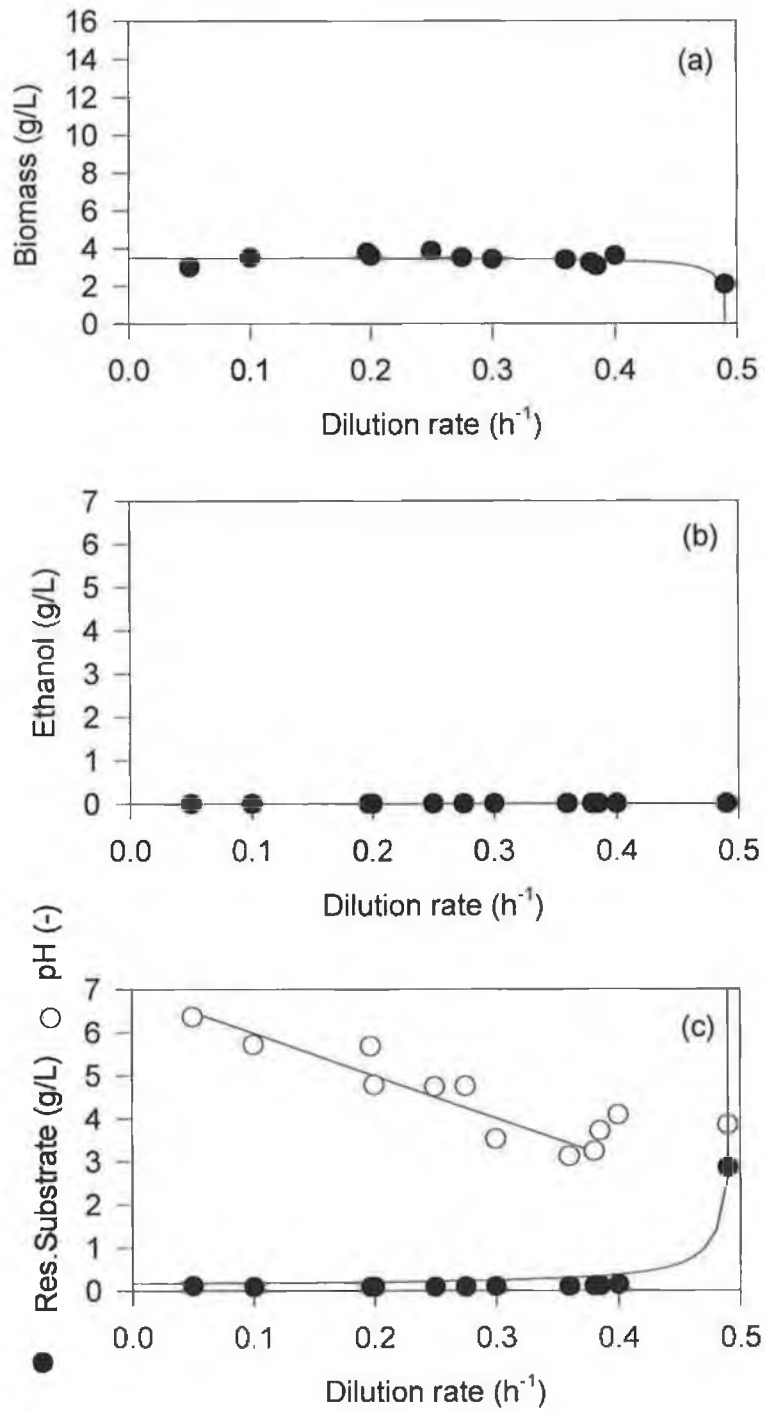


Figure 6.11. Chemostat Fermentation 4 - Kinetic overview of 5g/L run (a) biomass (b) ethanol (c) residual substrate and pH. Solid lines - model prediction of data ($S_0 = 5.2$ g/L).

stream indicating that the chemostat is lactose limited for all substrate feed concentrations. The critical dilution rate (dilution rate at which cell washout occurs with D surpassing μ_m) was observed to be approximately 0.5h^{-1} . Broth pH varies significantly over the range of dilution rates and substrate feed concentrations studied. This variation appears to be related to whether the culture is producing ethanol or not. In cultures that produce ethanol there is a sudden drop in the pH at the onset of ethanol production. This is thought to be due to the increased concentration of dissolved CO_2 associated with ethanol fermentation.

Considerable scatter was observed in the data for the 20g/L fermentation in the region of $D= 0.2\text{ h}^{-1}$. Broths in this region appear highly viscous in nature (see Figure 7.19) and this is thought to be due to a combination of high biomass and viscosity. This will be discussed in greater detail in Chapter 7.

The model data are observed to describe experimental data well over the range of S_0 examined.

6.5 BATCH CULTURE RESULTS

6.5.1 Overview of Whey-Based Batch Culture Studies

Figures 6.12 to 6.15 show the kinetic data for fermentations completed in batch culture on whey media over a variety of agitation speeds. The range of agitation speeds used in the experimental work, allowed a considerable variation in k_La (a factor of 10) of the range of the fermentations (Table 6.3).

The results obtained suggest that *Kluyveromyces marxianus* var. *marxianus* NRRLy2415 will not produce ethanol if excess oxygen is present. This is unusual among yeast and contradicts the theory of a limited respiratory capacity, (Sonnleitner and Käppelli, 1986; Barford, 1990a,b). As the k_La decreases, the yield of biomass drops in conjunction with an increase in the yield of ethanol.

These fermentations were completed to achieve a considerable variation in growth conditions. This has been successfully completed as the 800rpm fermentation is predominantly aerobic with little ethanol production and the 200rpm fermentation is predominantly ethanol producing with a low final biomass concentration. The

dashed line in each of the batch fermentation plots is that of the stoichiometric prediction discussed in Section 6.2.9.

Table 6.3 The effect of agitation on k_{La} in 10L batch whey fermentations

Agitation (rpm)	k_{La} (h^{-1})
800	0.0427
400	0.0182
300	0.0100
200	0.0048

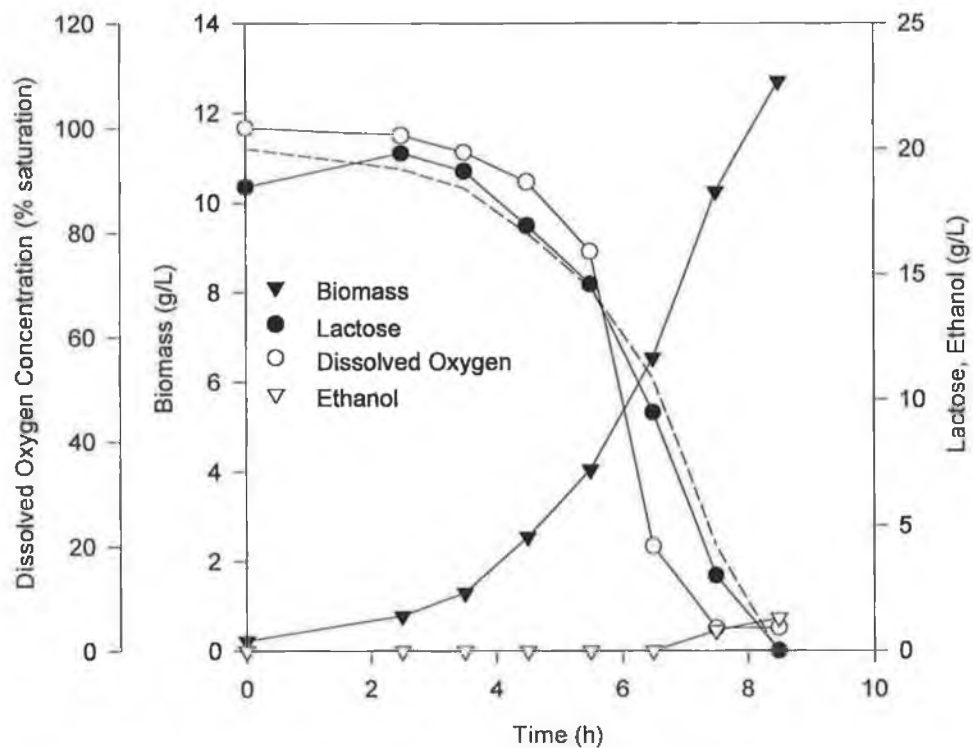


Figure 6.12 Batch Fermentation 1 – 800rpm, 1vvm whey medium. Broken Line – stoichiometric prediction for substrate concentration

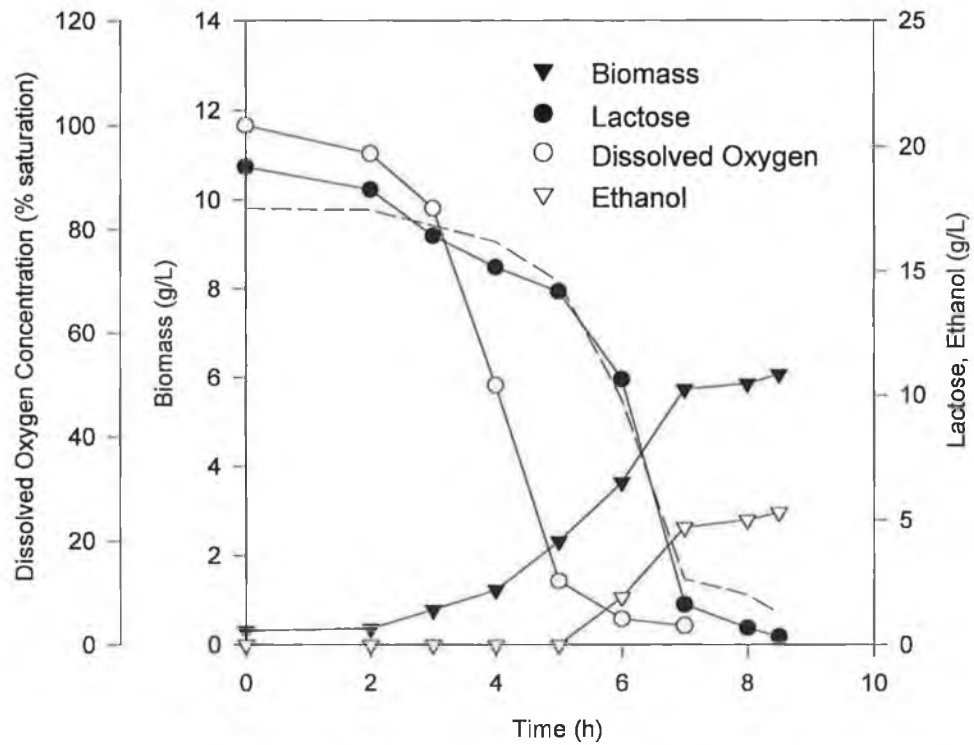


Figure 6.13 Batch Fermentation 2 – 400rpm, 1vvm whey medium. Broken Line – stoichiometric prediction for substrate concentration

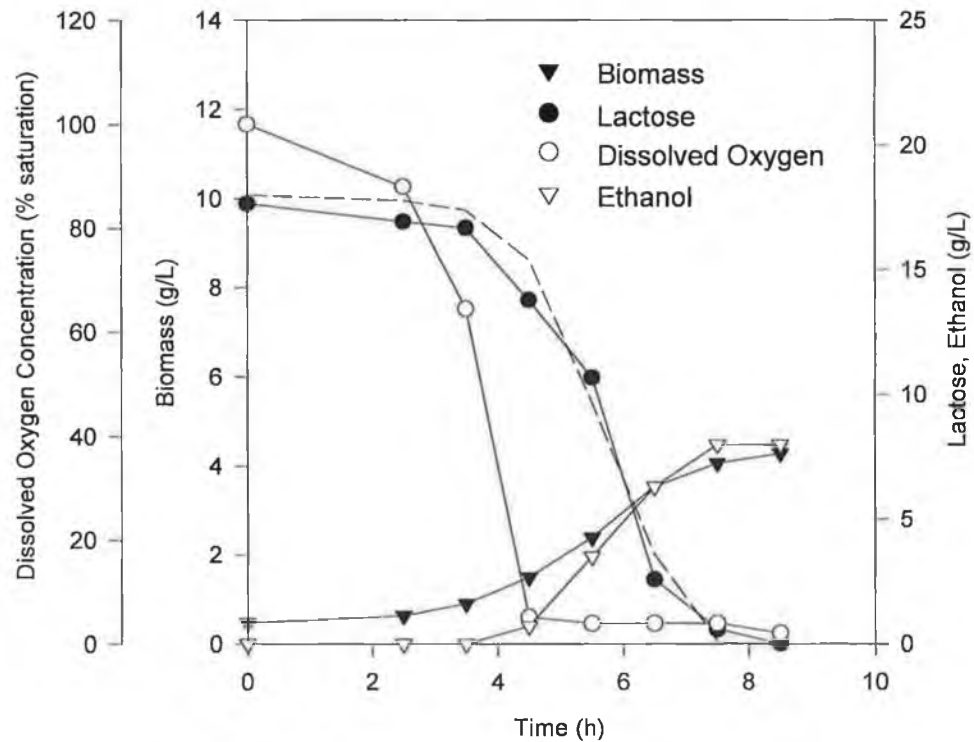


Figure 6.14 Batch Fermentation 3 – 300rpm, 1vvm whey medium. Broken Line – stoichiometric prediction for substrate concentration

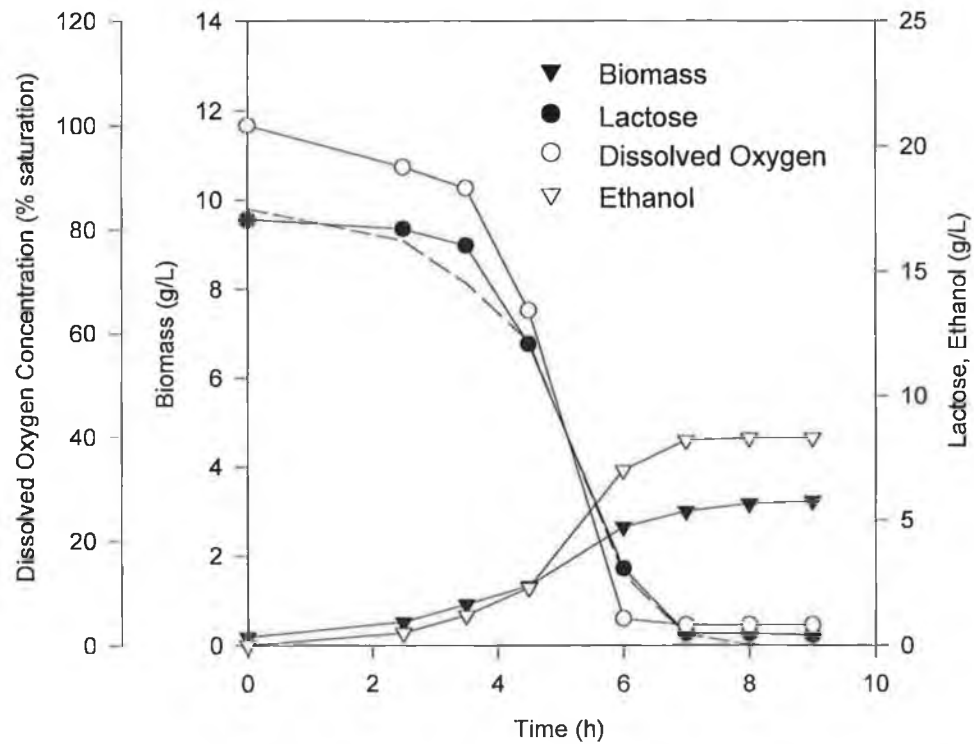


Figure 6.15 Batch Fermentation 4 – 200rpm, 1vvm whey medium. Broken Line – stoichiometric prediction for substrate concentration

6.5.2 Substrate Uptake Rates

All fermentations were completed in approximately the same amount of time (with respect to lactose consumption). As biomass concentrations varied significantly between fermentations therefore the specific uptake rates also vary in these fermentations.

Calculation of Specific Uptake Rates (R_s)

Specific substrate uptake rates were estimated from the model predictions of substrate concentrations as experimental data were too scattered to attempt such calculations. R_s was estimated by taking the mean biomass concentration over a short interval and dividing it into the difference in substrate uptake in the same time interval.

$$R_s = \frac{\Delta S}{\Delta X} \frac{1}{\Delta t} \quad (6.19)$$

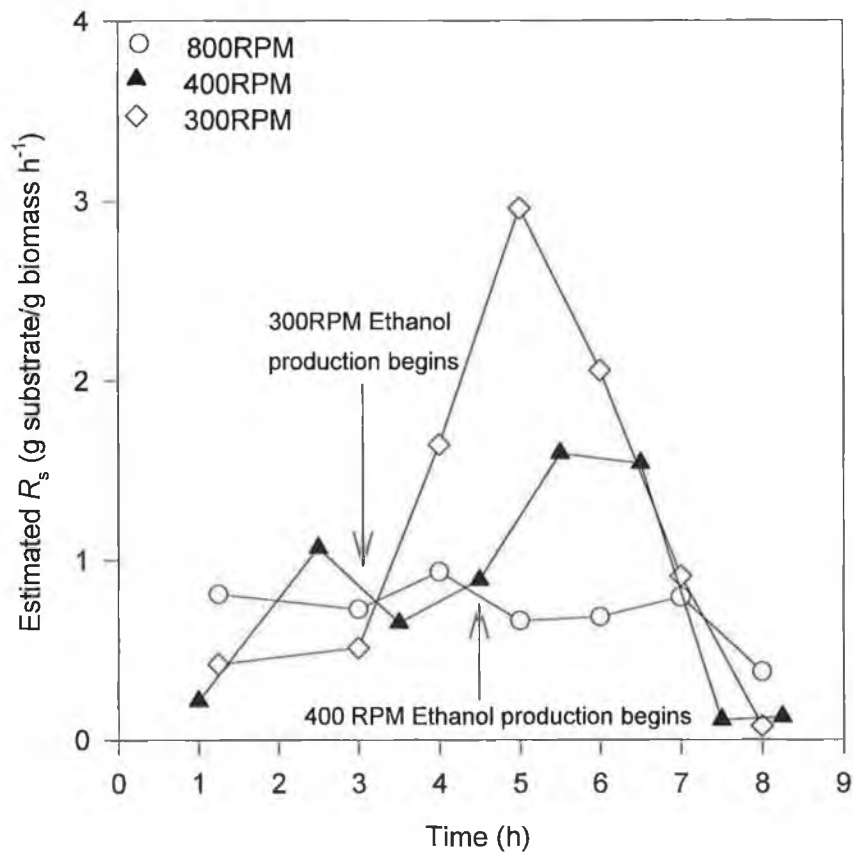


Figure 6.16 Estimated specific substrate uptake rates (R_s) vs. time for whey fermentations

Figure 6.16 shows the findings for three of the whey fermentations. R_s is seen to rise significantly after initiation of ethanol formation. This is possibly due to competitive substrate uptake that declines as the rate of new biomass production decreases. Such substrates are required less when the cells become oxygen limited thus opening more channels for the diffusion of substrate into the cell. More likely is the possibility that the glycolytic step,



catalysed by the enzyme, phosphofructokinase is impaired during aerobic growth. The enzyme, phosphofructokinase, is allosteric and is activated by ADP and P_i and deactivated by ATP. This results in the slowing down of the enzymatic step in regimes of high ATP/ADP ratios. During fully aerobic metabolism this is usually the case. As the rate of aerobic metabolism decreases, the rate of sugar uptake

increases. The cell requires significantly larger amounts of substrate fluxing through the glycolytic pathways, to maintain an equivalent ATP/ADP ratio thus the rate of reaction is increased accordingly (Shuler and Kargi, 1992). This will result in an overall increase in the specific substrate uptake rate, followed by a subsequent increase in the rate of glycolysis.

6.5.3 The Effect of $k_L a$ on $J_{s \text{ critical}}$

Figure 6.17 shows the effect of $k_L a$ on the critical substrate flux at which ethanol production begins. It is apparent that $k_L a$ controls ethanol production and any model developed to describe batch culture growth would have to address this finding.

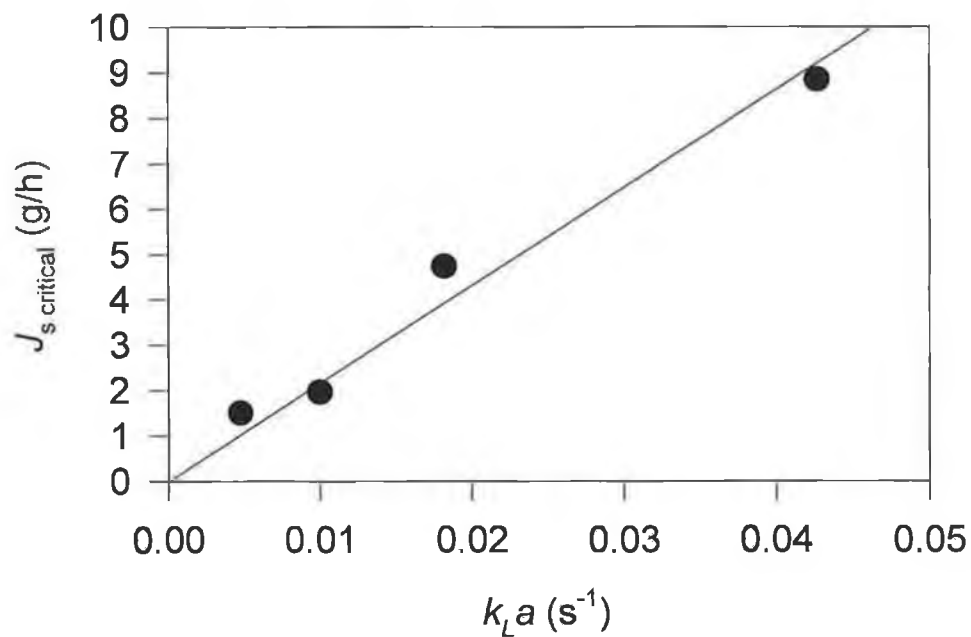


Figure 6.17 The effect of $k_L a$ on $J_{s \text{ critical}}$ in whey media batch culture

6.5.4 Overview of YEPD and YEPL Batch Fermentations

YEPD and YEPL based fermentations were carried out in order to compare the effect of medium alteration on the morphology of the organism. The fermentations behave similarly to the previous whey fermentations, showing similar trends in ethanol production and dissolved oxygen concentration. The results of the fermentations are displayed in Figures 6.18 to 6.21. The dashed lines on these plots represent stoichiometric predictions for residual substrate concentrations based on the Whey batch culture experiments. Due to their goodness of fit it can be assumed that the two medium are quite similar in performance to the whey based medium.

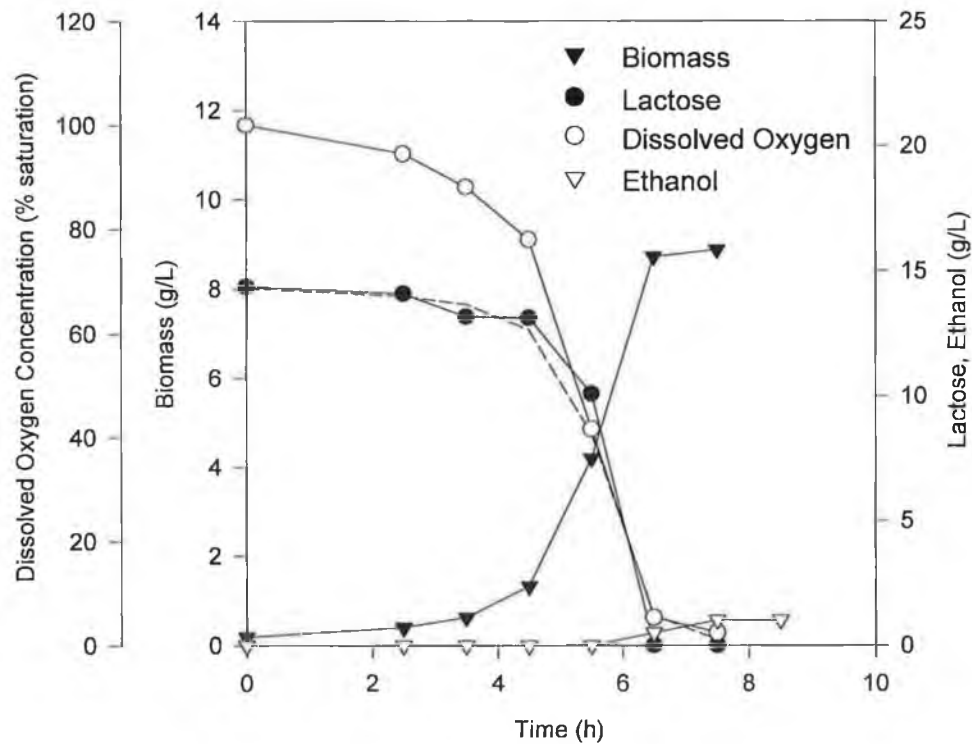


Figure 6.18 Batch Fermentation 5 – 800rpm, 1vvm YEPD medium, broken Line – stoichiometric prediction for substrate concentration

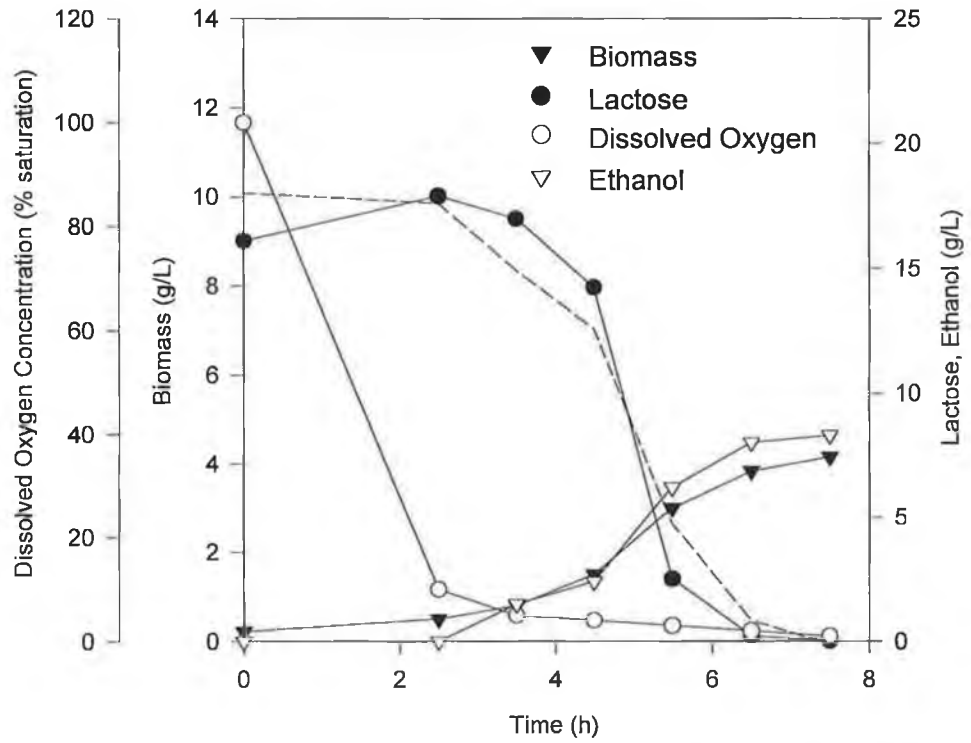


Figure 6.19 Batch Fermentation 6 – 200rpm, 1vvm YEPD medium, broken Line – stoichiometric prediction for substrate concentration

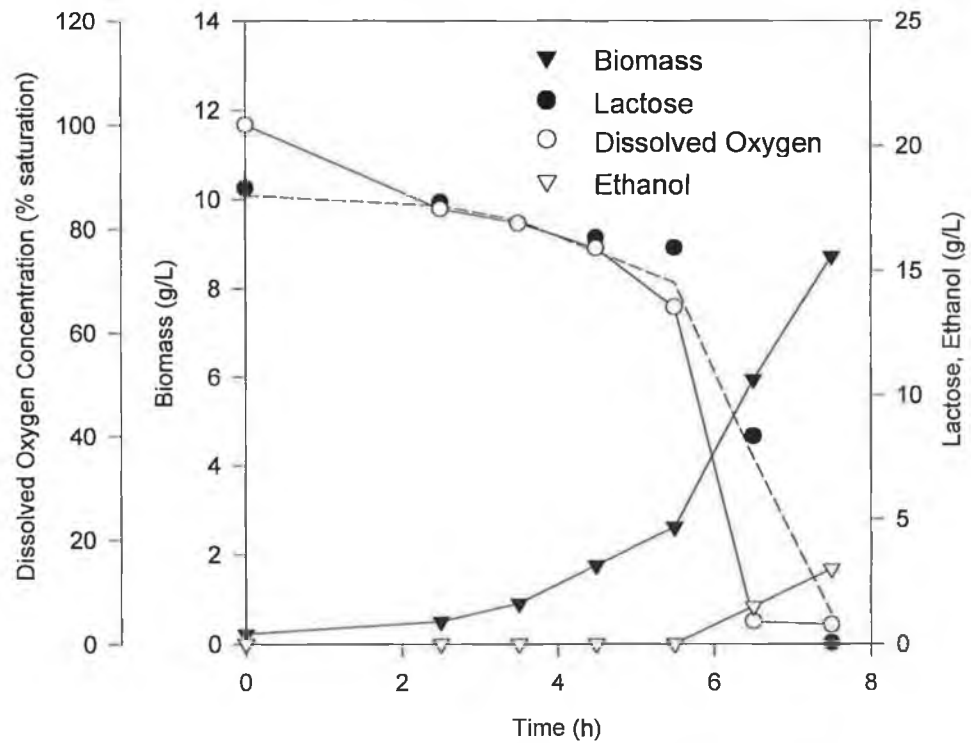


Figure 6.20 Batch Fermentation 7 – 800rpm, 1vvm YEPL medium, broken Line – stoichiometric prediction for substrate concentration

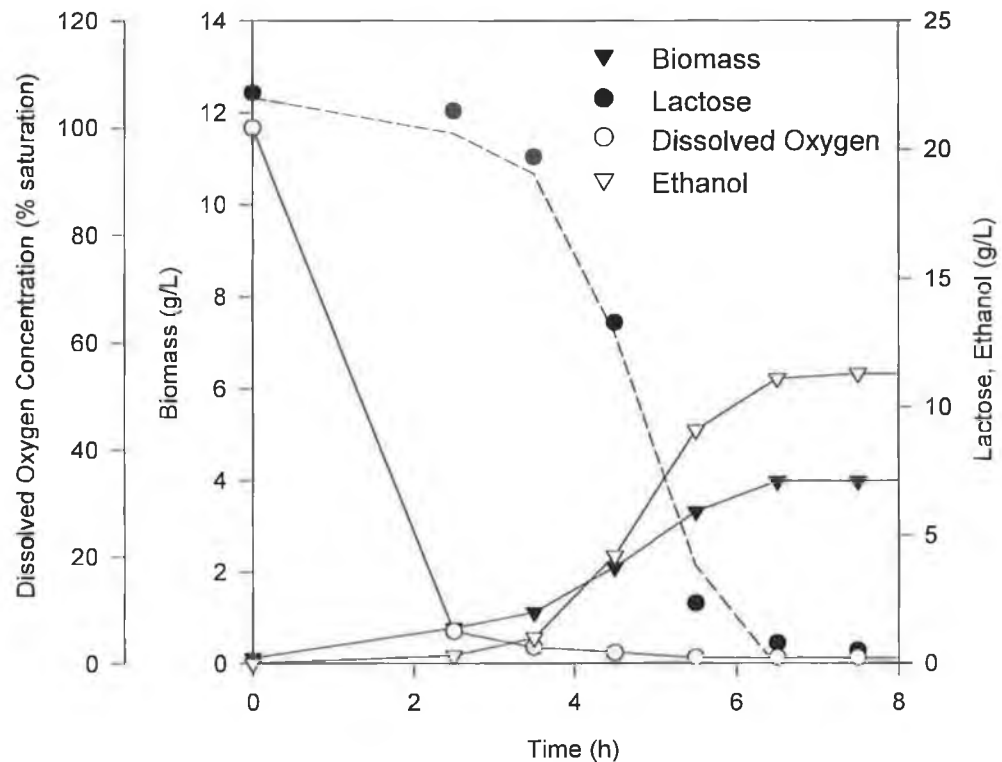


Figure 6.21 Batch Fermentation 8 – 200rpm, 1vvm YEPL medium, broken Line – stoichiometric prediction for substrate concentration

6.6 CONCLUSIONS

This work was carried out in order to attain the greatest diversity of fermentation conditions possible for the study of the effect of environmental conditions on the morphology of the dimorphic organism, *K marxianus* var. *marxianus* NRRLy2415. On examination of the fermentation data it is apparent that this objective has been achieved. The organism has been grown in two primary environments, the soluble substrate limited chemostat and soluble substrate excesses of batch cultures. Within each of the above environments the organism was subjected to both excess oxygen and partial oxygen limitation. Also within batch culture, the use of different media and carbohydrate substrates was also examined. This should allow the full assessment of the environmental effects on the morphology of the organism.

Creating this diversity of environmental conditions, allowed the detailed study of the kinetics of the organism. Figures 6.10 and 6.11 clearly demonstrate the lack of a limited respiratory capacity in the yeast *Kluyveromyces marxianus* var *marxianus* NRRLy 2415. This means that if the yeast has adequate oxygen supplies, it avoids

the production of ethanol. The presence of ethanol at higher substrate feed concentrations suggests that the fermentations are oxygen limited in these regions. Sonnleitner and Käppelli (1986) suggested a method to model metabolism which contained two pathways, an oxidative pathway and an oxidoreductive pathway. They decoupled aerobic and anaerobic metabolism and applied yield coefficients to each pathway. This approach was applied to a strain of *K. marxinaus* by Castrillo and Ugalde (1992) in order to model kinetic growth. This approach to modelling has now also been successfully applied to chemostat cultures of *K. marxianus* NRRLy2415 (NCYC 1425).

Several interesting findings arise from both the experimental data and model parameters. The primary finding is that the same model constants apply in both batch and continuous culture. The importance of this finding with respect to morphology will be discussed in Chapter 7. A point of interest may be the extremely high (0.69g/g) yield of biomass per gram of substrate. While this yield may be high compared to those reported in the literature, the media used in the literature typically contain a defined component. In this study a complex medium was utilised to sustain growth. Complex media require less component manufacture within the cell and rely on sugars primarily for energy. This typically will result in a higher $Y_{x/s}$. Secondly, the organism's kinetic performance is directly related to the $k_L a$, in the fermenter. As $k_L a$ is increased in the fermenter the yield of biomass increases to the detriment of ethanol production. The point of critical metabolic flux increases with increasing $k_L a$. The organism's ability to consume substrate is controlled by the type of metabolism in the cell. If excess oxygen is available to the cells then substrate uptake will be controlled to ensure no ethanol is produced. If the cells are oxygen limited, the cell will increase the specific rate of substrate uptake dramatically. This results in the rapid conversion of the remaining sugars to ethanol. To model the above phenomenon, several detailed experiments would have to be carried out, closely monitoring specific substrate uptake rates over much smaller time intervals and for a more extended range of $k_L a$ values, than those examined in this study

The YEPL and YEPD fermentations appear to behave similarly to the whey fermentations. It can be seen from Figures 6.18 – 6.21 that the stoichiometry of

the yeast extract fermentations is similar to that of the whey fermentations at all operating conditions. It would be assumed at this point that morphologically they should also be similar to the whey fermentations.

While the model developed in this chapter fits the experimental data for the chemostat well, the batch culture data, particularly the residual substrate traces, are of poor quality. This is due to a number of factors.

- Due to fermenter volume and quality of fabrication, the initial fermenter volume was prone to readjustment during autoclaving. This led to a slight dilution or concentration effect, resulting in inconsistent values for S_0 . The attainment of a consistent sterilisation temperature was also difficult. Different sterilisation temperatures and holding times can lead to different degrees of sugar caramelisation, leading to poor quality sugar data.
- The fermentations were carried out over a short time period (approx. 8 hrs.). It was attempted to sample the fermenter every hour. Approximately 200-500 mls was removed per sample. Thus, after 8 samples, approximately 24% of the fermenter volume was removed. The removal of more samples for intermediate analysis was deemed inappropriate, due to the resultant large variation in reactor volume.

Unfortunately the data, from a kinetic modelling standpoint, are poor. This is essentially due to a lack of the sophisticated equipment required to complete modern modelling exercises. Nielsen *et al.* (1991) state that new analytical techniques, suitable for accurate and reliable monitoring of key variables in fermentation processes, provide the necessary tools for improved modelling. Until more sensitive and accurate (possibly on-line) methods to determine the substrate utilisation curve are determined the analysis of the data will remain limited.

CHAPTER 7

THE CONSEQUENCES OF GROWTH CONDITIONS ON THE MORPHOLOGY OF *Kluyveromyces marxianus*

7.1 INTRODUCTION

In Chapter 2, the environmental causes for fungal dimorphism were outlined. Within groupings of similar organisms, certain trends were observed. Within ascosporogeneous yeast, for example, the following trends were observed.

- The primary morphology is yeast-like
- The organisms in this group revert to a filamentous/pseudohyphal morphology when put under stress.
- Stresses observed were generally attributed to poor quality substrates or substrate limitation.
- The mycelium formed is generally pseudohyphal, often consisting of chains of yeast cells

The work of Walker and O'Neill (1990), in which the morphology of *Kluyveromyces marxianus* var. *marxianus* NRRLy2415 was examined, is not in agreement with the above findings. They compared the organism to *Mucor*, a distant fungal relation, whose dimorphism is generally attributed to the presence or absence of oxygen. The primary morphology observed in aerobic culture was filamentous and when the organism was deprived of oxygen it grew in a yeast-like form. When culturing the organism in aerobic continuous culture the organism appeared to generate a more elongated filamentous form but no change from the dominant pseudohyphal/filamentous population was reported. They concluded that dimorphism was thus controlled by oxygen supply and that the organism could not be cultured in yeast-like form in aerobic culture.

This explanation was the most probable based on the experimental observation, yet it fits none of the criteria found for similar organisms. Hence the decision to investigate more thoroughly the causes for dimorphism in this organism. Two

different techniques will be employed in the present work to that of the study of Walker and O'Neill (1990).

- 1) The use of the image analysis protocol, as outlined in Chapter 5, will help monitor morphological alterations in more complete and objective detail and should be particularly useful in quantifying subtle changes in morphology.
- 2) All batch culture experimentation was performed in fermenters equipped with dissolved oxygen probes.

7.2 EFFECT OF AGITATION ON MORPHOLOGY IN BATCH CULTURE (WHEY BASED MEDIUM)

The following series of experiments attempted to assess the effect of increasing agitation intensity (thus increasing mass and oxygen transfer) on the morphology of *K. marxianus* in batch culture while growing on the whey-based medium outlined in Chapter 3.

The first fermentation was cultured at 800 rpm, 1 vvm (See Chapter 6 for kinetic data for all fermentations). This fermentation was completed to assess the effect of vigorous agitation on the morphology of the organism. The culture displayed a predominantly yeast-like morphology throughout. Figure 7.1 also demonstrates that the primary classification observed during the active growth phase was double yeast; a strong sign of an actively dividing culture. The mean total amount of the yeast classification present throughout the fermentation was 73 % by volume with the remainder being made up by 21 % elongated yeast and 6 % filamentous and pseudohyphal cells. These results obtained in this fermentation are at variance with the findings of Walker and O'Neill (1990) who indicated that the organism grew in pseudohyphal or filamentous form under aerobic conditions. As can be seen in Figure 6.17, the dissolved oxygen concentration remained in excess until hour 7 of the fermentation thus the fermentation was fully aerobic until this time. After this point a greater degree of heterogeneity is observed in the culture morphology.

It is apparent from an examination of the morphology data in batch fermentation runs 2 – 4 (Figures 7.2 to 7.4) that the morphology becomes increasingly

heterogeneous as the agitation intensity decreases, particularly at 300rpm and 200rpm (Runs 3 and 4). There are two possible factors involved in this morphological transition. The first is that as ethanol production begins a morphological transition is initiated. The second is that poor mixing and mass transfer in the fermenter causes the morphological alterations. The combination of both of the above effects is also possible.

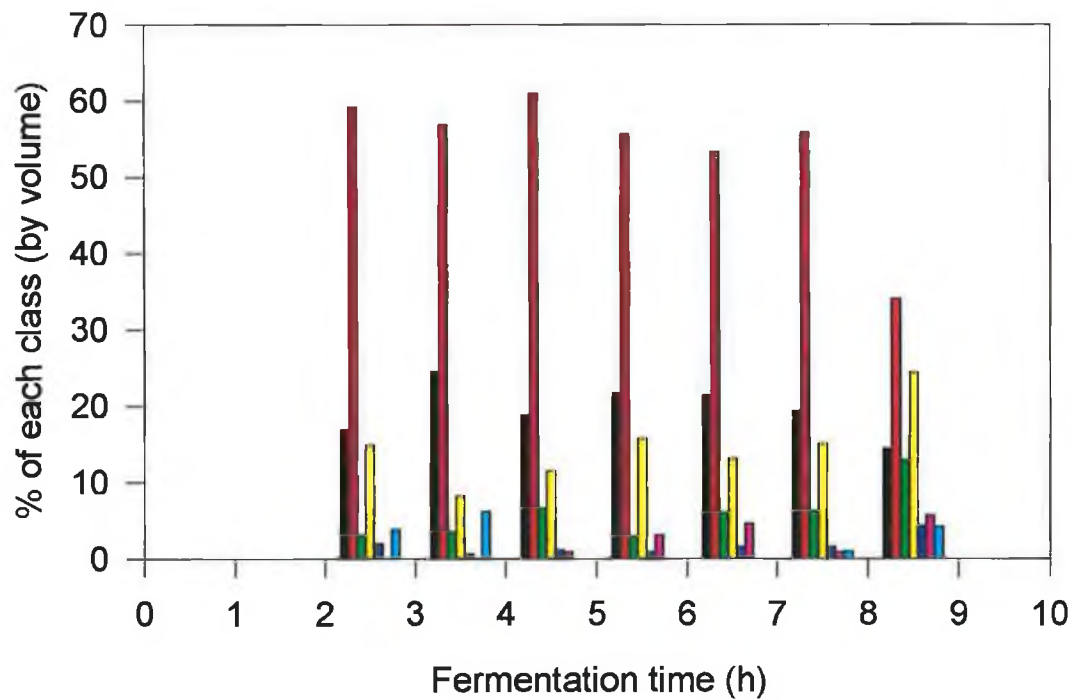


Figure 7.1 Morphology distribution versus time for whey batch culture grown at 800 rpm, 1vvm. Black – Yeast; Red – Double yeast; Green – Elongated yeast; Yellow - Double elongated yeast; Dark Blue – Filaments; Purple – Double filaments; Light Blue – Pseudohyphae

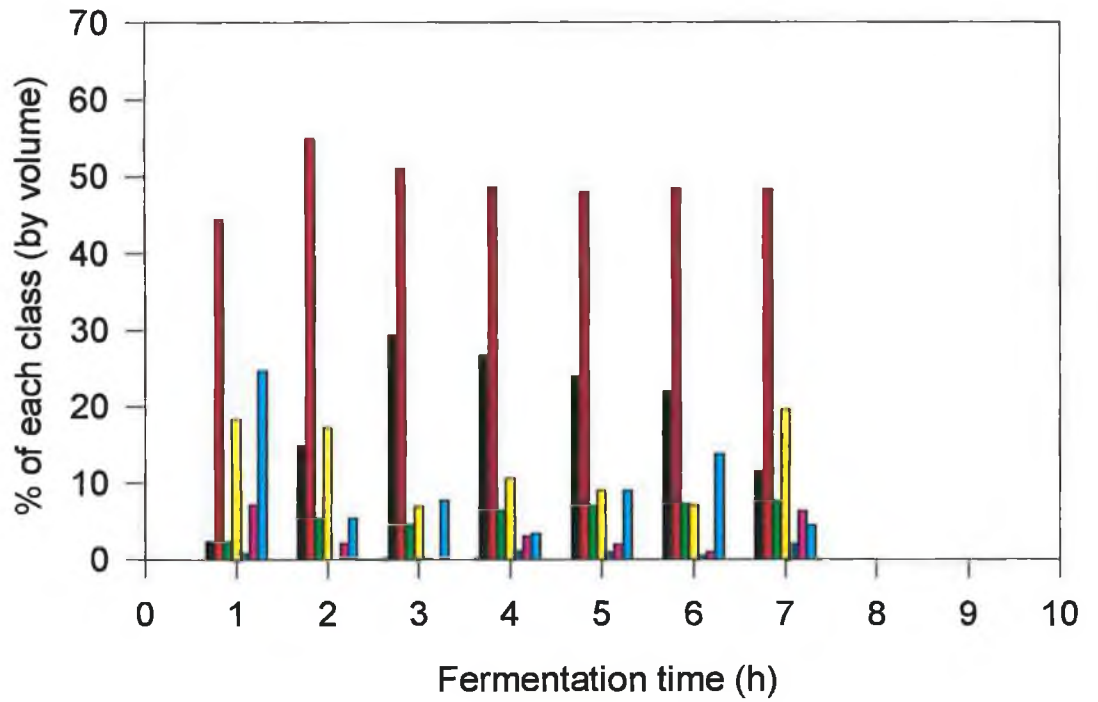


Figure 7.2 Morphology distribution versus time for whey batch culture grown at 400 rpm, 1vvm (Legends Figure 7.1)

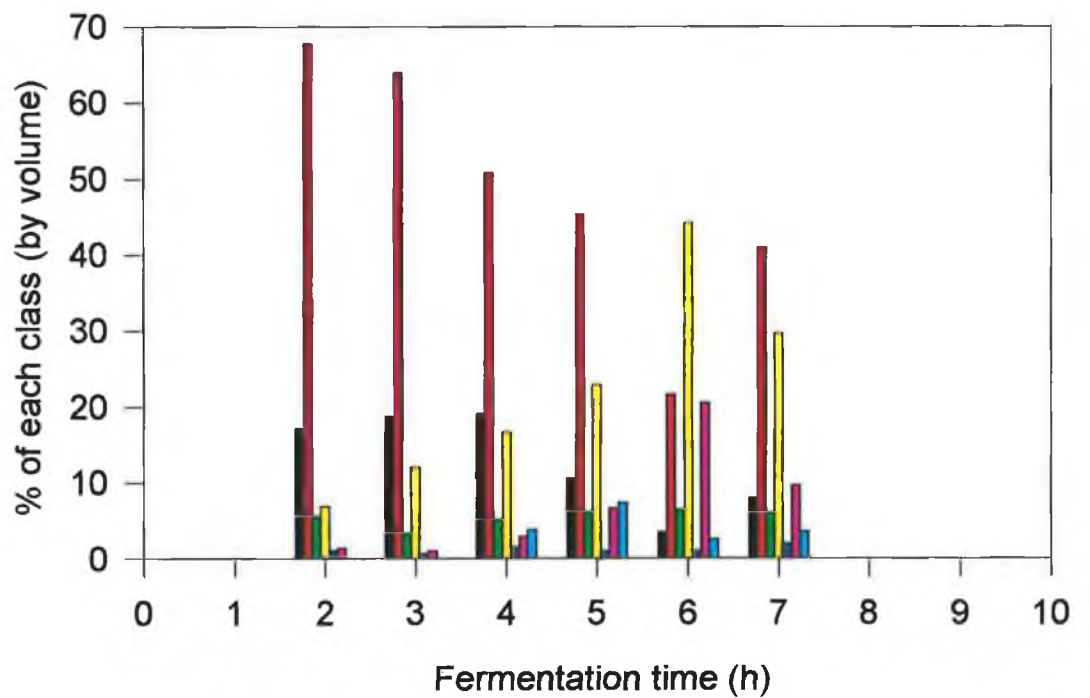


Figure 7.3 Morphology distribution versus time for whey batch culture grown at 300 rpm, 1vvm (Legends Figure 7.1)

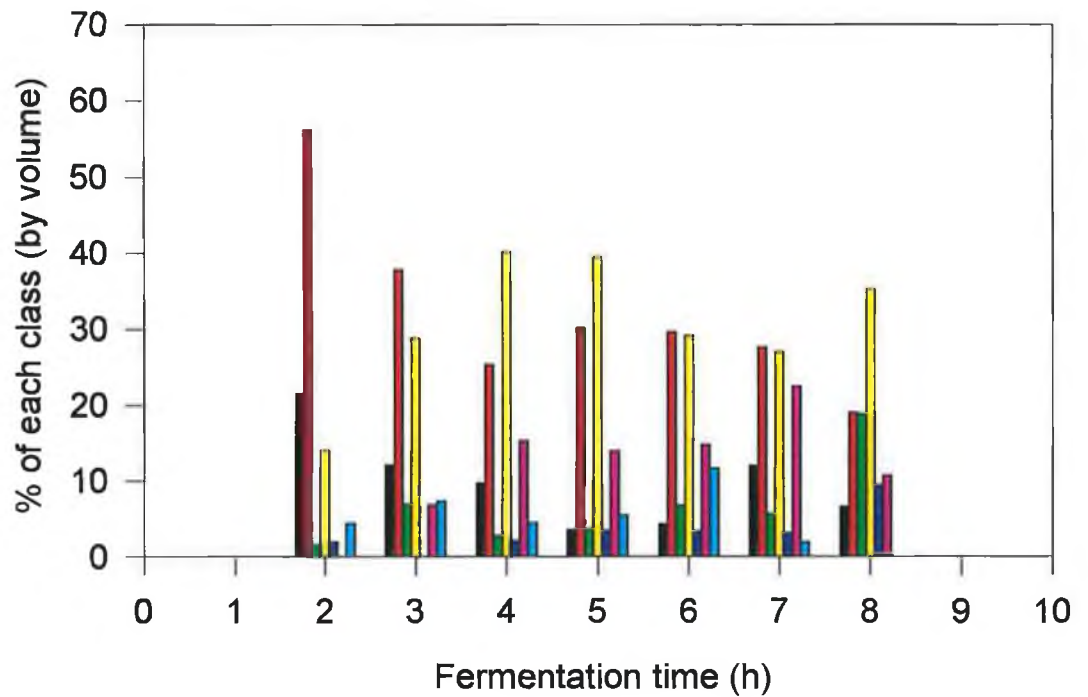


Figure 7.4 Morphology distribution versus time for whey batch culture grown at 200 rpm, 1vvm (Legends Figure 6.1)

By examination of Figures 7.1 to 7.4, it is apparent that the morphological transitions are gradual, leading to an increase in the heterogeneity of the cultures with respect to time. All fermentations appear to have a high concentration of yeast cells in the initial stages. This is probably due to the low concentrations of cells in the fermentations in the early hours; thus all nutrients, including oxygen, are in excess. It is probable that as the concentration of cells build up in the fermenter that nutrients, particularly oxygen, become limited in certain regions of the fermenter leading to morphological transitions of varying scale depending on the agitation speed. This examination also suggests that the morphological transition experienced in this work differs to that of *Candida albicans*, which forms filamentous cells or “germ tubes” directly from yeast cells (Odds, 1993). At no time was germ tube formation observed with this organism under the culturing conditions examined. This is verified by the results displayed. The formation of germ tubes would result in the bypassing of the elongated yeast phase.

One problem observed, with respect to automatic classification, was the formation of clusters of yeast cells very early in the fermentations. Zalewski and Buchholz (1996) have also observed this phenomenon for *Saccharomyces cerevisiae*. Figure

7.2 (400rpm) illustrates this finding. A large percentage of pseudohyphae are observed in the first sample (note; other fermentations were not morphologically sampled as early as this one). These “pseudohypha”, while, in theory, are being correctly classified, are geometrically different from previously observed pseudohyphae and thus their volume is being incorrectly calculated. It is probable that this is a problem experienced with reviving the starter culture (grown in YEPL) in a different nutrient medium. The cells in the chains are exclusively yeastlike but cell separation after division appears to be temporarily impaired. It was decided not to alter the image analysis protocols due to the rarity of the morphological form.

The predominance of double cells during the active growth phase is apparent. This appears to be independent of morphology and is more dependant on whether the organism is in the growth or stationary phase. A decrease in the percentage of double cells (by volume) is observed towards the end of each fermentation as the stationary phase is entered. This is a common phenomenon in yeast fermentations with many observations in the literature for *Saccharomyces cerevisiae* (Pons *et al.*, 1993; Zalewski and Bucholz, 1996). Zalewski *et al.* (1994) related the amount of cells in clusters of four or “tetrads” to the active growth rate. Due to the morphological alterations occurring here it is impossible to attempt such analysis. It is, however, possible to state that a high percentage of double cells indicates active growth.

7.3 EFFECT OF DIFFERENT MEDIA ON CELL MORPHOLOGY IN BATCH CULTURE

It was decided, based on the above results, to assess the effect of a different medium base on the morphology of the organism in batch culture. The medium used was a standard yeast medium with both glucose (dextrose) and lactose used as carbohydrate sources in order to assess whether the hydrolytic step in lactose metabolism had any affect on the morphology of the organism.

The morphology for the 800 rpm fermentations (Both YEPL (Figure 7.5) and YEPD (Figure 7.6)) are very similar in content to the whey fermentation conducted under similar conditions (Figure 7.1). This is also evident when the mean cell geometric properties are examined (Figure 7.7). The graphs are plotted versus biomass concentration rather than time to normalise all parameters such as initial substrate concentration and inoculum concentration. It is apparent that under optimal growth conditions that changing the medium has no effect on the morphology of the organism.

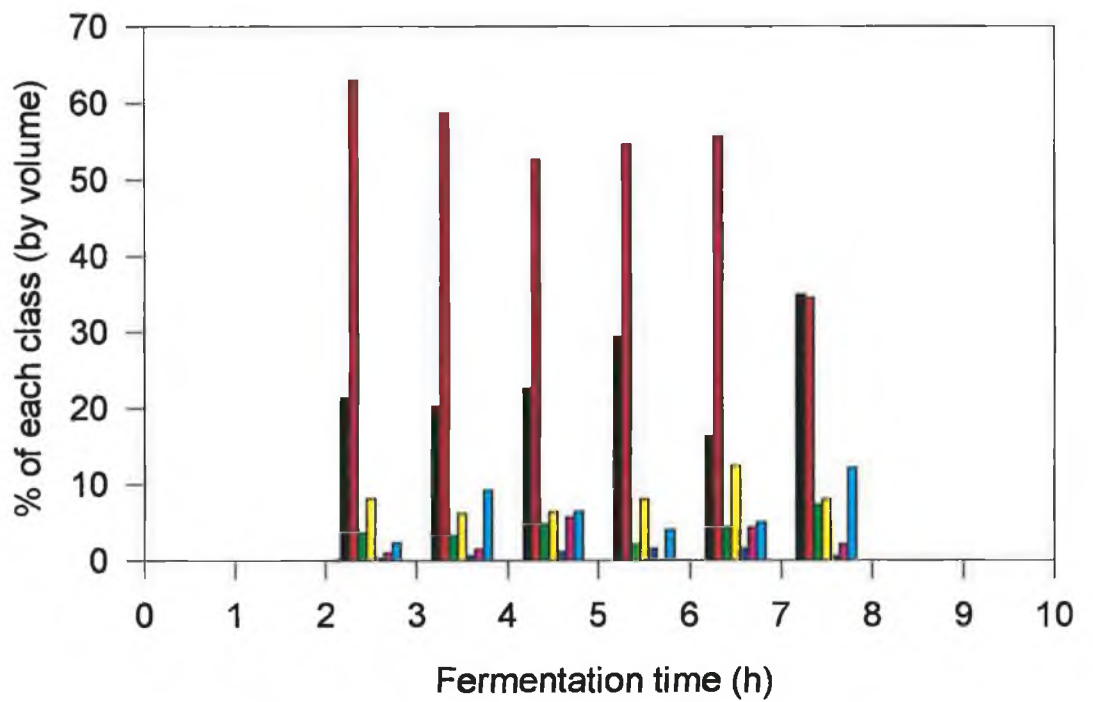


Figure 7.5 Morphology distribution versus time for YEPL batch culture grown at 800 rpm, 1vvm (Legends Figure 7.1)

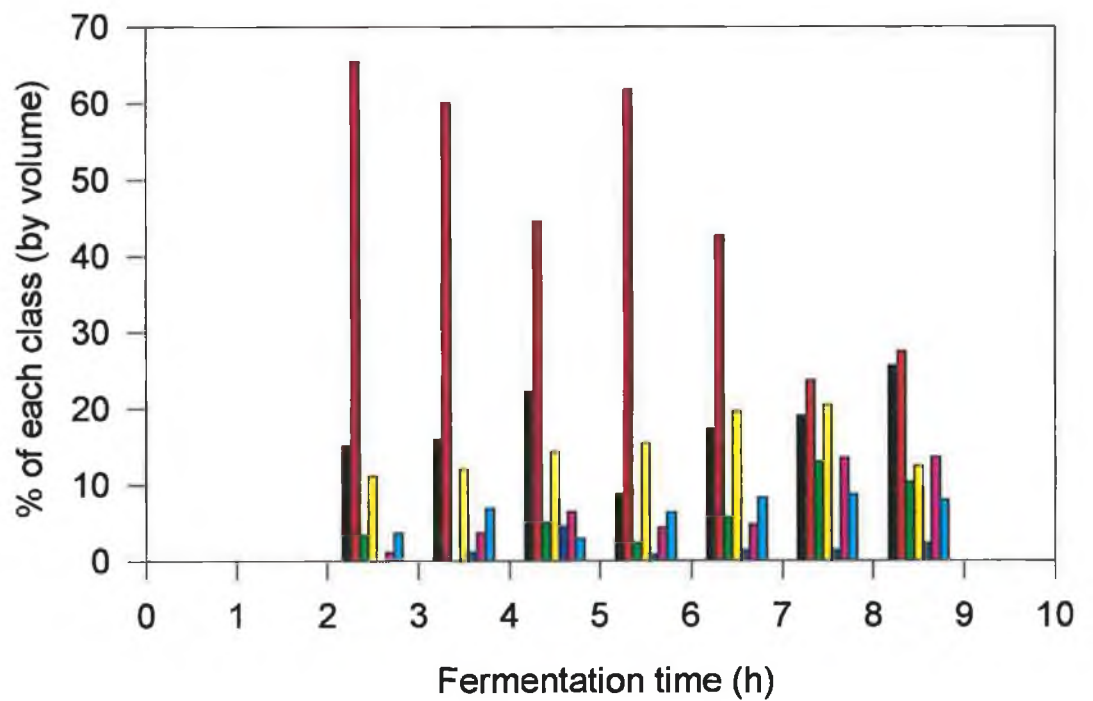


Figure 7.6 Morphology distribution versus time for YEPD batch culture grown at 800 rpm, 1vvm (Legends Figure 7.1)

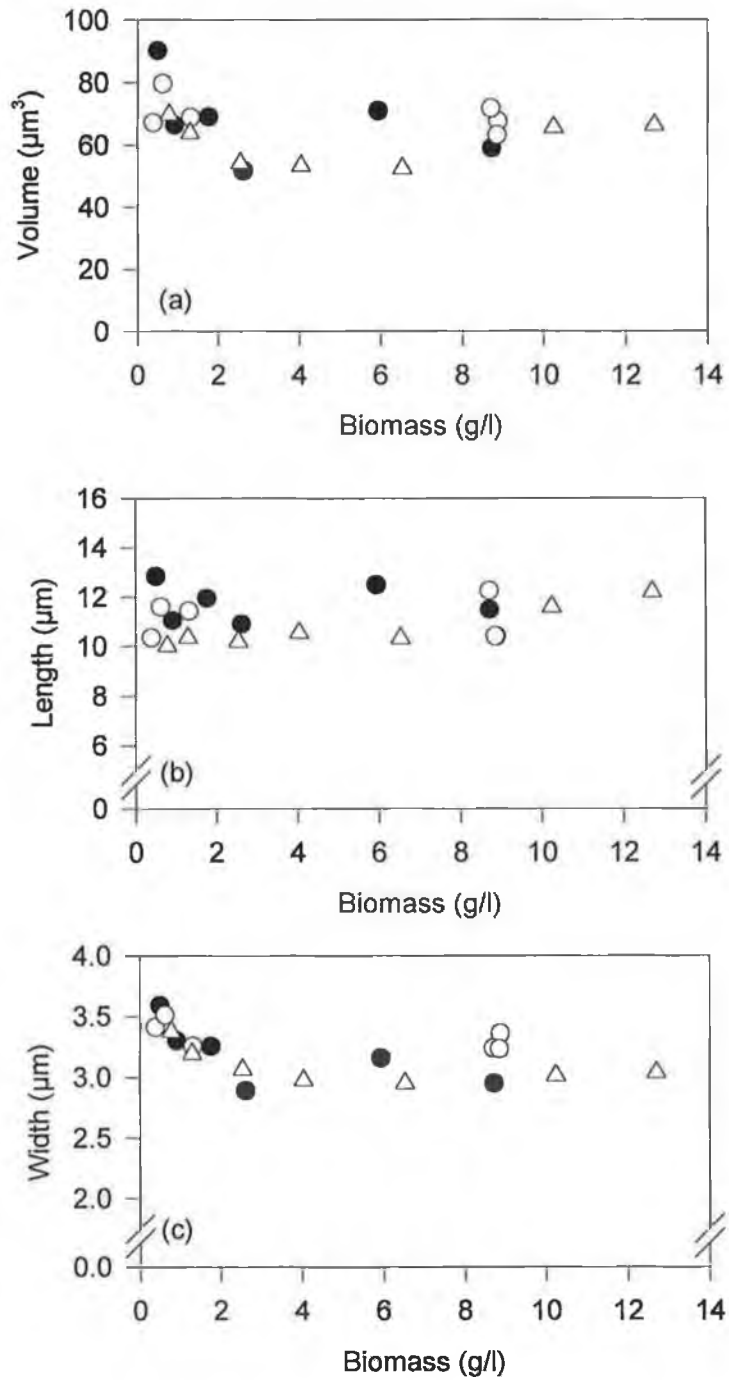


Figure 7.7 Mean geometric parameters of cells in batch cultures grown at 800 rpm, 1 vvm on various media. (a) mean cell volume, (b) mean cell length, (c) mean cell width. filled circles - YEPL, open circles - YEPD, open triangles - Whey. Data presented versus biomass concentration due to differences in inoculum size and initial substrate concentration.

This is not, however, true for all conditions. From an examination of the classification data and the mean geometric parameters presented for the 200rpm fermentations (Figure 7.8 (lactose) and Figure 7.9 (glucose)) it is apparent that significantly more pseudohyphae are being produced in the YEP based media than in the whey medium (Figure 7.4).

This trend is verified in the plots of mean cell volume and length versus biomass concentration (Figure 7.10) where the volume and length of the YEP based fermentations is approximately double that of the whey fermentations on completion. It is noteworthy that the mean cell widths of the three fermentations match each other closely (Figure 7.10c), and are significantly different from those presented for the 800rpm fermentations (Figure 7.7c). This suggests that the cell subunit morphology is similar for all the 200rpm fermentations and that the ability to form pseudohyphal structures without subunit breakup is enhanced in YEP based media. From the data presented thus far, it is apparent that the end point morphology of *K. marxianus* is not determined by carbohydrate source for YEP media. Ecologically this would suggest that certain key nutrients regulate the ability of the organism to form foraging pseudohyphal structures under adverse environmental conditions yet have little or no effect on the morphology or growth of the organisms under ideal conditions. Possible nutrients include Zn^{2+} and Fe^{3+} (Reeslev and Jensen, 1995). The enzyme responsible for chitin synthesis, which in turn controls the ability of a cell to separate after budding, is regulated by the presence or absence of Zinc (Berry, 1982). When the growth of the organism in YEPL and YEPD media (nutritionally balanced) is compared to that of the whey based media under ideal conditions it is apparent that the organism grows equally well on both compositions, with similar growth rates. The yield coefficient is also similar for the whey-based media and the YEP based media. This suggests that the whey medium is as equally balanced nutritionally as the YEPL and YEPD media. Further work is needed in this area to fully establish the reasons for this difference.

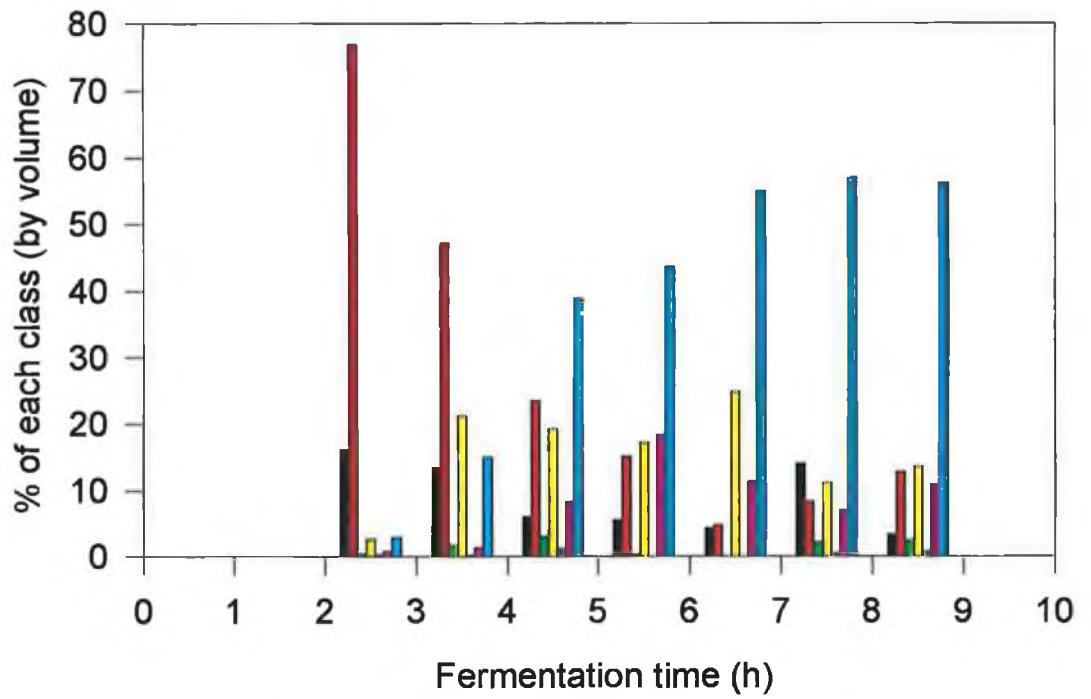


Figure 7.8 Morphology distribution versus time for YEPL batch culture grown at 200 rpm, 1vvm (Legends Figure 7.1)

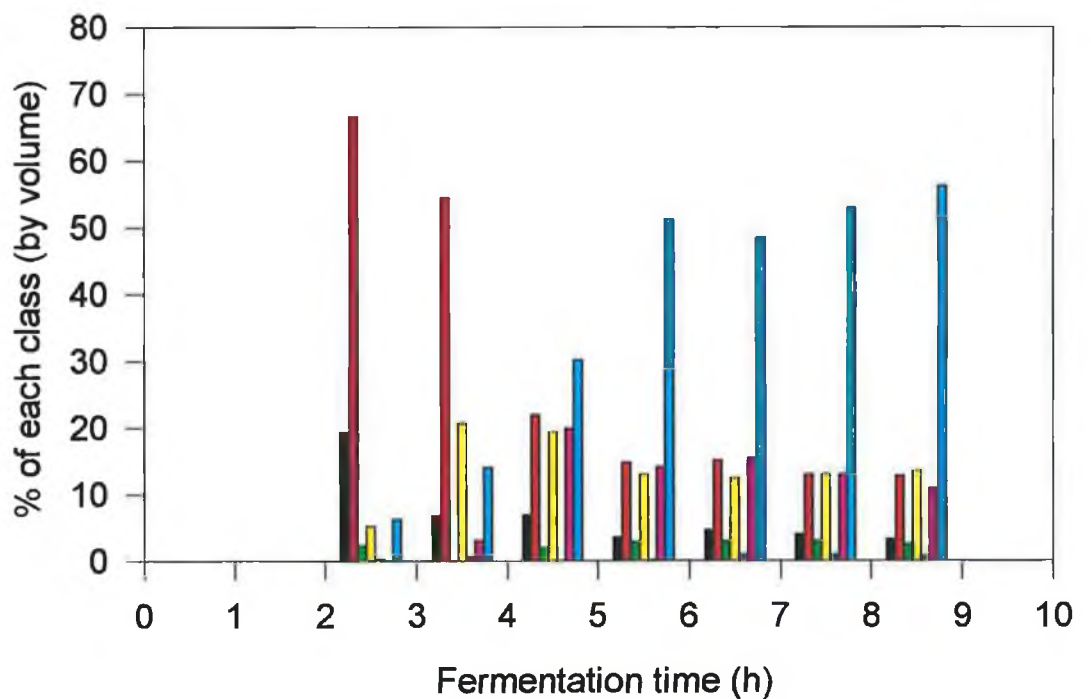


Figure 7.9 Morphology distribution versus time for YEPD batch culture grown at 200 rpm, 1vvm (Legends Figure 7.1)

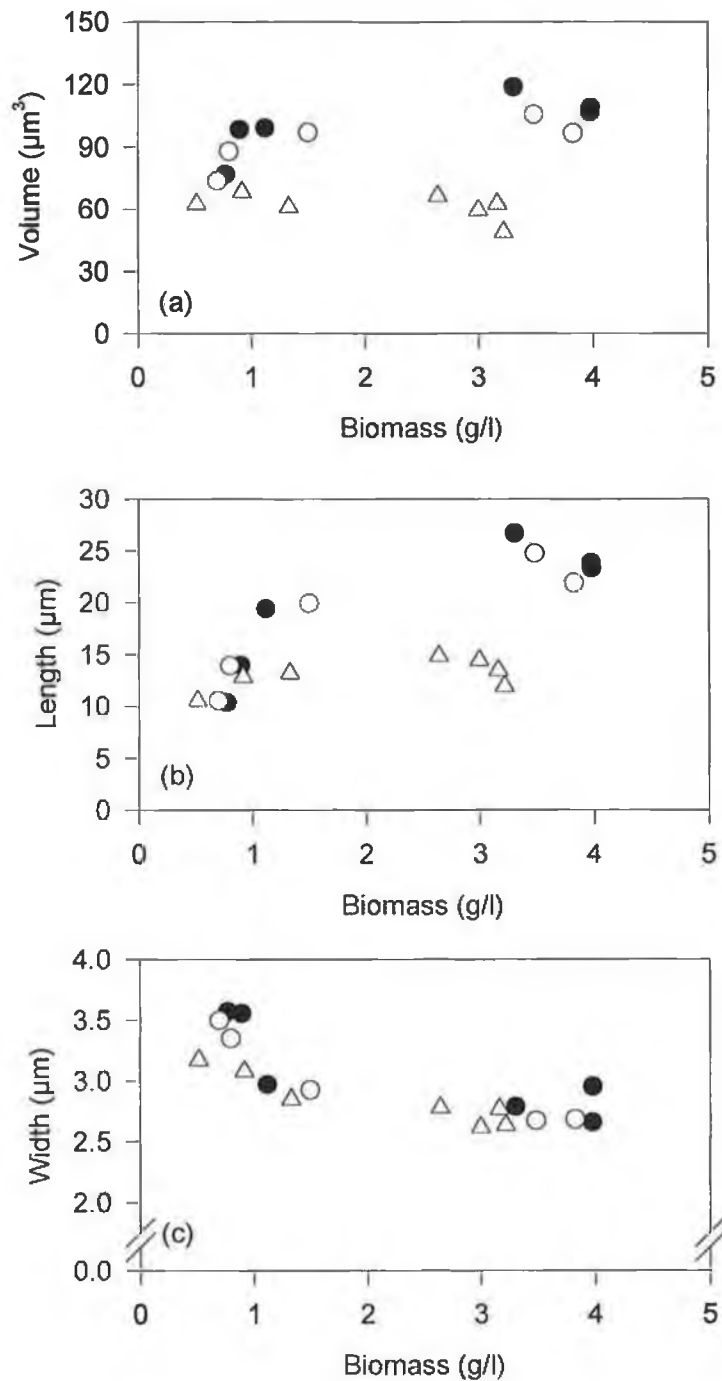


Figure 7.10 Mean geometric parameters of cells in batch cultures grown at 200 rpm, 1 vvm on various media. (a) mean cell volume, (b) mean cell length, (c) mean cell width. filled circles - YEPL, open circles - YEPD, open triangles - whey. Data presented versus biomass concentration due to differences in inoculum size and initial substrate concentration

7.4 MORPHOLOGY IN CHEMOSTAT CULTURE

7.4.1 Introduction

Chemostat culturing allows the study of steady state environments, where all parameters have established constant values. The batch culture work, described earlier, provided some reasons for morphological transitions in the organism but was limited by the nature of batch culture. It was hoped that the use of chemostat cultures would allow better control of the environment and allow morphology to adjust fully to a “morphological steady state” based on any set of environmental conditions. Wiebe and Trinci (1991) have also illustrated the importance of growth rate on the morphology of *Fusarium graminearum*, a filamentous fungus.

7.4.2 Chemostat Morphological Classification Data.

The first attempts at chemostat culture led to some surprising discoveries. Initially it was attempted to culture the organism aerobically, (i.e. no ethanol production). This was achieved as described in Chapter 3, by diluting the basic media four fold to generate a 5g/L lactose whey-based media. This was effective in completely eliminating ethanol production at any dilution rate, suggesting that the culture was completely aerobic. Yet the morphology on examination, in general, was pseudohyphal. Furthermore, the pseudohyphae observed in chemostat culture were unlike any seen previously. The global structure of the pseudohyphae was much more developed than that seen in batch culture and the individual subunits of the pseudohyphae were much more elongated than any seen previously. A more detailed overview of this set of results is presented below.

The overall morphological classifications (both by volume fraction and object count) for the four runs are presented in Figures 7.11 – 7-18. At low dilution rates, where maintenance is a significant factor, a mixed morphology prevails with yeast and elongated yeast predominant in all runs. As dilution rate increases ($>0.2 \text{ h}^{-1}$) filamentous and pseudohyphal morphologies predominate. The ratio of filaments to pseudohyphae is seen to increase with increasing substrate feed concentration. In the 20g/L fermentation, the population is almost completely composed of pseudohyphae in dilution rates greater than 0.15 h^{-1} . As the fermentation approaches $D = \mu_m$ and substrate is no longer limiting, there is a reversion back to a more yeast-like morphology in all fermentations. While certain deviations form

this behaviour may occur at both ends of the range of dilution rate, it is apparent from this study, that while the organism is being cultured in substrate limited chemostat culture, irrespective of whether the cell is in oxygen excess or in partial oxygen limitation, the predominant morphology will be filamentous/pseudohyphal.

The chemostat data illustrates the usefulness of both a numerical and volumetric based classification system, with the numerical classification system indicating the presence of cells with smaller volumes, such as yeast and elongated yeast, the presence of which may not be significant when using the volumetric classification system. The numerical classification graph for the 20g/L fermentation indicates a region in the environs of 0.2h^{-1} dilution rate, where a sudden increase in % pseudohyphae from 30% to 90%, followed by a drop to 50%, is noted. This observation is also observed for the 15g/L fermentation, but to a lesser extent. As dilution rate approaches the washout value there is an increase in the % of yeast and elongated yeast for all runs indicating a possible return to a yeast-like morphology at μ_m .

The presence of significant numerical fractions of single and double yeast and elongated yeast cells under almost all conditions indicates that a population exclusively composed of pseudohyphal cells is unattainable. The presence of so many small cells suggest that they may play an important role in the maintenance of a steady state, morphologically speaking, in the bioreactor, allowing the rejuvenation of pseudohyphae as they are removed from the chemostat.

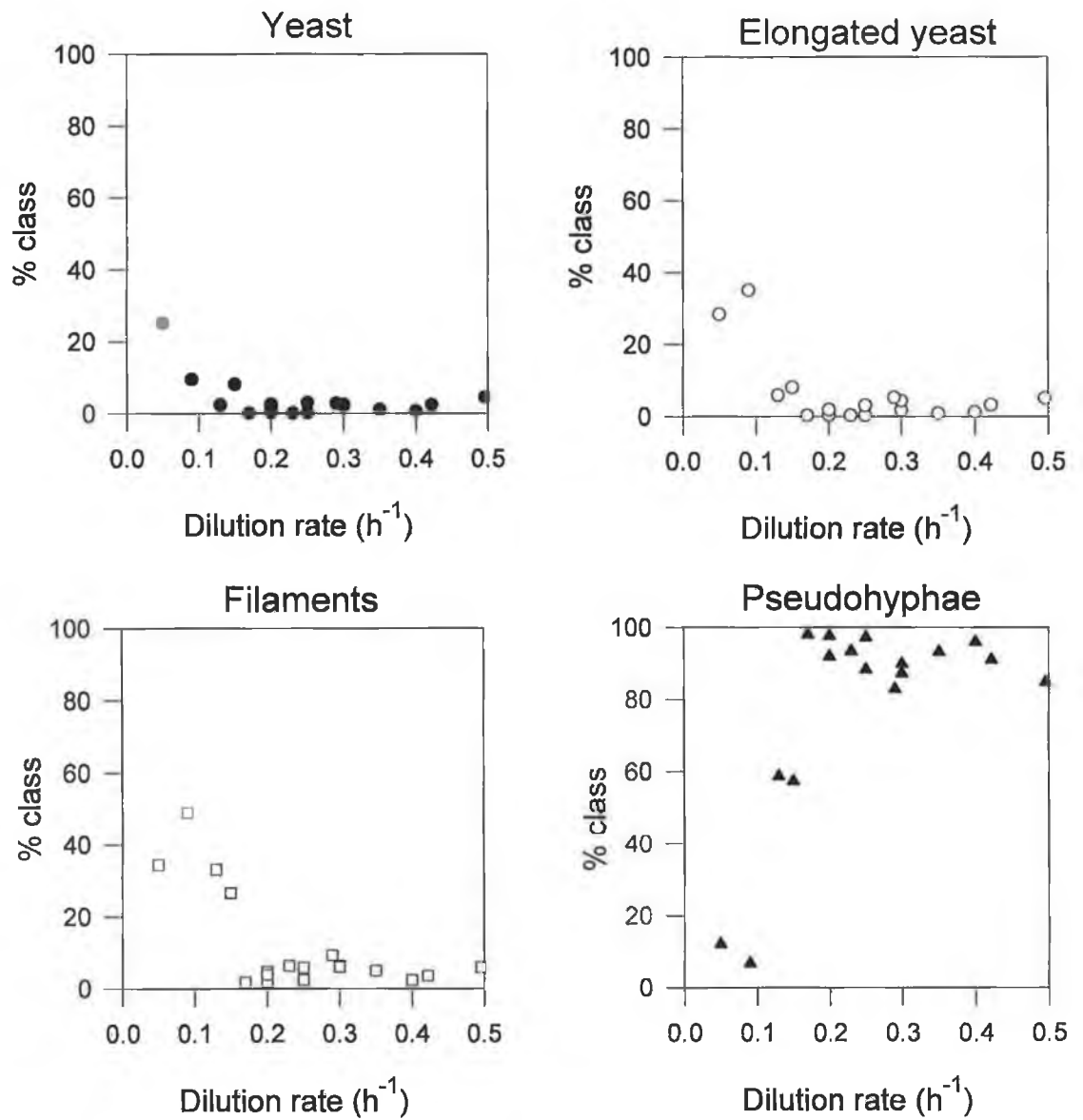


Figure 7.11 Classification data for 20g/L chemostat fermentation (based on cell volume fraction in each class)

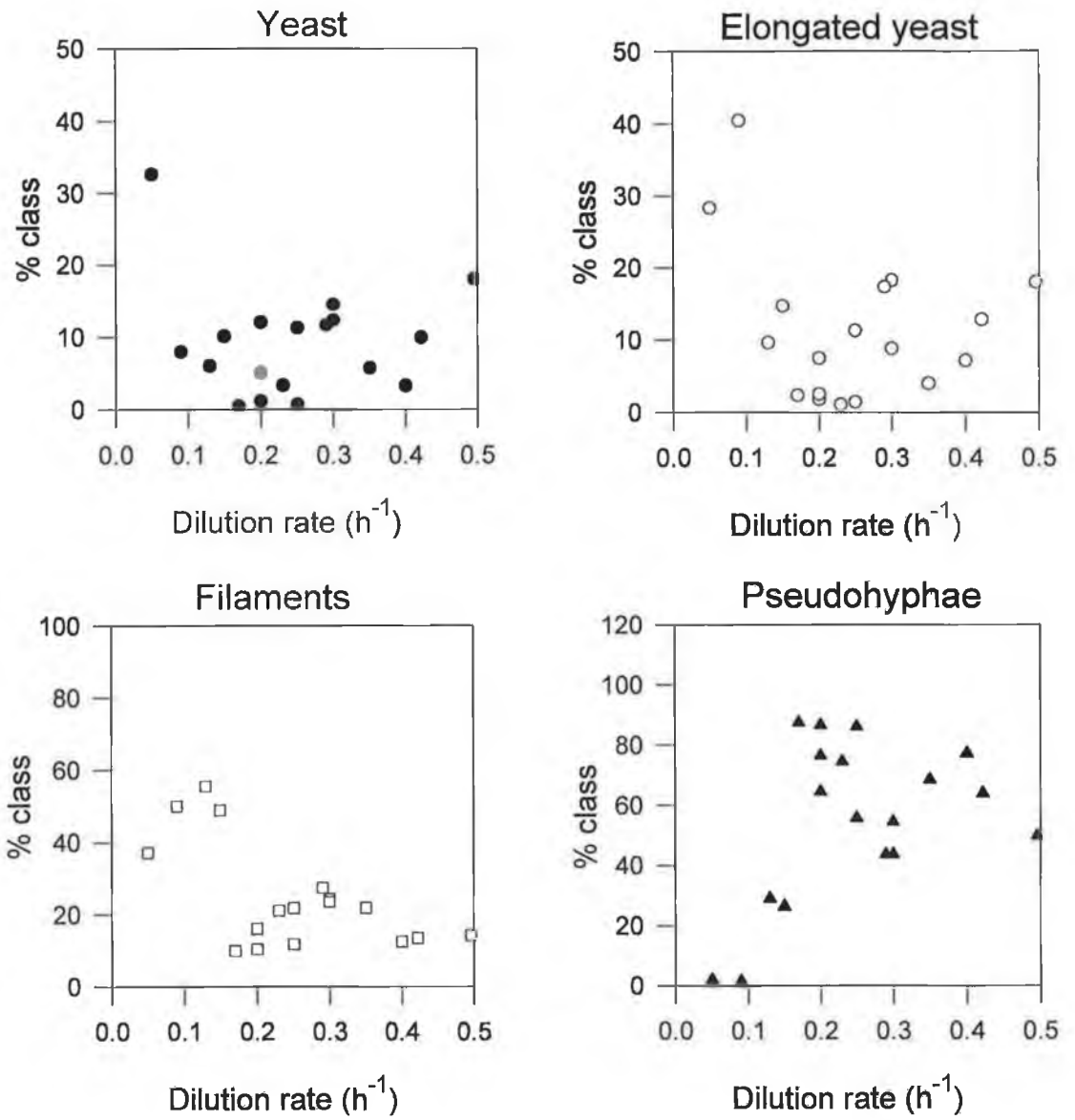


Figure 7.12 Classification data for 20g/L chemostat fermentation (based on cell numerical fraction in each class)

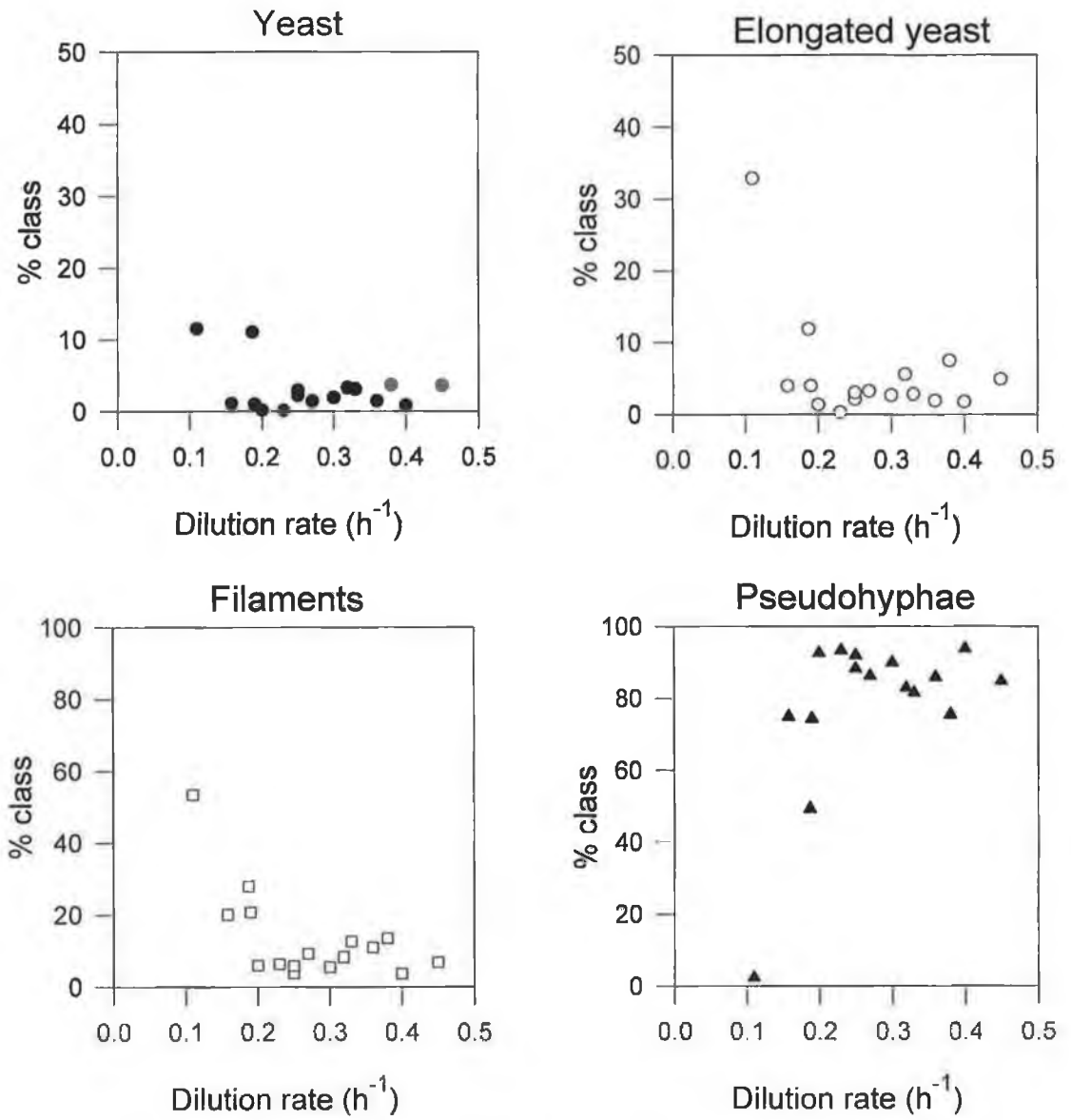


Figure 7.13 Classification data for 15g/L chemostat fermentation (based on cell volume fraction in each class)

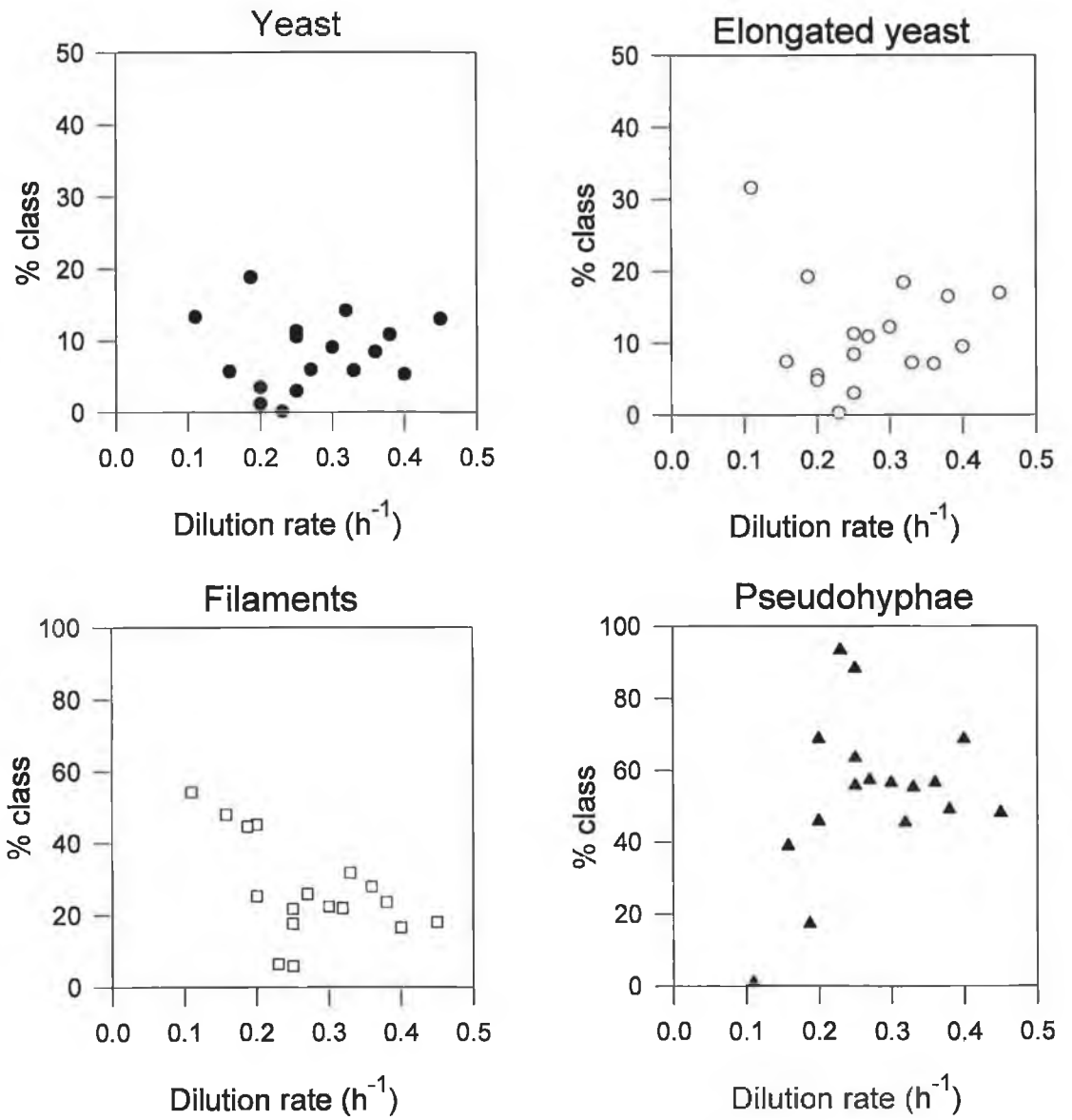


Figure 7.14 Classification data for 15g/L chemostat fermentation (based on cell numerical fraction in each class)

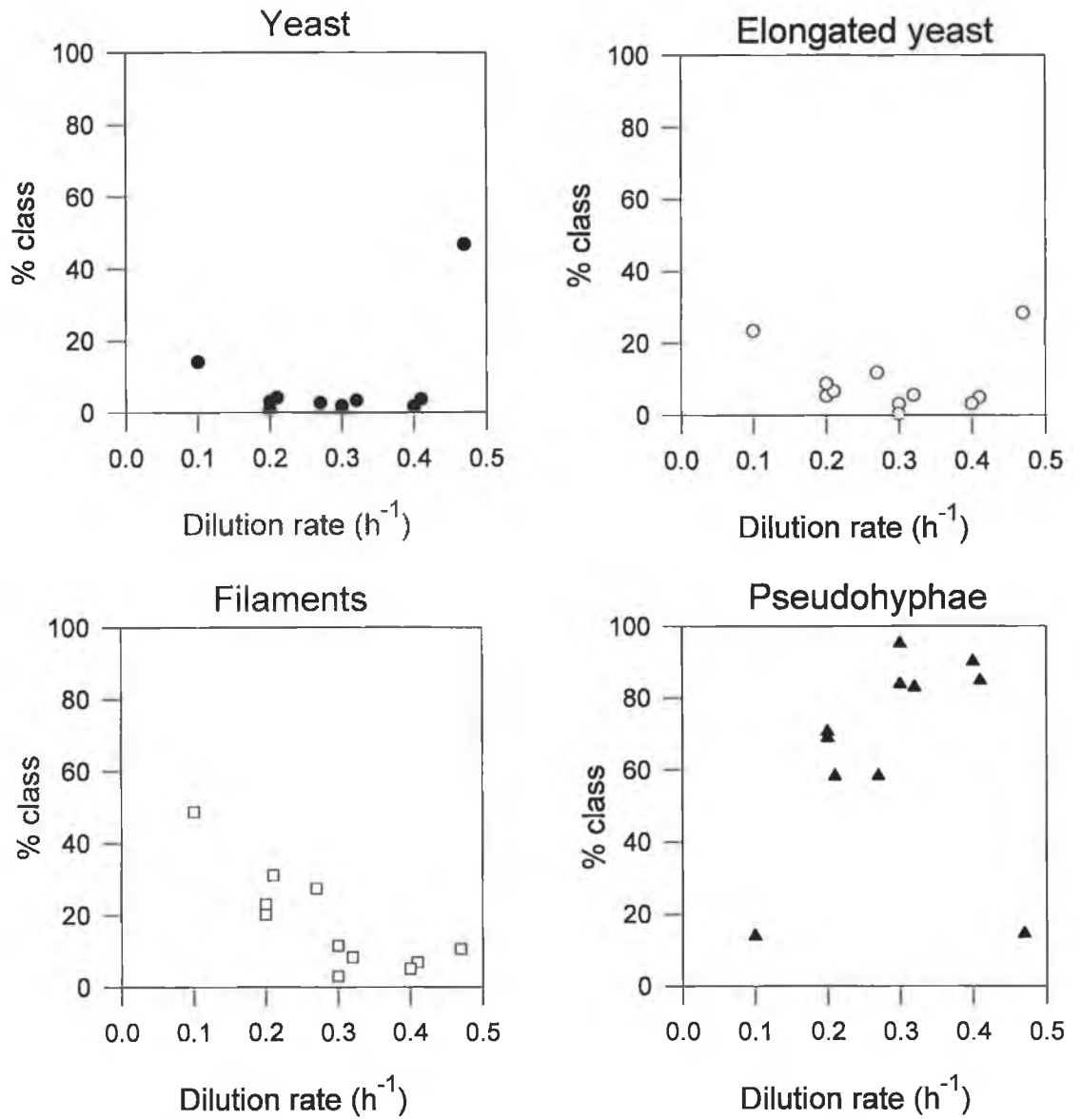


Figure 7.15 Classification data for 10g/L chemostat fermentation (based on cell volume fraction in each class)

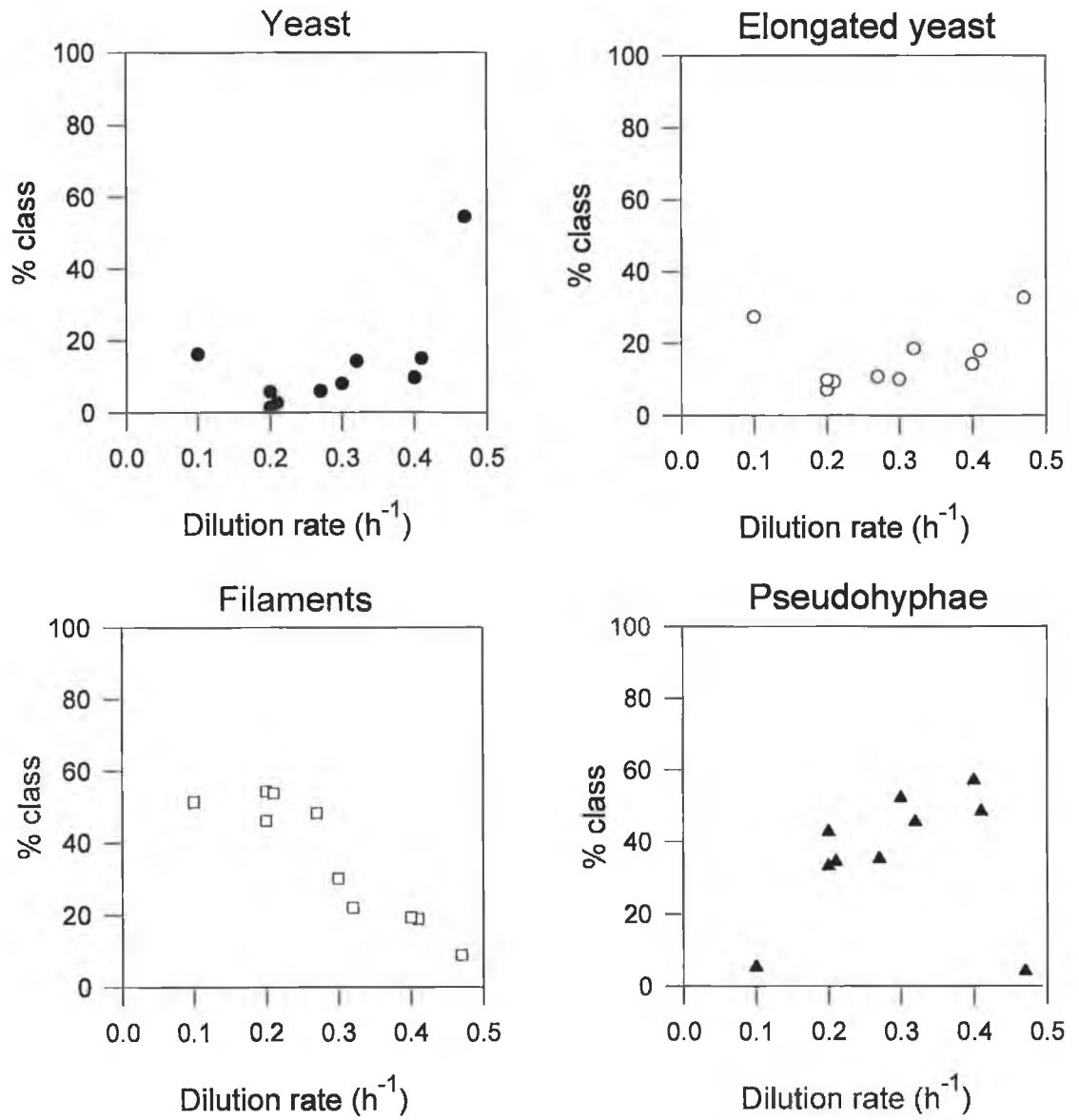


Figure 7.16 Classification data for 10g/L chemostat fermentation (based on cell numerical fraction in each class)

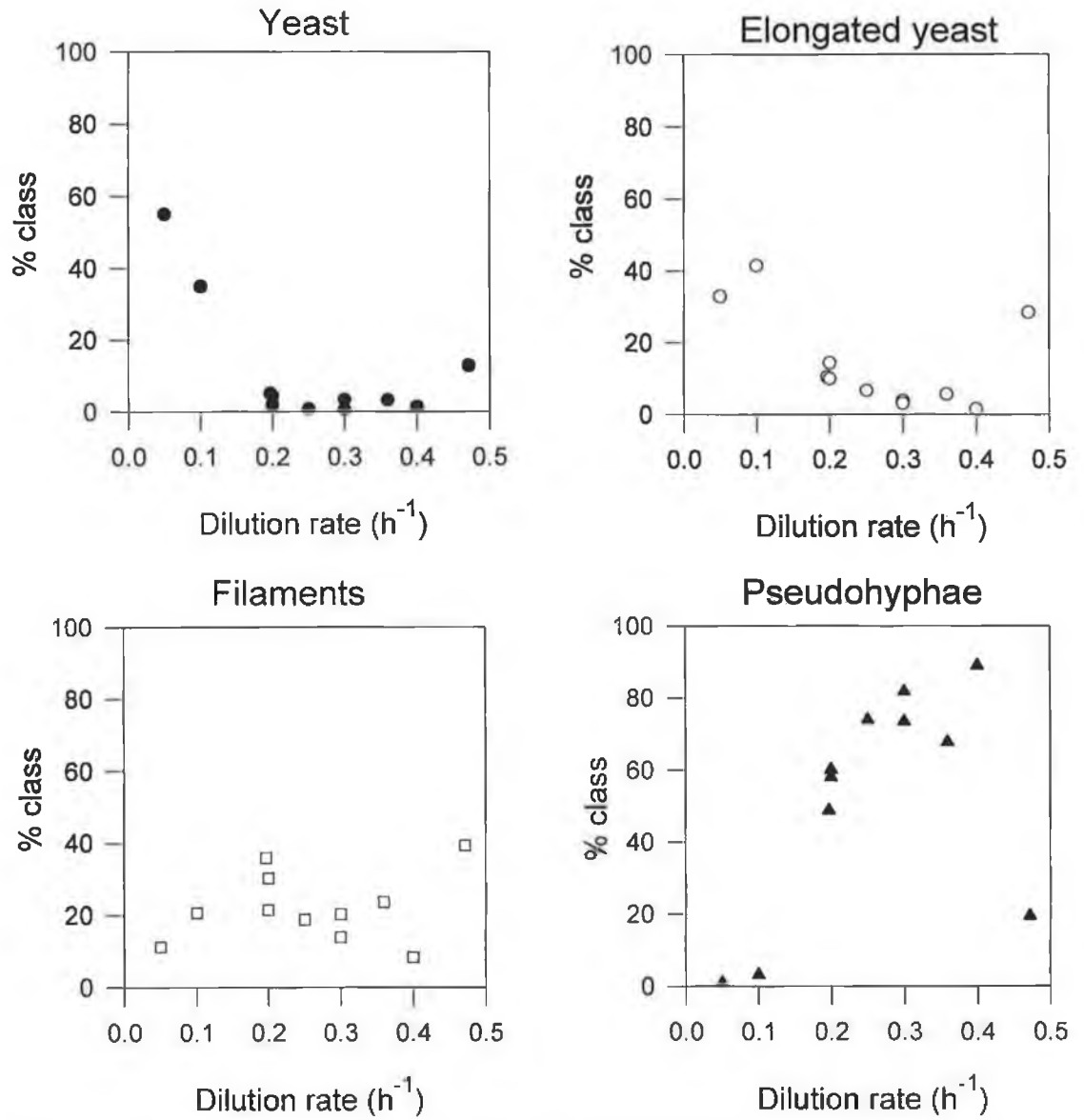


Figure 7.17 Classification data for 5g/L chemostat fermentation (based on cell volume fraction in each class)

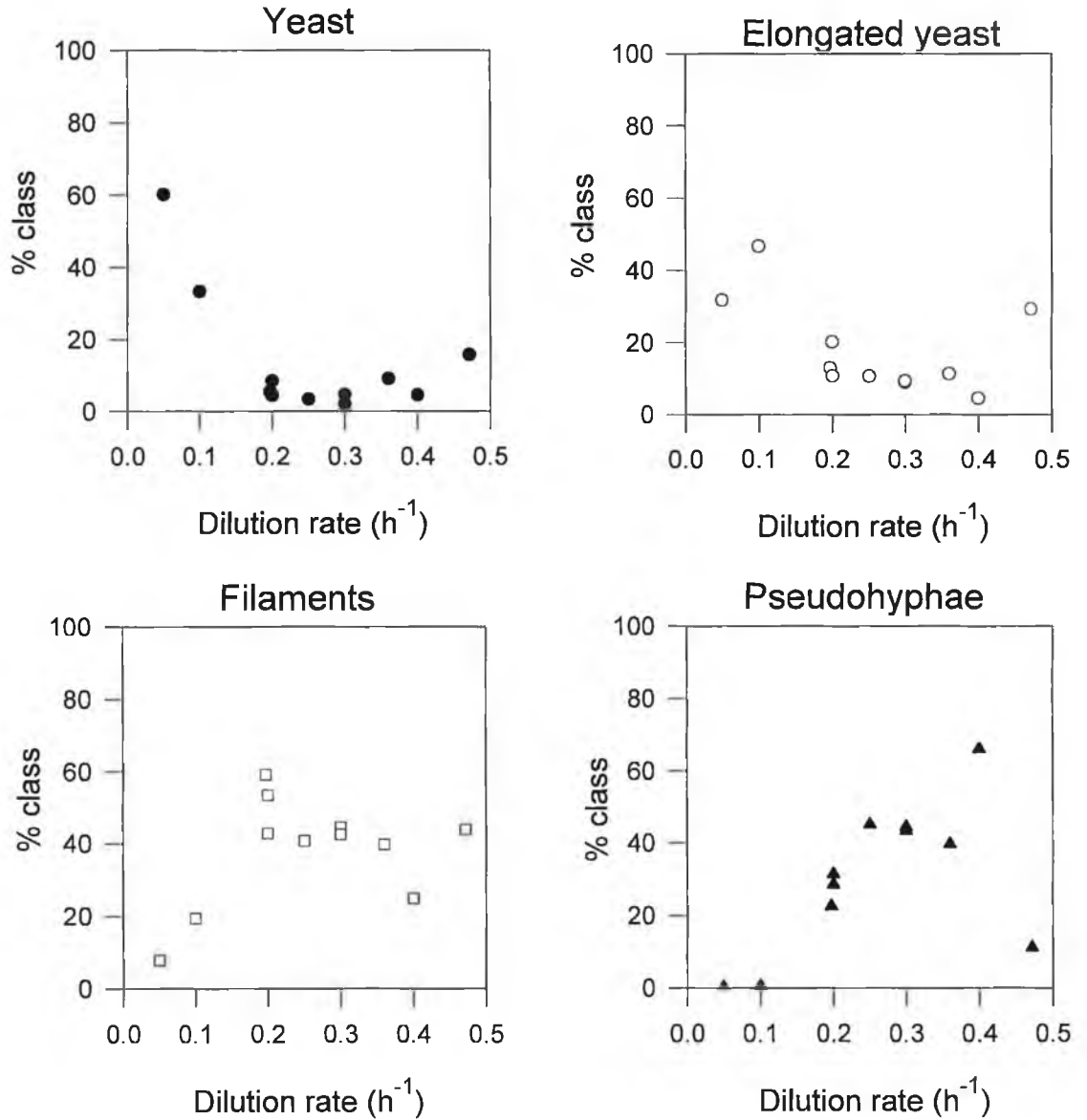


Figure 7.18 Classification data for 5g/L chemostat fermentation (based on cell numerical fraction in each class)

7.4.3 Geometric Properties of Cells

Data for mean volume, length and width of the cells are shown in Figures 7.20 – 7.23. The data reflect what was observed in the classification graphs. All runs show an increase in volume and length with increasing dilution rate indicating the transition from smaller cells such as yeast and elongated yeast to pseudohyphal cells. It is apparent at this stage that even though all fermentations indicate the presence of large quantities of pseudohyphae, that the pseudohyphae present vary

greatly in size. Mean cell width is seen to decrease rapidly initially and increase linearly from $D = 0.2\text{h}^{-1}$ to washout. There is a small increase in cell width with respect to increasing substrate feed concentration.

As mentioned previously in the discussion of percentage classification (by number), an area of interest was noted for the 20g/L fermentation in the region surrounding $D = 0.2\text{h}^{-1}$. A sudden increase in volume and length is noted in this region followed by a sharp decline. The fact that four points (all taken from different fermenter setups) are involved in this phenomenon suggests that it is more than experimental variability. In this region, the rheological behaviour of the broth was different due to the concentration of biomass and the filamentous morphology (all other regions were approximately Newtonian in nature). The fluid became strongly power law in nature. This resulted in non-uniform mixing with almost stagnant regions in the vicinity of the vessel wall. This irregular mixing may be responsible for the sudden change in morphology experienced in this region. Similar behaviour was observed for the 15g/L fermentation in the same range of D values.

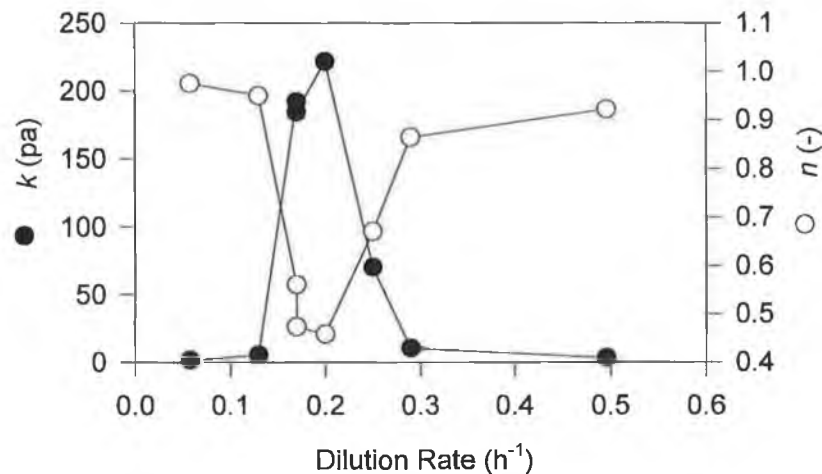


Figure 7.19 Plot of Power law constant (k) and Power law index (n) versus dilution rate for 20 g/L Chemostat fermentation

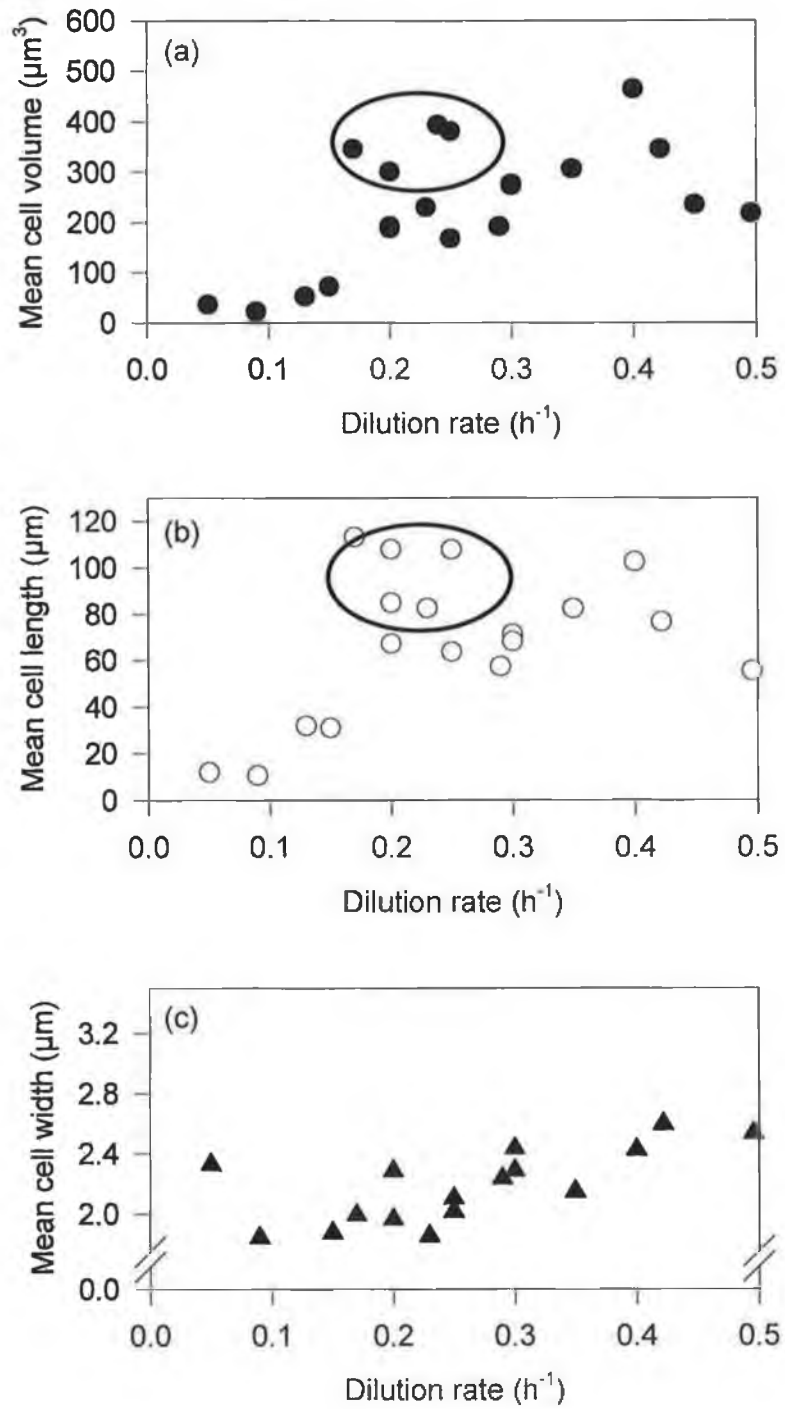


Figure 7.20 Mean geometric parameters of cells for 20g/L chemostat fermentation; (a) cell volume, (b) cell length, (c) cell width

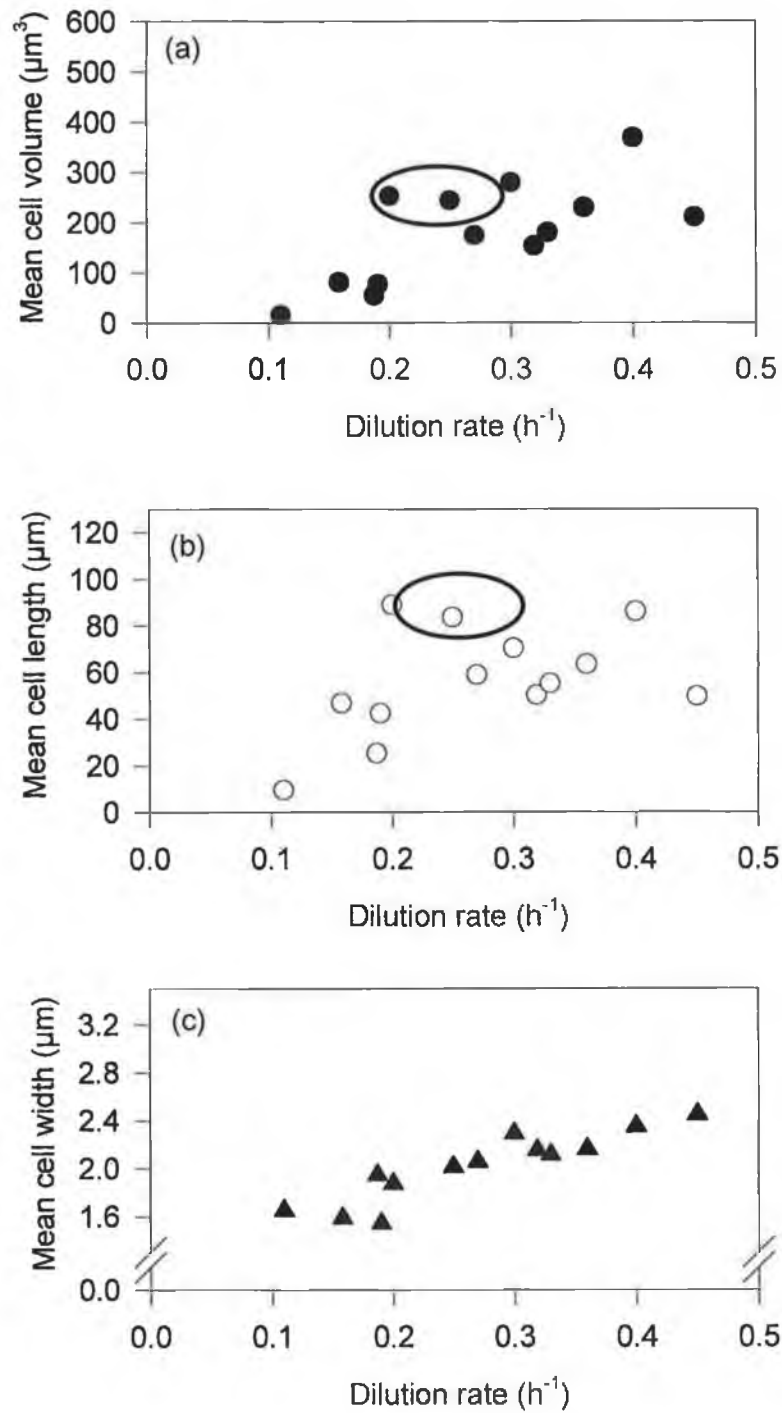


Figure 7.21 Mean geometric parameters of cells for 15g/L chemostat fermentation; (a) cell volume, (b) cell length, (c) cell width

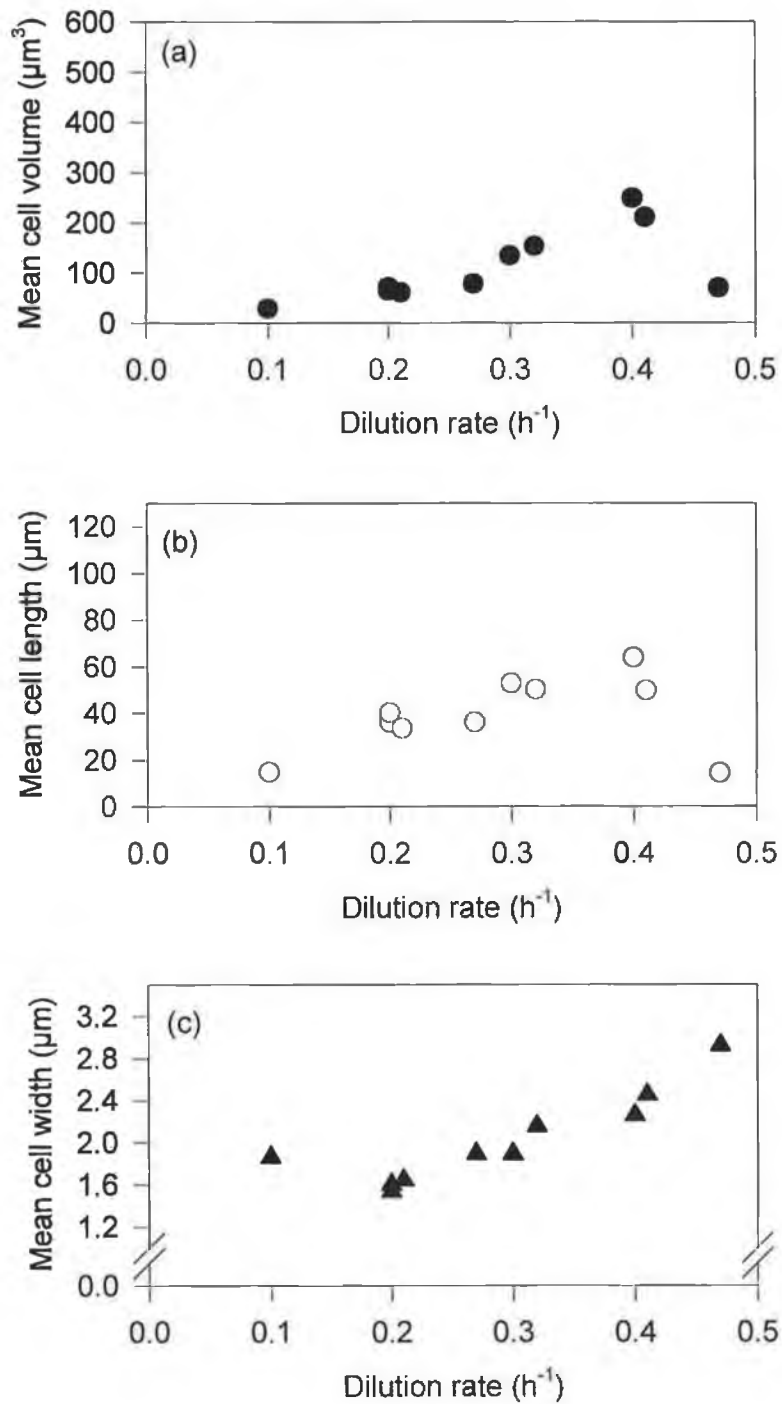


Figure 7.22. Mean geometric parameters of cells for 10g/L chemostat fermentation; (a) cell volume, (b) cell length, (c) cell width

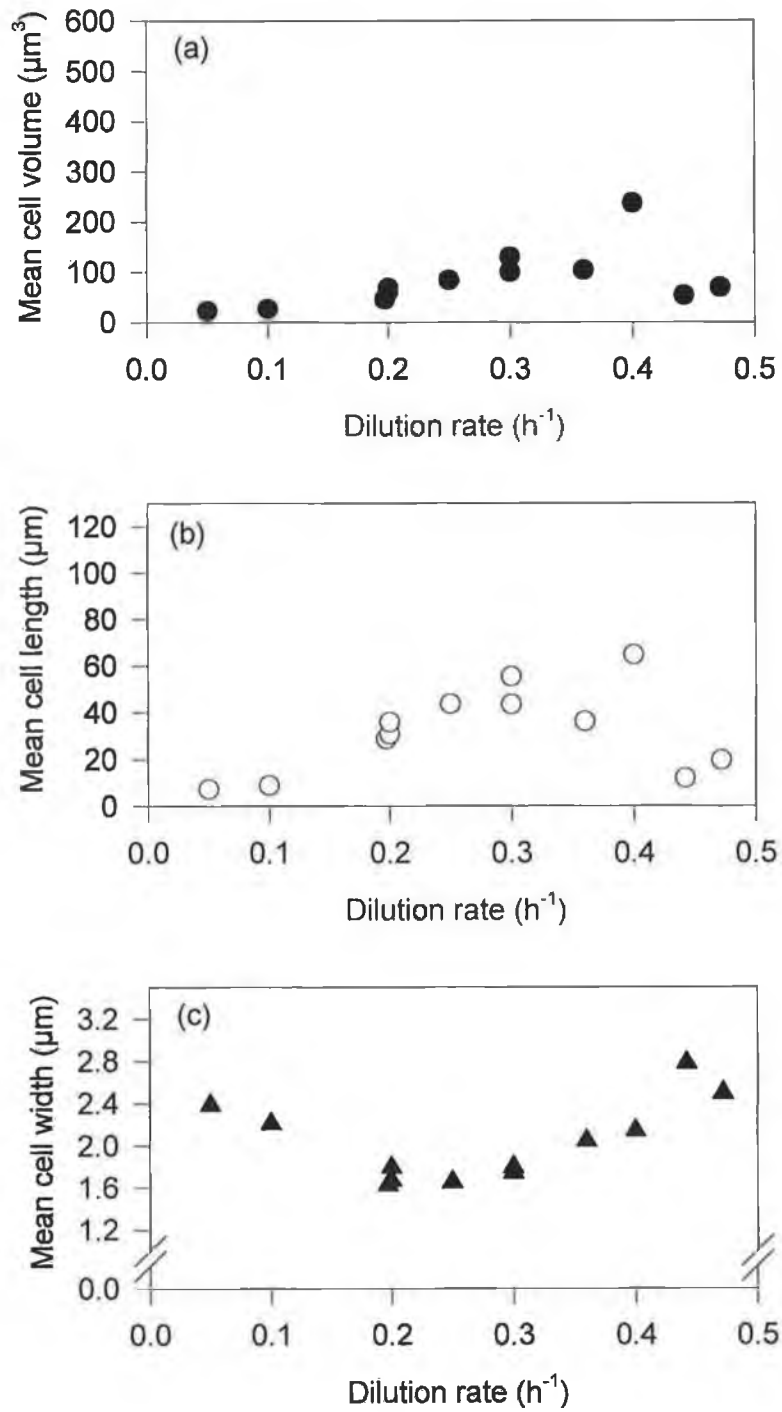


Figure 7.23 Mean geometric parameters of cells for 5g/L chemostat fermentation; (a) cell volume, (b) cell length, (c) cell width

As can be seen in Figures 7.20-7.23, the initial substrate concentration has a considerable effect on development of the pseudohyphae. The average length of the cell population, at any dilution rate, increases with increasing substrate feed concentration. The width of the cells in the fermentation increase linearly after an initial decrease for $D = 0.0-0.2 \text{ h}^{-1}$. This linear increase has been observed for other filamentous organisms while growing in continuous culture, for example, *Fusarium graminearum* (Wiebe and Trinci, 1991).

7.4.4 Pseudohyphal Growth Unit

The hyphal growth unit length (L_{hgu}) is a good indicator of hyphal structure. It is calculated by dividing the total hyphal length (L_t) by the number of hyphal tips (N). A low L_{hgu} is indicative of a highly branched mycelium whereas a high L_{hgu} suggests a less branched structure. The latter is better, on a solid surface, for extending and relocating to regions containing greater amounts of nutrients. L_{hgu} is plotted for each fermentation in Figure 7.24

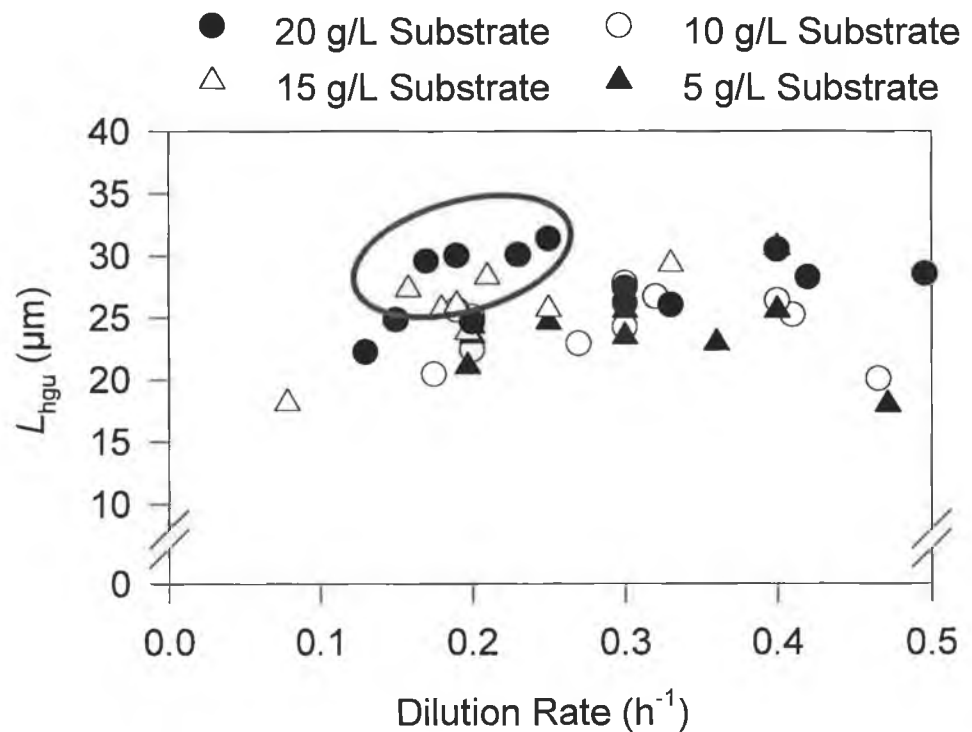


Figure 7.24 Mean L_{hgu} versus dilution rate for four initial substrate concentrations. The mean L_{hgu} of pseudohyphae show a general increase with increasing D for all runs. Again the region surrounding $D = 0.2 \text{ h}^{-1}$ generates some erratic results.

suggesting the viscosity problem also interferes with L_{hgu} . This increase in L_{hgu} with increasing dilution rate is similar to that found by Wiebe and Trinci (1991) with a filamentous fungus, although, the scale of increase in L_{hgu} was much greater. Increases in L_{hgu} generally reflect a transition from a densely branched, morphological form to a less branched, more diverse form capable of a greater degree of foraging. As stated previously, the changes observed here are not significant enough to make a considerable difference to the foraging pattern of the organism.

7.5 GEOMETRIC CONSIDERATIONS FOR MORPHOLOGICAL TRANSITIONS

Morphological transitions in a micro-organism are usually a response to environmental changes. The organism adapts its morphology in an attempt to gain advantage in its natural environment.

The organism absorbs nutrients through the cell wall. Substrate diffusion into the cell has the potential to increase with increasing surface area. The surface area of a prolate ellipsoid is given by the following equation.

$$S_{\text{yeast}} = 2\pi LW \left(\frac{\arcsin\left(\sqrt{1 - \frac{W^2}{L^2}}\right)}{\sqrt{1 - \frac{W^2}{L^2}}} + \frac{W}{L} \right) \quad (7.1)$$

The surface area of a filamentous/pseudohyphal cell can be estimated using equation 7.2

$$S_{\text{fm}} = \pi W \left(L - \frac{NW}{4} \right) \quad (7.2)$$

Where N equals the number of tips in the pseudohypha. By dividing the above values of surface area by the calculated volume of the cell an estimate of the foraging power of the cell can be generated.

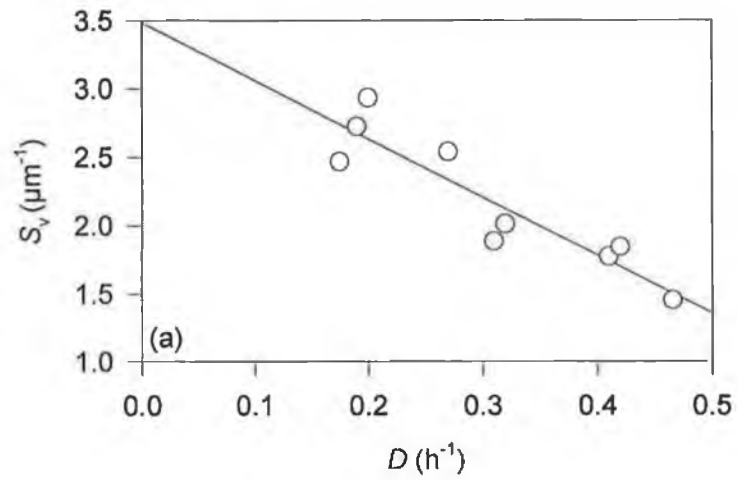
$$S_v = \frac{S}{V} \quad (7.3)$$

The surface area to volume ratio would be expected to be high in an organism with good foraging ability. Also by dividing the surface area term by the cell length, a value associated with the amount of localised surface area can be generated.

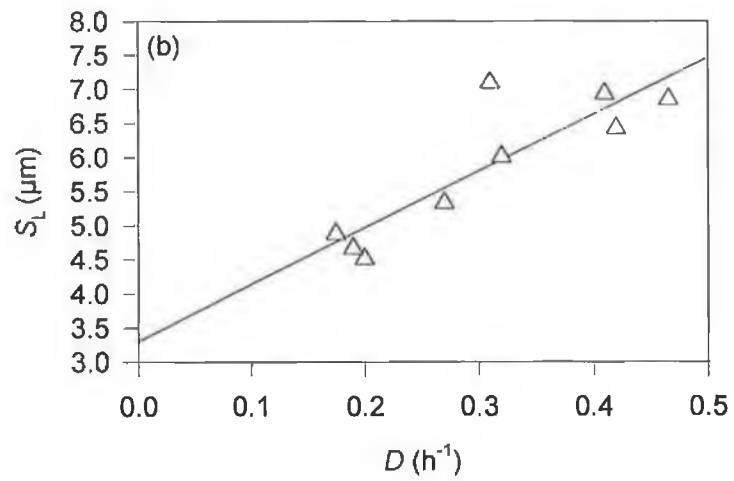
$$S_L = \frac{S}{L} \quad (7.4)$$

This value should lend some information regarding a cell's ability to accumulate localised substrate.

Figure 7.25 shows the change of S_v and S_L with increasing dilution rate for the 10g/L chemostat fermentation.



(a)



(b)

Figure 7.25 Plots of S_v and S_L versus dilution rate for 10g/L chemostat fermentation (a) S_v (b) S_L .

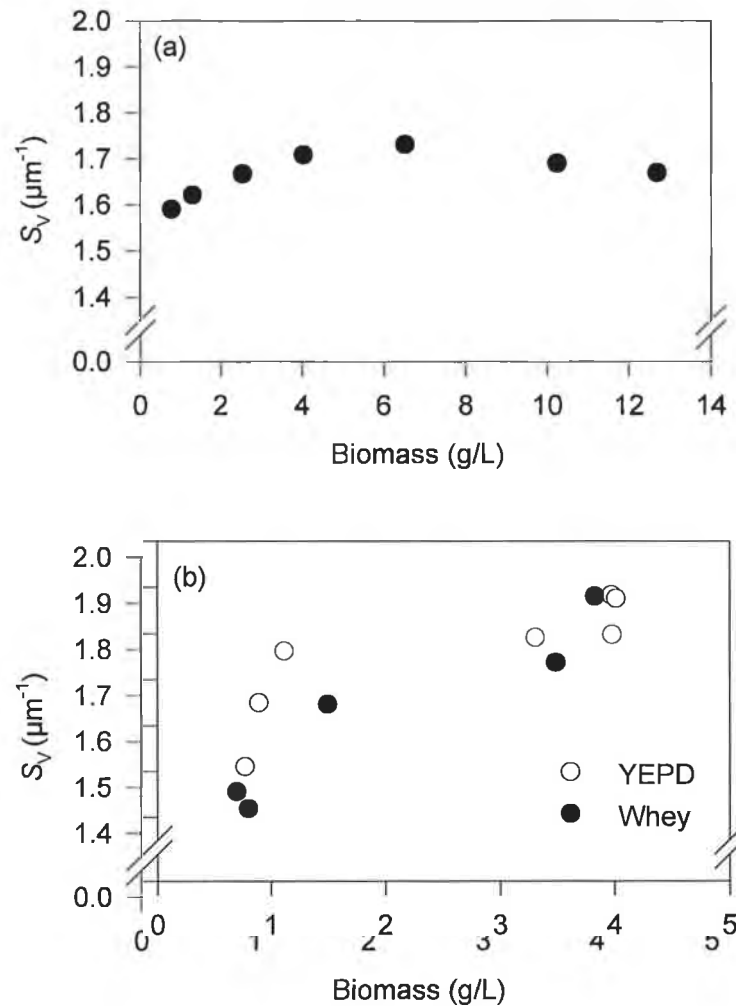


Figure 7.26 Plots of S_V versus biomass concentration for various batch culture fermentations. (a) 800rpm (b) 200rpm.

Figure 7.25 reveals that the foraging power of the organism is at its peak at low dilution rates and decreases as the dilution rate increases. In batch culture, foraging power is low whereas the ability to accumulate localised substrate is high. S_V remains low and the S_L is high (mean value of $8.14\mu\text{m}$ for 800rpm whey fermentation). It is apparent that by a simple manipulation of morphological form the organism has adapted to each environment. This is achieved by presenting the greatest amount of surface area per unit length in batch culture where the concentration of substrate is highest. On a solid substrate this is the equivalent of localising as much surface area as possible in one region. This results in the development of raised colonies on agar plates. The alternative is to present the

highest possible surface area per unit volume. This allows the organism to forage across surfaces and the development of a flat colony is the result.

Figure 7.26 examines the effect of batch culturing on the S_V term. In the 800rpm Whey fermentation, the S_V remains low and constant, reflecting the yeastlike morphology experienced in the fermentation. In the 200rpm fermentations, there is a steady rise in the S_V term with increasing biomass. The fact that both YEPD and whey fermentation's S_V profiles are similar at 200rpm, again suggests that the organism has the same morphological substructure in both fermentations but fails to develop chains of subunits in the whey culture.

7.6 CONCLUSIONS

This set of data suggests that, irrespective of the presence or absence of oxygen, that the organism will grow predominantly in pseudohyphal form while in a substrate limited chemostat. This statement does not hold for the extrema of dilution rate. At low dilution rates, the cell population has to expend large amounts of energy on maintaining itself, prior to any replication. This results in a significant drop in the cell yield coefficient. It also does not hold at high dilution rates when $D \cong \mu_m$. This is where the organism is no longer suffering from substrate limitation. This is a classic response to environment, whereby the cell metamorphoses into a foraging form when concentrations of substrates required for growth are reaching growth limiting levels. It is apparent that the organism cannot sustain such a morphological transition at very low dilution rates (the equivalent of very adverse conditions in a natural environment) and remains in a yeast-like form. This appears to be the equivalent of a dormant phase. The complexity of pseudohyphae increases as the dilution rate increases. This suggests that the higher the growth rate, the greater the foraging power of the yeast. The size of the pseudohypha adjusts accordingly to the increased substrate throughput.

In batch culture, the predominant morphology displayed is yeast-like (yeast and elongated yeast). Double cells predominate during active growth periods. This contradicts the findings of Walker and O'Neill (1990). This is due to a series of misinterpretations on their behalf. The organism was grown at a low agitation rate

in high initial substrate concentrations resulting in large quantities of ethanol. Any fermentations completed in this present work that produced large quantities of ethanol were generally heterogeneous in morphology and in the case of the YEP based cultures extremely filamentous and pseudohyphal. These cultures were deemed “aerobic” by Walker and O’Neill and hence the conclusion was made that aerobic growth supports filamentous growth. When the cultures were made anaerobic, growth rates were slowed to a point where maintenance again becomes an issue. This resulted in the “dormant state” observed in the chemostat at very low dilution rates. This led them to conclude incorrectly that anaerobic cultures produced yeastlike cells because they were deprived of oxygen rather than the fact that the growth rate limited the development of hyphal cells.

Walker and O’Neill contradict their own conclusions by demonstrating a predominantly yeastlike morphology for a culture grown aerobically on glycerol. Glycerol is a very poor, and slowly metabolised substrate resulting in very slow growth rates. Hence the requirements for oxygen are lower in such fermentations and generally oxygen is in excess, resulting in a yeastlike morphology, as observed for the 800rpm whey fermentation.

The current findings are in agreement with previous research. *K. marxianus* responds strongly to substrate limitation, this has been noticed, to a lesser extent in *Saccharomyces cerevisiae* (Hill and Robinson, 1988). The organism also responds to partial oxygen limitation, where the oxygen is only partly limiting and conditions are not completely anaerobic. Any morphological transition experienced in batch culture was minor, in terms of pseudohyphal length and structure, compared to those found in substrate limited chemostat culture. The study also reveals that the organism’s morphology is different in different media when the organism experiences adverse conditions yet behaves identically when under ideal conditions. Although the average length of cells in the YEPL and YEPD cultures surpasses those of the whey-based medium, the average width and S_V were almost identical (Figure 7.10(c), Figure 7.26). This suggests that the morphology of the subunits in pseudohyphae is identical to the single and double cells in the whey medium but the ability to form pseudohyphal chains is greater in the YEPL and YEPD based media. This area requires further research in the

future, to identify the key nutrient or nutrients causing the organism to change so dramatically.

CHAPTER 8

POPULATION DISTRIBUTIONS OF VARIOUS MORPHOLOGIES OF *Kluyveromyces marxianus*

8.1 INTRODUCTION

Populations can generally be described in terms of distributions, functions that describe the frequency of a measured parameter at given values. The most widely used distribution to describe populations is known as the Gaussian or Normal distribution. The probability distribution is described by the following function (Montgomery and Runger, 1994).

$$p(x) = \frac{1}{\sigma\sqrt{2\pi}} \exp\left[\frac{-(x - \bar{x})^2}{2\sigma^2}\right] \quad (8.1)$$

This results in a distribution where the mean (\bar{x}) is equal to the median and 95% of the population is contained within two standard deviations (σ) on either side of the mean. Often statistical analysis of parameters assumes that populations are distributed normally about the mean and that the mean and standard deviation of the population is adequate information to fully describe the size and scatter of a parameter. Often this is not the case.

Certain biological systems are not described by the above distribution due to exponential development with respect to time. Filamentous fungi develop linearly from each hyphal tip yet the whole hypha develops exponentially with respect to time (Trinci, 1969) When such organisms are growing in continuous culture there is a normal distribution in terms of hyphal residence time. This means that hyphal volume or length will not be distributed normally. The lognormal distribution can often be applied to such systems to describe the population distribution. The probability distribution is described by the following function.

$$p(x) = \frac{1}{\sigma_{\ln x} \sqrt{2\pi}} \exp\left(\frac{-(\ln(x) - \overline{\ln x})^2}{2\sigma_{\ln x}^2}\right) \quad (8.2)$$

A variant of the above function has been used by Kieran *et al.* (1993) to describe the population distribution of *Morinda citrifolia*, a plant cell strain that develops in shear-sensitive chains, in suspension culture. While the development of these cells is linear, the cells were more susceptible to shear as the length increased (see Chapter 2) hence the generation of a skewed distribution.

One of the aims of the present work was to develop a population model distribution that will successfully describe the range of data experienced. It was also hoped to investigate whether the morphological classes described in Chapter 4 have any bearing on this process.

8.2 INITIAL INVESTIGATIONS.

Three populations were used to assess the potential of different population distribution models

- A predominantly yeast-like population taken from batch culture
- An mixed morphology population taken from chemostat culture
- A predominantly pseudohyphal population taken from chemostat culture

Table 8.1 details the culture conditions for each Sample.

Table 8.1 Origins of Samples used for population model development

Sample no.	Description	Culture conditions	Number of cells analysed
1	Yeast-like	800 rpm whey medium – Sample time = 5.5 h	302
2	Intermediate	Chemostat 5g/L lactose feed concentration $D =$ 0.20 h^{-1}	397
3	Pseudohyphal	Chemostat 20g/L lactose feed concentration $D =$ 0.35 h^{-1}	250

The first stage of the evaluation was to assess the potential of normal and lognormal distributions, to describe the populations. Frequency distributions generated from cell volume data, were converted to probability distributions using the following equation.

$$p(x) = \frac{f(x)}{wN_t} \quad (8.3)$$

Where w is the histogram bucket width and N_t is the total sample size. A suitable histogram bucket width was determined using the recommendation of Kanazawa (1988).

$$w = 3.5\sigma N_t^{-0.33} \quad (8.4)$$

Figures 8.1 to 8.3 present the probability distributions of cell volume for each of the test samples.

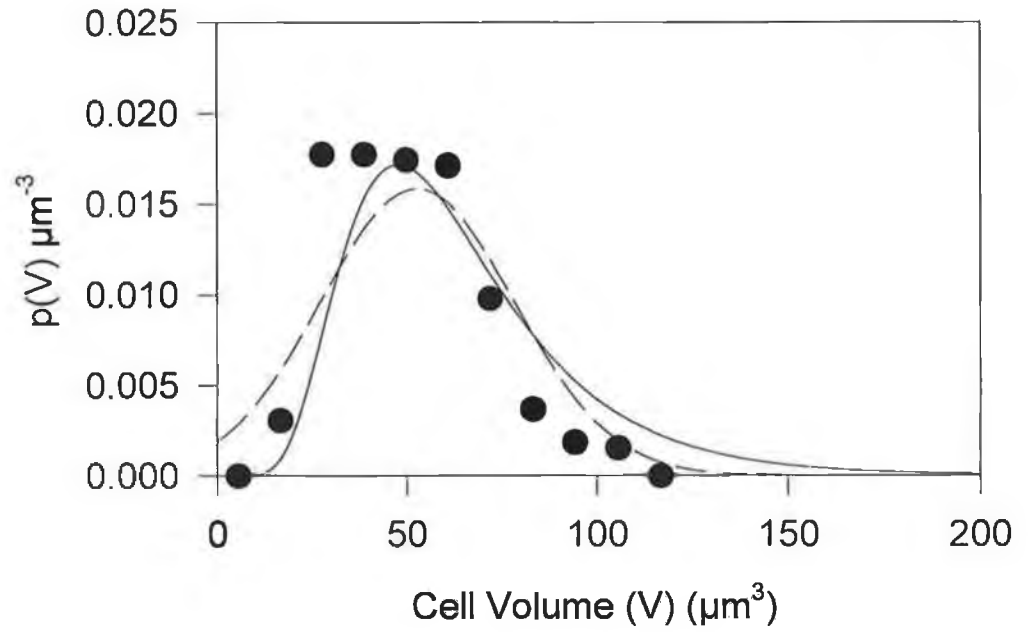


Figure 8.1 Lognormal and Gaussian volume distributions for Sample 1. Solid line – lognormal distribution, dashed line – normal distribution (sample size=302)

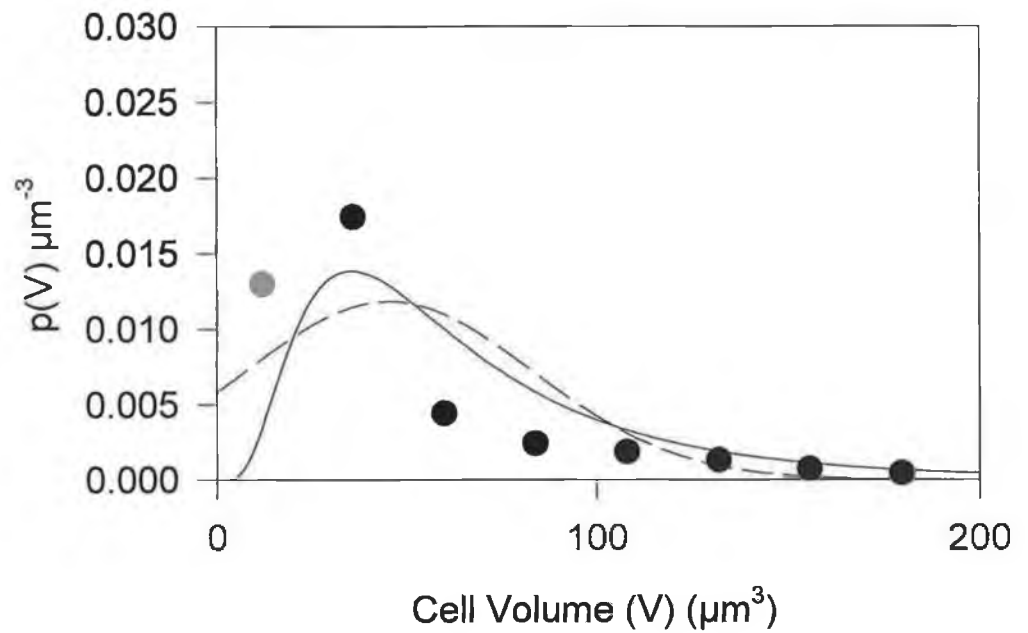


Figure 8.2 Lognormal and Gaussian volume distributions for Sample 2 Solid line – lognormal distribution, dashed line – normal distribution (sample size = 297)

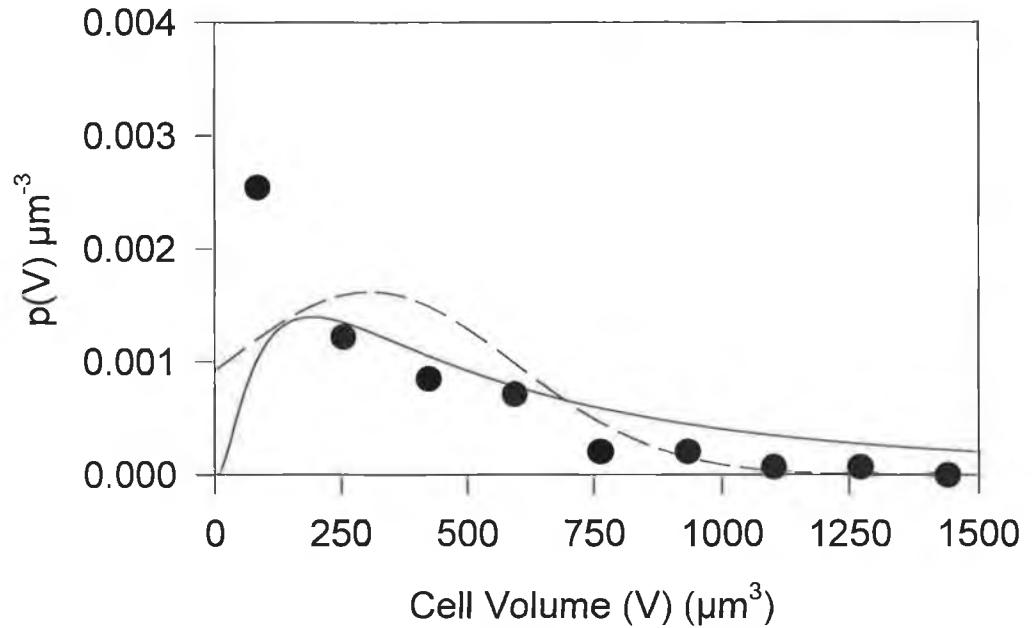


Figure 8.3 Lognormal and Gaussian volume distributions for Sample 3 Solid line – lognormal distribution, dashed line – normal distribution (sample size = 250)

The global population models both fail, particularly the Gaussian distribution, to adequately describe the cell population over the entire range of operating conditions.

8.3 DISTRIBUTIVE CHARACTERISTICS OF CELL SUB-POPULATIONS

It was decided to divide the population into three distinct classes, single cells, double cells and pseudohyphae and assess the types of distribution associated with each. If this approach proved successful it was hoped to develop a distribution which is the sum of several sub-distributions, where,

$$p(x) = \sum_i^{n_c} N_i f_i(x) \quad (8.4)$$

Where n_c is the number of classes used to describe the population and N_i is the number fraction of objects in class i . By examining the distributive characteristics of the three sub-populations, it was hoped that a more sensitive population model could be developed that permitted a better fit to the data.

8.3.1 Single cells

Single cells are composed of single yeast, elongated yeast and filaments. Figures 8.4 and 8.5 shows the probability distribution for single cells in Sample 1 and Sample 2. Not enough single cells were present in Sample 3 to attempt statistical analysis. While both the lognormal and the normal distributions approximates the data from Sample 1 (Figure 8.4) well, both fail to approximate the data in Sample 2 (Figure 8.5). The lognormal distribution approximates both population distributions to a more uniform degree.

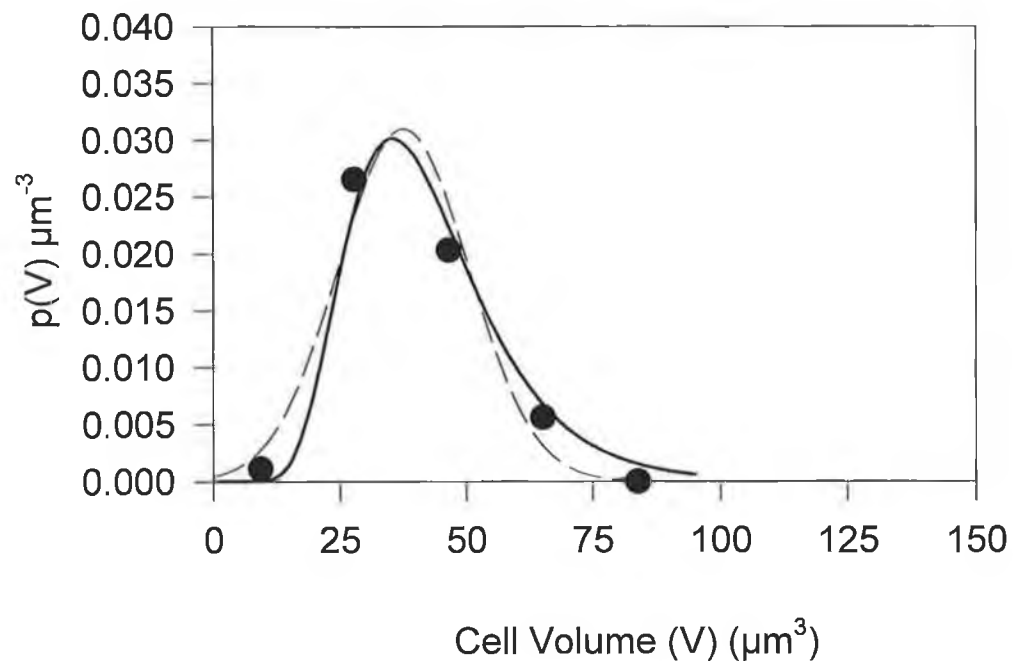


Figure 8.4 Volume distribution of single cells for Sample 1. Solid line – lognormal distribution, dashed line – normal distribution (sample size = 95)

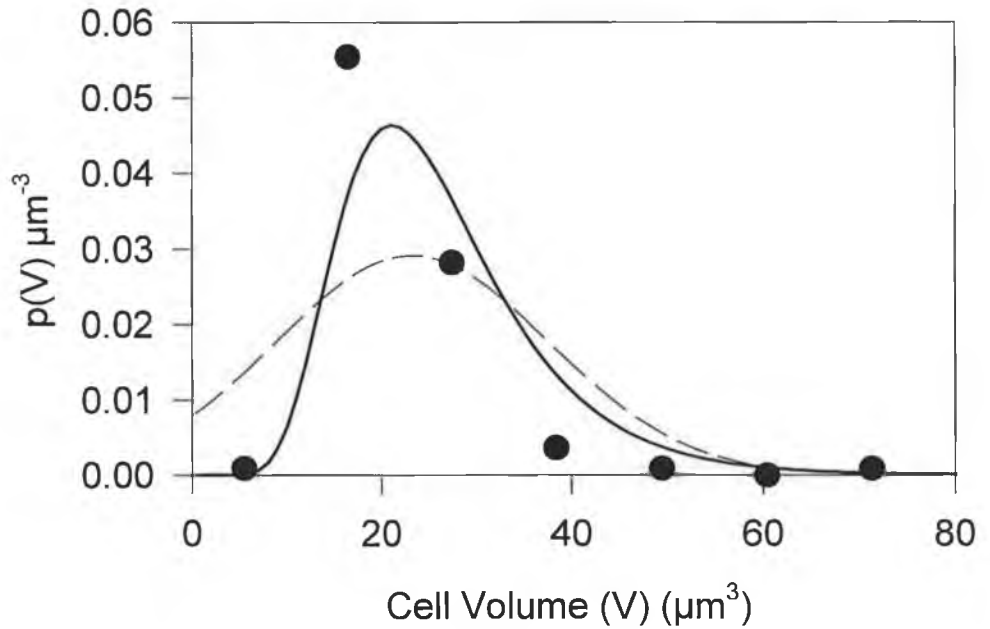


Figure 8.5 Volume distribution of single cells for Sample 2. Solid line – lognormal distribution, dashed line – normal distribution (Sample size = 101)

The poor data fit obtained in Figure 8.5 can be explained in terms of the classification of cells examined. The classification breakdown for each populations single cells is shown in Table 8.2.

Table 8.2 Summary of classification breakdown for single cells for Sample 1 and 2

Sample	%Yeast	%Elongated yeast	%Filaments	Number of single cells
Sample 1	79	16	5	95
Sample 2	16	24	61	101

Sample 1 is mainly composed of yeast and elongated yeast, whereas Sample 2 has significant quantities of filaments in the culture. The gross morphology difference between filaments and the yeast-like forms is significant thus the development of the population may not be continuous, in terms of yeast – elongated yeast - filaments. The filament population was examined for distributive properties.

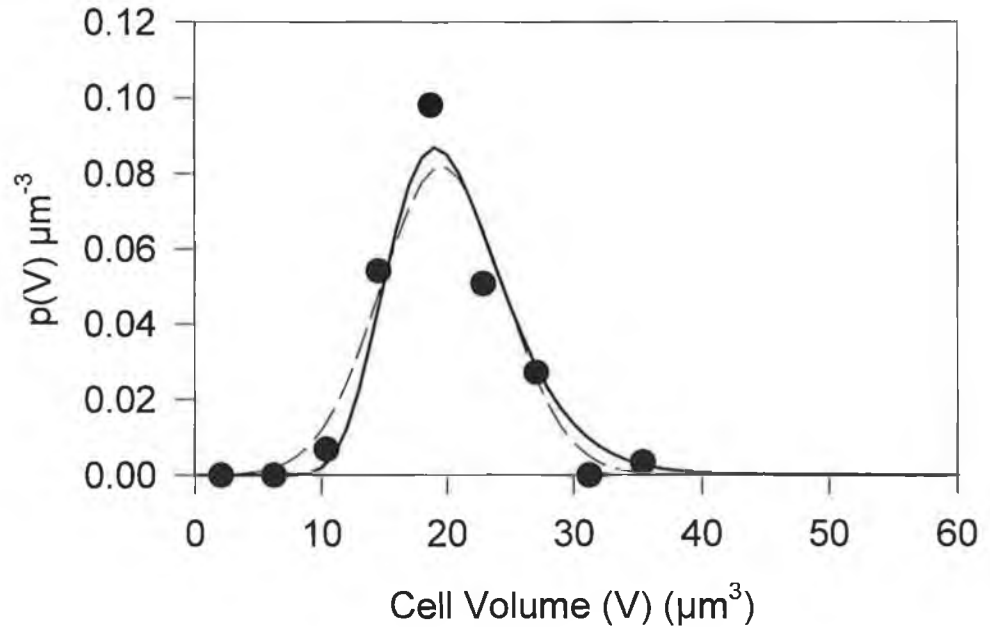


Figure 8.6 Volume distribution for single filaments in Sample 2, solid line - lognormal distribution, dashed line – normal distribution (Sample size = 72)

It is clear from Figure 8.6 that the filaments are normally distributed, although the lognormal distribution does account well for the slight skew experienced in the 30-40 μm subrange. Based on observation of Figures 8.4 and 8.6, it can be said that Yeast and Elongated yeast are part of the same population whereas filaments are a discrete population that require separate treatment. The following approach is proposed to describe single cell populations.

$$p(V)_{\text{singles}} = N_y p_y(V) + N_f p_f(V) \quad (8.5)$$

where N_y is the number fraction of yeast and elongated yeast, N_f is the number fraction of filaments, $p_y(V)$ and $p_f(V)$ probability distribution functions for yeast and filament volume respectively. The two probability distribution functions used are lognormal due to the slightly better description of the population distributions. Figure 8.7 demonstrates the effectiveness of this approach in describing the population of single cells in Sample 2.

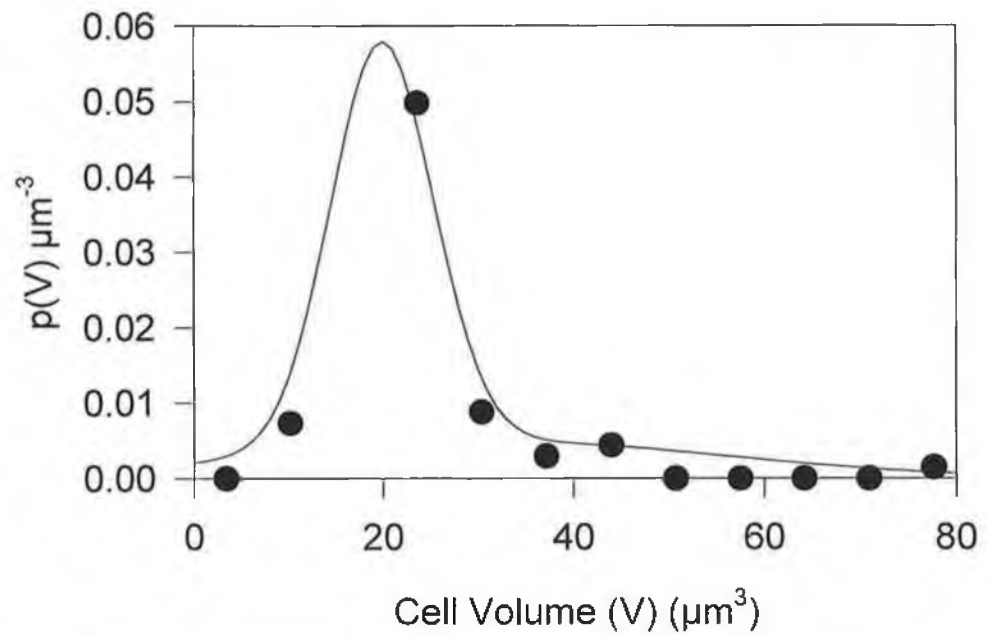


Figure 8.7 The use of the summed distribution of yeastlike cells and filaments to describe the overall volume distribution of single cells for Sample 2. ($N_y = 0.29$, $N_f = 0.71$) (Sample size = 101)

8.3.2 Double cells

Figure 8.8 and 8.9 show the probability distributions of volume for the double cells in Samples 1 and 2.

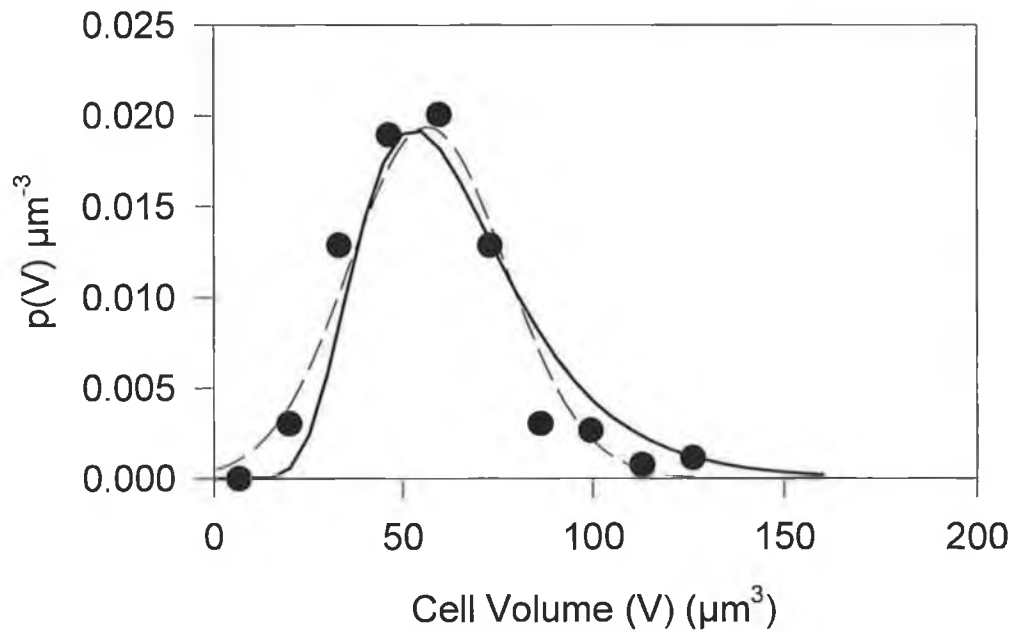


Figure 8.8 Volume distribution of double cells for Sample 1, solid line – lognormal distribution, dashed line – normal distribution (Sample size = 201)

On examination of the double cell distribution from Sample 1 it can again be seen that the normal distribution adequately describes the population, although again the lognormal distribution deals with the slight skew experienced. Table 8.3 shows the population breakdown for double cells in Sample 1 and 2.

Table 8.3 Summary of classification breakdown for double cells for Samples 1 and 2

Sample	%Yeast	%Elong. yeast	%Filaments	Sample size
Sample 1	75	20	5	201
Sample 2	9	32	59	221

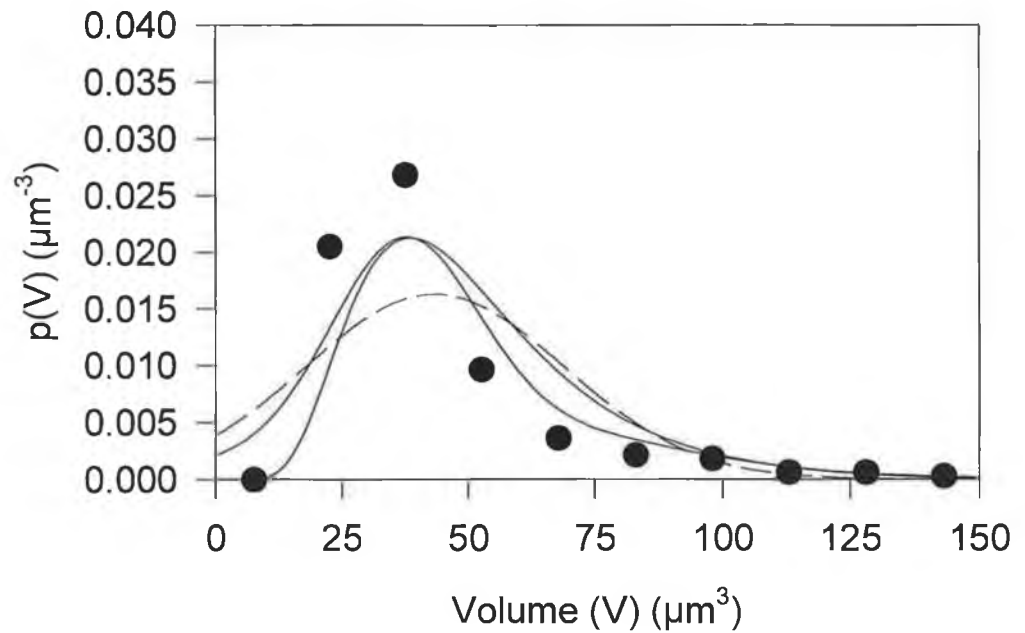


Figure 8.9 Volume distribution of double cells for Sample 2, solid line – lognormal distribution, dashed line – normal distribution (Sample size = 221)

The normal or lognormal distribution fails to completely describe the population containing significant quantities of double filaments. The same approach as applied in the previous section will be used to describe the population. Both filaments and yeast-like cells are separated, a log-normal distribution generated for each and the weighted results summed. Figure 8.10 shows the resultant distribution that describes the double cell population. As can be seen in Figure 8.10, the use of this approach provides a better description of the data.

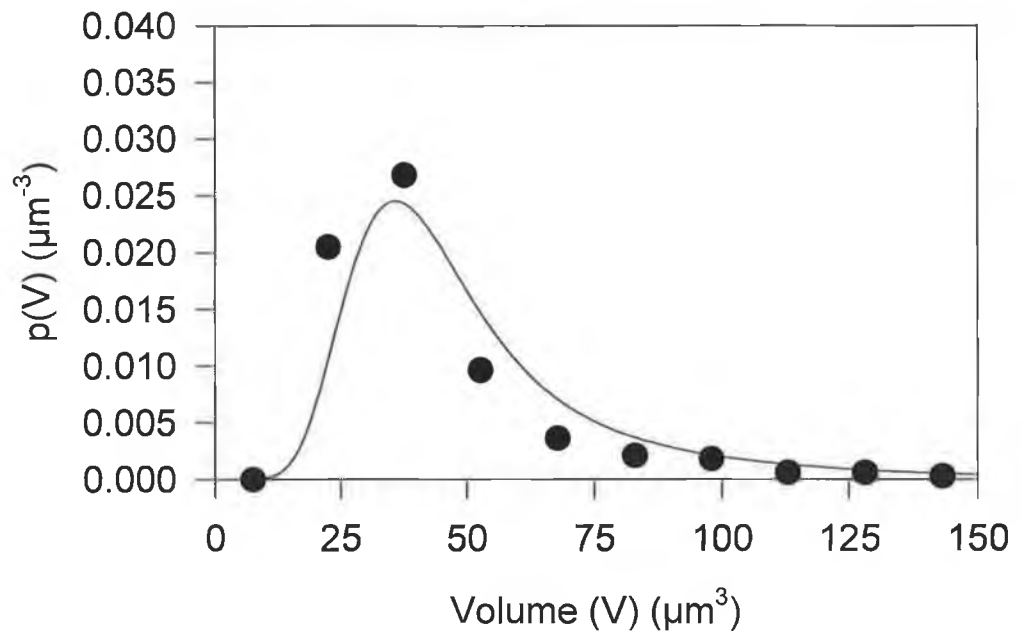


Figure 8.10 The use of the summed distribution of yeastlike cells and filaments to describe the overall volume distribution of double cells for Sample 2. ($N_{dy} = 0.41$, $N_{df} = 0.59$)

8.3.3 Pseudohyphae

Hyphae, in theory, extend their volume exponentially (Trinci, 1969). The distributions are therefore expected to be lognormal in nature. Figure 8.11 and 8.12 show the probability distributions of pseudohyphal volume for Samples 2 and 3. The calculated distributions in both figures show a slight bias towards larger cells. This is due to the sensitivity of the calculation; if a few extremely large cells are measured the distribution will be biased in favour of large cells. It is also possible that due to the scale of the pseudohyphae that an operator bias in favour of measuring shorter pseudohypha may have existed. The use of an automated microscope stage may have produced better results than a human operator in this case.

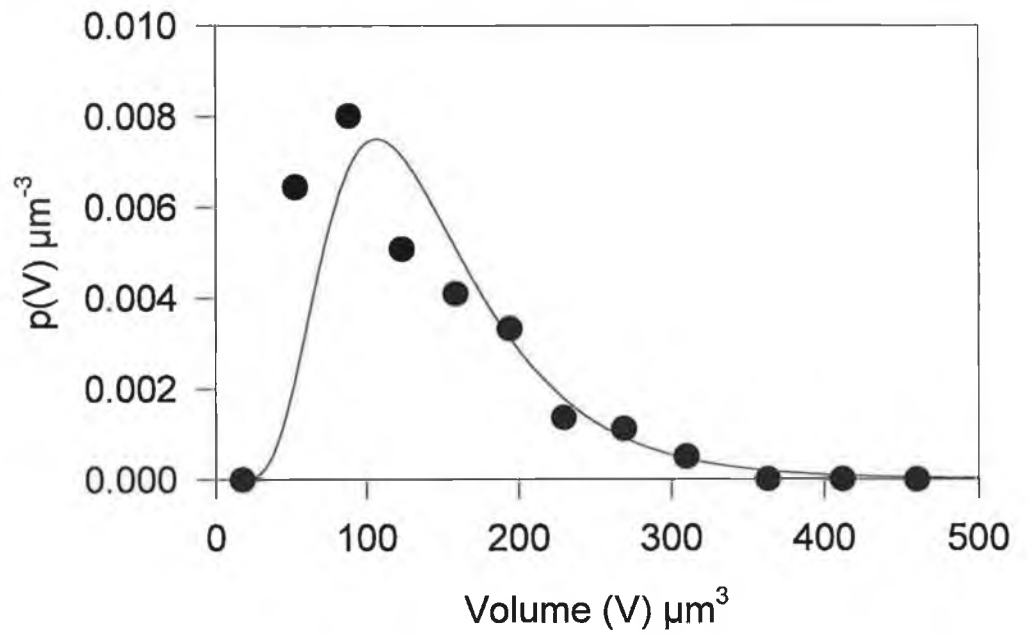


Figure 8.11 Distribution of pseudohyphae for Sample 2, solid line – lognormal distribution (sample size = 146)

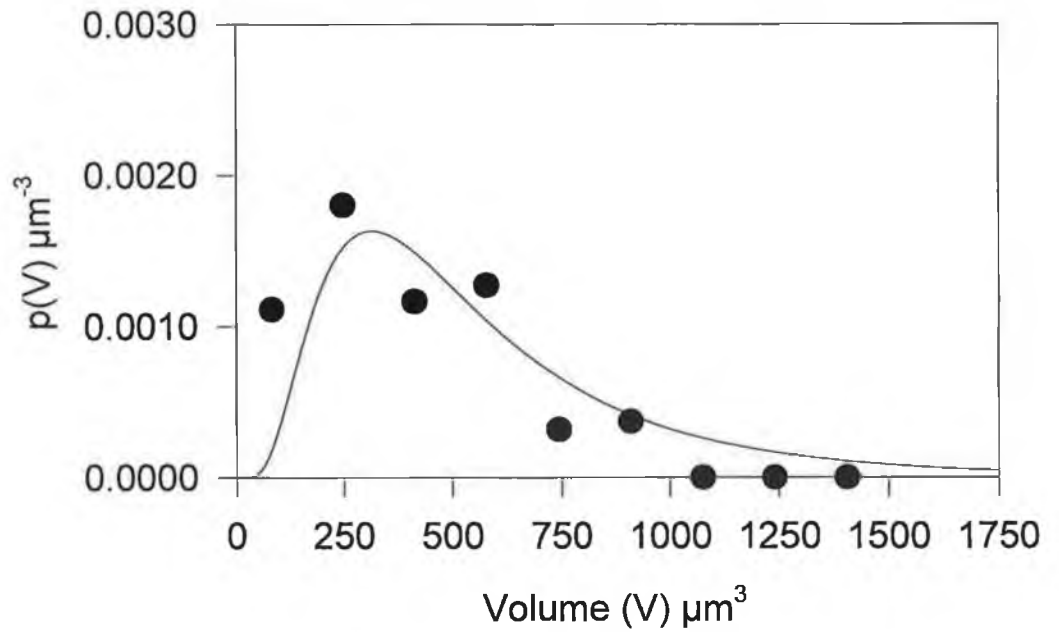


Figure 8.12 Distribution of pseudohyphae for Sample 3, solid line – log-normal distribution (sample size = 164)

8.4 GENERATION OF SUMMED DISTRIBUTION FUNCTION

The summed distribution was the weighted sum of the following lognormal distributions.

- Yeastlike single cells $N_y, p_y(V)$
- Filamentous single cells $N_f, p_f(V)$
- Yeastlike double cells $N_{dy}, p_{dy}(V)$
- Filamentous double cells $N_{df}, p_{df}(V)$
- Pseudohyphae $N_m, p_m(V)$

The distributions were weighted according to their number fraction in the population. A transform was written using Sigmaplot [™] (Jandel Scientific, CA, USA) to calculate the distributions based on the raw data supplied by the image analysis system. If any subpopulation had a numerical representation of less than 5, they were omitted due to the generation of “spikes” in the distributions. Figures 8.13 to 8.15 show the effectiveness of this approach in describing the test populations.

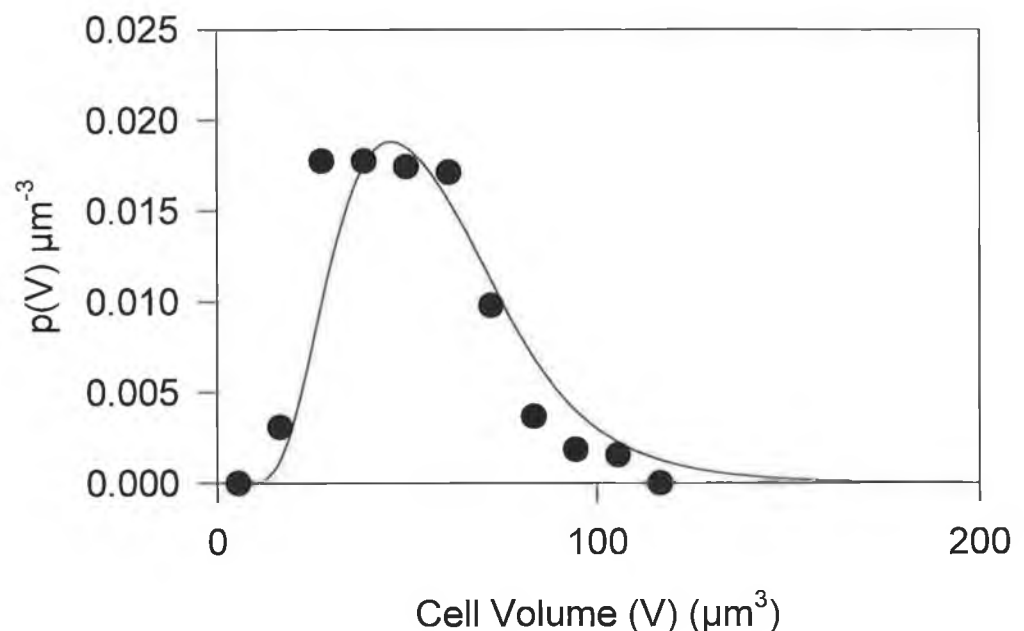


Figure 8.13 Summed volume distribution for sample 1, $N_y = 0.31$, $N_{dy} = 0.63$, $N_f = 0.02$, $N_{df} = 0.03$, $N_m = 0.00$ (sample size = 302)

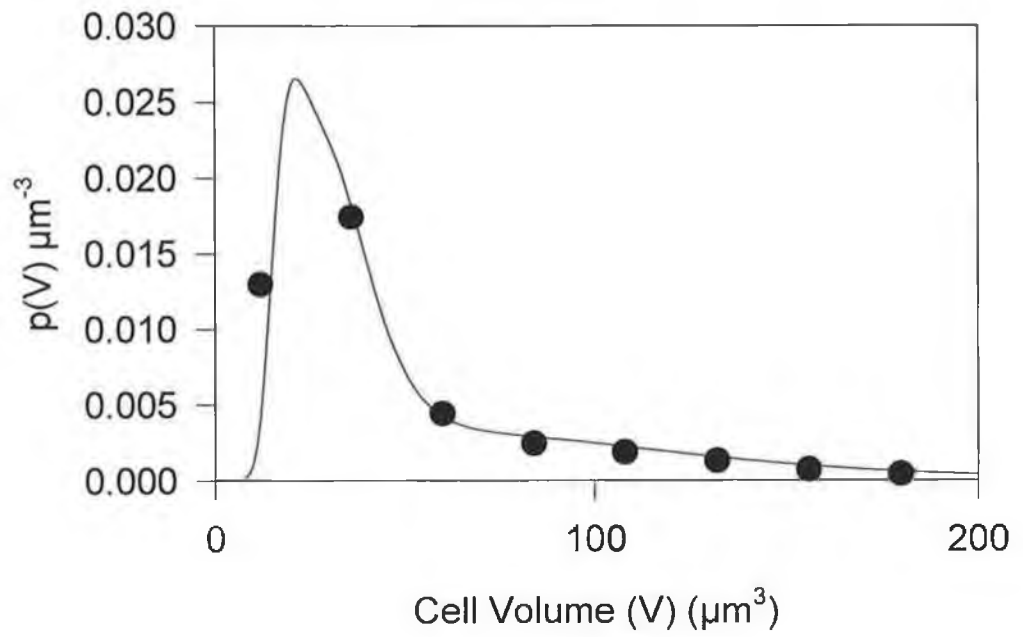


Figure 8.14 Summed volume distribution for sample 2, $N_y = 0.10$, $N_{dy} = 0.09$, $N_r = 0.25$, $N_{df} = 0.34$, $N_m = 0.23$ (sample size = 297)

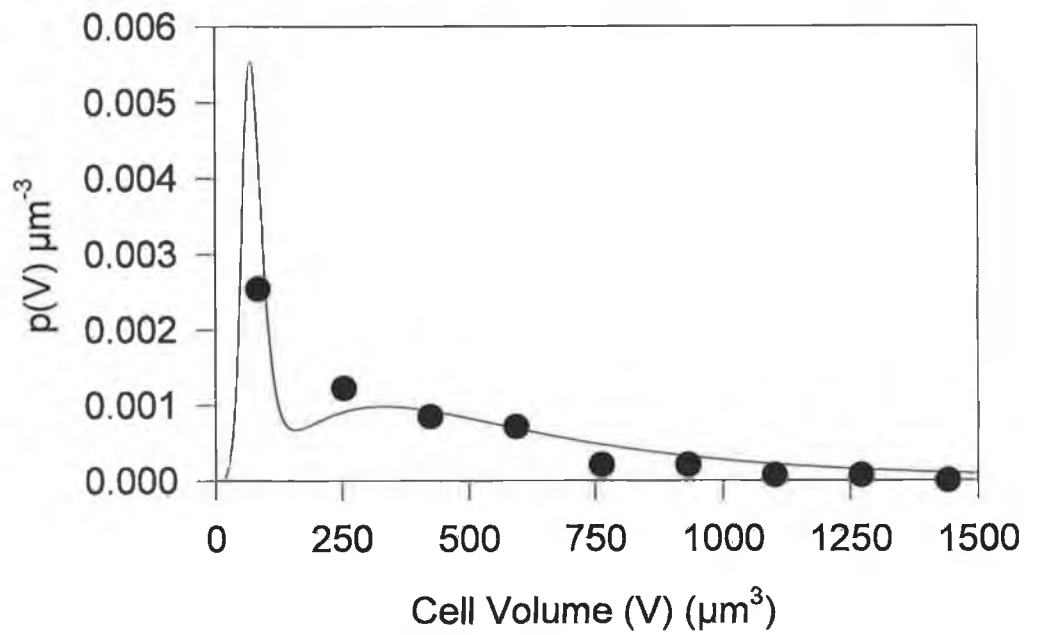


Figure 8.15 Summed volume distribution for sample 3, $N_y = 0.01$, $N_{dy} = 0.09$, $N_r = 0.02$, $N_{df} = 0.20$, $N_m = 0.68$ (sample size = 250)

8.5 APPLICATION OF THE SUMMED DISTRIBUTION TO CELL LENGTH AND CELL WIDTH

The same approach was applied to distributions of cell length and cell width. As can be seen from Figures 8.16 to 8.22, the use of summed distributions describes the experimental data very well. From an examination of the cell width distributions (Figures 8.19-8.22) the two primary morphological forms, yeastlike and pseudohyphae, are evident by their difference in width.

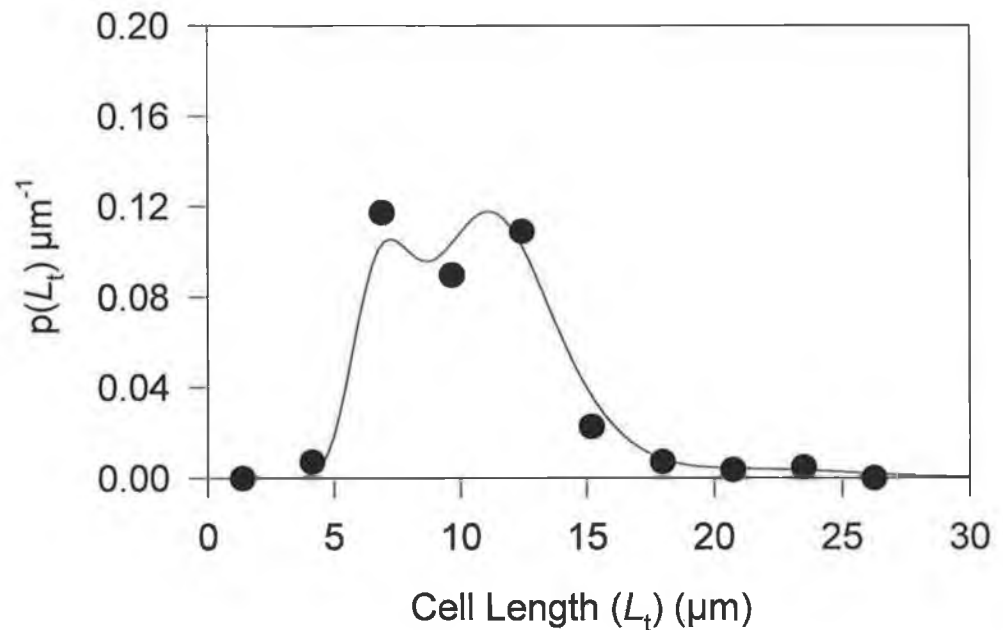


Figure 8.16 Summed length distribution for Sample 1 cell length, $N_y = 0.31$, $N_{dy} = 0.63$, $N_f = 0.02$, $N_{df} = 0.03$, $N_m = 0.00$ (Sample size = 302)

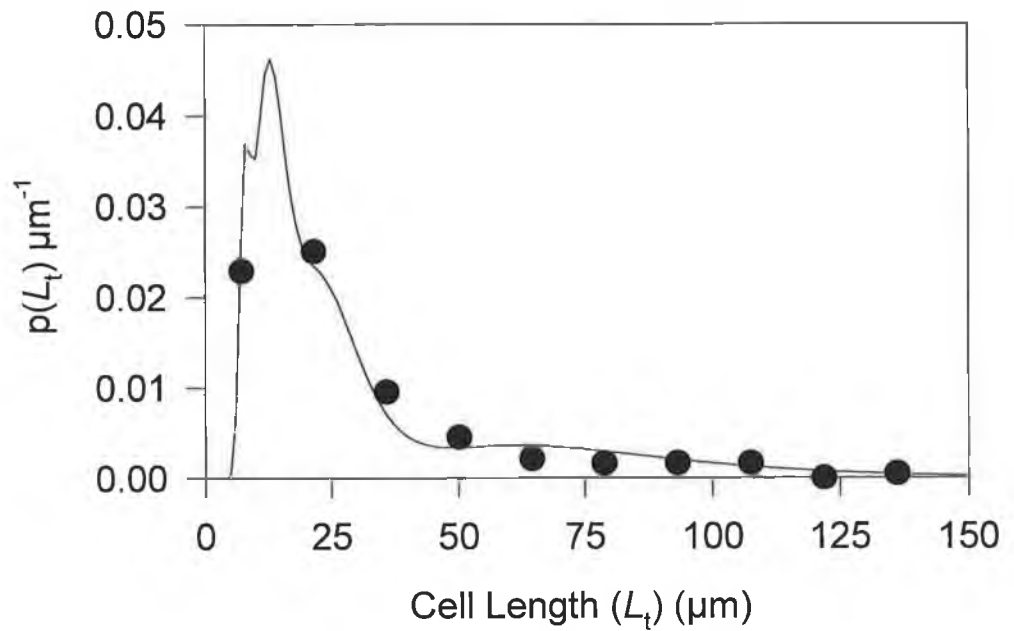


Figure 8.17 Summed length distribution for intermediate Sample 2, $N_y = 0.10$, $N_{dy} = 0.09$, $N_f = 0.25$, $N_{df} = 0.34$, $N_m = 0.23$ (Sample size = 297)

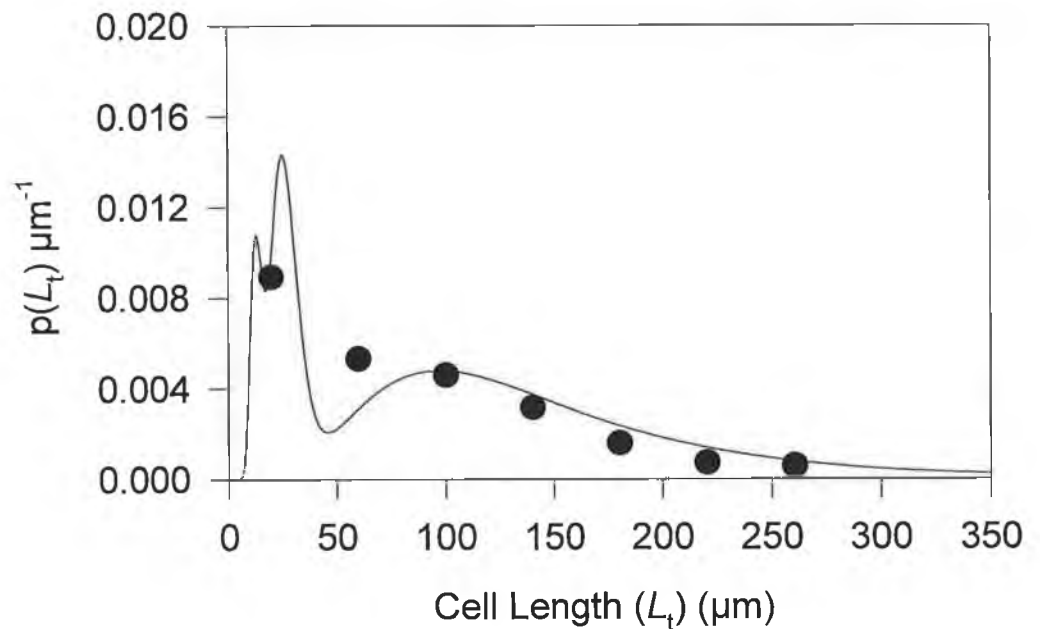


Figure 8.18 Summed length distribution for pseudohyphal Sample 3, $N_y = 0.01$, $N_{dy} = 0.09$, $N_f = 0.02$, $N_{df} = 0.20$, $N_m = 0.68$ (Sample size = 250)

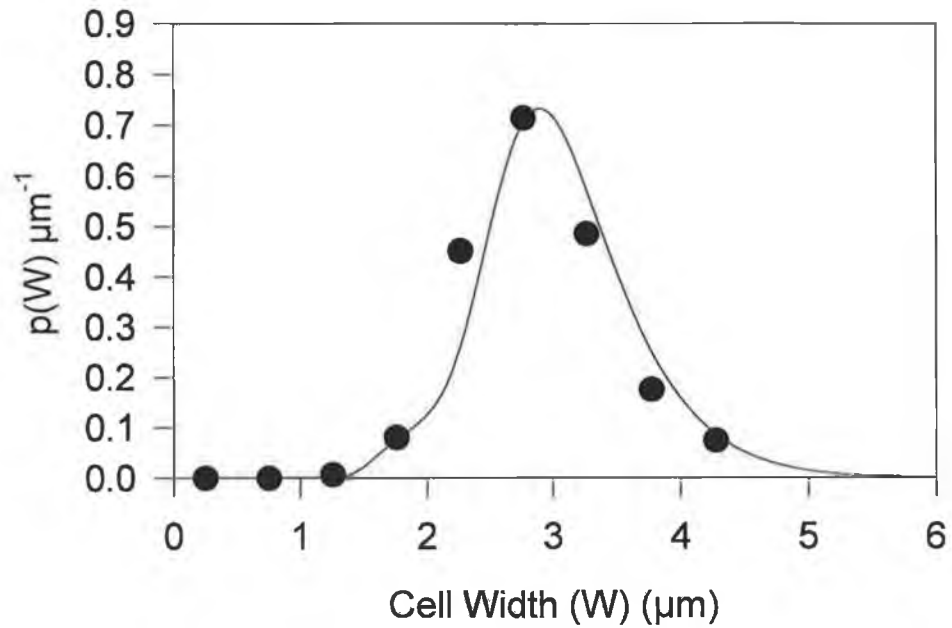


Figure 8.19 Summed width distribution for yeast-like Sample 1, $N_y = 0.31$, $N_{dy} = 0.63$, $N_f = 0.02$, $N_{df} = 0.03$, $N_m = 0.00$.(Sample size = 302)

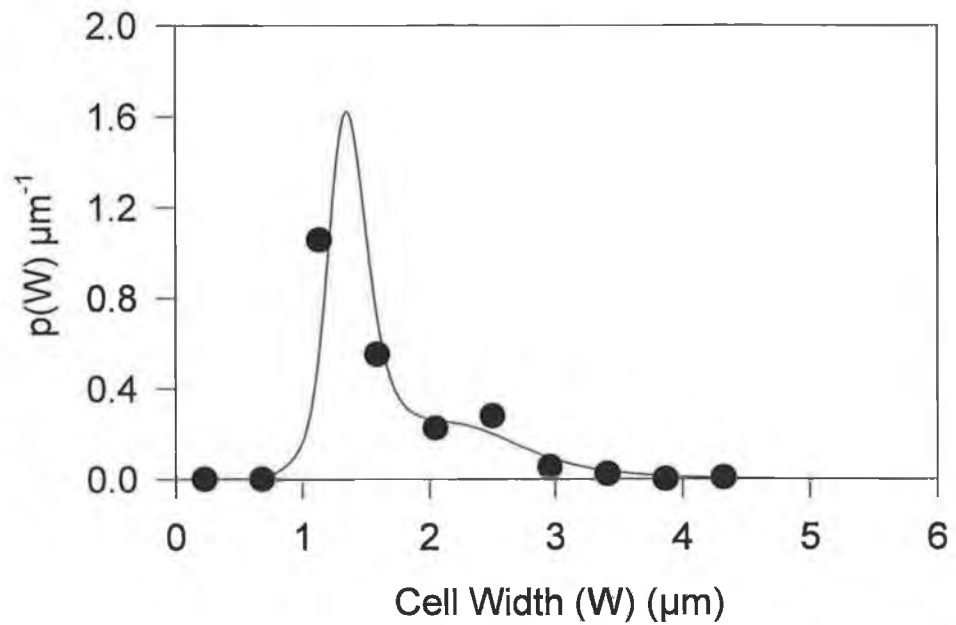


Figure 8.20 Summed width distribution for yeast-like Sample 2, $N_y = 0.10$, $N_{dy} = 0.09$, $N_f = 0.25$, $N_{df} = 0.34$, $N_m = 0.23$ (Sample size = 297)

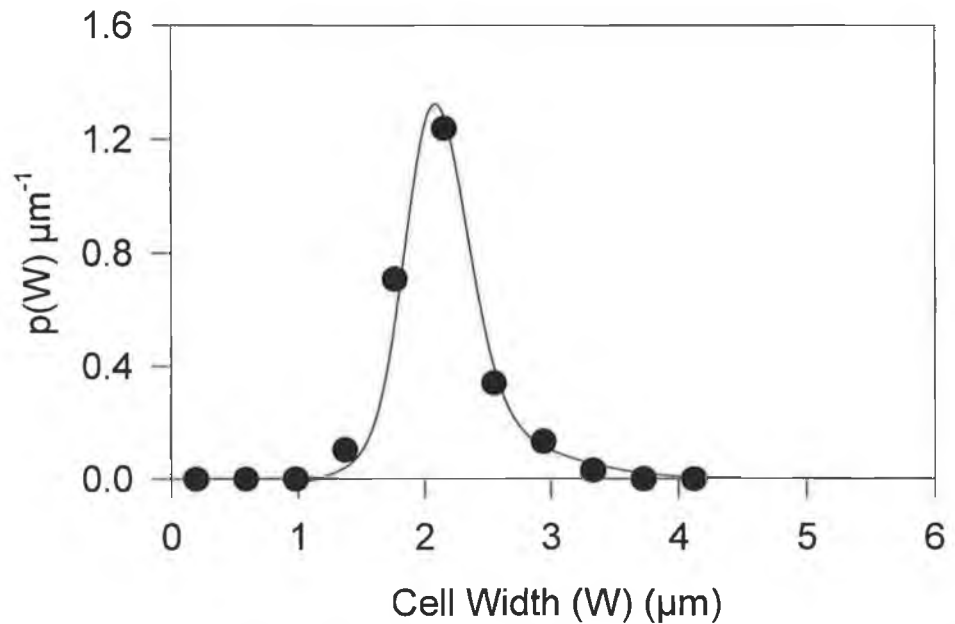


Figure 8.21 Summed width distribution for pseudohyphal Sample 3, $N_y = 0.01$, $N_{dy} = 0.09$, $N_f = 0.02$, $N_{df} = 0.20$, $N_m = 0.68$ (Sample size = 250)

8.6 APPLICATION OF DISTRIBUTION TO FERMENTATION DATA

The volume distributions with respect to dilution rate for the 20g/L and 5 g/L substrate feed concentrations are shown in Figures 8.22 and 8.23. Both chemostat fermentations have a tight volumetric distribution at low dilution rates ($D \leq 0.1$). As the dilution rate increases the distribution for all runs broadens, developing the characteristic shape of a sharp peak followed with a gradual decline at low probabilities. The shape of these curves is uncharacteristic of filamentous fermentation data which shows a more gradual decline with respect to increasing volume. There are obviously significant differences in the mechanism of population regeneration between this organism and typical filamentous fungi.

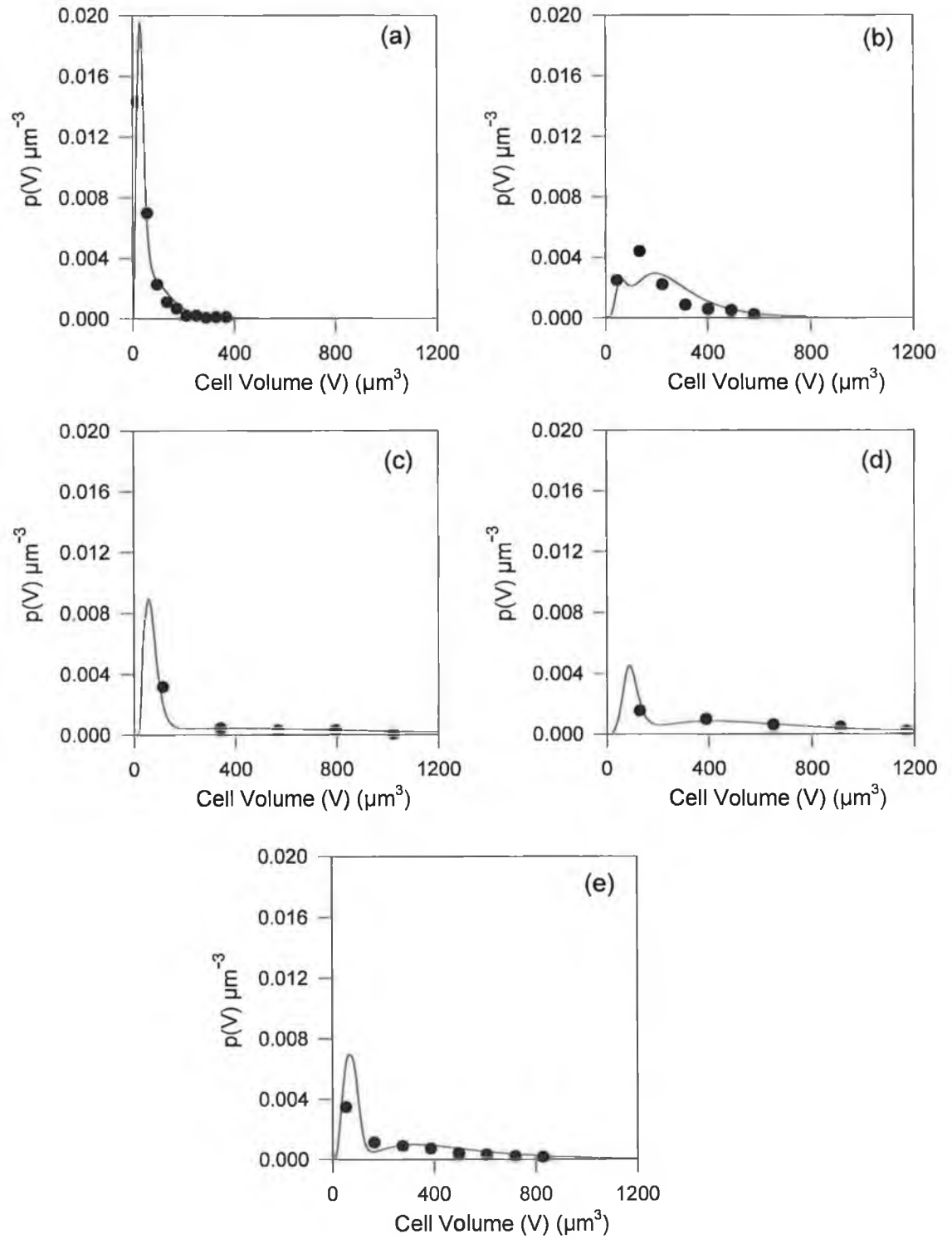


Figure 8.22 Distribution of volume for selected dilution rates for chemostat with 20g/L feed substrate concentration: (a) 0.12 h^{-1} (b) 0.20 h^{-1} (c) 0.3 h^{-1} (d) 0.4 h^{-1} (e) 0.49 h^{-1}

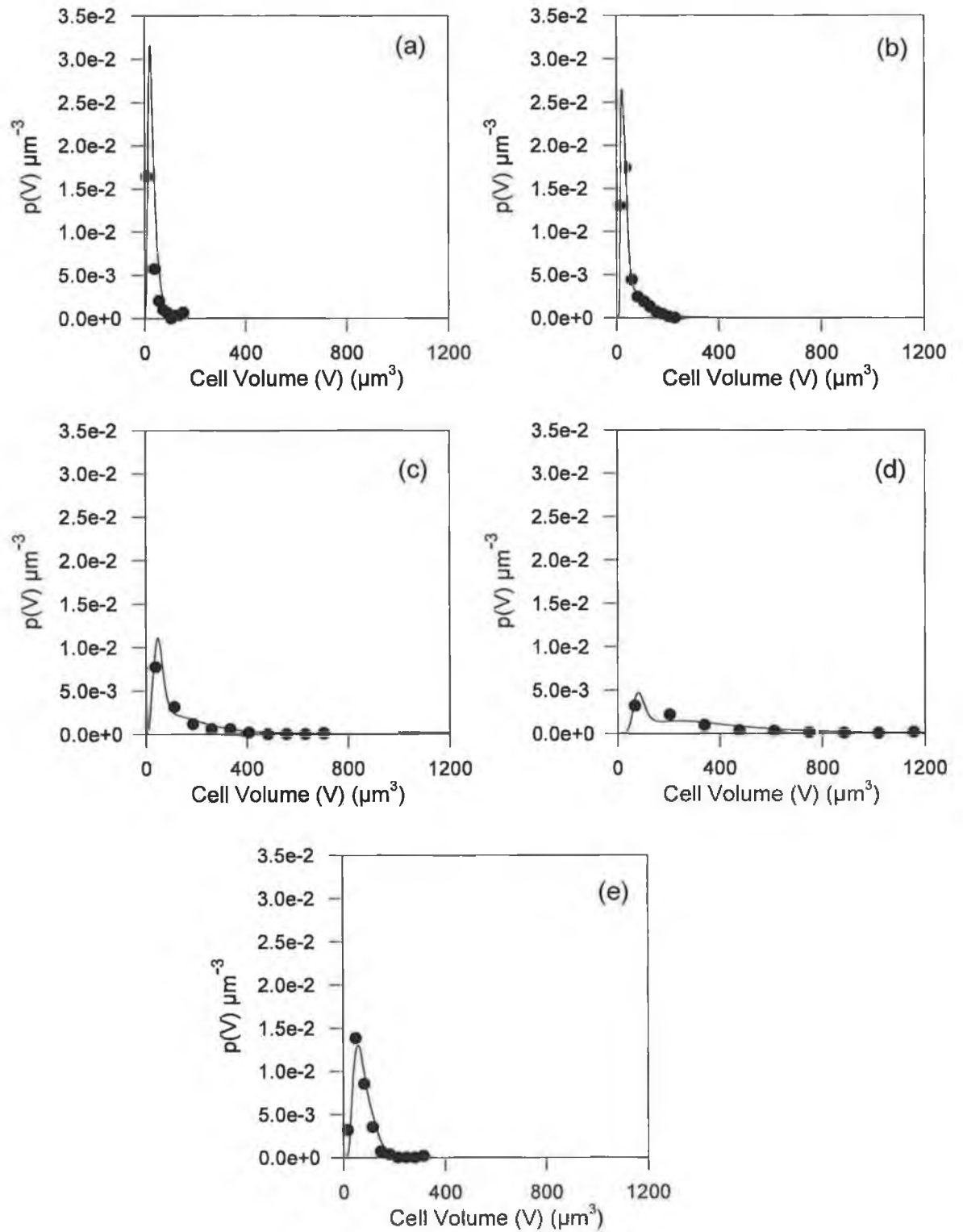


Figure 8.23 Distribution of volume for selected dilution rates for chemostat with 5g/L feed substrate concentration: (a) 0.10 h⁻¹ (b) 0.20 h⁻¹ (c) 0.3 h⁻¹ (d) 0.4 h⁻¹ (e) 0.47 h⁻¹

Distribution changes in batch culture are more subtle, with smaller inter-sample variance than experienced in the chemostat results. The volumetric distribution data from two selected fermentations is presented in Figures 8.24 and 8.25. Figure 8.24 shows the 800rpm batch culture whey fermentation. This fermentation was predominantly yeast-like throughout with a slight morphological diversification at later stages. This can be seen in the volume distributions where a relatively uniform distribution is presented throughout the fermentation. This is not the case, however, for the 200rpm YEPL fermentation presented in Figure 8.25. This figure also outlines how the characteristic shape of the distributions develop in a transition from yeast-like to pseudohyphal.

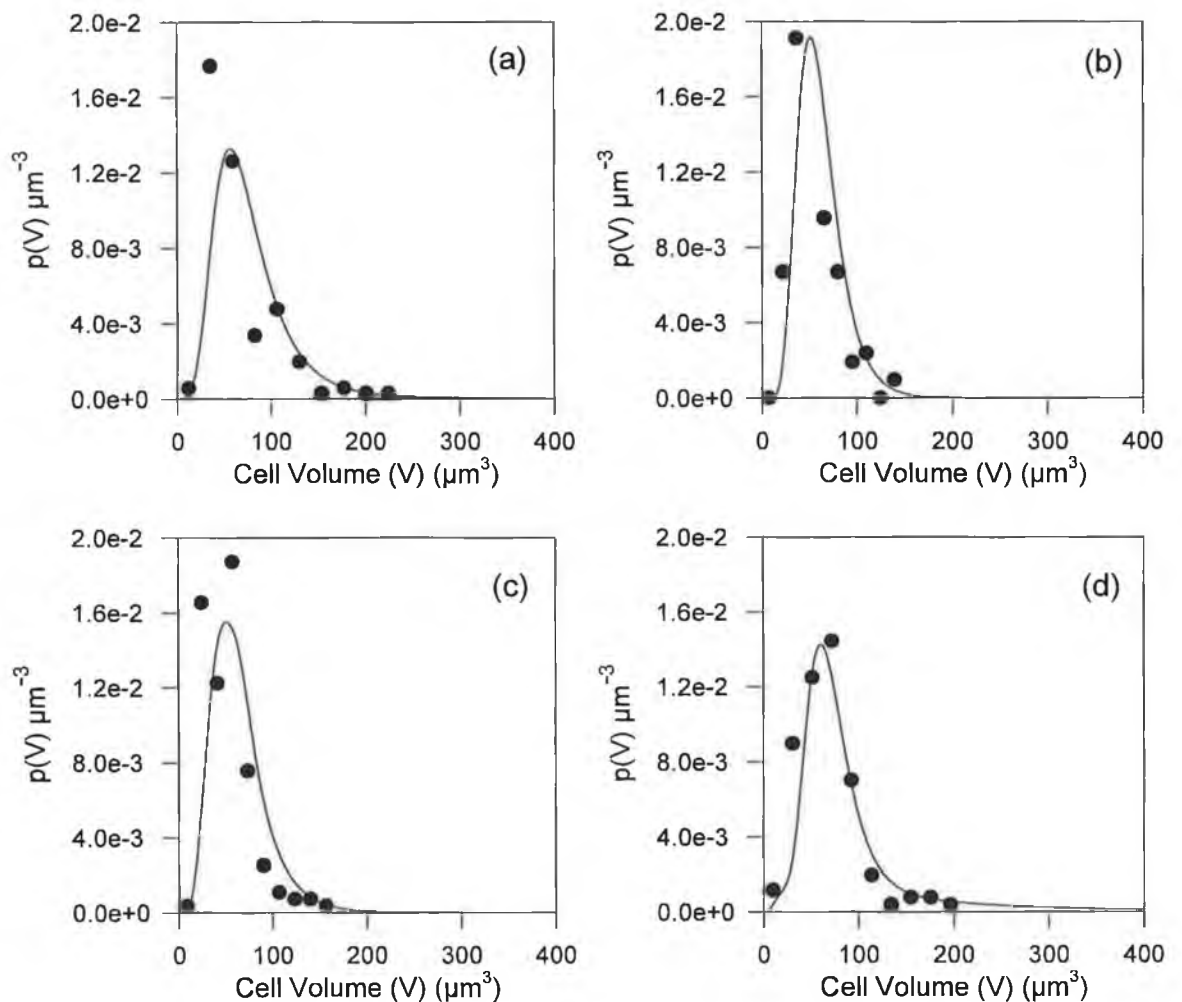


Figure 8.24 Distribution of volume for selected time points for whey media batch culture fermentation at 800rpm 1vvm (a) 2.5 h (b) 4.5 h (c) 6.5 h (d) 8.5 h.

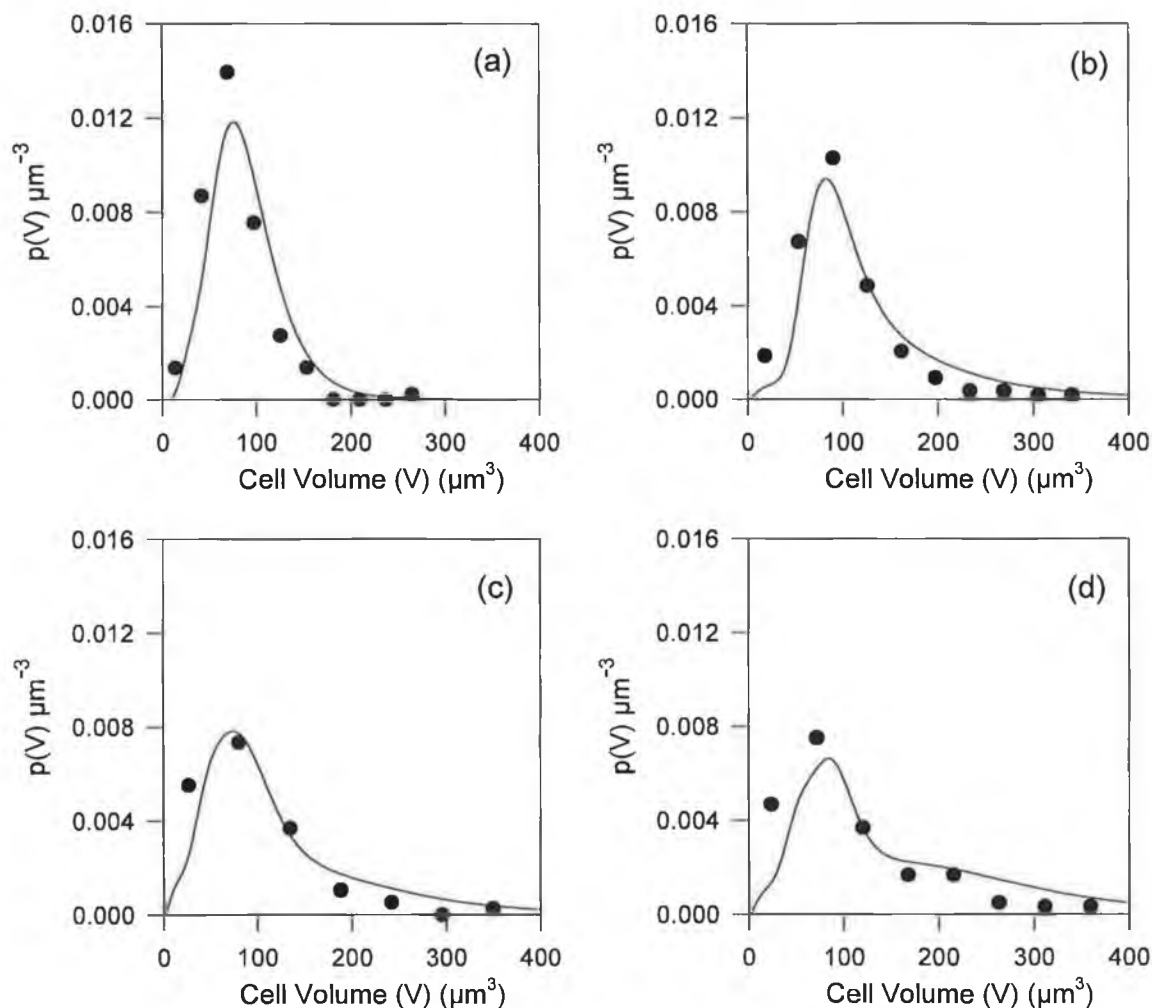


Figure 8.25 Distribution of volume for selected time points rates for YEPL media batch culture fermentation at 200rpm 1vvm (a) 2.5 h (b) 4.5 h (c) 6.5 h (d) 8.5 h.

8.7 CONCLUSIONS

The probability distribution for the volume, length and width of the diversity of samples experienced can be described in terms of a weighted sum of the lognormal distributions of certain key sub-populations in the sample. The key sub-populations identified were yeastlike single cells, yeastlike double cells, filamentous single cells, filamentous double cells and pseudohyphae. The term yeastlike refers to both yeast and elongated yeast cells. This means that the yeast and elongated yeast populations are not discrete and are invalid as true classes in the classification regime implemented in Chapter 4. While they may be invalid as “true” classes, they still act as an indicator of slight morphological transitions in the yeastlike subrange. Certain problems exist with respect to applying lognormal

distributions to pseudohyphal populations due to the sensitivity of the calculation rather than the inherent shape of the distribution. The presence of a small percentage of very large cells can cause the distribution to skew in favour of larger pseudohyphal. The approach used by Kieran (1993), which allows small adjustments to the distribution parameters in the case of poor fits, may provide better description of the population distribution.

The distributions experienced are unusual in shape, particularly for samples containing predominantly pseudohyphal cells. For such samples, there is an unusual sharp peak in the smaller cells subrange followed by a long gradual decrease as volume increases. This is due to the method of regeneration used by the pseudohyphae, which is obviously different from conventional hyphae. Preferential degradation of smaller cells in preference to larger pseudohyphae must occur to obtain the distributions observed.

The generation of a function of this nature has use, when the volumetric distribution is required as part of a mathematical model. Foley *et al.* (1995) has demonstrated the importance of yeast size polydispersity in crossflow microfiltration and has developed a mathematical model incorporating a cell size distribution function. As *K. marxianus*'s filtration characteristics are currently being evaluated (McCarthy *et al.*, 1998), a function describing the size distribution of the cell population may be useful.

CHAPTER 9

THE STRUCTURAL DEVELOPMENT OF *Kluyveromyces marxianus* PSEUDOHYPHAE IN CONTINUOUS CULTURE

9.1 INTRODUCTION

Much work has been done towards understanding the growth and morphological development of true hyphae (Trinci, 1974; Fiddy and Trinci, 1976a,b) yet little has been done in the area of mathematically describing the growth and development of pseudohyphae. This work hopes to identify key aspects of morphological development in pseudohyphae and subsequently propose a model to describe such growth.

Chapter 5 outlined an automatic imaging method capable of classifying the morphology of the organism displaying a diverse range of morphological forms. It allowed for the assimilation of data on pseudohyphae including main hyphal length, effective hyphal length, hyphal growth unit length, number of tips and mean branch lengths. This appears to be a comprehensive repertoire of hyphal measurements, yet it does not provide any information towards the macro-structure of the hyphae, such as the mean length of subelements in the pseudohyphae, number of subunits in the main hyphae, number of subunits in the branches etc. It was attempted during the development of the automated routine to follow a comprehensive “subunit” based analysis through to the longest pseudohypha from single and double subunits, but it was found to be impossible due to poor curvature at the subunit interfaces in pseudohyphae. It was decided to generate a manual measurement based protocol in which the user measures the subunits of interest and records the data in a manner that allows easy data retrieval on a number of different problems.

9.2 MANUAL IMAGING PROTOCOL

A 35 μ L quantity of a suitably diluted sample was placed on a slide and covered with a coverslip. The coverslip was applied with a pressing motion in order to introduce planarity in the slide. A computer program was written to compile

information on pseudohyphae. Measurements taken include the length and geometric position of each subunit in pseudohypha.

A coding system was devised for subunits in pseudohyphae. It was apparent on examination of many pseudohyphae that there was a lead subunit from which all subunits in the pseudohyphae were descended. This subunit was to be found at the start of a chain and all branches appeared at an obtuse angle to the lead subunit (Figure 9.1). The main hypha was deemed the longest continuous line through the subunit starting at the lead subunit. Any other subunit was deemed part of a branch. Subunits on the main hypha were numbered 2.0, 3.0 etc. according to their distance, in subunits, away from the lead subunit (1.0). The active growing end of the subunits in the pseudohypha was deemed to be that furthest away from the lead subunit. Thus branches emerge from a subunit at the point furthest away from the lead subunit and not from the start of the subsequent subunit in the main hypha. Branch subunits were numbered according to the subunit on the main hypha that they originated from and their position on the main hypha. Figure 9.1 demonstrates the coding system employed in the study of pseudohyphae.

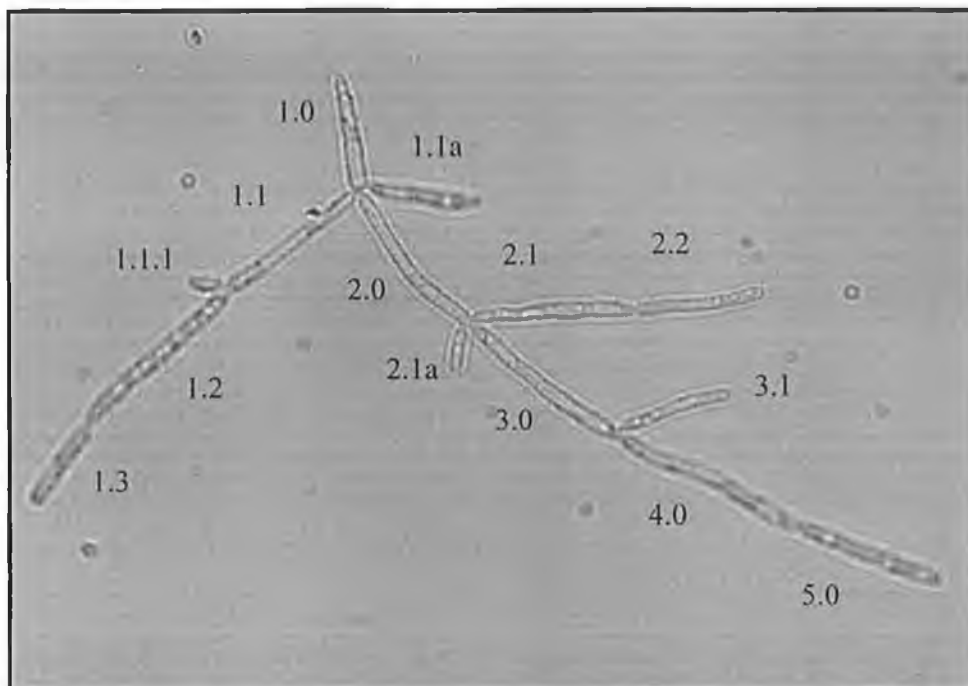


Figure 9.1 Example of pseudohyphal coding system employed in the study of *K. marxianus* pseudohyphae

As can be seen in Figure 9.1, each subunit on the main hypha can generate two or more branches. For ease of description, the subunits on the second branch will have the postscript a, subunits on a third branch will have the postscript b etc. Any branch that generates a sub-branch will be referred to as 1.1.1, a second subunit on this sub-branch will be referred to as 1.1.2, etc.

To study the relationship between mother subunits and daughter subunits the following terminology will be used. In Figure 9.1, the progeny of subunit 1.0 are 2.0, 1.1 and 1.1a in order of age. The progeny of subunit 2.0 are subunit 3.0, subunit 2.1 and subunit 2.1a. The term daughter will be used to describe the progeny of subunits. Subunit 2.0 in Figure 9.1 will be referred to as Daughter 1 of subunit 1.0, subunit 1.1 will be Daughter 2 and subunit 1.1a will be Daughter 3. Daughters will be numbered according to age assessments based on the overall length of the subsequent growth originating from each daughter subunit. The daughter subunit supporting the most subsequent development is termed the oldest daughter and so on.

9.3 INITIAL OBSERVATIONS

All pseudohyphae observed follow a distinct pattern of development. The lead subunit (1.0) buds once, sending out a cylindrical subunit (2.0) which does not detach from the lead subunit (Figure 9.2). This subunit subsequently buds adding a third subunit (3.0) to the chain (Figure 9.3). As subunit 3.0 is being formed, subunit 1.0 develops a second bud (1.1), which grows at an angle to the main "hypha". Subunit 1.1 then develops at approximately the same rate as the main "hypha" leading to branch formation. Each subunit will bud a second time approximately one cycle after the emergence of the first bud (Figure 9.4). The development of a third bud on the lead subunit (1.1a) can be seen in Figure 9.5. As all subunits remain attached to each other, the structure develops into a complex branched entity (Figure 9.6). The complexity of the branching is thus controlled by the age of the lead subunit, which is controlled by the residence time of the pseudohypha in the reactor. Thus a finite maximum object size is inevitable. It is obvious that a certain degree of breakage or bud release has to occur to maintain the

population in steady state. Unusual phenomena occur in very long (old) pseudohyphae such as the disappearance of the longest (oldest) branches and the development of bipolar budding and budding from the middle of the subunits (Figure 9.7). It is presumed that the subunit buds too frequently from one apex and the budding mechanism moves around to counter this problem. Streiblova (1970) observed a spiral budding pattern, for *S. cerevisiae*, moving from one pole to the other. Lord and Wheals (1980) observed this phenomenon but also found that the bud scar was able to move from one pole to the other without intermediate bud scars. Unfortunately cells in this form were not observed regularly in the fermentation.



Figure 9.2 The initiation of pseudohyphal formation with the lead subunit budding into a long thin subunit



Figure 9.3 The development of the second bud from the lead subunit

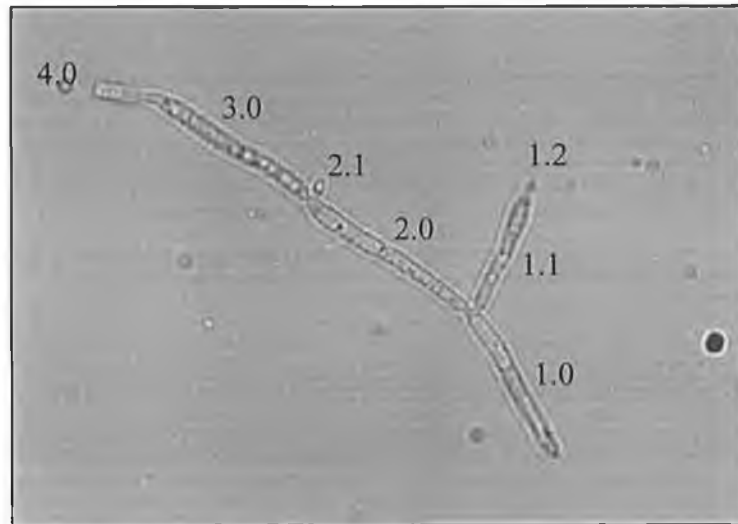


Figure 9.4 New bud formation at the tip of branch 1 and on subunit 2 in the main hypha

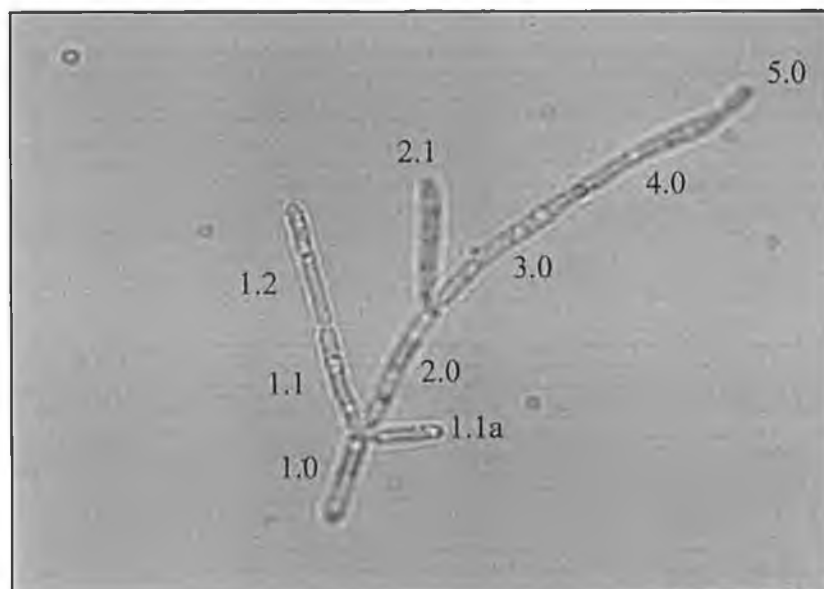


Figure 9.5 Development of third bud from lead subunit

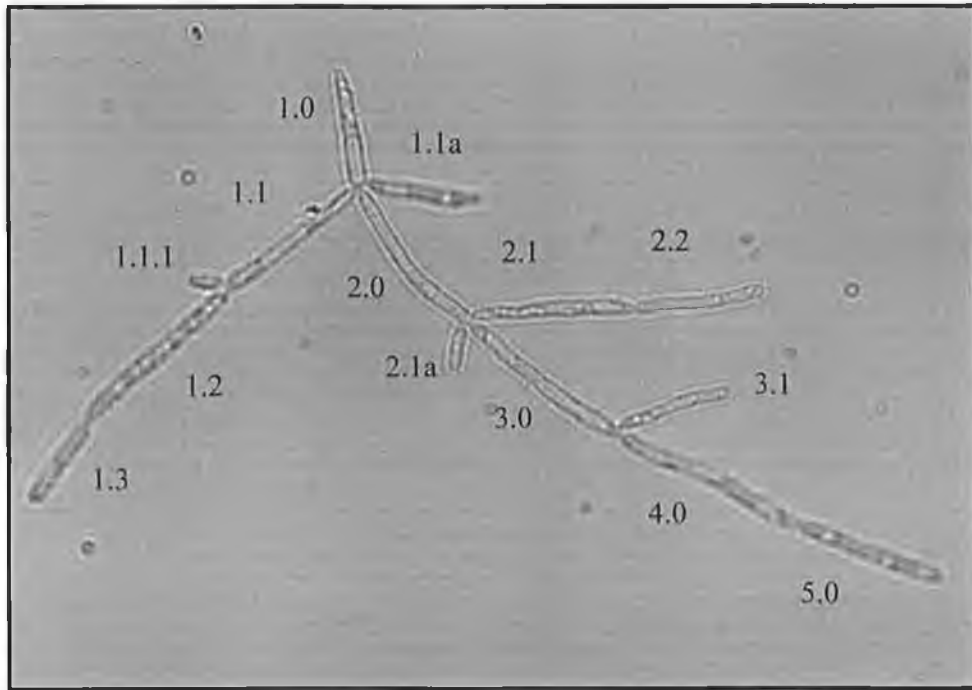


Figure 9.6 Development of a second bud on the first branch concurrent with the development of a third bud on the second subunit on the main hypha

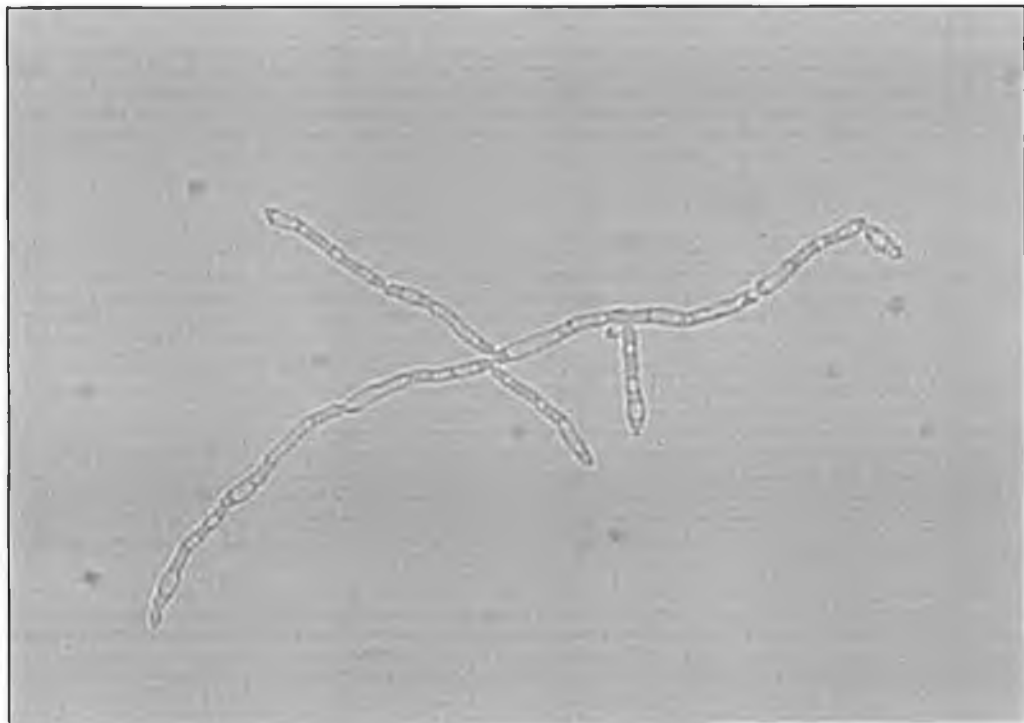


Figure 9.7 Unusual morphological structure in "old" pseudohypha

9.4 PROPOSED MODEL FOR PSEUDOHYPHAL DEVELOPMENT

Figure 9.8. shows a proposed model for pseudohyphal development based on structures observed in Figures 9.2 to 9.6. The model is based on each subunit in the structure producing daughter subunits on a regular interval and at a regular rate.

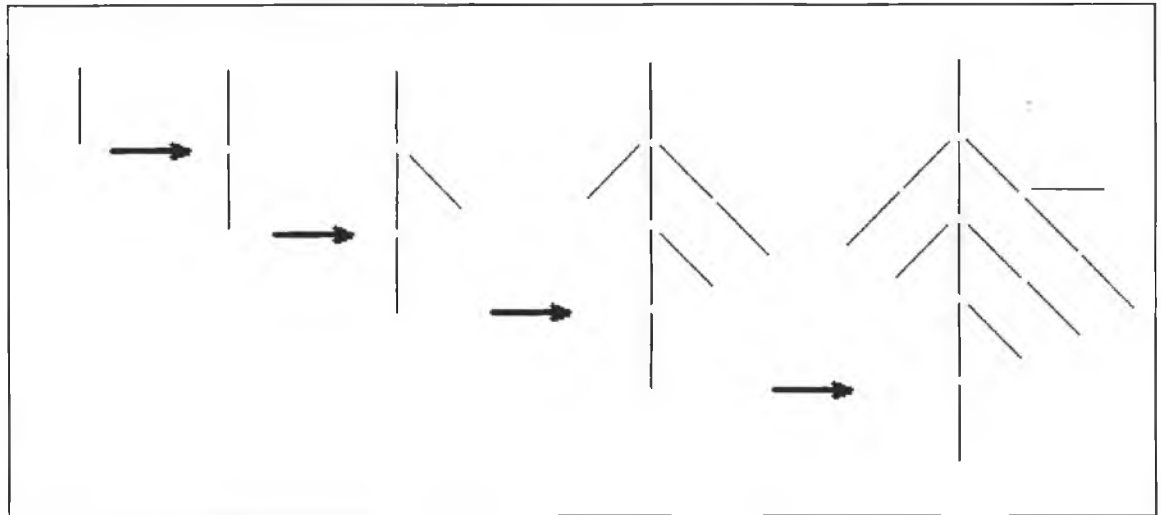


Figure 9.8 Diagrammatic representation of pseudohyphal development for *K. marxianus*

The initial structures are quite close to what is observed in chemostat cultures. As the structures develop, however, the branches do not appear as well developed in reality. Examination of age dependant growth cycles are reported in the literature, where yeast do not bud at equal rates for each progeny produced, but instead slow down with the production of each new subunit. The data of Lord and Wheals (1980) demonstrates this with repeatedly higher percentages of virgin yeast (have not formed progeny of their own) than would be expected for a synchronously dividing population.

9.5 ANALYSIS OF SUBUNIT BEHAVIOUR

9.5.1 Introduction

Based on the above observations of pseudohyphal development and the hypothesis for subunit development presented in Section 9.4, the following questions need to be addressed if a model for pseudohyphal development is to be proposed.

- On a statistical basis, are the subunits the same length in a pseudohypha or does the length of the subunits change with position in the pseudohyphal structure?
- Does the subunit stabilise post budding or does it keep extending. This is important if the overall length of the developing hyphae is to be predicted?
- In the literature, several references are made to an age dependant budding rate. Does a subunit's progeny develop at different rates according to their mothers subunit's cycle number?
- Are the progeny of a subunit morphologically related?
- How does mechanical shear affect the overall structure?
- How does growth rate and growth in different substrate concentrations affect pseudohyphal structure?

9.5.2. Subunit Lengths Relative to Position in Pseudohyphae

Figure 9.9 shows the mean subunit length versus subunit position in the main hyphae for pseudohyphae of various main hyphal lengths (in subunits). As can be seen in Figure 9.9 the subunits develop while they are in the terminal subunit position and subsequently do not extend significantly. This is in agreement with the definition of pseudohyphal structure suggested in Chapter 2 whereby the terminal subunit is generally shorter than previous subunits. It also appears that as subunits get further away from subunit 1.0, they are more elongated. The additional graph in Figure 9.9 illustrates the typical standard deviations exhibited by this data. The scatter appears to be higher for subunit 1.0 and the terminal subunit (6.0) than the

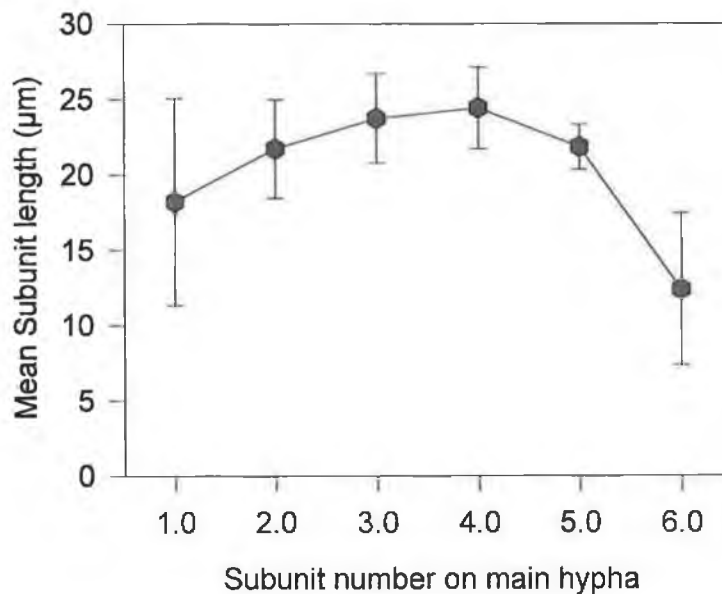
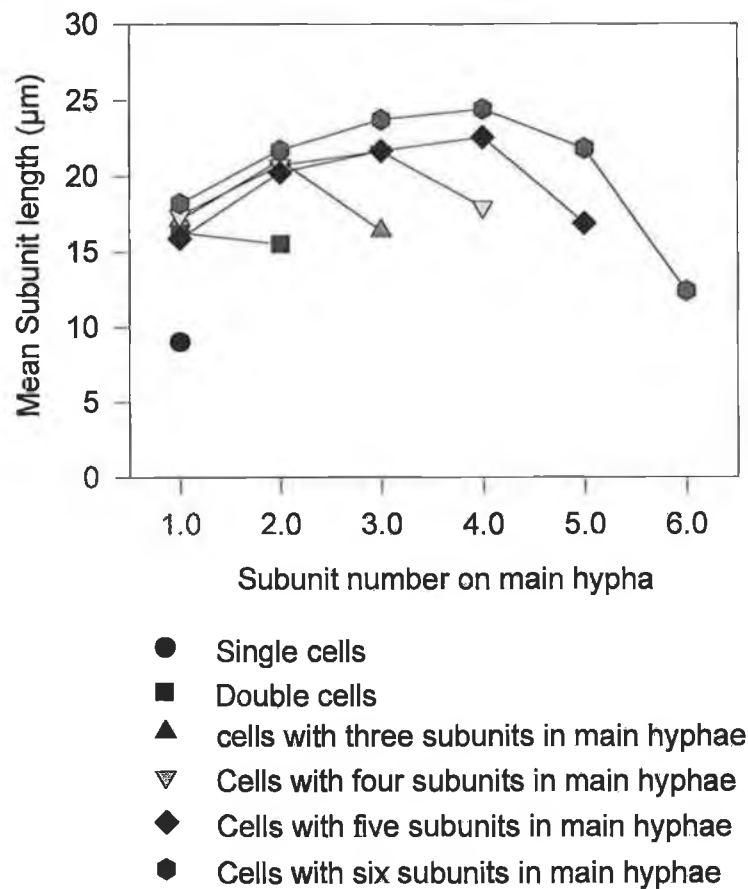


Figure 9.9 Lengths of subunits in main hyphae (5g/L substrate feed concentration, $D = 0.4\text{h}^{-1}$). Additional graph demonstrates the standard deviations on the values obtained for six subunits in the main hypha.

other subunits. This suggests a heterogeneity in length of the starting cell in pseudohyphae. This may be due to pseudohyphae originating from both yeastlike cells (resulting in an overall shortening of the mean length of subunit 1.0) and breakdown products of pseudohyphae. Heterogeneity in the terminal subunit length is simply due to the fact that it is still in active development and can range in length from a small bud (just after formation) to a large cell (just about to produce progeny of its own).

The development of subunits in the main hypha is also illustrated by examination of the growth of specific subunits in the main hypha with respect to the development of the total main hypha (Figure 9.10). It is apparent that while the subunit is in the terminal position it grows quickly, after budding it extends at a much reduced rate. Assuming the extension rate of the terminal subunits in the hyphae is constant with respect to time, extension rates, relative to the extension of the main hyphae, for subunits after budding are shown in Table 9.1.

Table 9.1 Relative extension rates of subunits post budding (5g/L substrate feed concentration, $D = 0.4\text{h}^{-1}$)

Subunit number.	Relative extension rate (post budding)
1	0.039
2	0.034
3	0.070
4	0.021
5	0.081

It is apparent that all subunits in the hyphae extend slowly post budding and that based on the decrease of the relative extension rates of the lead subunits that this secondary extension has to be taken in to account if mathematical modeling of the development of the structure. A mean post budding extension rate of 0.05 was calculated for this sample.

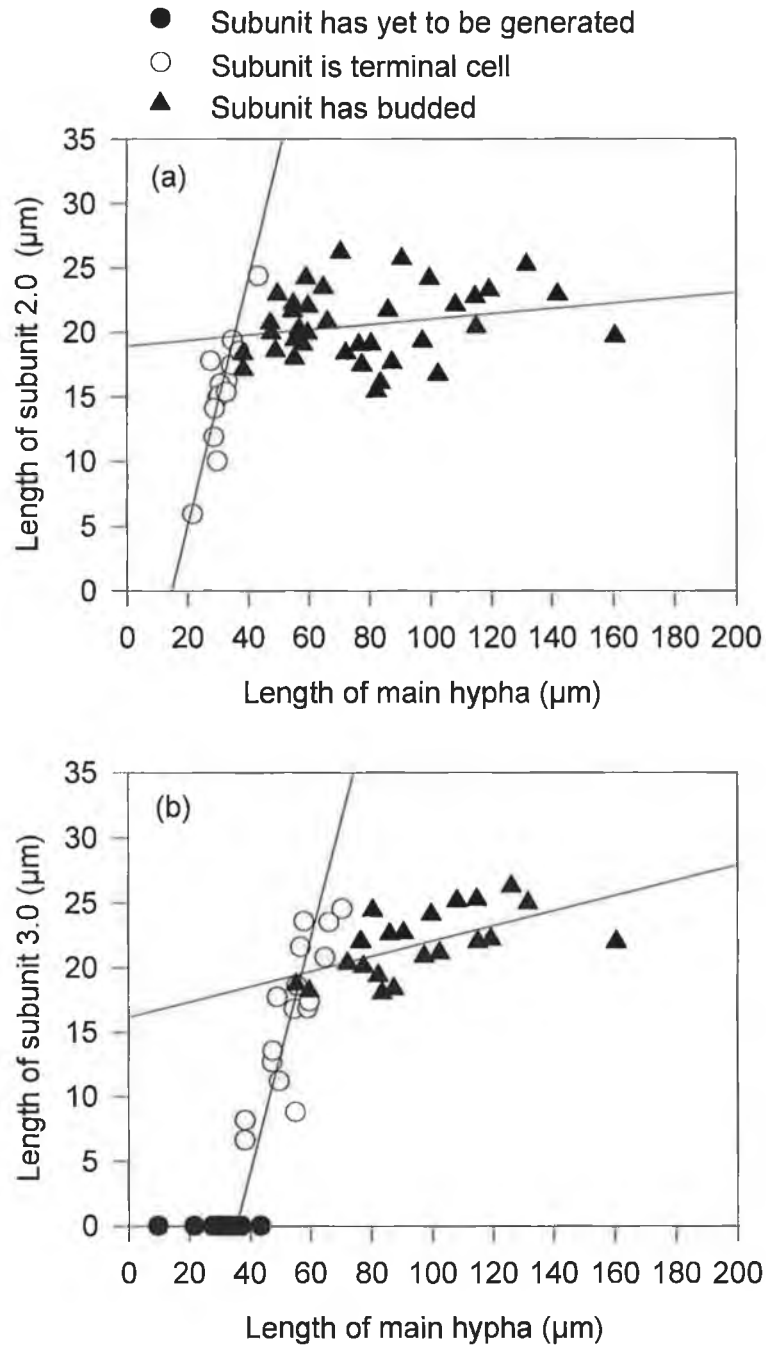


Figure 9.10 Development of subunits in main hyphae with respect to main hyphal length development of subunit two, (b) development of subunit three. (20g/L substrate feed concentration, $D = 0.4\text{h}^{-1}$)

Figure 9.9 demonstrates that each subunit appears to grow to a greater length than its mother subunit. Based on this observation it was decided to examine whether any relationship existed between the length of the mother subunit and that of the

daughter subunit. As can be seen in Figure 9.11 there does appear to be a tenuous relationship between the two parameters suggesting that as the length of mother subunits increases, so does that of any fully developed daughter subunits. The data presented Figure 9.11 encompasses all operating conditions utilised in chemostat culturing, including changes in dilution rate and S_0 . All daughter subunits had to possess a granddaughter subunit before they were measured. The results demonstrated in Figure 9.11 suggest a “destiny” for each subunit, whereby a daughter subunit’s length is preordained by the length of the mother subunit. The low regression coefficient has to be noted for the data.

It was also attempted to assess the relationship between the length of fully grown daughter subunits and the mother subunit. Figure 9.12 shows that a tenuous relationship exists between the lengths of daughter subunits generated from the same mother subunit.

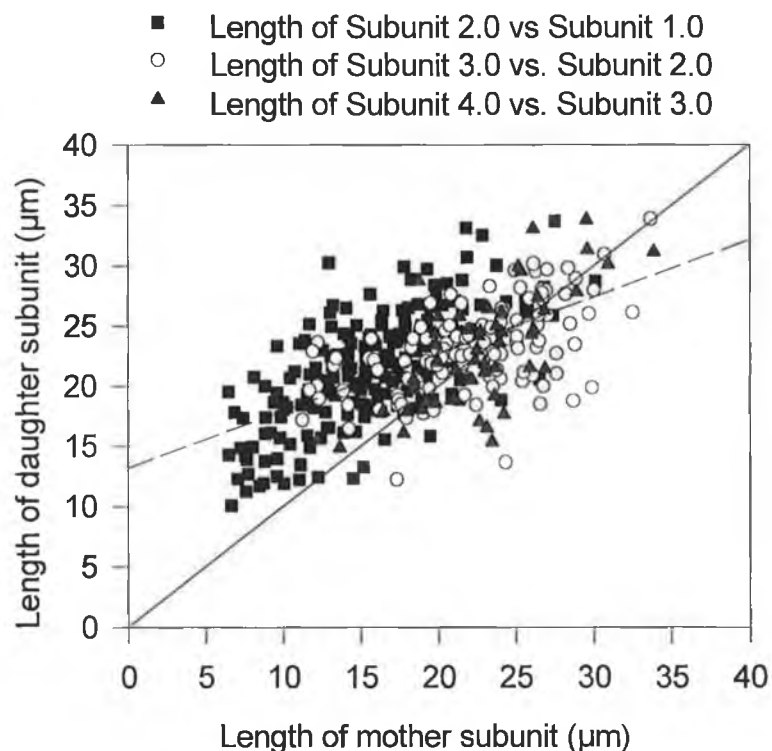


Figure 9.11 Relationship between the length of mother and daughter subunits. Solid Line – parity plot, dashed Line - linear regression ($r^2 = 0.38$)

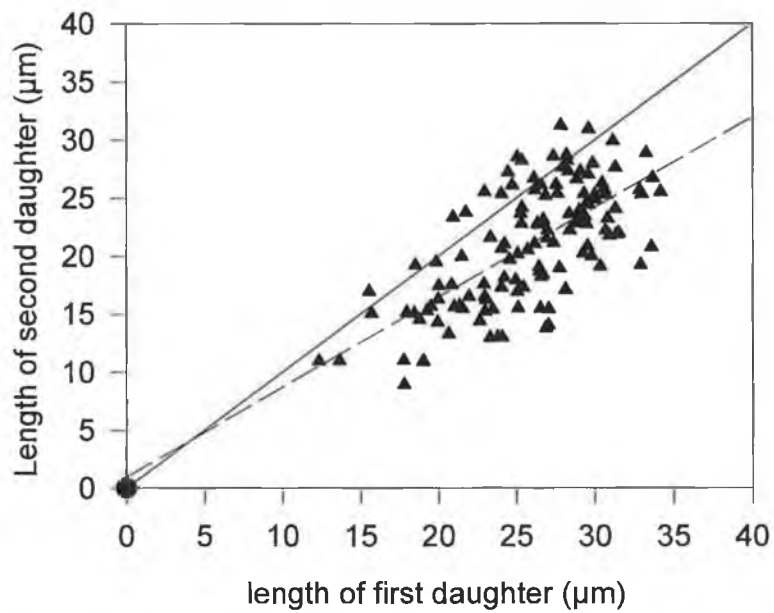


Figure 9.12 The relationship between the fully grown length of the first and second progeny of a subunit. Solid Line – parity plot, dashed line - linear regression ($r^2 = 0.46$)

Both of the above findings are essential for the development of a proper mathematical model for the development of pseudohyphae.

9.6 ANALYSIS OF BRANCH DEVELOPMENT

9.6.1 Introduction

The second issue to be examined is the development of branches. Pseudohyphal growth is the result of subunits not separating after formation, thus studying the development of branches is the equivalent of studying the “family tree” of mother subunits. The life cycle of the subunit has to be examined in order to determine whether the budding rate is constant with respect to time or whether the subunit cycle time increases with the age of the subunit. The length of branches is plotted with respect to the length of the main hyphae to compare rates of development of both. There are recognised limitations with this analysis.

- While subunits predominantly develop while in the terminal position, they do exhibit slight growth after formation (Figure 9.9). The number of subunits in the

main hypha is always greater than the number in a branch. Therefore the amount of residual extension will always be greater in the main hypha than in the branch. For example, the pseudohypha presented in Figure 9.4 has four subunits in the main hypha and two in the branch evolving from subunit 1.0. Therefore the amount of residual extension in each component is as follows. The main hypha has a terminal subunit extending at a relative rate of 1.0. It also has three other subunits extending at an average relative rate of 0.05 each. This contributes a total extension rate of 1.15. The branch has one terminal subunit extending at a relative rate of 1.0 and one other subunit extending at a rate of approximately 0.05. This makes a combined total extension rate of 1.05. Therefore if both terminal subunits are extending at the same rate the branch should be extending at an approximate rate of 0.91 relative to the main hypha.

- Another possible error is the assumption that the main hypha's terminal subunit always extends at the same rate. The subunits are observed to elongate as they get further away from subunit 1.0. This either means that the subunit develops at the same rate and that the establishment of the subunit interface is varying with respect to time or that the rate of interface establishment is fixed and the extension rate is varying.

While the above observations may create errors in the data analysis, it is impossible to measure any morphological characteristics of a single subunit with time for this system. Any experiments examining the extension rates for filamentous fungi are done on solid substrates (López-Franco *et al.*, 1994), whereas in the present work, the method of growth is in suspension culture and it is impossible to follow the history of any one pseudohypha over time. All that can be done is to examine a population whereby one assumes, that due to the simple nature of yeast, replicas of previous morphological forms of a particular pseudohypha are present in the population and thus the whole life cycle of the pseudohypha can be estimated.

9.6.2 Branch Extension Rates

Figure 9.13 illustrates the lengths of branches originating from subunit 1.0 with respect to overall length of the main hypha. The first finding is that the extension rate of new “branches” from subunits that have already budded is significantly slower than that of the main hyphae. The more often a subunit buds the slower the development of its progeny. This is illustrated in Figure 9.13. It was mentioned before that the slow post budding extension of each sub element will artificially increase the main hyphal extension rate yet when this is compensated for the difference it makes does not significantly alter the findings. The first branch extends at relative rate of $0.59 \mu\text{m}/\mu\text{m}$ to the main hypha with the second branch extending at a relative rate of $0.20 \mu\text{m}/\mu\text{m}$ of the main hypha for the sample illustrated.

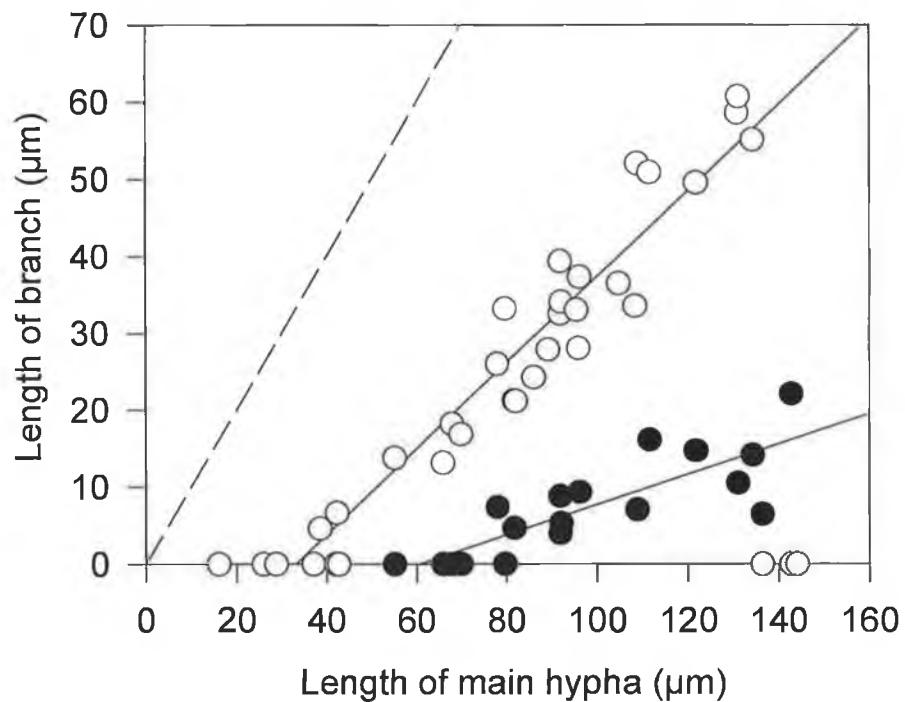


Figure 9.13 Extension of branches from lead subunit (1.0); Unfilled symbols, first branch; Filled symbols second branch; dashed line - parity plot (20g/L, substrate feed concentration, $D = 0.4\text{h}^{-1}$)

The fact that the plots are linear suggests that the extension rate of the main hypha in the pseudohypha is constant with respect to that of the branches.

Another interesting feature of this graph is that some of the branches examined are composed of more than one subunit yet the extension rate of the progeny of the first subunit in the branch appear to be equal to the extension rate of the first branch subunit. This suggests possible developmental problems for subunits born of an old mother subunit. Unfortunately due to the limited development of hyphae within the chemostat before washout it was only possible to do limited work on this phenomenon. Another phenomenon preventing the study of such events was the apparent "dropping off" of branches once subunits reach a certain age (effective hyphal length). Figure 9.13 illustrates the disappearance of the first branch on the hyphae in the environs of 140 μm effective hyphal length. This was observed in all samples with a greater and more random affect observed at lower dilution rates. Also apparent was the increased extension rate of subsequent branches. Figure 9.14 shows the extension rate for the first branch on the subunit 1.0 and first branch on the subunit 2.0. It is apparent that the first branch on subunit 2.0 extends at a greater rate than that of the first branch on subunit 1.0 (0.79 $\mu\text{m}/\mu\text{m}$).

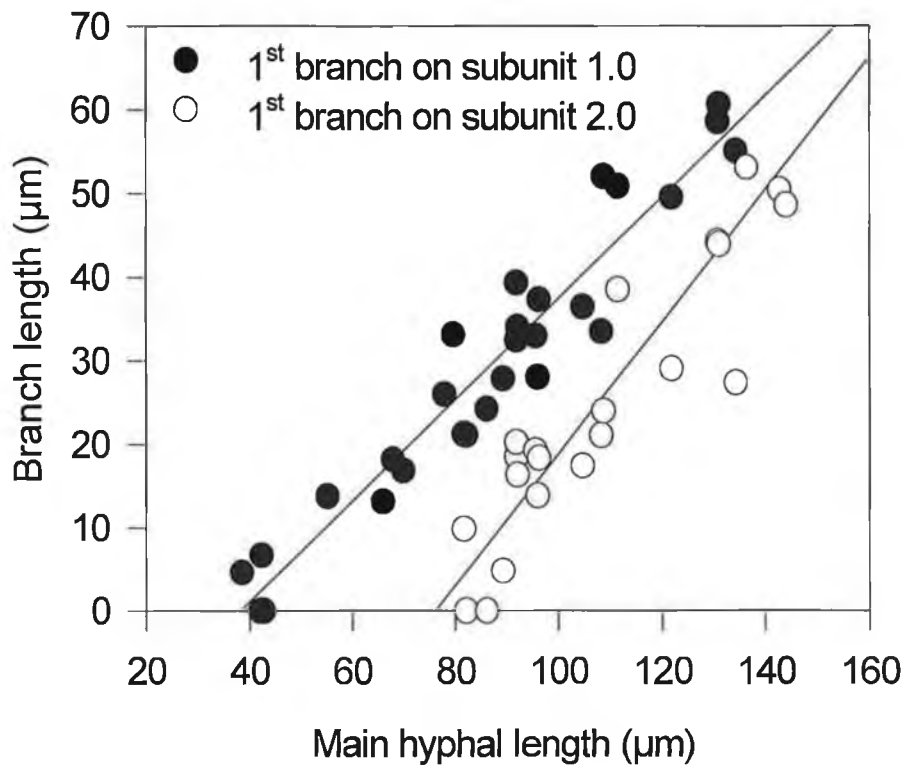


Figure 9.14 Extension rate differences between branches generated from first and second subunit on main hyphae. (20g/L substrate feed concentration, $D = 0.2\text{h}^{-1}$)

9.7 EFFECT OF ENVIRONMENT ON PSEUDOHYPHAL DEVELOPMENT

9.7.1 Effect of Operating Conditions on Branching Pattern

It was decided to examine the effect of operating conditions such as substrate feed concentration, dilution rate and agitation on the development of structural complexity within the pseudohyphae. Figure 9.15 shows the effect of changing both dilution rate and substrate feed concentration on the complexity of the pseudohyphae. For low S_0 concentrations there are slight differences between $D = 0.2\text{ h}^{-1}$ and other dilution rates. This difference becomes less significant as substrate feed concentration increases.

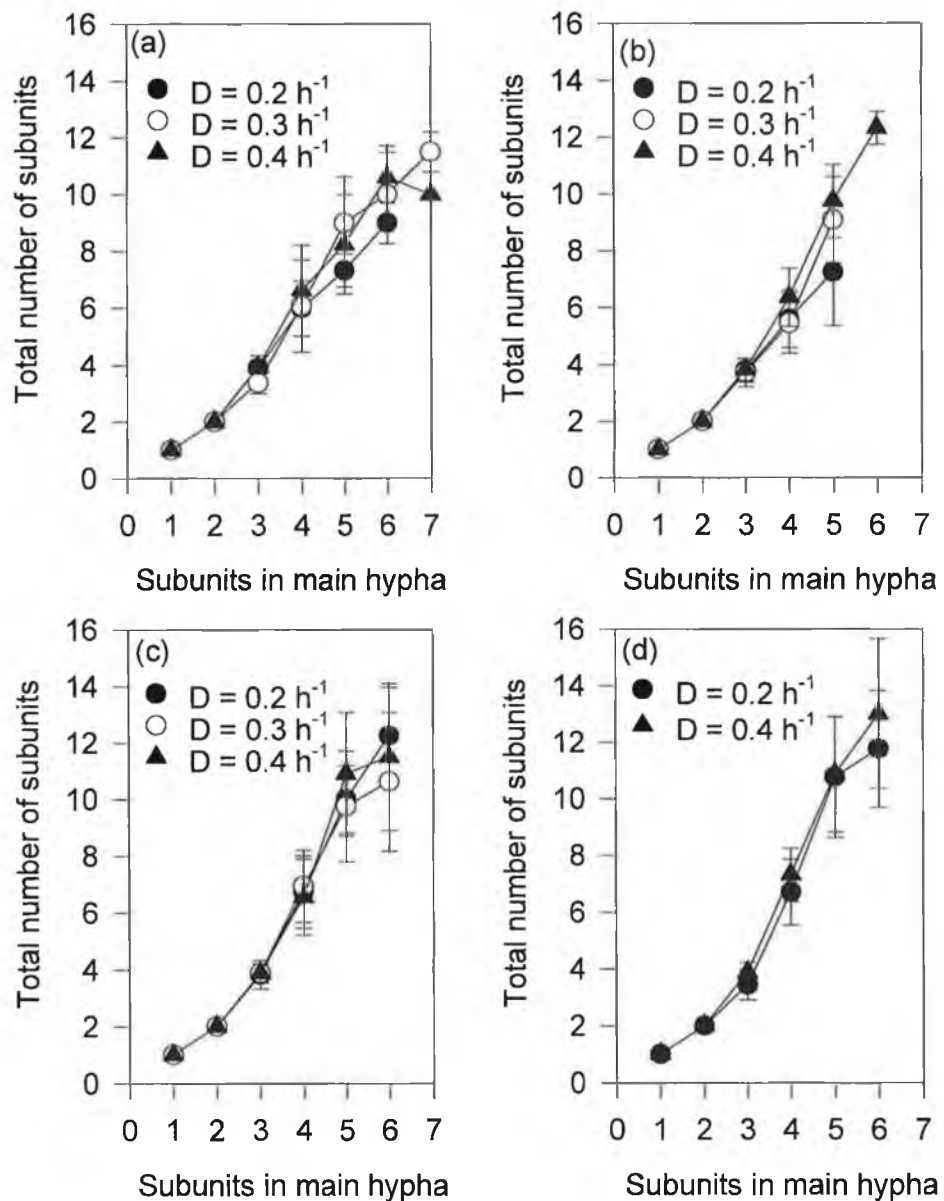


Figure 9.15 Effect of dilution rate and substrate feed concentration on the structure of pseudohyphae, (a) 5g/L substrate feed concentration, (b) 10g/L substrate feed concentration, (c) 15 g/L substrate feed concentration, (d) 20 g/L feed concentration.

When agitation is changed at a fixed dilution rate and substrate feed concentration (Figure 9.16) there are negligible differences in the structures of the pseudohyphae observed. While this may be true, there were significant differences in the population classifications under these conditions (Table 9.2).

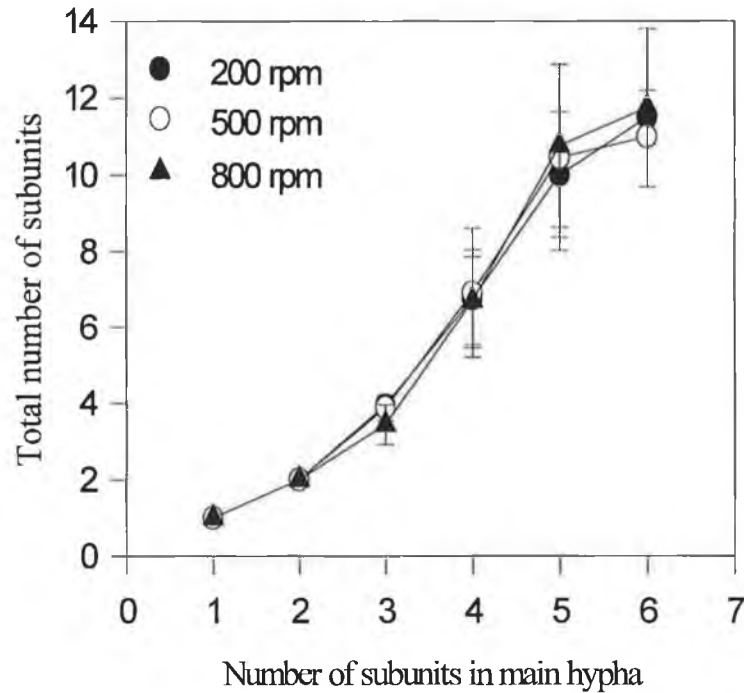


Figure 9.16 The effect of agitation on the structural characteristics of pseudohyphae ($D = 0.2 \text{ h}^{-1}$, $S_0 = 20\text{g/L}$)

Table 9.2 Classification (numerical fraction) data for samples used in Figure 9.16

Sample	Y	DY	EY	DEY	F	DF	M
200RPM	3.59	8.38	2.39	9.58	5.38	22.16	48.50
500RPM	3.79	9.00	2.37	11.37	2.37	16.59	54.50
800RPM	3.18	1.91	1.91	3.18	12.74	12.74	76.43

To ensure that this analysis was sufficient to guarantee structural similarity, a more complex analysis was utilised in Figure 9.17. This Figure demonstrates the structural similarity on a subunit by subunit basis. The range of impeller tip speed used in this study suggests that the organism does not undergo mechanical breakage but undergoes natural breakage under a preprogrammed regime. It is apparent that overall diversity of structures may change from sample to sample yet if the same pseudohyphal structure is maintained then population dynamics are controlled by factors other than artificial breakage, which would result in a myriad

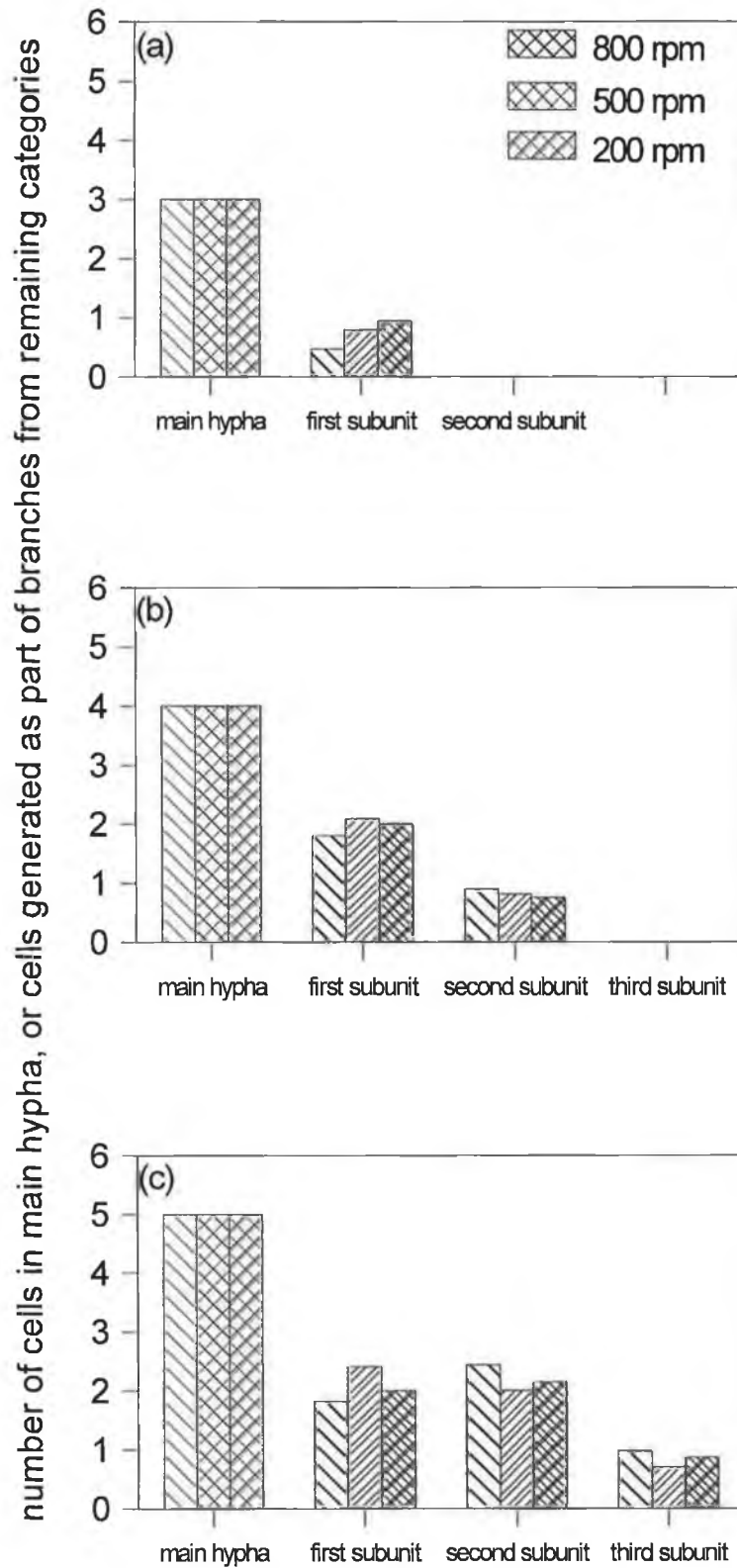


Figure 9.17 Branching pattern analysis for various subunits under different agitation conditions (a) pseudohyphae with three subunits in the main hypha, (b) pseudohyphae with four subunits in the main hypha, (c) pseudohyphae with five subunits in the main hypha ($D = 0.2 \text{ h}^{-1}$)

of structures. It is also possible to speculate that the breakdown products are fractal in nature and assume the shape of shorter pseudohyphae on breakage.

9.7.2 The Effect of Growth Conditions on Pseudohyphal Subunit Length

It is apparent that operating conditions have no apparent affect on the growth patterns of pseudohyphal in continuous culture. It will now be established whether this is also true for subunit length within the pseudohyphal. It has been demonstrated previously that the length of subunits within pseudohyphal change with respect to age thus it will be necessary to study the length of the subunits with respect to the structure they are part of. Little difference in mean subunit length for the various categories was found when samples from each of the different agitation speeds were examined (Figure 9.18). On examination of the effect of changing dilution rate and substrate feed concentration on the mean length of subunits within a pseudohypha, small differences were observed (Figure 9.19). It was apparent that increasing substrate feed concentration or dilution rate increases mean subunit length within categories. The effect of dilution rate was less noticeable at lower substrate feed concentrations. The length increases were noted particularly for subunits with the longest effective hyphal length. Little change was observed for single and double subunits under all conditions.

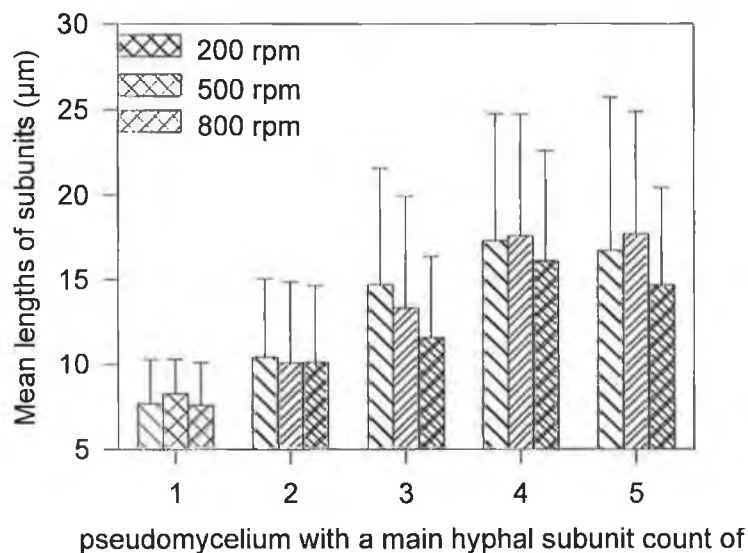


Figure 9.18 The effect of agitation on the mean subunit lengths of subunits within pseudohyphae of various chain lengths

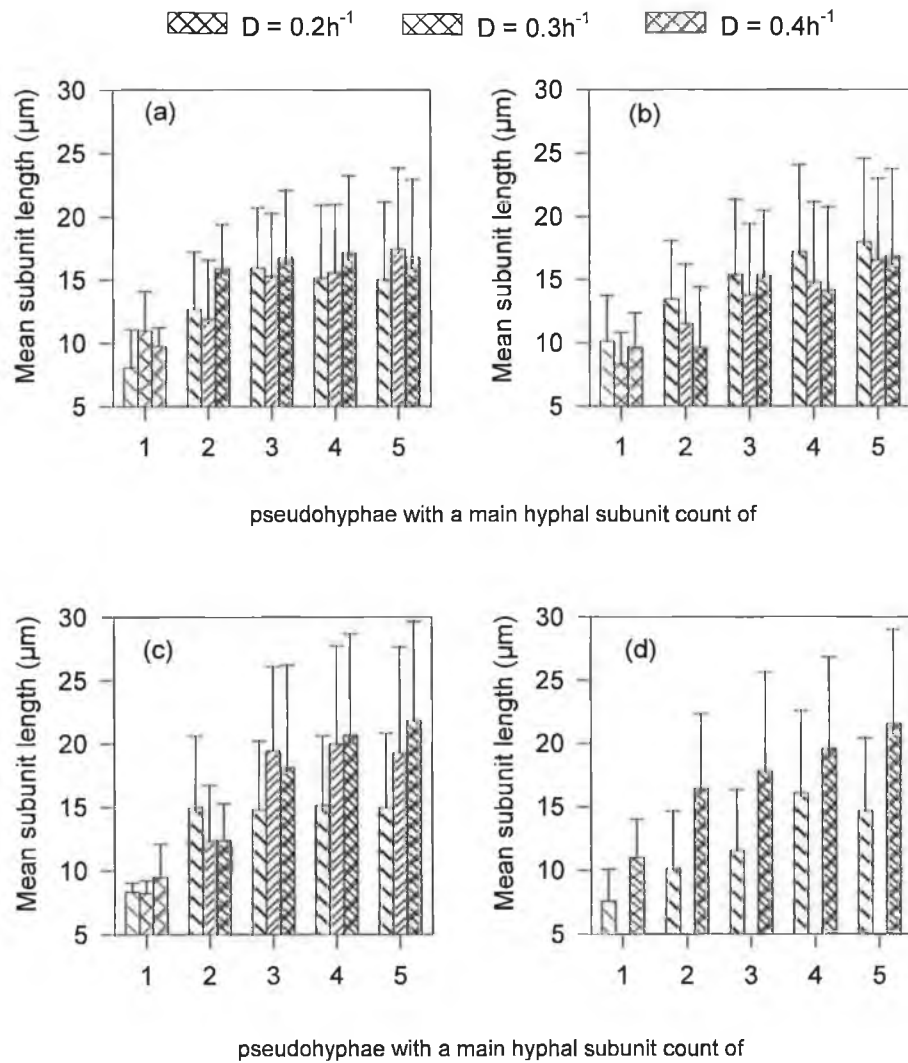


Figure 9.19 The effect of dilution rate and substrate feed rate on the mean subunit length of subunits within pseudohypha of various chain lengths (a) 5g/L substrate feed concentration (b) 10g/L substrate feed concentration (c) 15g/L substrate feed concentration (d) 5g/L substrate feed concentration.

9.8 NOTE ON THE CLASSICAL VALUE OF L_e

The classical morphological value, L_e , described in the literature as the longest interconnected path through the hypha, is meant as an indicator of the hyphal age. This term, however, is inappropriate for the morphological form in the present work. If Figures 9.2 to 9.6 are examined, the longest interconnected line is not related to the true physiological length of the pseudohypha, the central main hypha starting at subunit 1.0 and running to subunit X.0 where X is the number of subunits in the main hypha. Thus, therefore it is important to define this new value as $L_{e \text{ physiological}}$ in case of confusion with the above definition. It is highly probable that this length has been misinterpreted for other organisms for the purpose of simplifying image analysis. It is unfortunate that, when the automated image analysis protocol was developed for the present work, the method of Tucker *et al* (1992) was utilised which calculates L_e rather than $L_{e \text{ physiological}}$, and so it was not possible to analyse the data in the required manner. The design of an automated image analysis protocol to quantify length of the main hypha in a pseudohypha, would be a difficult but rewarding exercise.

9.9 CONCLUSIONS

The pseudohyphal structure appears to be a mimic of a budding yeast population whereby each pseudohypha is a “family tree” with all subunits descending from the one parental subunit. Each subunit may proceed to create an observed maximum of four daughter subunits, three from the active growing end and a fourth occasionally from the opposite pole. There is a finite limit to the structural development of a pseudohypha in a chemostat due to the inevitable washout of older and thus longer pseudohyphae. The rate of development of daughter subunits appears to be controlled by the age and position of the mother subunit at the time of budding.

The pseudohyphal structure, observed in this work, behaves completely differently to that of a true hypha. Septae in true hyphae form erratically, both in terms of intersepta distance and position, new septa can form either before or after a previously formed septa. Intracellular divisions in *K. marxianus* are formed

regularly and always after the previous intracellular division. The position of branches in true hyphae is controlled by the structure of the septa. If pores exist in the septa of true hyphae, allowing protoplasmic streaming, branch formation is an irregular affair, with branches often emerging from mid-compartment positions (*A. nidulans*). If pores are absent, branch formation is polar, originating from the active pole of the compartment (*G. candidum*). The latter agrees with observations for *K. marxianus*, which suggests that subunits are individual and do not interact with each other. The compartments formed by septa in true hypha generally contain multiple nuclei, whereas yeast compartments are generally mono-nuclear (Fiddy and Trinci, 1976a,b).

Interesting features observed for pseudohyphal structures include the elongation of subunits with respect to their distance from subunit 1.0. This is accompanied by a greater degree of homogeneity in subunit length. This gives some information about the formation and regeneration of pseudohyphae in continuous culture. The fact that subunits are shorter at the start of pseudohyphae suggests that some pseudohyphae may have originated from yeast-like subunits or terminal subunits. A high standard deviation in the length of subunit 1.0 also suggests that the breakdown products of pseudohyphae may also be used for this process. This would not be the case if the pseudohypha regenerated exclusively from random hyphal breakage. It is hypothesised that as a terminal subunit is formed its connection to the pseudohypha can be either strong or weak. This results in either the subunit remaining attached to the pseudohypha and developing to its full extent or it will disconnect from the main hypha resulting in the formation of a small single subunit. This subunit is a virgin subunit and can go on to form a new pseudohypha. This mechanism for pseudohyphal regeneration would also explain the unusual shape of the volume distributions in Chapter 8 for the 20g/L substrate feed concentration chemostat. The distributions had a sharp peak at low values for volume followed by a gradual decrease. This can be explained in terms of the population regenerating itself predominantly from single subunits. For such a probability distribution to occur, however, there has to be preferential breakoff of terminal subunits in smaller pseudohyphal than in larger ones. This is not

unreasonable, as it is apparent that subunits appear to commit to pseudohyphal growth to a greater extent as the overall length of the pseudohypha increases.

The global pseudohyphal structure observed, on a subunit basis, is approximately constant with respect to main hyphal length (in subunits) over a wide range of operating conditions. Any particular main hyphal length (in subunits) will have a corresponding defined branch structure. A population of pseudohyphae is thus composed of amounts of discrete morphological forms, rather than the products of random hyphal breakage. This rule applies up to a main hyphal length (in subunits) of 6. After this point branches start falling off the pseudohyphae and erratic budding patterns are observed whereby the organism assumes bipolar budding patterns and budding is observed from the middle of subunits (Figure 9.8). This may be a response to a heavily bud scarred apex. The rarity of such morphological forms was due to the finite residence time in the bioreactor. The reversal of bud polarity may be a genetic response, whereby the subunit 1.0 produces buds firstly in one direction and then completely reverse poles and initiate growth in another direction. This behaviour may be an attempt by the subunit to forage in as many directions as possible.

The mean lengths of the subunits were seen to vary both with substrate feed concentration (S_0) and dilution rate (D). As the substrate feed concentration increases so does the length of the subunits. It is also apparent that the widths of the subunits are increasing with increasing S_0 and D in Chapter 7. The effect of changing D on subunit length increases with increasing S_0 . In chemostat fermentations with 5g/L substrate feed concentration, the subunits are approximately the same length for all values of D . At a 20g/L substrate feed concentration the difference in overall subunit length is more apparent.

Most investigations of hyphal development in the literature, involve the study of hyphae on solid media (Fiddy and Trinci, 1976a,b; Gimeno *et al*, 1993). This approach allows the direct measurement of rates of extension with time. Unfortunately, the changing environmental conditions experienced on solid media

result in a heterogeneity of morphology, thus making it impossible to examine the morphology of populations behaving uniformly. Such culturing problems would have to be overcome before the extension rates of main hyphae and branches can be examined with time.

CHAPTER 10

SUMMARY AND RECOMMENDATIONS FOR FURTHER WORK

10.1 SUMMARY

On initial examination of the morphology of *K. marxianus*, it was noted that the morphology displayed by the organism could not be described as dimorphic but was best described as polymorphic in that it displayed a myriad of morphological forms between the yeast form and the pseudohyphal form. This fits well with recent dimorphism studies that suggest the term dimorphism is unsuitable for the description of morphology of such organisms, and that terminology such as plaeomorphism or polymorphism would be more suitable.

To describe the morphology of polymorphic organisms, requires the introduction of a more rigorous classification system. The current descriptors of yeast-like or filamentous are inadequate to fully describe the observed morphology in fermentation. The introduction of a seven class system was deemed appropriate, based on observations of fermentation samples. The classes introduced were as follows:

- Yeast - spherical to ovoid single cells
- Double yeast - the double variant of the above
- Elongated yeast - ovoid single cells with a high length to width ratio
- Double elongated yeast - The double variant of the above
- Filament - single rod-like cell
- Double filament - double rod-like cell
- Pseudohyphae - pseudohyphae composed generally of chains of filaments, often displaying a complex branched structure.

With a classification system of this nature, certain complications arise in the interpretation of small morphological differences between certain classes. An example of this is the difference between a slightly elongated “yeast” and an

“elongated yeast” with a low length to width ratio. Differences of this nature are inherently prone to interoperator misclassification. It was decided that a more objective system was needed to correctly classify the organism into the above classes. Based on an examination of the literature, it was concluded that image analysis was the best means of achieving this goal.

The image analysis algorithm constructed was an amalgamation of several other protocols previously used for the description of various monomorphic morphological forms. The classification of yeast and elongated yeast was based on the principle of subunit separation using object segmentation. This allows the measurement of the geometric parameters of each of the subunits in the cell structure. Initially it was hoped to extend this approach to the classification of filaments and pseudohyphae, but when this approach was applied to the cells it was inadequate. The poor degree of curvature at the subunit interfaces and the lower cell width resulted in the formation of false “subunits”. Thus it was decided to examine the morphology of filaments and pseudohyphae by classical means, using skeletonisation and pruning to determine the geometric properties of such cells. The two morphologies therefore had to be separated from each other before any processing could be done. This was achieved using global size and shape criteria. Segmentation was applied to smaller cells and skeletonisation to pseudohyphae and long double filaments. The algorithm allowed the study of the resultant classifications, on a numerical and volumetric basis. It also allowed the examination of gross measurement data such as the cell volume, length and width.

Certain problems exist with this current algorithm, particularly in its ability to morphologically examine the subunits in filamentous cells and pseudohyphae. This limitation was software based. The software package used, was useful for simple morphological operations and allowed the application of a combination of simple operators to achieve a desired effect, but did not include the possibility of development of custom operators. It also did not allow access to pixel level data. This limited the development of the overall algorithm. There is also a recognised problem with the classification of elongated yeast and filaments. As the length to

width ratio increases the morphology will change gradually from yeast to elongated yeast to filaments. As the elongated yeast develop into filaments, the transition is smooth whereas the transition as predicted by the algorithm is abrupt. It may be more suitable to calculate volume on the basis of a contour rotation method as suggested by Huls *et al* (1992) which should, in theory, deal with calculating this smooth transition more appropriately. Again the development of such a protocol was limited by the software package utilised.

It was determined that to fully understand the effect of environment on morphology, the effect of environment on the microbial kinetics on the organism also had to be assessed. A simple kinetic model was proposed that described the stoichiometry adequately in both batch and continuous culture. The model, was adapted from Sonnleitner and Kappelli (1986) and involves splitting the cell's sugar metabolism into two discrete kinetic routes, an aerobic and an anaerobic pathway. Each kinetic pathway has distinct cell yield coefficients and ethanol can only be generated from the anaerobic pathway. The model developed adequately described chemostat kinetic data solely by changing the S_0 term. For the model to describe the effect of variation in k_La , a relationship between k_La and $J_{s \text{ critical}}$ will have to be established. Preliminary examinations in batch culture suggest linearity between the two parameters. The yield coefficients determined from the chemostat studies, when applied to batch culture data, describes the kinetic data well, suggesting that the kinetics of the organism are essentially the same in both batch and continuous culture. Due to large variations in the specific substrate uptake rates in batch culture, and the poor quality of the experimental substrate data, the model could not be adapted to batch culture data. The model proposed was ineffective in regions with low growth rates ($\mu < 0.1\text{h}^{-1}$). This is where cell maintenance becomes important. The kinetics of cell maintenance are not fully understood and are generally not addressed in models of this nature.

When the morphology of the organism was examined in batch culture under various operating conditions, it was found that decreasing agitation rate caused a greater heterogeneity in the morphology with an increase in the volumetric

fractions of elongated yeast and filaments with time. Contrary to previous investigations, the morphology displayed under fully aerobic conditions was predominantly yeastlike. All cultures were observed to have large volumetric fractions of yeastlike cells in the early stages of fermentations. When dissolved oxygen became partially limiting, an increase in the morphological heterogeneity of the cultures was observed. This increase was relative to the degree of agitation, and consequently the degree of gas-liquid mass transfer occurring in these regions. When YEPL and YEPD media were assessed in a similar fashion it was observed that similar morphologies were observed in fully aerobic yeastlike cultures whereas in cultures subject to lower agitation rates a greater development of pseudohyphal forms was observed. When both cell width and surface area to volume ratios were compared between these fermentations and the comparable whey fermentation, it was observed that the results for both YEPL and YEPD match those of the whey medium. This suggests that the subunit morphology in each form is the same but YEPL and YEPD suppress subunit separation to a greater extent than the whey based media. No difference in morphology was observed between YEPL and YEPD suggesting that the hydrolytic step that splits lactose into glucose and galactose or the subsequent metabolism of galactose have no effect on morphology. Thus it can be concluded that either poor mixing or poor gas-liquid mass transfer causes morphological transitions in the organism from a yeastlike form under ideal conditions to a mixed morphology in poor conditions.

When the organism was cultured in a chemostat the primary morphology observed was pseudohyphal under almost all environmental conditions. Exceptions to this rule occur at low dilution rates where the cells have a strong maintenance requirement and at D approaching μ_m . While the morphologies displayed in both of these regions was returning to yeastlike, the yeast cells produced at low dilution rates were much smaller than those produced at higher dilution rates. The pseudohyphae produced increased in length and complexity as dilution rate increased. This was also accompanied by an increase in pseudohyphal width. The effect of the presence or absence of oxygen appeared to be negligible on the morphology in these fermentations. There was a significant numerical fraction of

yeast and elongated yeast cells in all samples (up to approximately 20%) but this fraction was negligible on a volumetric basis. A global increase in the mean cell volume and length with dilution rate was observed. The rate of increase of these parameters appeared to be related to increasing S_0 . It is apparent that substrate limitation is the parameter that gives the strongest morphological transition in this organism and not oxygen as previously thought.

As the kinetic model proposed is equally effective in describing both batch and continuous culture data and the gross morphology of batch and continuous are very different it has to be concluded that the cells in batch and continuous culture are essentially the same on a metabolic basis. For the kinetic balances to be effective the cells in both culturing conditions have to be manufacturing equal amounts of dry matter from substrate. The yeast like cells present a lower surface area per unit volume than pseudohyphal cells, therefore more wall building materials per unit volume should in theory be required to manufacture pseudohyphae. A compensation may be made in terms of storing carbohydrates (glycogen and trehalose) under ideal environmental conditions, when yeastlike morphologies prevail. Further work is required in to study this phenomenon.

If the population distributions are examined, it is apparent that geometric parameters such as volume, length and width cannot be described using global population models such as Gaussian or lognormal distributions. By distributing various cell subpopulations, it was discovered that the global population distribution could be described in terms of summed weighted distributions of the subpopulations. Lognormal distributions were calculated for each subpopulation and the results weighted using the numerical fraction of each subpopulation in the total population. The distinct subpopulations identified were single yeastlike cells, double yeastlike cells, single filaments, double filaments and pseudohyphae. The term yeastlike included both yeast and elongated yeast, as it was found that both were essentially part of the same population. The use of the "elongated yeast" class is therefore restricted to descriptive purposes only. The global distributions observed for pseudohyphal populations had an unusual shape, displaying a sharp

peak at low values of volume and length and subsequently declining gradually over a large range of volume or length. The shape of distributions is completely determined by the method of replication of the pseudohyphae, hence some information from this data should point to mechanisms for pseudohyphal replication.

Pseudohyphae are composed of subunits that fail to separate on division. It was decided to study the mechanism of pseudohyphal formation using manual image analysis as automatic image analysis proved too difficult to implement. It was found that the pseudohyphae observed, developed as if each subunit was a budding yeast and that all daughter cells remained attached to their mothers. Thus a family tree developed whereby all cells in the pseudohypha were descended from one individual subunit. Subunits were also observed to elongate as the pseudohypha extended, suggesting that pseudohyphae are not generated by random breakage, but rather develop from shorter cells, i.e. yeast and elongated yeast. The ultrastructure of hypha increases uniformly with increasing main hyphal length, under all operating conditions except at combined low S_0 and D . This suggests that populations are composed of quantities of discrete elements. For example, pseudohyphae were typically observed to develop from one cell to two cells to four cells, very few pseudohyphae with three cells were observed. This may explain the bimodal appearance of the distributions for predominantly pseudohyphal populations in Chapter 8. It was found that subunit length increased with increasing D and S_0 , but the effect was most significant in the cases of combined high D and S_0 . Also observed in this section of the work was the fact that when a subunit is in the terminal position of a hypha, it extends rapidly. Once a bud has been produced, the extension rate of the mother subunit is minimal. There also appears to be a predestiny for a subunit's length to be related to the length of its mother subunit. It was observed that this occurrence applied to cells on the main hyphae and cells in branches.

10.2 OVERALL CONCLUSIONS

To propose a hypothesis for morphological transition all evidence gathered in this work has to be examined carefully. Firstly, the transition does not significantly alter cell metabolism. This would indicate, as suggested in Chapter 2, that dimorphism is simply the response of a slight change in the rates of various enzymatic pathways responsible for wall formation, rather than a global cellular change. Chemostat data suggests that cell width is increasing linearly with dilution rate. If carefully examined, it is seen that values of width increase linearly towards those values observed in batch culture. This suggests that the elongation component of dimorphism is completely controlled by growth rate. In batch culture, this also correlates with observations that as the cells elongate as agitation decreases (accompanied by a decrease in growth rate). The decreases, in growth rate, in batch culture are not as significant as those in chemostat culture, so the transitions reported are not as significant. Cells will always grow at the maximum possible growth rate and generally the only factor controlling growth rate in a cell is the acquisition of nutrients. This is controlled in regions of substrate limitation and hence this is how substrate limitation affects elongations. In the matter of subunits not separating after generation, this appears to be an on-off effect with cells either predominantly separating or not separating according to environmental conditions. Generally cell separation does not occur if the cells are sufficiently elongated.

Cells in chemostat culture have to regenerate themselves at the same rate as they are removed from the reactor. If all cells keep extending without cell separation, hypothetically, the culture could end up containing one pseudohypha encompassing the entire fermenter. This is obviously not the case, as the culture reaches an observed morphological steady state. Therefore, the population requires some means of self-maintenance. This regeneration is hypothesised to originate from two different sources. The large numerical fraction of yeast and elongated yeast in such populations can provide a reservoir of cells from which to generate a population of pseudohyphae. Secondly, old pseudohyphae were observed to disintegrate into smaller pseudohyphae. This would explain the high standard

deviation in the length of the first subunit in pseudohyphae, as there are two probable routes for first subunit formation. The yeast cell population must be predominantly self-maintaining, as it seems less probable that they originate from the tips of pseudohyphae. Figure 10.1 outlines a possible route for cell cycling in the reactor.

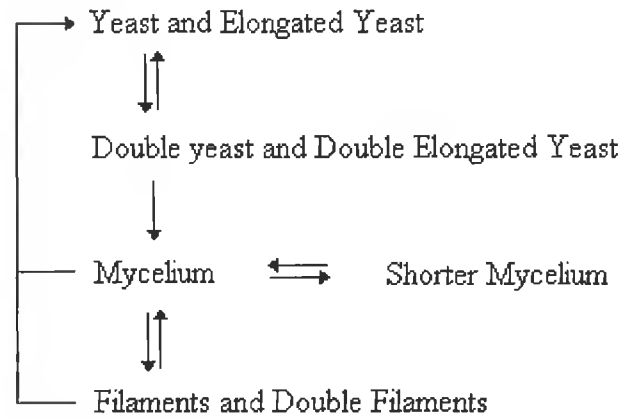


Figure 10.1 Overview of possible morphological pathways based on experimental observations

This body of work provides several novel techniques and approaches useful in the examination of the morphology of dimorphic organisms and has shown conclusively that the dimorphic transition does not affect process performance but rather is a response to process environment. It does not claim to have fully explained the mechanisms behind dimorphism, but rather highlights deficiencies in current approaches to dimorphic research. Currently there is a strong emphasis on genetic investigations in this area which are looking for on-off mechanisms in dimorphic organisms. It is probable that a lot of this work is misguided as dimorphism appears to be controlled by rate balances in the cells mechanism of wall development. If progress is to be made in this area, more mechanistic studies of this nature need to be carried out to fully understand the control processes behind this unusual biological phenomenon.

10.3 POSSIBLE AREAS OF FUTURE RESEARCH

10.3.1 Image Analysis

To develop an algorithm that examines the morphology of all cells on a subunit basis and calculates volumes based on a contour rotation method is essential to future studies. The experimental work described in Chapter 9 was very time consuming and tedious and it proved difficult to generate the quantities of data required for a more complex analysis of this nature. A method based on current imaging software would allow the isolation of perimeter points from which it would be possible to identify points of constriction in pseudohyphae with greater ease. This would also allow the generation of contour rotation methods to estimate the volume of the various morphologies more accurately.

10.3.2 Kinetic Modelling

The kinetic study uncovered some interesting phenomena that require further study. Firstly, the model needs to be verified using off-gas analysis whereby the amount of CO₂ evolved and O₂ consumed could be used in mass balances to validate the above approach. The model also has to be adapted to include a variable k_La term. This was not possible due to the lack of a dissolved oxygen probe for the chemostat fermenter. A dynamic batch culture model has to be developed which needs to address the variable substrate uptake rate observed when ethanol production begins. Again this will require more sensitive mechanisms of substrate utilisation measurement, such as off-gas analysis and possibly on-line analysis of lactose concentration in the fermenter.

10.3.3 Morphology Studies

While several key issues have been identified in this work concerning model development for hyphal extension, more detailed studies will have to take place to analyse phenomena to a greater degree.

- Batch to continuous culture transition studies will yield information about the speed of the transition from yeastlike to filamentous/pseudohyphal forms. This should allow the assessment of whether there is a genetic effect in dimorphism or not.

- The morphological transition is now understood to be a growth rate dependent phenomenon. Mathematical analysis should attempt to relate kinetic model findings to overall population morphological dynamics.
- In terms of predicting pseudohyphal development, a model should be developed that encompasses some of the above findings. Models describing the cell cycles of budding yeast should be a good starting point for this work. Such models propose that division is a function of age and time. This model hypothetically should have a third parameter, the global position of the subunit with respect to subunit 1.0.

BIBLIOGRAPHY

Adams, H.L. and Thomas, C.R. (1988). The use of image analysis for morphological measurements on filamentous microorganisms. *Biotechnol. Bioeng.* **32**, 707 - 712.

Allen, D.G. and Robinson, C.W. (1990). Measurement of rheological properties of filamentous fermentation broths. *Chem. Eng. Sci.* **45**, 1, 37 - 48.

Bail, T. (1857). Uber Hefe, Flora (Jena). **40**, 417 - 444.

Barford, J.P. (1990a) A general model for aerobic yeast growth: Batch growth, *Biotechnol. Bioeng.*, **35**, 907-920.

Barford, J.P. (1990b) A general model for aerobic yeast growth: Chemostat growth, *Biotechnol. Bioeng.*, **35**, 921-927.

Bartnicki-Garcia, S. (1968). Control of dimorphism in mucor by hexoses: control of hyphal morphogenesis. *J. Bacteriol.* **96**, 3, 1586 - 1594.

Bartnicki-Garcia, S. and Gierz, G. (1991). Predicting the molecular basis of mycelium-yeast dimorphism with a new mathematical model of fungal morphogenesis. In: More Gene Manipulations in Fungi. Bennett, J.W. and Lasure, L.L. (eds), Academic Press, SanDeigo, 27-47.

Bartnicki-Garcia, S. and Gierz, G. (1993). Mathematical modelling of the cellular basis of fungal dimorphism. in: Dimorphic fungi in Biology and Medicine. Vanden Bossche, H., Odds, F.C. and Kerridge, D. (Eds.), Plenum Press, New York and London, 3 - 10.

- Bartnicki-Garcia, S. and Nickerson, W.J. (1962a). Induction of yeast-like development in mucor by carbon dioxide. *J. Bacteriol.* **84**, 829 - 840.
- Bartnicki-Garcia, S. and Nickerson, W.J. (1962b). Isolation, composition and structure of cell walls of filamentous and yeast-like forms of *Mucor rouxii*. *Biochem. Biophys. Acta.* **58**, 102 - 119.
- Bartnicki-Garcia, S. and Nickerson, W.J. (1962c). Nutrition, growth and morphogenesis of *Mucor rouxii*, *J. Bacteriol.* **84**, 841 - 858.
- Bergen, M.S., Voss, E. and Soll, D.R. (1990). Switching at the cellular level in the white opaque transition of *Candida albicans*. *J. Gen. Microbiol.* **136**, 1925-1936.
- Berkeley, M.J. (1838). Cited in: de Bary, A. (1887), Comparative Morphology and Biology of the Fungi Mycetoza and Bacteria. Clarendon Press, Oxford.
- Berry, D.R. (1982) The Biology of Yeast, Edward Arnold Publishers Ltd., London
- Bongenaar, J.I.T.M., Kossen, N.W.F., Metz, B. and Meijboom, F.W. (1973). A method for characterising the rheological properties of viscous fermentation broths, *Biotech. Bioeng.* **15**, 201 - 206.
- Brooks, L.D. and Northey, W.T. (1963). Studies on *Coccidioides immitis*, II. Physiological studies on *in vitro* spherulation. *J. Bacteriol.* **85**, 12 - 15.
- Brown, C.M. and Hough, J.S. (1965). Elongation of yeast cells in continuous culture. *Nature*, **206**, 4985, 676 - 678.
- Carter, B.L.A. and Bull, A.T. (1971). The effect of oxygen tension in the medium on the morphology and growth kinetics of *Aspergillus nidulans*. *J. Gen. Micro.* **65**, 265 - 273.

Castrillo, J.I., Ugalde, U.O. (1992) Energy metabolism of *Kluyveromyces marxianus* in deproteinated whey. Chemostat studies. Modelling, *J. Biotechnol.*, **22**, 145-152.

Castrillo, J.I., Ugalde, U.O. (1993) Patterns of energy metabolism and growth kinetics of *Kluyveromyces marxianus* in whey chemostat culture, *Appl. Microbiol. Biotechnol.*, **40**, 386-393.

Catley, B.J. (1980). The extracellular polysaccharide, pullulan, produced by *Aureobasidium pullulans*: A relationship between elaboration rate and morphology. *J. Gen. Microbiol.* **120**, 265 – 268.

Charles, M. (1978). Technical aspects of the rheological properties of microbial cultures. *Adv. Biochem. Eng.* **8**, 1 - 64.

Chattaway, F.W., Holmes, M.R. and Barlow, A.J.E. (1968). Cell wall composition of the mycelial and blastospore forms of *Candida albicans*. *J. Gen. Micro.* **51**, 367 - 376.

Chi, C.M., Zhang, C., Staba, E.J., Cooke, T.J., Hu, W.S. (1996) An advanced image analysis system for evaluation of somatic embryo development, *Biotechnol. Bioeng.*, **50**, 65-72.

Cox, P.W. and Thomas, C.R. (1992). Classification and measurement of fungal pellets by automated image analysis. *Biotechnol. Bioeng.* **39**, 945 - 952.

Cooper, L.A., Edwards, S.W. and Gadd, G.M. (1985). Involvement of adenosine 3:5-cyclic monophosphate in the yeast-mycelium transition of *Aureobasidium pullulans*. *J. Gen. Micro.* **131**, 1589 - 1593.

Cooper, L.A. and Gadd, G.M. (1984). The induction of mycelial development in *Aureobasidium pullulans* (IM 45533) by yeast extract. *Antonie van Leeuwenhoek*, **50**, 249 - 260.

De Kee, D., Turcotte, G., Fildey, K. and Harrison, B. (1980). New method for the determination of yield stress. *J. Texture Stud.* **10**, 281 - 288.

Deacon, J.W. (1984). Introduction to Modern Mycology. Blackwell Scientific Publications.

Dion, W.M., Carilli, A., Sermonti, G. and Chain E.B. (1954). The effect of mechanical agitation on the morphology of *Penicillium chrysogenum* in stirred fermenters. *Rend. Ist. Super. De Sanita.* **17**, 187 - 205.

Donnelly, D.P., Wilkins, M.F., Boddy, L. (1995) An integrated image analysis approach for determining biomass, radial extent and box-count fractal dimension of macroscopic mycelial systems, *Binary*, **7**, 19-28.

Doran, P.,M., (1995) Bioprocess Engineering Fundamentals, Academic Press Ltd., London.

Duffy, N., Lacey, G. (1997) Colour Profiling, *Proc. Irish Machine Vision and Image Processing Conference (IMVIP-1997)*, 36-43.

Esener, A.A., Roels, J.A. and Kossen, N.W.F. (1981). Fed-Batch culture: Modelling and Applications in the study of microbial energetics, *Biotechnol. Bioeng.* **23**, 1851-1871.

Evans, E.G.V., Richardson, M.D., (1989) Medical Mycology: a practical approach, Information press Ltd., Oxford.

Fatile, I.A. (1985). Rheological characteristics of suspensions of *Aspergillus niger*: correlation of rheological parameters with microbial concentration and shape of the mycelial aggregate. *Appl. Microbiol. Biotechnol.* **21**, 60 - 64.

Fiddy, C. and Trinci, A.P.J. (1976a). Mitosis, septation branching and the duplication cycle in *Aspergillus nidulans*. *J.Gen. Microbiol.* **97**,169 - 184.

Fiddy, C. and Trinci, A.P.J. (1976b). Nuclei, septation branching and growth of *Aspergillus nidulans*. *J.Gen. Microbiol.* **97**,169 - 184.

Flegel, T.W. (1977). Lets call a yeast a yeast. *Can. J. Microbiol.* **23**, 945 - 946.

Foley, G., Malone, D.M. and MacLoughlin, F. (1995). Modelling the effects of particle polydispersity in crossflow filtration. *J. Membrane Sci.* **99**, 77 – 88.

Girbardt, M. (1957). Der spitzenkörper von *Polystictus versicolor*. *Planta*, **50**, 47.

Gimeno, C.J., Ljungdahl, P.O., Styles, C.A., Fink, G.R. (1993) Characterization of *Saccharomyces cerevisiae* pseudohyphal growth. in: Dimorphic Fungi in Biology and Medicine. Vanden Bossche, H., Odds, F.C. and Kerridge, D. (Eds.), Plenum Press, New York and London, 83-103.

González Siso, M.I., Ramil, E., Cerdán, M.E., Freire-Picos, M.A. (1996) Respirofermntative metabolism in *Kluyveromyces lactis*: Ethanol production and the Crabtree effect, *Enzyme Microb. Technol.*, **18**, 585-591.

Gopal, P.K., Sullivan, P.A. and Shepherd M.G. (1984a). Isolation and structure of glucan from regenerating spheroplasts of *Candida albicans*. *J. Gen. Microbiol.*, **130**, 325-335.

Gopal, P.K., Sullivan, P.A. and Shepherd M.G. (1984b). Metabolism of [C¹⁴] glucose by regenerating spheroplasts of *Candida albicans*. *J. Gen. Microbiol.* **130**, 1217-1225.

Gupta, R.K. and Howard, D.H. (1971). Comparative studies of the yeast and mycelial forms of *Histoplasma capsulatum*: Uptake and incorporation of L-Leucine, *J. Bacteriol.*, **105**, 3, 690 - 700.

Guterman, H. and Shabtai, Y. (1996). A self-tuning vision system for monitoring biotechnological processes. I. Application to production of pullulan by *Aureobasidium pullulans*. *Biotechnol. Bioeng.*, **51**, 501 - 510.

Häder, D.P., (1992) Chapter 6: Analysis of 2-D Electrophoretic Gels, in: *Image Analysis in Biology*, Hader D.P.(ed), CRC Press, London.

Haidle, C. W. and Storck, R. (1966). Control of dimorphism in *Mucor rouxii*, *J. Bacteriol.* **92**, 1236 - 1244.

Hamburger, W.W. (1907). A comparative study of four strains of organisms isolated from four cases of generalised blastomycosis. *J. Infect. Dis.* **4**, 201.

Harsa, S. and Zaror, C.A. (1993). Production of polygalacturonases from *Kluyveromyces marxianus* fermentation: preliminary process design and economics. *Process Biochemistry*, **28**, 187 - 195.

Heald, P.J. and Kristiansen, B. (1985). Synthesis of polysaccharide by yeast-like forms of *Aureobasidium pullulans*. *Biotechnol. Bioeng.*, **27**, 1516 - 1519.

Hill, G.A. and Robinson, C.W. (1988). Morphological behaviour of *Saccharomyces cerevisiae* during continuous fermentation. *Biotechnol. Letts.*, **10**, 11, 815 - 820.

Hitchcock, D., Glasbey, C.A., Ritz, K. (1996) Image analysis of space-filling by networks: application to a fungal mycelium, *Biotechnol. Techniques*, **10**, 205-210.

Huls, P.G., Nanninga, N., van Spronsen, E.A., Valkenburg, J.A.C., Vischer, N.O.E. and Woldringh, C.L. (1992). A computer-aided measuring system for the characterisation of yeast populations combining 2D-image analysis, electronic particle counter, and flow cytometry. *Biotechnol. Bioeng.* **39**, 343 - 350.

Inderlied, C.B. and Sypherd, P.S. (1978). Glucose metabolism and dimorphism in *Mucor*. *J. Bacteriol.* **133**, 1282 - 1286.

Jain, A.K. (1989). Fundamentals of Digital Image Processing. Prentice Hall, Engelwood Cliffs, NJ.

Joung, J.J. and Blaskovitz, R.J. (1985). Role of ammonium nitrate in morphological differentiation of *Aspergillus niger* in a submerged culture. *Dev. Ind. Microbiol.* **26**, 487 - 494.

Jüsten P., Paul G.C., Nienow, A.W. and Thomas, C.R. (1996). Dependence of mycelial morphology on impeller type and agitation intensity. *Biotechnol. Bioeng.* **52**, 672 - 684.

Kanazawa, Y. (1988) An optimal variable cell histogram, *Commun. Statist. – Theory Meth.*, **17**, 1401-1422.

Kerridge, D. (1993). Fungal dimorphism: A sideways look. in: *Dimorphic Fungi in Biology and Medicine*. Vanden Bossche, H., Odds, F.C. and Kerridge, D. (Eds.), Plenum Press, New York and London, 3 - 10.

Kieran, P.M., Malone, D.M. and MacLoughlin, P.F. (1993). Variation of aggregates size in plant cell suspension batch and semi-continuous cultures. *Trans. IChemE.* **71**, (C1): 40 - 46.

Kieran P.M. (1993) An investigation of the hydrodynamic shear susceptibility of suspension cultures of *Morinda citrifolia*. Ph.D. thesis, University College Dublin.

Kreger-van Rij, N.J.W. (1984). In: The yeasts (a taxonomic study). Kreger-van Rij, N.J.W. (Ed), Elsevier Science Publishers B.V.

Ku, M.A. and Hang, Y.D. (1992). Production of yeast lactase from saurkraut brine. *Biotechnol. Letts.* **14**, 925 - 928.

Kuriyama, H., Slaughter, J.C. (1995) Control of cell morphology of the yeast *Sacharomyces cerevisiae* by nutrient limitation in continuous culture. *Letters in Applied Microbiology*, **20**, 37-40.

Langerton, M. and Talice, R.V. (1932). Nouvelles méthodes d'étude et essai de classification des champignons levuriformes. *Ann. Parasitol. Hum. Comp.* **10**, 1 - 80.

Larralde-Corona, C.P., González-Blanco, P.C., Viniegra-González, G. (1994) Comparison of alternative kinetic models for estimating the specific growth rate of *Gibberela fujikuroi* by image analysis techniques, *Biotechnol. Techniques*, **8**, 261-266.

LeBoit, P.E., Van Fletcher, H. (1987) A comparative study of Spitz Nevus and Nodular Malignant Melanoma using image analysis cytometry, *J. Invest. Dermatol*, **88**, 753-757.

Levine, S. and Ordal, J.Z. (1946). Factors influencing the morphology of *Blastomyces dermatitidis*. *J. Bacteriol.* **52**, 687 - 694.

Lipke, P.N., Taylor, A. and Ballou, C.E. (1976). Morphogenic effects of α -factor on *Saccharomyces cerevisiae* a Cells. *J. Bacteriol.* **127**, 1, 610 - 618.

Lones, G.W. and Peacock, C.L. (1960). Role of carbon dioxide in the dimorphism of *Coccidioides immitis*. *J. Bacteriol.* **79**, 308 - 309.

López-Franco, R., Bartnicki-Garcia, S., Bracker, C.E. (1994) Pulsed growth of fungal hyphal tips, *Proc. Natl. Acad. Sci. USA*, **91**, 12228-12232.

Lord, P.G., Wheals, A.E. (1980) Asymmetrical division of *Saccharomyces cerevisiae*, *J. Bacteriol.*, **142**, 808-818.

Makagiansar, H.Y., Ayazi Shamlou, P., Thomas, C.R. and Lilly, M.D. (1993). The influence of mechanical forces on the morphology and penicillin production of *Penicillium chrysogenum*. *Bioprocess Eng.* **9**, 83 - 90.

Marchant, J.A., (1990) Intelligent machinery for agriculture, *J. of the Royal Agricul. Soc. Of England*, **151**, 177-186.

Mariat, F. (1969). Saprophytic and parasitic morphology of parasitic fungi. In: The Fourteenth Symposium of The Society for General Microbiology. Smith, H. and Taylor, J. (Eds.), 85 - 109.

McIntyre, M., McNeil, B. (1997) Dissolve carbon dioxide effects on morphology, growth, and citrate production in *Aspergillus niger* A60, *Enzyme Microb. Technol.*, **20**, 135-142.

Maruhashi, F., Murakami, S., Baba, K., (1994) Automated monitoring of cell concentration and viability using an image analysis system, *Cytotechnology*, **15**, 281-289.

McCarthy, A.A., O'Shea, D.G., Murray, N.T., Walsh, P.K. and Foley, G. (1998). Effect of cell morphology on dead-end filtration of the dimorphic yeast *Kluyveromyces marxianus* var *marxianus* NRRLy2415., *Biotechnol. Prog.*, **14**, 279-285.

- McNeill, B. and Harvey, L.M. (1993). Viscous fermentation products. *Crit. Rev. Biotechnol.* **13**, 4, 275 - 304.
- McNeil, B. and Kristiansen, B. (1987). Influence of impeller speed upon the pullulan fermentation. *Biotechnol. Letts.* **9**, 2, 101 - 104.
- McNeil, B., Kristiansen, B. and Seviour, R.J. (1989). Polysaccharide production and morphology of *Aureobasidium pullulans* in continuous culture. *Biotechnol. Bioeng.* **33**, 1210 - 1212.
- Melamed, M. (1996) Artificial Intelligence and Pathology: Ready or Not?, *Laboratory Investigation*, **75**, 291-293.
- Metz, B., De Bruijn, E.W. and Van Suijdam, J.C. (1981). Method for quantitative representation of the morphology of moulds. *Biotechnol. Bioeng.* **23**, 149 - 162.
- Metz, B. and Kossen, N.W.F. (1977). The growth of molds in the form of pellets - a literature review. *Biotechnol. Bioeng.* **19**, 781 - 799.
- Metz, B., Kossen, N.W.F. and Van Suijdam, J.C. (1979). The rheology of mould suspensions. *Adv. Biochem. Eng.* **11**, 103 - 156.
- Metzner, A.B. and Otto, R.E. (1957). Agitation of viscous Newtonian and non-Newtonian fluids *AICHEJ*, **7**, 3 - 10.
- Mitard, A. and Riba, J.P. (1988). Morphology and growth of *Aspergillus niger* ATCC 26036 cultivated at several shear rates. *Biotechnol. Bioeng.* **32**, 835 - 840.
- Monod J. (1942). Reserches sur croissance des cultures bacteriennes, Hermann et C^{ie}, Paris.

Montgomery, D.C. and Runger, G.C. (1994). Applied statistics and probability for engineers. Wiley and sons, U.S.A.

Moor, H. (1967). Endoplasmic reticulum as the initiator of bud formation in yeast, (*S. cerevisiae*). *Arch. Mikrobiol.* **57**, 135-146.

Moser, A. and Kung W. (1986). *Trichosporon cutaneum* as a biological test system with two forms of morphology. *Proc. International Conference on Bioreactor Fluid Dynamics*, 329 - 340.

Nécas O. and Svoboda A. (1981). Morphogenesis in protoplasts. In: Yeast Cell Envelopes: Biochemistry, Biophysics and Ultrastructure (Vol 2), Chpt. 6, 105-127, Arnold W.N. (Ed.), CRC Press.

Nickerson, W.J. and Edwards, G.A. (1949). Studies on the physiological basis of morphogenesis in fungi, I. The respiratory metabolism of dimorphic fungi. *J. Gen. Physiol.* **33**, 41 - 55.

Nickerson, W.J. and Falcone, G. (1956). Identification of protein disulphide reductase as a cellular division enzyme in yeast. *Science*, **124**, 722 - 723.

Nielsen, J., Johansen, C.L., Jacobsen, M., Krabben, P. and Villadsen, J. (1995). Pellet formation and fragmentation in submerged cultures of *Penicillium chrysogenum* and its relation to penicillin production. *Biotechnol. Prog.* **11**, 93 - 98.

Nielsen J. and Villadsen, J. (1994). *Bioreaction Engineering Principles*. Plenum Press, New-York.

Nienow, A.W. (1990). Agitators for mycelial fermentations. *TIBTech.* **8**, 224 - 233.

Nombela, C., Pla, J., Herreros E., Gil, G., Molina, M., Sanchez, M. (1992) Novel targets for antifungal drugs. in: *New Strategies for Fungal Disease*, Bennet, J.E., Hay, R.J., Peterson, P.K. (eds), Churchill Livingstone, Edinburgh.

Novick, A. and Szilard, L. (1950). Description of the chemostat. *Science*, **112**, 715-720

Odds, F.C. (1988). In: *Candida and candidosis*, Odds, F.C. (Ed.). Baillière Tindall, London.

Odds F.C. (1993). Quantification of *Candida* morphology *in vitro* and *in vivo*. In: *Dimorphic fungi in Biology and Medicine*, Vanden Bossche, H., Odds, F.C. and Kerridge, D. (Eds.). Plenum Press, New York and London, 3 - 10.

Ohsumi, M., Uchiyama, K. and Ohsumi, Y. (1993). Density fluctuation during the cell cycle in the defective vacuolar morphology mutants of *Saccharomyces cerevisiae*. *J. Bacteriol.* **175**, 5714 - 5716.

Olsson, S. (1994) Uptake of glucose and phosphorous by growing colonies of *Fusarium oxysporum* as quantified by image analysis, *Exp. Mycol.*, **18**, 33-47.

Olsvik, E. and Kristiansen, B. (1994). Rheology of filamentous fermentations. *Biotechnol. Adv.* **12**, 1 - 39.

Ono, K., Yasuda, N. and Ueda, S. (1977). Effect of pH on pullulan elaboration by *Aureobasidium pullulans* S-1. *Agric. Biol. Chem.* **41**, 11, 2113 - 2118.

Oolman, T. and Liu, T.C. (1991). Filtration properties of mycelial microbial broths. *Biotechnol. Prog.* **7**, 534 - 539.

Packer, H.L., Keshavarz-Moore, E., Lilly, M.D., Thomas, C.R. (1992). Estimation of cell volume and biomass of *Penicillium chrysogenum* using image analysis. *Biotechnol. Bioeng.* **39**, 384 - 391.

Packer, H.L. and Thomas, C.R. (1990). Morphological measurements on filamentous microorganisms by fully automatic image analysis. *Biotechnol. Bioeng.* **35**, 870 - 881.

Papagianni, M., Matthey, M. and Kristiansen, B. (1994). Morphology and citric acid production of *Aspergillus niger* PM1. *Biotechnol. Letters*, **16**, 9, 929 - 934.

Pasteur, L. (1876), *Études sur la Bière*, Gauthier-Villars, Paris.

Paul, G.C., Kent, C.A., Thomas, C.R. (1992). Quantitative characterisation of vacuolisation in *Penicillium chrysogenum* using automatic image analysis. *Trans. I. Chem. E.* **70**, C, 13 - 20.

Paul, G.C., Kent, C.A., Thomas, C.R. (1994a). Image analysis for characterising differentiation of *Penicillium chrysogenum*. *Trans. I. Chem. E.* **72**, C, 95 - 105.

Paul, G.C., Kent, C.A. and Thomas, C.R. (1994b). Hyphal vacuolation and fragmentation in *Penicillium chrysogenum*, *Biotechnol. Bioeng.* **44**, 655 - 660.

Paul, G.C., Thomas, C.R. (1994). A structured model for hyphal differentiation and penicillin production using *Penicillium chrysogenum*. *Biotechnol. Bioeng.* **51**, 558 - 572.

Plomley, N.J.B. (1959). Formation of the colony in the fungus *Chaetomium*. *Aust. J. Biol. Sci.* **12**, 53 - 64.

Pons, M.N., Mona, H., Drouin, J.F., Vivier, H. (1995) Texture characterisation of colonies on solid substrates, In: 6th International conference on computer applications in biotechnology, Garmish-Partenkirchen, Germany, May 14th-17th Schügerl, K., Munack, A., Elsevier Science Ltd., Oxford, 154-189.

Pons, M.N., Vivier, H., Rémy, J.F. and Dodds, J.A. (1993). Morphological characterisation of yeast by image analysis. *Biotechnol. Bioeng.* **42**, 1352 - 1359.

Prosser, J., Rattray, L., Silcock, D., Glover, A., Killham, K. (1994) Spatial characterisation of luminescence marked bacterial cells by CCD image-enhanced microscopy, *Binary*, **6**, 49-54.

Reeslev, M., Jensen, B.(1995), Influence of Zn^{2+} and Fe^{3+} on polysaccharide production and mycelium/yeast dimorphism of *Aureobasidium pullulans* in batch cultivations. *Appl. Microbiol. Biotechnol.*, **42**, 910-915.

Reeslev, M., Nielsen, J.C., Olsen, J., Jensen, B. and Jacobsen, T. (1991). Effect of pH and the initial concentration of yeast extract on regulation of dimorphism and exopolysaccharide formation of *Aureobasidium pullulans* in batch culture. *Mycol. Res.* **95**, 2, 220 - 226.

Reichl, U., King, R. and Gilles, E.D. (1992a). Characterisation of pellet morphology during submerged growth of *Streptomyces tendae* by image analysis. *Biotechnol. Bioeng.* **39**, 164 - 170.

Remes Biomedical, Field Road, Busby, Scotland (Personal Communication)

Reuss, M. (1988). Influence of mechanical stress on the growth of *Rhizopus nigricans*. *Chem. Eng. Technol.* **11**, 178 - 187.

Reuss, M., Debus, D. and Zoll, G. (1982). Rheological properties of fermentation fluids. *Chem. Eng.* **381**, 233 - 236.

Roels, J.A., Van Der Berg, J. and Vonken, R.M. (1974). The rheology of mycelial broths. *Biotechnol. Bioeng.* **16**, 181 - 208.

Rouwenhorst, R.J., Hensing, M., Verbakel, J., Scheffers, W.A. and Van Dijken, J.P. (1990). Structure and properties of the extracellular inulinase of *Kluyveromyces marxianus* CBS 6556. *Applied and Environmental Microbiology*, **56**, 3337 - 3345.

San-Blas, G. and San-Blas, F. (1984). Molecular aspects of fungal dimorphism. *CRC Critical Reviews in Microbiology*, **11**, 2, 101 - 127.

Scherr, G.H. and Weaver, R.H. (1953). The dimorphism phenomenon in yeasts. *Bacteriol. Rev.* **17**, 51 - 92.

Schuler, M.L., Kargi, F. (1992) *Bioprocess Engineering: Basic Concepts.*, Prentice Hall, New Jersey, USA.

Schwan, R.F. and Rose A.H. (1994). Polygalacturonase production by *Kluyveromyces marxianus*: effect of medium composition. *J. App. Bacteriol.* **76**, 62 - 67.

Sentandreu, R., Elorza, M.V., Mormeneo, S., Sanjuan, R. and Iranzo, M. (1993). Possible roles of mannoproteins in the construction of *Candida albicans* cell wall. In: *Dimorphic Fungi in Biology and Medicine*. Vanden Bossche, H., Odds, F.C. and Kerridge, D. (Eds.). Plenum Press, New York and London, 169 - 176.

Sentheshanmuganathan, S. and Nickerson, W.J. (1962a). Nutritional control of cellular form in *Trigonopsis variabilis*. *J. Gen. Microbiol.* **27**, 437 - 440.

Sentheshanmuganathan, S. and Nickerson, W.J. (1962b). Composition of cell and cell walls of triangular forms of *Trigonopsis variabilis*. *J. Gen. Microbiol.* **27**, 451 - 464.

Shepherd, M.G. and Gopal, P.K. (1993). Nature and control of cell wall biosynthesis. In: *Dimorphic Fungi in Biology and Medicine*. Vanden Bossche, H., Odds, F.C. and Kerridge, D. (Eds.). Plenum Press, New York and London, 3 - 10.

Smith, J.E. (1975). In: The Filamentous Fungi: Volume 1 – Industrial Mycology. Smith, J.E. and Berry, D.R. (Eds.).

Smith, M.D. and Ho, C.S. (1985). The effect of dissolved carbon dioxide on penicillin production: Mycelial morphology. *J. Biotechnol.* **2**, 347 - 363.

Smith, J.J., Lilly, M.D. and Fox, R.I. (1990). The effect of agitation on the morphology and penicillin production of *Penicillium chrysogenum*. *Biotechnol. Bioeng.* **35**, 1011 - 1023.

Soll, D.R. (1991). Current status of the molecular basis of *Candida* pathogenicity, In: The fungal spore and disease in plants and animals. Cole G.T. and Hoch, H.P. (Eds.). Plenum Press, New York and London.

Sonnleitner, B., Käppeli, O. (1986) Growth of *Saccharomyces cerevisiae* is controlled by its limited respiratory capacity: Formulation and Verification of a hypothesis, *Biotechnol. Bioeng.*, **28**, 927-937.

Staebell, M. and Soll, D.R. (1985). Temporal and spatial differences in cell wall expansion during bud and mycelium formation in *Candida albicans*. *J. Gen. Microbiol.* **131**, 1467 –1480

Streiblova, E. (1970) Study of scar formation in the life cycle of heterothallic *Saccharomyces cerevisiae*, *Can. J. Microbiol.*, **16**, 827-831.

Suhr, H., Wehnert, G., Schneider, K., Bittner, C., Scholz, T., Geissler, P., Jahne, B., Scheper, T. (1995) *In situ* microscopy for on line characterisation of cell populations in bioreactors, including cell concentration measurements by depth from focus. *Biotechnol. Bioeng.*, **47**, 106-116.

Sundhagul, M. and Hedrick, L.R. (1966). Effect of tryptophan on growth and morphology of *Hansenula schneegii* cells. *J. Bacteriol.* **92**, 1, 241 - 249.

Svoboda, A. and Nécas, O. (1974). Morphogenesis during protoplast reversion in dimorphic yeast. *proc. 4th Int. Symp. On Yeast*, Part 1, Vienna, p. D-74.

Swain, M.J., Ballard, D. (1991), Colour Indexing, *International Journal of Computer Vision*, **7**, 11-32.

Takahashi, J. and Yamada, K. (1959). Studies on the effect of some physical conditons on the submerged mold culture, *J. Agric. Chem. Jpn.* **33**, 707 - 709.

Treskatis, S.K., Orgeldinger, V., Wolf, H., Gilles, E.D., (1997) Morphological characterisation of filamentous microorganisms in submerged cultures by on-line digital image analysis and pattern recognition, *Biotechnol. Bioeng.*, **53**, 191-201.

Thomas, C.R., Department of Chemical Engineering, University of Birmingham, U.K. (Personal Communication)

Thomas, C.R. and Paul, G.C. (1996). Applications of image analysis in cell technology. *Current Opinion in Biotechnology*, **7**, 35 - 45.

Trinci, A.P.J. (1969). A kinetic study of the mode of growth of *Aspergillus nidulans* and other fungi. *J. Gen. Microbiol.* **57**, 11 - 24.

Trinci, A.P.J. (1974). A study of the kinetics of hyphal extension and branch initiation of fungal mycelia. *J. Gen. Microbiol.* **81**, 225 - 236.

Trinci, A.P.J., Robson, G.D., Wiebe, M.G., Cunliffe, B. and Naylor, T.W. (1990). Growth and morphology of *Fusarium graminearum* and other fungi in batch and continuous culture. In: *Microbial Growth Dynamics*, Poole, R.K., Bazin, M.J., Keevil, C.W. (Eds.) IRL Press: Oxford.

Tsuchido, T., Takeuchi, H., Kaewahara, H., Obata, H. (1994) Evaluation of bacterial injury by image analysis of cell motion, *J. Ferment. Bioeng.*, **78**, 185-187.

Tucker, K.G., Kelly, T., Delgrazia, P. and Thomas, C.R. (1992). Fully-automatic measurement of mycelial morphology by image analysis. *Biotechnol. Prog.* **8**, 353 - 359.

Tucker, K.G., Chalder, S., Al-Rubeai, M., Thomas, C.R. (1994) Measurement of hybridoma cell number, viability, and morphology using fully automated image analysis, *Enzyme Microb. Technol.*, **16**, 29-35.

Tucker, K.G. and Thomas, C.R. (1993). Effect of biomass concentration and morphology on the rheological parameters of *Penicillium chrysogenum* fermentation broths. *Trans. I. Chem. E.* **71**, C, 111 - 117.

Tyson, C.B., Lord, P.G. and Wheals, A.E. (1979). Dependency of size of *Saccharomyces cerevisiae* cells on growth rate. *J. Bacteriol.* **138**, 92 – 98.

Van Suijdam, J.C. and Metz, B. (1981). Influence of engineering variables upon the morphology of filamentous molds. *Biotechnol. Bioeng.* **23**, 111 - 148.

Van Urk, H., Mak, P.R., Scheffers, W.A., Van Dijken, J.P. (1988) Metabolic responses of *Saccharomyces cerevisiae* CBS8066 and *Candida utilis* CBS621 upon transition from glucose limitation to glucose excess, *Yeast*, **4**, 283-291.

Vanhoutte, B., Pons, M.N., Thomas, C.R., Louvel, L. and Vivier, H. (1995). Characterisation of *Penicillium chrysogenum* physiology in submerged cultures by color and monochrome image analysis. *Biotechnol. Bioeng.* **48**, 1 - 11.

Vecht-Lifshitz, S.E., Magdassi, S. and Braun, S. (1990). Pellet formation and cellular aggregation in *Streptomyces tendae*. *Biotechnol. Bioeng.* **35**, 890 - 896.

Walker, G.M. and O'Neill, J.M. (1990). Morphological and metabolic changes in the yeast *Kluyveromyces marxianus* var. *marxianus* NRLL y 2415 during fermentation on lactose. *J. Chem. Tech. Biotechnol.* **49**, 75 - 89.

Weibe, M.G. and Trinci, A.P.J. (1991). Dilution rate as a determinant of mycelial morphology in continuous culture. *Biotechnol. Bioeng.* **38**, 75 - 81.

Wickerham, L.J. (1951). Taxonomy of Yeasts, Technical Bulletin No. 1029. United States Department of Agriculture.

Wimpenny, J., Wilkinson, T., Peters, A. (1995) Monitoring microbial colony growth using image analysis techniques, *Binary*, **7**, 14-18.

Wirtanen G., Ahola, H., Mattila-Sandholm, T. (1995) Evaluation of cleaning procedures in elimination of biofilm from stainless steel surfaces in open process equipment. *Trans. Inst. Chem. Engineers.*, **73 [Part C]**, 9-16.

Withers, J.M., Wiebe, M.G., Robson, G.D. and Trinci, A.P.J. (1994). Development of morphological heterogeneity in glucose limited chemostat cultures of *Aspergillus oryzae*. *Mycol. Res.* **98**, 95 - 100.

Yamasaki, H., Lee, M.S., Tanaka, T. and Nakanishi, K. (1993a). Characteristics of cross-flow filtration of pullulan broth. *Appl. Microbiol. Biotechnol.* **39**, 26 - 30.

Yamasaki, H., Lee, M.S., Tanaka, T. and Nakanishi, K. (1993b). Improvement of performance for cross-flow membrane filtration of pullulan broth. *Appl. Microbiol. Biotechnol.* **39**, 21 - 25.

Yanagishima, N. (1963). Effect of auxin and antiauxin on cell elongation in yeast. *Plant & Cell Physiol.* **4**, 257 - 264.

Yanagishima, N. and Masuda, Y. (1964). RNA functional in auxin action to elongate yeast cells. *Plant & Cell Physiol.* **5**, 369 - 372.

Zalewski, K. and Bucholz, R. (1996). Morphological analysis of yeast cells using an automated image processing system. *J. Biotechnol.* **48**, 43 - 49.

Zalewski, K., Götz, P. and Bucholz, R. (1994). On-line estimation of yeast growth rate using morphological data from image analysis. In: *Advances in Bioprocess Engineering*, Galindo E. and Ramirez, O.T. (Eds.), Kluwer Academic Publishers, 191 - 195.